Summer 2021

Enhanced heavy oil recovery by low salinity polymer flood combined with microgel treatment

Yang Zhao

ENHANCED HEAVY OIL RECOVERY BY LOW SALINITY POLYMER FLOOD

COMBINED WITH MICROGEL TREATMENT

by

YANG ZHAO

A DISSERTATION

Presented to the Graduate Faculty of the

MISSOURI UNIVERSITY OF SCIENCE AND TECHNOLOGY

In Partial Fulfillment of the Requirements for the Degree

DOCTOR OF PHILOSOPHY

in

PETROLEUM ENGINEERING

2021

Approved by:

Dr. Baojun Bai, Advisor
Dr. Mingzhen Wei, Co-advisor
Dr. Randall S. Seright
Dr. Ralph Flori
Dr. Shari Dunn-Norman
Dr. Parthasakha Neogi

PUBLICATION DISSERTATION OPTION

This dissertation consists of the following seven articles, formatted in the style used by the Missouri University of Science and Technology:

Paper I, "Enhancing Heavy Oil Recovery Efficiency by Combining Low Salinity Water and Polymer Flooding", found on pages 12–55, was published in *SPE Journal*.

Paper II, "Experimental Study of Transport Behavior of Microgel Particles in Superpermeable Channels for Conformance Control", found on pages 56–97, is intended for submission to *Journal of Petroleum Science and Engineering*.

Paper III, "Selective Penetration of Microgels in Superpermeable Channels and Reservoir Matrices", found on pages 98–123, is intended for submission to *Journal of Petroleum Science and Engineering*.

Paper IV, "Critical Pressure Gradients During Microgel Propagation", found on pages 124–152, is intended for submission to *Fuel*.

Paper V, "A Comprehensive Laboratory Method to Evaluate Microgel Conformance Control Performance Using Sandwich-like Channel Models", found on pages 153–185, is intended for submission to *SPE Journal*.

Paper VI, "Transport, Placement, Fluid Diversion and Matrix Damage Behavior of Microgels for Conformance Control in Reservoirs Containing Superpermeable Channels", found on pages 186–219, is intended for submission to *SPE Journal*.

Paper VII, "Experimental Study of Microgel Conformance-Control Treatment for A Polymer-Flooding Reservoir Containing Superpermeable Channels", found on pages 220–257, has been published online by *SPE Journal*.

ABSTRACT

Heavy oil resources account for a large portion of the total oil reserves around the world. The target heavy oil reservoir is located on Alaska's North Slope (ANS). Advantages of low-salinity HPAM polymer (LSP) over high-salinity polymer (HSP) were demonstrated. LSP could recover more oil with 40% less polymer consumption. No additional oil was recovered by HSP after LSP flood. The first-ever polymer flood pilot on ANS showed remarkable success regarding water cut reduction, oil production increase, delayed breakthrough, and projected oil recovery improvement. Polymer alone was insufficient to achieve satisfactory recovery as the reservoirs were highly heterogeneous. Microgels could improve the effectiveness of polymer flood by reducing water cut and increasing oil recovery. Favorable working conditions were identified. Microgel transport behavior was studied using superpermeable sandpacks (27-221 darcies) with multiple pressure sensors. The particle-to-pore matching size ratio significantly impacted the effectiveness of the gels. A threshold differential pressure (ΔP_{th}) and critical pressure gradient (∇P_{cr}) were required to push the gels to penetrate and propagate through the channels. The ΔP_{th} and ∇P_{cr} revealed the underlying mechanisms of selective penetration/placement behavior of microgels in heterogeneous reservoirs. Diagrams were developed to estimate the maximum propagation distance of the gels in channels in conceptual field applications. Sandwich-like channel models and methodologies were developed to comprehensively evaluate the effectiveness of gel materials. Gel retention in the channels was quantified. Results also indicated that the retained gels were dehydrated. Fluid diversion and sweep improvement after gel treatments were evaluated by tracer tests.

ACKNOWLEDGMENTS

First and foremost of all, I would give my deepest appreciation to my dear advisor, Dr. Baojun Bai for his nice advising, outstanding guidance, constant encouragement and generous financial support through my Ph.D. career. Thanks for bringing me to the wonderful world of enhanced oil recovery, for giving me the chance to be part of a creative team, and for teaching me to learn how to think critically, how to perform lab work creatively, and how to present results logically. His instructions and inspirations certainly benefit not only my four-year Ph.D. life, but also my future career. My sincere gratitude should also be given to my co-advisor Dr. Mingzhen Wei for her patient advice and help.

I appreciate my nice committee members Dr. Randall S. Seright, Dr. Ralph Flori, Dr. Shari Dunn-Norman, and Dr. Parthasakha Neogi. Their rich knowledge always inspires me to get new understanding of the topics of my research from different perspectives. Their comments and feedbacks always help me fresh my thoughts and broaden my mind.

The funding support (DE-FE0031606) from the Department of Energy and Hilcorp is acknowledged. Dr. Abhijit Dandekar, Dr. Yin Zhang, Dr. Samson Ning, Dr. Dongmei Wang and the other members of the project team greatly help me improve my research. I thank the former and current lab members, to name a few, Jiaming Geng, Yifu Long, Jingyang Pu, Mustafa Almahfood, Shize Yin, Ze Wang, Tao Song, Junchen Liu, Shuda Zhao, Bowen Yu, Adriane Melnyczuk, Ali Al Brahim, Jianqiao Leng and other nice colleagues for their help.

The work is impossible without the support of my family. Their love and support are always there to rise me up.

TABLE OF CONTENTS

SECTION

LIST OF ILLUSTRATIONS

LIST OF TABLES

PAPER VI

PAPER VII

NOMENCLATURE

Symbol	Description
A_c	Cross-sectional area of channel, cm^2
A_m	Cross-sectional area of matrices, cm^2
ANS	Alaska's North Slope
d	Average diameter of the pores, µm
E_{bw}	Water blocking efficiency
EOR	Enhanced oil recovery
f_{CK}	Carman-Kozeny factor
F_{rr}	Residual resistance factor
f_w	Water cut, $f_w=q_w/(q_w+q_o)$
FW	Formation water
HSP	High-salinity polymer, salinity=FW
HSW	High-salinity water, salinity=FW
I_b, I_a	Injectivity before and after the gel treatment
IFT	Interfacial tension
K_c	Initial permeability of channel, md
K_{cw}	Permeability of the channel to water after the gel treatment, md
K_{cwi}	Permeability of the channel to water before the gel treatment, md
K_m	Initial (absolute) permeability of matrices, md
K_t	Overall permeability of the channel model
LSE	Low salinity effect
LSP	Low salinity polymer, prepared with injection source brine in Milne Point Unit

LSW	Low-salinity water, injection source brine in the Milne Point field
MSR	Particle-to-pore matching size ratio
N_{ca}	Capillary number
OOIP	Oil originally in place
P_{cr}	Critical pressure, psi
PPG	Preformed Particle Gel
ppm	Parts per million
PV	Pore volume
q_m	Flow rate in the matrices, ml/min
S_{or}	Residual oil saturation, fraction
S_{wi}	Initial water saturation, fraction
Φ	Porosity, fraction
η	Oil recovery factor
τ	Tortuosity, dimensionless

SECTION

1. INTRODUCTION

1.1. BACKGROUND

Heavy oil resources are abundant and account for a large portion of the total oil reserves around the world. Thermal methods, like steam flooding, are effective techniques to develop the heavy oil resources. However, in some areas the thermal methods are not feasible. For example, the Milne Point heavy oil reservoir on Alaska's North Slope (ANS) is covered with a thick permafrost layer. Heat loss and environmental concerns make thermal recovery methods unacceptable. Waterflooding can maintain the production at the early stage, but it shows quick breakthrough and fast rise of water cut. Polymer flood was proposed to unlock the heavy oil resources in this area (Dandekar et al. 2019, 2020, 2021; Ning et al. 2019, 2020). Successful field applications of polymer flood in heavy oil reservoirs have been reported around the world, like in Canada (e.g., Pelican Lake, Seal, and Cactus Lake), China (e.g., Bohai Bay), Middle East (e.g., South Oman), Suriname (e.g. Tambaredjo), and Trinidad and Tobago (Delamaide et al. 2014, 2018; Saboorian-Jooybari et al. 2016; Saleh et al. 2017; Zhang et al. 2016).

The first-ever polymer-flood pilot test on the ANS has been implemented since August 2018. Detailed background information about the geology, stratigraphy, minerology, reservoir, well configurations, fluids, and production history are available in the literature (Dandekar et al. 2019, 2020, 2021; Ning et al. 2019, 2020; Paskvan et al. 2016; Attanasi & Freeman 2014). The key information is summarized in Table 1.1. The

heavy oil reservoir is located at the J-Pad of Milne Point Unit (Figure 1.1). The target Schrader Bluff formation consists of O-sands and N-sands (Figure 1.2). The O-sands are subdivided into OA and OB sands, and the N-sands are subdivided into NA through NF. OA sand and NB sand are the main oil layers of the Schrader Bluff formation in Milne Point field. The pilot well pattern is located in the NB sand, which is a thin, unconsolidated shallow marine sandstone formation. The thickness is in the range of 10-18 feet. The porosity is 31-35%, and the permeability is 500-5,000 md. The depth of formation is about 3,550 feet. The API gravity of the crude oil is around 15-19 °API, and 200-330 cp under reservoir conditions. The average reservoir temperature and pressure are about 71 °F and 1750 psi, respectively. The well pattern consists of two horizontal injectors and two horizontal producers (Figure 1.3). The horizontal lengths of the wells are in the range of 4200 to 5500 feet. The inter-well distances are about 1100 feet. The injectors are equipped with injection control devices (ICD) to regulate the water flow profiles in different segments along the wellbore.
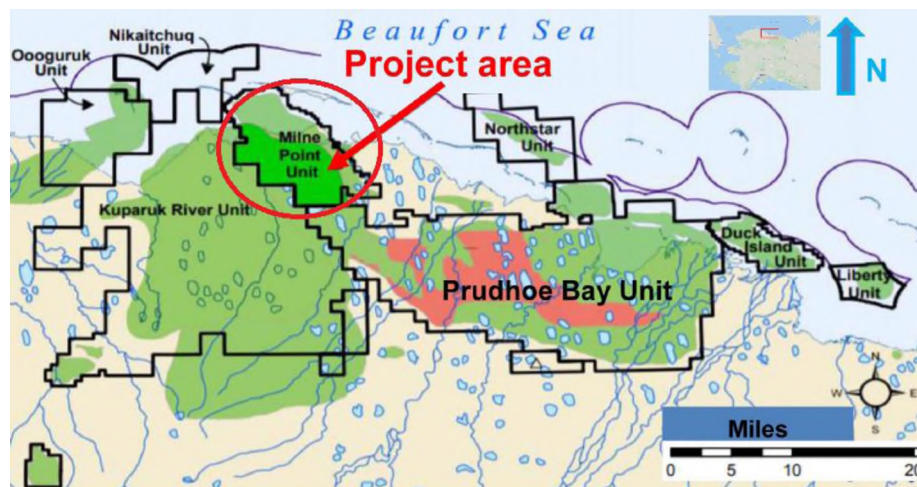
Figure 1.1. Location of the target reservoir. (Modified from Dandekar et al. 2019, originally from AK DNR, Div. of Oil & Gas, 2006.)

Table 1.1. Reservoir information. [The data was collected from Dandekar et al. (2019, 2020, 2021), Ning et al. (2019, 2020), and Paskvan et al. (2016).]

Item	Value
Location	Alaska's North Slope (ANS), USA
Oil field	Milne Point Unit (~50,000 acres)
Operator	Hilcorp Alaska
Formation	Schrader Bluff NB-sand (thin, unconsolidated shallow marine sandstone)
Development	Production since 1985 ~490 wells (2020) First-ever polymer flood pilot: from August 2018
Vertical depth, ft	3550 ft
Thickness	10-18 ft
API gravity, Oil viscosity	15-19 °API 200-330 cp (in-situ)
Porosity and permeability	31-35%; 500-5000 md
Reservoir temperature, pressure	71 °F; 1750 psi
Well Pad	J-Pad
Well pattern	Two horizontal injectors and two horizontal producers
Pattern area	~450 acres, isolated by sealing faults
Horizontal lateral	4200-5500 ft
Inter-well distance	1100 ft
Polymer	Flopaam 3630S
Formation water	Total dissolved solids (TDS) = 27500 ppm
Injection source water	TDS=2500 ppm
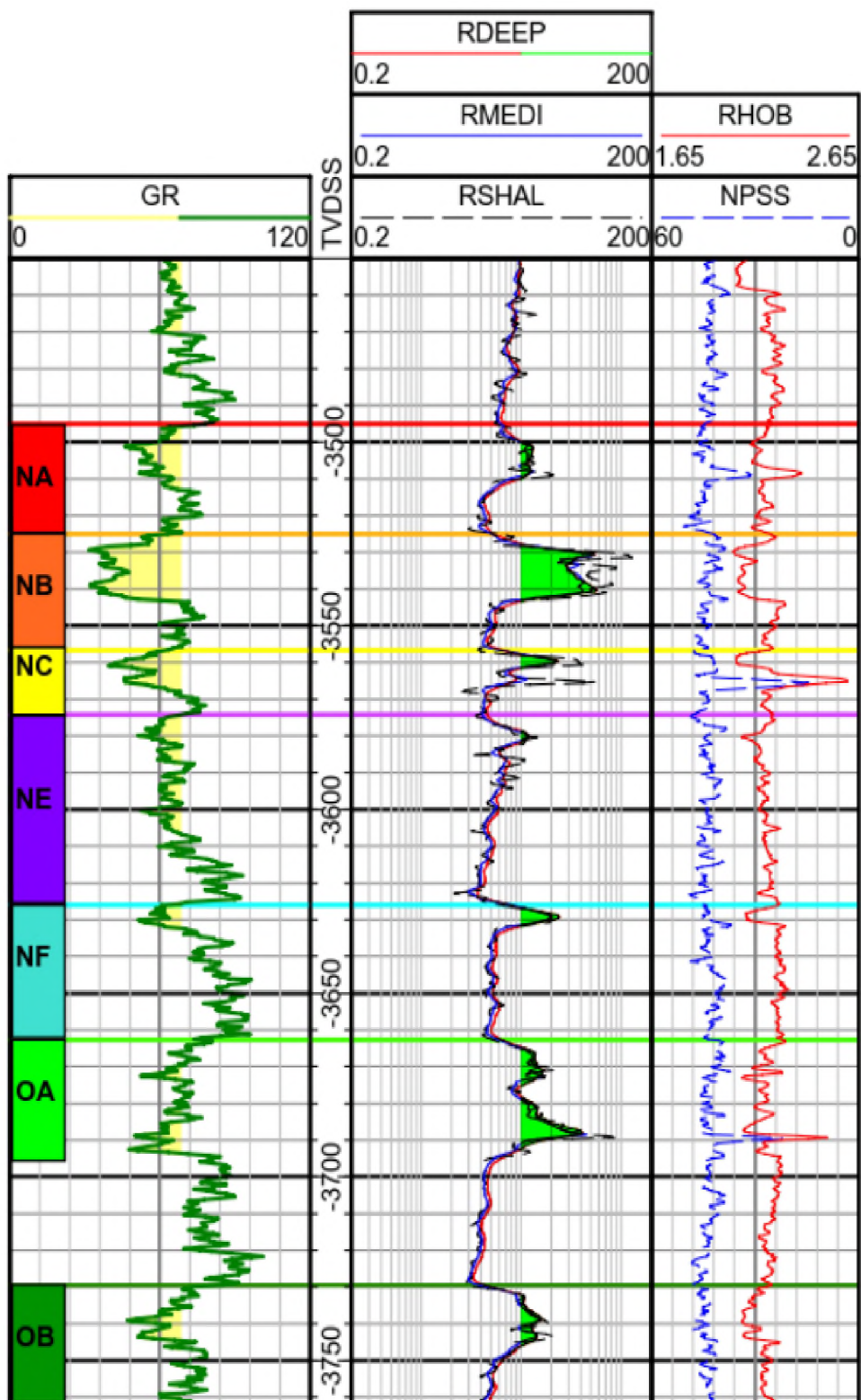
Figure 1.2. Well logging information of the Schrader Bluff formation at Milne Point.
(Ning et al. 2019)
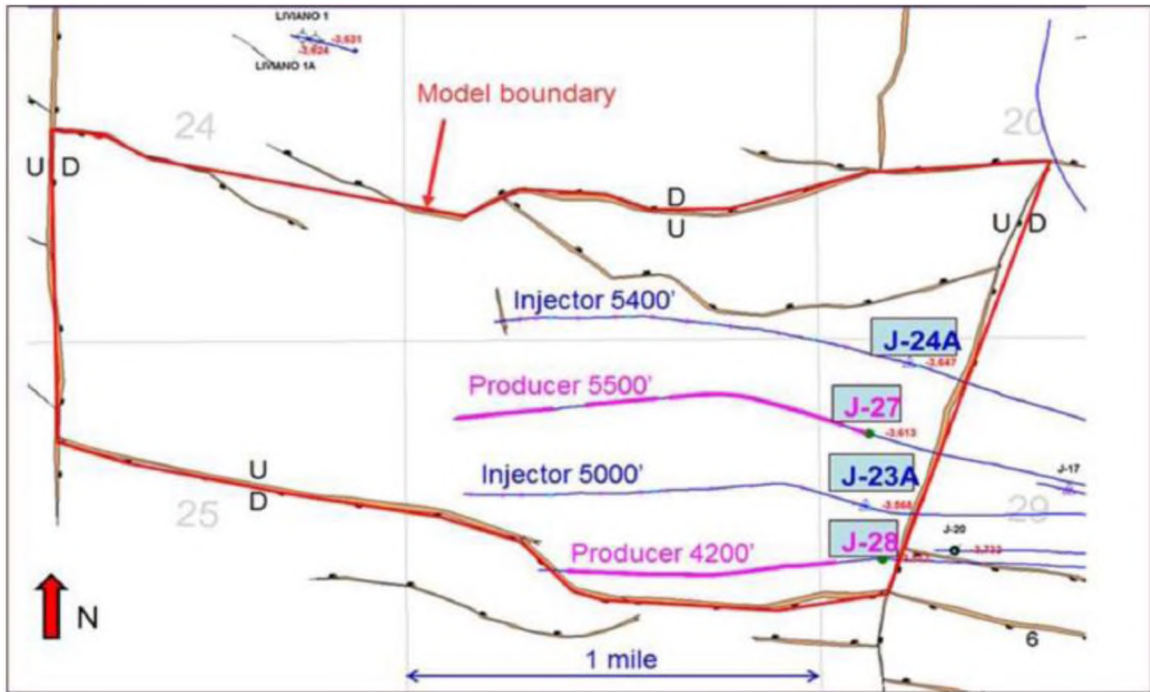
Figure 1.3. Injector-producer well patterns of the polymer flood pilot. (Dandekar et al. 2019)

Since a low-salinity water resource is readily available in the field and no additional facilities are required, it is possible to combine the advantages of low-salinity water (Sheng 2014; Morrow & Buckley 2012; Chavan et al. 2019) and polymer flooding in a technically and economically attractive way at Milne Point. Despite the convenient implementation of the hybrid EOR process, however, it is challenging to fully understand the physics of the complex polymer/brine/oil/rock system. Systematic laboratory research work is required to verify the synergic effect, identify favorable conditions for implementation, and maximize the oil-recovery performance.

Fast water breakthrough and excessive water production are commonly encountered in oil fields when local and large-scale heterogeneities (e.g., fractures, channels, conduits, and so forth) present in a reservoir act as preferential water pathways

from injection wells to production wells (Bai et al. 2013; Sun & Bai 2017; Sydansk & Romero-Zeron 2011). Polymer flood, although effective in reducing the mobility ratio between the water phase and the oil phase, might be insufficient to overcome the adverse effect caused by the heterogeneities and achieve satisfactory oil recovery. Considering the relatively high cost of the flooding fluid and the processing difficulties of the produced water (Chang et al. 2020; Dhaliwal et al. 2021), the excessive water production during polymer flooding is more undesirable compared with the issue encountered during waterflooding. The produced polymer would significantly increase the operational cost and raise environmental concerns. Conformance-control treatment can help improve the polymer-flooding performance and suppress the excessive water/polymer production. Gel treatment has proved to be effective to block fractures and fracture-like features in reservoirs and improve the conformance, and different types of gel systems have been developed over the last several decades (Bai et al. 2007a, 2007b, 2008, 2012, 2013, 2015; Seright et al. 2003; Seright & Brattekas 2021; Aldhaheri et al. 2020, 2021; Zhu et al. 2017; Kang et al. 2021; Leng et al. 2021). To overcome some drawbacks inherent with the in-situ gel (e.g., damage to oil zones, sensitivity to reservoir temperature, salinity, and so forth), preformed particle gels were developed in a variety of size series (Bai et al. 2007a). Successful applications by Chinese companies (Bai et al. 2008, 2012), Occidental Petroleum (Pyziak & Smith 2007), Halliburton (Vasquez et al. 2008), Kinder-Morgan (Larkin & Creel 2008), and ConocoPhillips (Peirce et al. 2014) have demonstrated the effectiveness of this type of gel system. Recently, a new PPG (Pu et al. 2019), named RPPG (i.e., Recrosslinkable PPG) has been successfully used by ConocoPhillips in low-temperature West Sak reservoirs on Alaska's North Slope (Targac et al. 2020).

Numerous studies have been reported with the focus on the transport and water blocking efficiency of the milli-sized PPGs in open fractures or partial open fractures (Zhang & Bai 2011; Sun et al. 2018, 2020; Wang & Bai 2018; Alhuraishawy et al. 2018; Wang et al. 2019a, 2019b). However, the understanding of micrometer-sized gel (microgel) particles transporting through porous-medium type channels is still not sufficient. Therefore, this dissertation will study the enhanced heavy oil recovery performance by low-salinity HPAM polymer flooding. Also, in order to overcome the channeling problems, microgels will be used to improve the effectiveness of the polymer flooding in heavy oil reservoirs. The transport, placement, and water-blocking efficiency of the microgels will be systematically studied using different models. Proper physical models and methodologies will be developed to comprehensively evaluate the effectiveness of the gel materials.

1.2. OBJECTIVES OF THIS WORK

The specific objectives of this study include:

(1) To demonstrate the technology of combining low salinity water and polymer flooding in enhancing heavy oil recovery, and to determine the favorable conditions for the combined effect of low-salinity water and polymer flooding.

(2) To investigate the transport behavior of microgels in superpermeable channels.

(3) To develop proper physical models and methodologies to systematically evaluate the placement behavior, water-blocking performance, fluid diversion, and sweep improvement of microgels.

(4) To test the performance of microgel treatments in improving the effectiveness of polymer flooding in heavy oil reservoirs containing superpermeable channels, and to figure out the favorable working conditions for conformance control treatments with microgels.

1.3. STRUCTURE OF THE DISSERTATION

According to the research objectives, this dissertation focuses on four topics and consists of seven papers. The four topics are: 1) Enhancing heavy oil recovery efficiency by combining low salinity water and polymer flooding (Paper I); 2) Microgel transport behavior in superpermeable channels (Paper II, Paper III, and Paper IV); 3) Microgel placement and water-blocking performance in superpermeable channels (Paper V and Paper VI); and 4) Microgel conformance-control treatment in polymer-flooding reservoirs containing superpermeable channels (Paper VII). The literature review is distributed in the introduction section of each paper, and a separate literature review section is not included in this dissertation.

In Paper I, a series of coreflooding experiments were performed using representative brine/oil/core materials under various flooding schemes. The possible mechanisms responsible for the synergic benefit of combining the low-salinity water and polymer were explored. The performance of the two-year field pilot test in the target field was also briefly discussed.

In Paper II, a series of experiments were carried out to investigate the transport behavior and explore the effective working conditions of microgels in superpermeable porous media. Sandpacks prepared with silica sands were used to mimic superpermeable

channels in reservoirs. Specifically, the following key questions would be addressed: 1) whether the microgel particles can be injected and placed into the in-depth region of the superpermeable channels? 2) Could the microgels establish reliable resistance to the post water injection? and 4) what are the proper working conditions for the tested microgel to be effective (in terms of successful in-depth placement and efficiently shutting off water flow)?

Paper III is focused on the threshold (minimum) differential driving pressure required for the microgel particles to penetrate and propagate in superpermeable channels. A series of experiments were carried out using different models to elucidate the threshold pressure of the microgel particles in such superpermeable channels. Microgel dispersions were injected into superpermeable sandpacks, heterogeneous models with superpermeable channels, and sandstone cores with relatively low permeabilities at various conditions. The implications of the experimental results to gel treatment field applications is demonstrated. The effect of the particle-to-pore matching size ratio is discussed. The results are expected to provide crucial support for the gel treatment design, and to evaluate how far the gel can be placed into the reservoir away from the wellbore.

Paper IV is focused on the critical (minimum) pressure gradient (∇P_{cr}) was required to drive the microgel particles to propagate the superpermeable porous channels. The effect of particle-to-pore matching size ratio (MSR) was investigated, and correlations were developed. A procedure was developed to estimate the maximum propagation distance of microgels in at given conditions.

Paper V explores proper physical models and methodologies to perform proper and comprehensive evaluations of a gel product and/or an enhanced oil recovery process before

deploying them in field applications. In this paper, a particular sandwich-like physical model and a set of comprehensive evaluation techniques were developed. The model consists of low-permeability matrices and a superpermeable porous channel. The comprehensive evaluations include: 1) selective penetration/placement in the target location, 2) sweep efficiency improvement (and fluid diversion) after the gel treatment, 3) water-blocking efficiency, 4) damage to matrices, and 5) potential oil recovery improvement.

In Paper VI, systematic laboratory studies were carried out to investigate the transport, placement, water-blocking ability, fluid diversion and sweep improvement, and matrix damage effect of micrometer-sized preformed particle gels (microgels) in reservoirs containing superpermeable channels. The impact of the channel/matrix permeability contrast, the particle/pore size ratio to the channels, the particle/pore size ratio to the matrices were studied. The favorable conditions of the gel treatment were identified. The results of this study are expected to provide important support for gel product selection, and successful gel treatment design and implementations.

Paper VII is focused on the excessive-water-production problem caused by the presence of superpermeable channels (ten to several hundred darcies) during polymer flooding. The sandwich-like channel models were used to study the selective-penetration, water-blocking, and oil-recovery-improvement performance of microgel particles. A series of experiments were carried out to examine whether polymer flooding alone is sufficient to overcome the adverse effect of the superpermeable channels and achieve satisfactory oil recovery, and to investigate the potential of microgel treatment in reducing the water cut and improving the sweep efficiency and oil-recovery performance.

The achievements of this study can help get a better understanding of the crucial issues involved in the polymer flooding in heavy oil reservoirs. The results can help to select proper gel products and identify the proper working conditions for conformance control treatment. The results are expected to provide important laboratory support to the polymer flood pilot project in the target oil field. Moreover, the results of this study would provide insights for the development of similar oil resources around the world.

PAPER

I. ENHANCING HEAVY OIL RECOVERY EFFICIENCY BY COMBINING LOW SALINITY WATER AND POLYMER FLOODING

(This paper, SPE-204220-PA, has been published in SPE Journal.)

ABSTRACT

Combining low salinity water (LSW) and polymer flooding was proposed to unlock the tremendous heavy oil resources on Alaska's North Slope (ANS). The synergy of low salinity water and polymer flooding was demonstrated through coreflooding experiments at various conditions. The results indicate that the high-salinity polymer (HSP, salinity=27,500 ppm) requires nearly two thirds more polymer than the low-salinity polymer (LSP, salinity=2,500 ppm) to achieve the target viscosity at the condition of this study. Additional oil was recovered from LSW flooding after extensive HSW flooding (3-9% OOIP). LSW flooding performed in secondary mode achieved higher recovery than that in tertiary mode. Also, the occurrence of water breakthrough can be delayed in the LSW flooding compared with the HSW flooding. Strikingly, after extensive LSW flooding and HSP flooding, incremental oil recovery (~8% OOIP) was still achieved by LSP flooding with the same viscosity as the HSP. No noticeable incremental oil was recovered by HSP flooding performed after LSP flooding. The residual oil saturation (Sor) reduction induced by the low salinity effect in the area unswept during the LSW flooding (mainly smaller pores) would contribute to the increased oil recovery. LSP flooding performed

directly after waterflooding recovered more incremental oil (~10% OOIP) compared with HSP flooding performed in the same scheme. Apart from the improved sweep efficiency by polymer, the low-salinity-induced Sor reduction also would contribute to the increased oil recovery by the LSP. Nearly two-year pilot test in the Milne Point field on the ANS has shown impressive success of the proposed hybrid enhanced oil recovery (EOR) process: water cut reduction (70% to below 15%), increasing oil rate, and no polymer breakthrough so far. This work has demonstrated remarkable economical and technical benefits of combination of low salinity water and polymer flooding in enhancing heavy oil recovery.

1. INTRODUCTION

Heavy oil resources are abundant and account for a large portion of the total oil reserves around the world. Thermal methods, like steam flooding, are effective techniques to develop the heavy oil resources. However, in some areas the thermal methods are not feasible. For example, the Milne Point heavy oil reservoir on the Alaska North Slope (ANS) is thin and covered with a thick permafrost layer. Heat loss and environmental concerns make thermal recovery methods unacceptable. Solvent-based methods (solvent agent: CO_2, CH_4, C_3H_8, etc. and/or their mixture) show potential in reducing the in-situ oil viscosity and enhancing the oil recovery (Jiang et al. 2019; Sun et al. 2020). However, the high mobility of the displacing agent would make it challenging to achieve the anticipated enhanced oil recovery performance without additional measures. The cost is also a key concern as massive relatively expensive solvent is required. Waterflooding can maintain the production at the early stage, but it soon shows premature breakthrough and fast rise of

water cut (Kargozarfard et al. 2019). Polymer flooding is believed an effective method to unlock the heavy oil resources in this area. Successful field applications of polymer flooding in heavy oil reservoirs have been reported around the world, like in Canada (e.g., Pelican Lake, Seal, Cactus Lake), China (e.g., Bohai Bay), Middle East (e.g., South Oman), Suriname (e.g., Tambaredjo), and Trinidad and Tobago (Saboorian-Jooybari et al. 2016).

The first ever polymer flood pilot test on the ANS has been implemented since August 2018 (Dandekar et al. 2019, 2020; Ning et al. 2019; Wang et al. 2020). As a low-salinity water resource is readily available in the field and no additional facilities are required, it is possible to combine the advantages of low-salinity water and polymer flooding in a technically and economically attractive way at the Milne Point. Despite the convenient implementation of the hybrid EOR process, however, it is challenging to fully understand the physics of the complex polymer/brine/oil/rock system. Systematic laboratory research work is required to verify the synergic effect, identify favorable conditions for implementation, and maximize the oil recovery performance.

Low salinity water has drawn increasing attention during the last two decades since the pioneering work of Morrow and his co-workers (Tang & Morrow 1997, 1999). Various researches have demonstrated encouraging EOR potential in laboratory experiments, pilot tests and field applications (Sheng 2014; Awolayo et al. 2018; Chavan et al. 2019). The salinity of the injection water should be low enough for the presence of low salinity effect (LSE), usually below 1500 ppm, but the LSE has been observed at the salinity as up to 5000 ppm (Morrow & Buckley 2011). There is no clear boundary to define the low and high salinity. Generally, the salinity of the injected brine was about 5-10% of the connate brine (Awolayo et al. 2018). Various mechanisms were proposed in the literature. No

consensus is now available on the major mechanism(s) that responsible for the improved oil recovery during LSW flooding. The most often discussed mechanisms for sandstone porous media include (Sheng 2014): 1) wettability alteration; 2) multi-component ion exchange (MIE); 3) Clay swelling, fines destabilization and migration; 4) Salt-in effect; 5) Osmosis pressure; and 6) alkaline-like flooding.

Several researchers have discussed the technical and economic benefits of combining low salinity water and polymer flooding. The oil used in the published studies so far has a relatively low viscosity (<50 cp). By using low salinity water, one of the most direct benefits is significant reduction of the polymer consumption. For example, Vermolen et al. (2014) reported that the required polymer concentration could be reduced 2-4 times using low-salinity water as make-up brine compared with high-salinity water. Shiran and Skauge (2013) investigated the diluted seawater as both secondary and tertiary in strongly water-wet and intermediate wet outcrop Berea sandstone cores. Also, they tested the low-concentration polymer solution (3630S, 300 ppm, 2.6 cp) in improving oil recovery beyond the residual oil saturation established with diluted seawater. Secondary-mode LSW showed improved oil recovery, especially in intermediate-wet cores, while tertiary-mode LSW only showed very marginal low salinity benefit for intermediate-wet cores. The 300-ppm polymer flooding showed no improvement in strong water-wet cores after secondary or tertiary LSW flooding. An increase in oil recovery of 5% OOIP was observed in intermediate-wet cores after tertiary LSW flooding, and 12-17% oil recovery increase after secondary LSW flooding. Kozaki (2012) performed several coreflood experiments to investigate the performance of LSP flooding after water flooding in aged Berea sandstone

cores. Beneficial recovery was observed from tertiary LSP flooding, both after limited and extensive HSW flooding.

The research reported by ENI also demonstrated the EOR potential of LSP over HSP with aged reservoir sandstone cores (Moghadasi et al. 2019). Their experiments showed that LSP could achieve 8% additional oil after extensive HSP with the same viscosity. Moreover, the LSP showed remarkable economic benefit as much lower polymer concentration was used for LSP (300 ppm versus 1000 ppm). Almansour et al. (2017) performed six coreflooding experiments with Berea and Bentheimer sandstone cores. They reported that in intermediate-wet sandstone cores (Berea), a tertiary LSP significantly improved the oil recovery, and the improvement was greater after a secondary HSW flood (16.7% after HSW versus 11.6% after LSW). However, the recovery by LSW and the ultimate recovery was much higher (55.4% vs. 40.3%; 67.0% vs. 57%). They attributed the beneficial low salinity effect to the release of mixed-wet fines, as supported by fines production in effluent and the fluctuation in pressure drop during LSW flooding. The initial wettability had a significant impact on the secondary LSW recovery rate and efficiency, and on the incremental recovery of the tertiary LSP and the final recovery. Torrijos et al. (2018) studied the effect of injection scheme on the oil recovery performance of LSP. In their experiments, obvious pH increase was observed during the LSP flooding. The beneficial effect of LSP flooding was also reported by a very recent study (Kakati et al. 2020).

However, the reported observations were made from relatively light oils. For example, in the cases discussed above, the oil viscosity is in the range of 2.4-33 cp. In this study, we aimed at the following problems.

(1) Whether the hybrid EOR method of combining LSW and polymer flood is effective for a 200-cp heavy oil? To what extent could the hybrid EOR method improve the oil recovery performance in the target heavy oil reservoir at the Milne Point field?

(2) Whether can the LSP further reduce the residual oil saturation established after extensive waterflooding and/or extensive HSP flooding of the same viscosity?

(3) What is the favorable flooding scheme that beneficial to maximizing the synergy effect?

(4) What are the possible mechanisms that responsible for the enhanced oil recovery?

To achieve these goals, a series of coreflooding experiments were performed using representative brine/oil/core materials under various flooding schemes. The possible mechanisms that responsible for the synergic benefit of combining the LSW and polymer were explored. The performance of the two-year field pilot test in the target field was also briefly discussed.

2. METHODOLOGY

Brines. The composition of formation brine and injection brine are shown in Table 1. The synthetic formation brine (SFB) and synthetic injection brine (SIB) were prepared in lab according to the corresponding brine compositions in the Milne Point field. The salinity of the SIB (2498 ppm) was about 9% of the SFB (27500 ppm), and they are regarded as HSW and LSW respectively in this paper (Awolayo et al. 2018; Sheng 2014). The ionic strength of the HSW and LSW is 0.492 and 0.046, respectively.

Table 1. Compositions of formation brine and injection brine.

Name	Properties (Measured at 71 °F)	Composition (ppm)
HSW (SFB, synthetic formation brine)	pH=7.30 μ=1.15 cp TDS=27500 ppm Ionic strength=0.492 Hardness: 1700 ppm	Na^+: 10086.0 K^+: 80.2 Ca^{2+}: 218.5 Mg^{2+}: 281.6 Cl^-: 16834.4
LSW (SIB, synthetic injection brine)	pH=7.50 μ=1.07 cp TDS=2498 ppm Ionic strength=0.046 Hardness: 280 ppm	Na^+: 859.5 K^+: 4.1 Ca^{2+}: 97.9 Mg^{2+}: 8.7 Cl^-: 1527.6

Polymer. The polymer used was an acrylamide-acrylate copolymer, Flopaam 3630S, provided by SNF Floerger. This polymer was selected for the pilot polymer flood project based on the availability and cost of the polymer products, and initial laboratory/numerical studies (Dandekar et al. 2019). The hydrolysis degree was 25−30% with a molecular weight of 18-20 million Daltons. HSP and LSP were prepared with the HSW and LSW, respectively. Prior to adding polymer powder, the brine was deoxygenated with argon. The desired amount of polymer was slowly added into the brine while being stirred with a magnetic bar at 300 rpm. The solution was stirred at room temperature for about 24 hours until all the polymer powders were well dissolved. The polymer solution was filtered through a 1.2-μm filter paper.

Oil. The crude oil was collected at a wellhead at the Milne Point (Well #B-28). The oil sample was centrifuged to remove water and solids (if any) and filtered through a 0.5-μm filter paper. The viscosity of the oil was 202 cp at reservoir temperature (71 °F), and the API gravity was 19.0° (0.940 g/ml). A heavy mineral oil (CAS 8042-47-5, Fisher Chemical) was used in one coreflooding experiment. The mineral oil was composed of paraffin oil and had a viscosity of 173 cp, comparable with the crude oil.

Sandpacks. As proper core plugs were not available, sandpacks prepared with formation sand were applied to perform the coreflooding tests. The sand was from a crushed core sample from the target reservoir formation (Schrader Bluff NB sand) from Liviano-01A well at the Milne Point Unit. The formation was poorly consolidated, and the core samples were not intact to use directly for coreflooding tests. The sand kept the native condition to some extent with crude oil attached on the sand surface, as shown in Figure 1a. The sand was used as received to prepare the sandpacks. The sand contained 1.5% illite, 1.5% chlorite, 1% dolomite, ~10% albite, and the remaining was quartz. The native-state sand and the SEM image are shown in Figure 1. The median size of the sand was about 170 μm. The sandpacks were prepared using a steel tube with an inner dimension of 2.54 cm × 20.4 cm. A piece of stainless-steel screen was attached to the outlet end plug to prevent sand from being flushed out of the sandpack tube. A wet-packing method was adopted to prepare the sandpacks. The sand was mixed with formation brine and set for about 24 hours to remove air bubbles attached on the sand. The sand was slowly added to the sandpack tube at multiple times. A hammer was used to knock the tube body to make sure the sand was well packed. The pore volume and porosity were measured through tracer

test. After measuring the permeability with formation brine, crude oil was injected to establish the irreducible water saturation (S_{wi}).
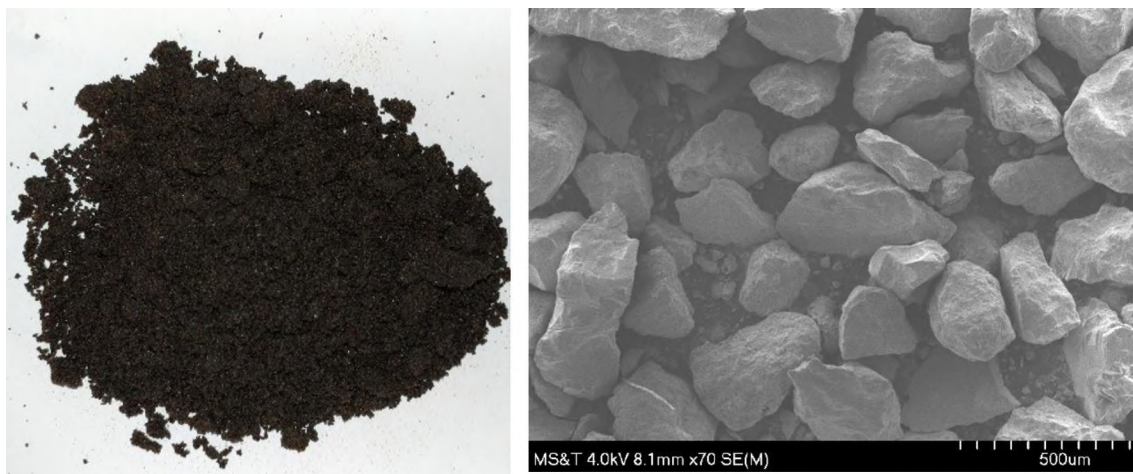
(a) Formation sand in native state.　　　　(b) SEM image of the sand.

Figure 1. Formation sand.

Rheology Measurement. The viscosity of injected and produced brine and polymer solutions was measured with a Brookfield viscometer for a wide range of shear rate 0.5-200 s-1 at reservoir temperature. The UL adapter system was used in the measurement. The viscosity of crude oil was also measured. The SC-34 spindle-container system was adopted because of the relatively high viscosity. The deviation of the measurement was within 0.1%. the viscoelasticity of the LSP and HSP. To evaluate the viscoelasticity of the polymer solutions, a rheometer (HAAKE MARS III) was used to measure the storage modulus (G') and loss modulus (G") of the polymer solutions through frequency sweep tests (0.1-100 rad/s) in the linear viscoelastic regime. The polymer showed power-law behavior, as shown in Figure 2. As the salinity was reduced, the required polymer

concentration decreased to achieve the target viscosity (45 cp). The viscosities of the two polymer solutions were very close to each other. The concentrations of the two polymers were 2,300 ppm and 1,400 ppm, respectively, which indicates the HSP required 64% more polymer than the LSP to achieve the target viscosity. The polymer molecules are more likely in a coiled state in a high-salinity environment. This is a result of the strong repulsive forces exerted by the surrounding dense ions (Muller et al., 1979). Consequently, the viscosifying ability of the polymer molecules is suppressed. On the contrary, the polymer molecules would be in a stretched status and have a greater viscosifying ability at low salinity conditions.
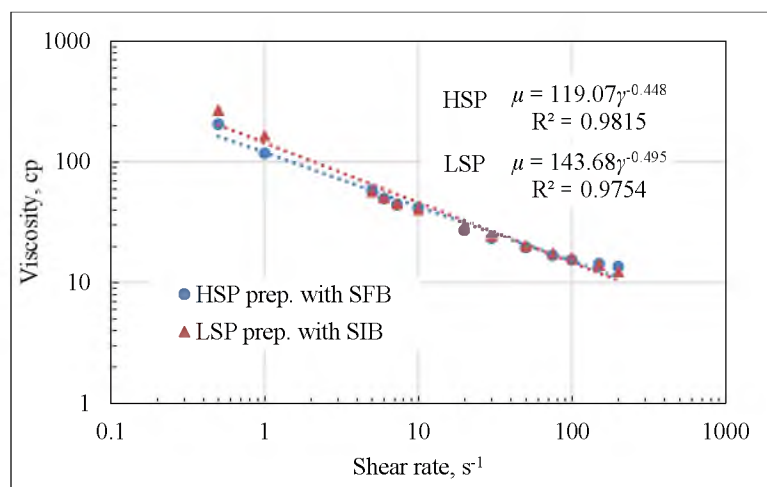
Figure 2. Polymer viscosity.

pH Measurement. The pH value of the brine, polymer solutions, and aqueous phase of the effluent was measured with a pH meter with an accuracy of ±0.002 pH (Orion™ 2-Star Benchtop, Thermo Scientific). The pH values of the HSW and LSW were 7.3 and 7.5, respectively. The pH values of the fresh HSP and LSP were 7.6 and 7.8, respectively.

Coreflooding Experiments. Figure 3 shows the coreflood setup. It consists of a D-series ISCO syringe pump, accumulators, the sandpack assembly, pressure transducers and data acquisition system, effluent collection system, and tubing lines and valves. The pump could work in constant-pressure and constant-flowrate mode. The flowrate accuracy was 0.001 ml/min, and the maximum operating pressure was 7,500 psi. A pressure sensor was mounted to monitor the injection pressure at the inlet of the sandpack model. The accuracy of the pressure sensor was within ±0.1%. The effluent samples were collected with graduated tubes at proper frequency. The samples were examined to get the oil recovery information and subject to further test of pH, salinity, and viscosity. A series of coreflooding experiments were carried out (Table 2). Exp-1 and Exp-2 were aimed at investigating LSW flooding performed in tertiary mode and secondary mode, respectively. From these two experiments, we intended to testify whether the low salinity brine could improve the recovery compared with the high salinity brine. Also, we would explore the favorable conditions in which the low-salinity benefit could be realized (i.e., performing the LSW flooding directly (secondary) was better or a tertiary scheme was preferable?).

After having a basic understanding of the behavior associated with the low salinity fluid, we investigated the more complex polymer flooding under different conditions (Exp-3-Exp-8). The questions we intended to answer are:

(1) Whether and to what extent more oil can be recovered with conventional polymer flooding after extensive water flooding? Can the polymer reduce the residual oil saturation established with extensive waterflooding (Exp-3, Exp-3R)?

(2) As a comparison to Exp-3, what is the oil recovery potential if the polymer flooding is performed earlier (without waterflooding prior to the polymer flood) (Exp-4)?

(3) Can the LSP further reduce the residual oil saturation established with extensive HSP flooding? What about the EOR potential of the LSP after HSP flooding with the same viscosity? (Exp-5, Exp-5R, Exp-6)?

(4) Compared to Exp-3, could the LSP flood achieve a better EOR performance compared with the HSP flood performed in the same scheme? What are the possible mechanisms that responsible for the improved recovery (Exp-7)?

In Exp-8, a heavy mineral oil, instead of the crude oil, was used. This experiment was intended to study the effect of the oil property (composition) on the oil recovery performance of LSP. The flow rate in the flooding process was set at 0.1 ml/min (equivalent to a Darcy velocity of ~1.2 ft/d). Due to the adverse mobility ratio between the displacing phase (water or polymer) and the heavy oil, the displacement is not stable. It is hard to reach the true residual oil saturation during a heavy oil recovery process. In view of this, for each flood process, many pore volumes of displacing fluid were injected to drive the system to the residual oil saturation condition for that fluid. During the last several pore volumes (PVs) of injection in each flood process, no oil was produced, which confirmed the completion of the displacement. Increased flow rates were used at the end of a flooding process to check the capillary end effect.
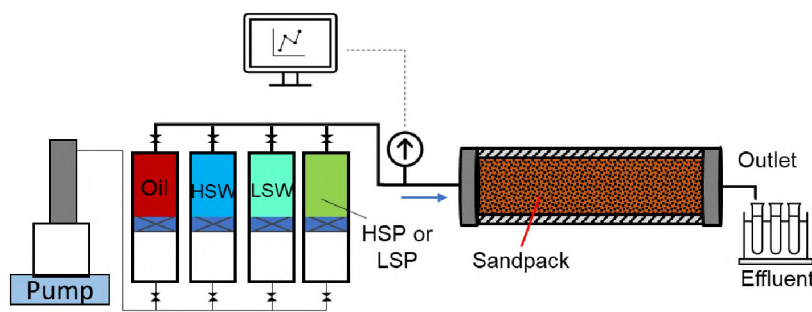
Figure 3. Coreflooding experiment setup.

Table 2. Basic information of core flooding experiments.

Exp #	Objective	d, cm	L, cm	porosity	K, md	S_{wi}	Flooding process
Exp-1	LSW in tertiary mode	2.54	20.40	0.415	1770	0.160	(1) HSW flooding to S_{or} (2) LSW flooding to no oil production
Exp-1R1	LSW in tertiary mode (Reproducibility test)	2.54	20.40	0.453	16,205	0.103	(1) HSW flooding to S_{or} (2) LSW flooding to no oil production
Exp-1R2	LSW in tertiary mode (Reproducibility test)	2.54	20.40	0.316	478	0.109	(1) HSW flooding to S_{or} (2) LSW flooding to no oil production
Exp-2	LSW in secondary mode	2.54	20.40	0.453	16,205	0.112	(1) LSW flooding to no oil production (2) HSW flooding to no oil production
Exp-3	HSP flooding after WF	2.54	20.40	0.415	1770	0.160	HSP flooding performed after Exp-1 until no oil production
Exp-3R	HSP flooding after WF (Reproducibility test)	2.54	20.40	0.453	16,205	0.112	HSP flooding performed after Exp-1R1 until no oil production
Exp-4	PF as secondary recovery	2.54	20.40	0.236	248	0.261	HSP flooding until no oil production
Exp-5	LSP after HSP&WF	2.54	20.40	0.415	1770	0.160	LSP flooding performed after Exp-3 until no oil production
Exp-5R	LSP after HSP&WF (Reproducibility test)	2.54	20.40	0.453	16,205	0.112	LSP flooding performed after Exp-3R until no oil production
Exp-6	LSP after secondary HSP flooding	2.54	20.40	0.236	248	0.261	LSP flooding performed after Exp-4 until no oil production
Exp-7	LSP right after waterflooding	2.54	20.40	0.316	478	0.109	LSP flooding performed after Exp-1R2 until no oil production
Exp-8	Effect of oil composition	2.50	30.50	0.372	4906	0.164	(1) HSW flooding to S_{or} (2) HSP flooding to no oil production (3) LSP flooding to no oil production

3. RESULTS AND DISCUSSION

3.1. LSW FLOODING: TERTIARY VERSUS SECONDARY

Exp-1 and Exp-2 were conducted to investigate the performance of LSW flooding performed in tertiary mode and secondary mode, respectively. The tertiary LSW flooding was performed at residual oil saturation (S_{or}) condition established after extensive HSW waterflooding. The results are shown in Figures 4 to 6.

Tertiary LSW Flooding. HSW flooding was first conducted in Exp-1 as a secondary recovery method. The water breakthrough occurred at 0.13 pore volumes (PV) of injection and 15.2% of the oil originally in place (OOIP) was recovered. After breakthrough, the water cut quickly increased up to 90% after 0.76 PV of injection. The water cut climbed to 99% after 2.9 PV. However, it took a long time (>15 PV) to visually reach the no-oil-production condition (water cut=100%). Then several additional PVs of water were injected to confirm no more oil could be produced. The long tail indicates the displacement was significantly distorted from a piston-like fashion. It resulted from the adverse mobility ratio between the injected brine and the viscous oil, which can be theoretically supported by the Buckley-Leverett theory (Buckley & Leverett 1942; Pope 1980; Maini 1998). For heavy oil, the displacement process is highly unstable, and the water tends to finger into the oil and further develop into channels preferential to water flow between the injectors and producers, as shown in Figures 7c and 7d. A total of 18.7 PV of HSW was injected. The endpoint oil saturation after such extensive flooding (> 10 PV) was regarded as the residual oil saturation in this work. It may be still not the exactly true residual oil saturation due to the high viscosity of the oil (Wassmuth et al. 2007). The oil recovery reached 37.9%

and the S_{or} was 0.522. About two thirds of the recovered oil was obtained after water breakthrough.
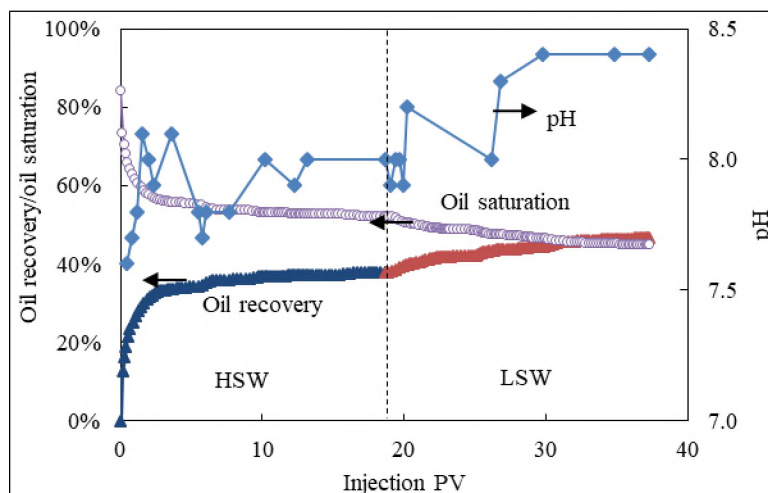
Figure 4. Tertiary LSW flooding (Exp-1).
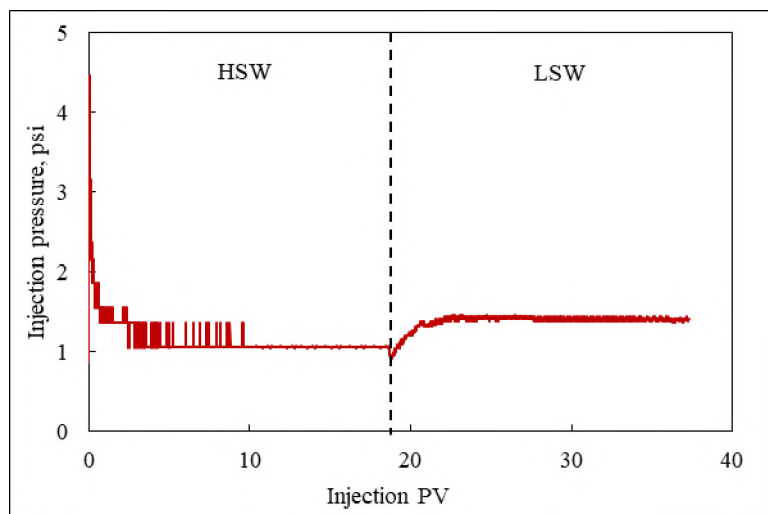
Figure 5. Injection pressure in Exp-1.

After the secondary HSW flooding, extensive PVs of LSW were injected into the core to test whether lowering the salinity could effectively recover more oil after the HSW

flooding. The water cut was obviously reduced and 8.7% OOIP additional oil was recovered. The oil recovery factor was increased to 46.6%. The results demonstrate the positive effect of low salinity in enhancing the heavy oil recovery efficiency. The results are consistent with the recent experimental work which showed improved oil recovery performance (6.3% OOIP) of LSW flooding (TDS=3,000 ppm) over HSW flooding (TDS=28,000 ppm) for the target Milne Point heavy oil (Cheng et al. 2018).

The capillary end effect was checked according to the Rapport-Leas scaling parameter, $Lv\mu$, which should be higher than 3.5 $cm^2min^{-1}cp$ (Rapoport & Leas 1953; Qi 2018), where L is the length of the core, cm; μ is the viscosity of the displacing fluid, cp; and v is the Darcy velocity, cm/min. The scaling parameter during water flooding was 0.43, thus a capillary end effect was likely. At the end of HSW flooding and LSW flooding, the flow rate was increased to 0.2, 0.5, 1.0 and 2.0 ml/min. No additional oil was produced at the increased flow rates. Note that the scaling parameter at 2.0 ml/min was 20 times higher and well above the critical value. The results indicated the end effect was negligible.

Exp-1R1 and Exp-1R2 were carried out following the same procedure on different sandpacks (Figures A1 and A2 in Appendix) to test the reproducibility. The results show that LSW recovered more oil after the normal salinity water. The improvement was quite significant as an oil incremental of 3.0% and 5.6% OOIP was achieved, respectively. The oil recovery efficiency increased from 41.4% to 44.3% for Exp-1R1, and from 43.9% to 49.5% for Exp-1R2. Accordingly, the residual oil saturation was significantly reduced. The results further confirmed the positive effect of low salinity on the oil recovery performance.

Secondary LSW Flooding. In Exp-2, the sandpack was directly flooded with LSW as the secondary recovery method. The water breakthrough occurred at 0.18 PV. The

breakthrough occurred later, and more oil could be recovered compared to the secondary HSW flooding in Exp-1. The water cut increased up to 90% after 0.96 PV of injection, and further rose to 99% after 4.9 PV. The production duration at relatively-lower-water-cut level lasted remarkably longer than the secondary HSW flooding. The behavior indicates the displacement was more stable during the LSW flooding. A total of 27 PV of LSW was injected. Compared with the secondary HSW flooding, the secondary LSW flooding achieved a higher recovery efficiency (49.4% vs. 37.9%) and drove the core to a lower S_{or} (0.482 vs. 0.522). The LSW flooding could recover 8% more oil than the HSW flooding using the same sandpack. Tertiary HSW flooding after the LSW flooding was attempted, but no appreciable incremental oil recovery was observed, as shown in Figure 6. The overall oil recovery after the tertiary flooding was 49.9%, which was higher than that in Exp-1R1 (44.3%).

Considering the breakthrough behavior and oil recovery efficiency, the results suggest that the LSW flooding can achieve a better performance than the HSW flooding, and secondary LSW flooding is better than that performed in tertiary stage. The results are qualitatively consistent with the observations reported by Shiran and Skauge (2013). They suggested that a secondary LSW was better than a tertiary one because during the secondary HSW flooding, the residual oil was trapped in pore throat structures in the swept area. The tertiary LSW tended to follow the water pathways, and thus the oil recovery performance was not as good as a secondary LSW. Also, the snap-off events were weakened during a secondary LSW flood. For heavy oils, due to unfavorable mobilities, the bypassed oil is significant after waterflooding. Therefore, the tertiary LSW still has a

better chance to recover additional oil compared with the cases with less viscous oil as Shiran and Skauge (2013).
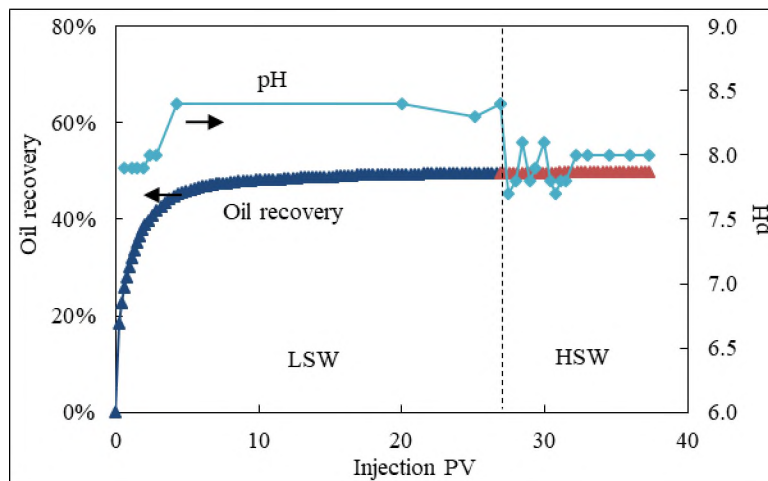
Figure 6. Secondary LSW flooding (Exp-2).

As shown in Figure 5, the injection pressure during LSW flooding was higher than that during HSW flooding, and no fines production was observed during the entire flooding process. It suggests the low salinity fluid did not result in formation damage and ruin the injectivity. Also, in the target oil field, low salinity waterflooding had been performed before the polymer flood pilot test (see the Field Application Evaluation section). For the polymer flood pilot test, the polymer solution was prepared with LSW that had the same salinity as used in the coreflooding experiments. The low salinity did not induce formation damage during waterflooding or polymer flooding (Ning et al. 2019). The increased injection pressure may be due to the wettability alteration induced by ion exchange and release of polar components from the pore surfaces. The relative permeabilities were reduced, as supported by the decreased endpoint K_{rw} at S_{or} condition.

The pH change of the produced aqueous phase in Exp-1 and Exp-2 was plotted in Figures 4 and 6. As shown in Figure 4, the pH was stabilized at 8.0 during HSW flooding, while during the tertiary LSW flooding, the pH quickly increased from 7.9 to above 8.2 and gradually stabilized at 8.4, which was almost 1.0 pH unit higher than the injected value. The major pH increase synchronized well with the incremental oil recovery process. A similar trend was observed in Exp-2, as shown in Figure 6. The pH increase was induced by the injected low salinity brine. Several mechanisms could ascribe to the pH change, such as ion exchange, dissolution of carbonate or plagioclase minerals (Rezaeidoust et al. 2011; Shiran & Skauge 2013). The native-state reservoir sand was relatively oil-wet as the sand had contacted the oil for millions of years (Figure 1). At the initial stage, polar components of the crude oil were adsorbed onto the pore surface either directly or through divalent cations. The cations acted as a bridge to attach the polar components onto the pore surface (mainly the clay surfaces). The adsorbed oil films could not be detached from the sand surfaces by the HSW as it was the same with the connate brine, as shown in Figure 7a. The invasion of LSW disturbed the adsorption equilibrium status. Ion exchange occurred as a result of the ion concentration gradient between the invading LSW and the in-situ brine, especially at the pore surfaces. The hydrogen ions were adsorbed onto the surfaces and the divalent cations were released. Also, the hydroxide ions could react with the acidic and basic components through acid-base reaction (Rezaeidoust et al. 2011), thus the polar components attached to the pore surface were released. The sand surfaces become more water wet as the polar components were detached and the oil films became thinner, as shown in Figure 7b. Consequently, the residual oil was mobilized, and the residual oil saturation was reduced.

3.2. HSP FLOODING AFTER WATERFLOODING

In Exp-3, the performance of HSP flooding was investigated after extensive HSW flooding and LSW flooding. The results are shown in Figure 8. The results show that the polymer can still improve the oil recovery performance even after extensive water flooding (37 PV of HSW and LSW). The oil recovery incremental was 7.4% OOIP, and the oil recovery was increased to 53.9%. In the reproducibility test experiment (Figure A3), Exp-3R, the incremental oil recovery was 6.5% OOIP, and the oil recovery was increased from 49.9% to 56.3%.
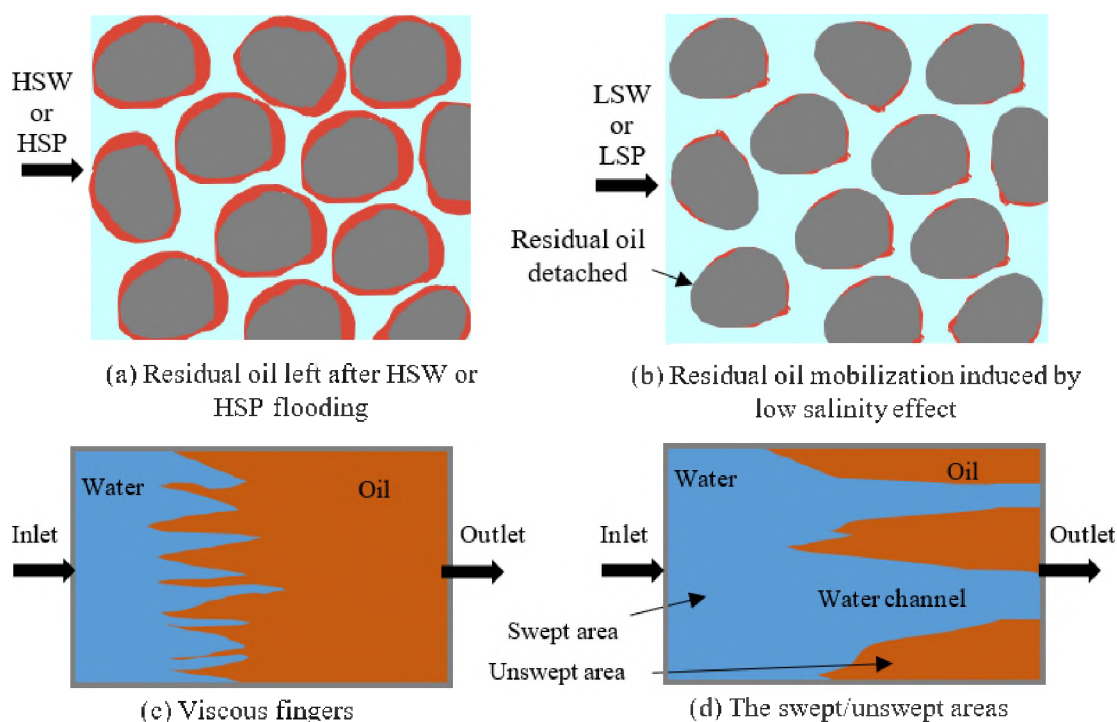
Figure 7. Residual oil mobilization induced by low salinity effect and development of preferential water channels. (a) Polar components attach on the sand surface and residual oil is left after HSW or HSP flooding. (b) The residual oil is detached from the sand surface induced by the low salinity effect during LSW or LSP flooding. (c) The water fingers into the oil phase due to the adverse mobility ratio between the water and oil phases. (d) Local heterogeneities can exacerbate the viscous fingering and some parts would be left unswept.

Due to the adverse mobility ratio during waterflooding, the sweep efficiency is hard to reach 100%. The adverse mobility ratio would cause fingering problem (Figure 7c), and local heterogeneity (e.g., pores with different sizes) would make the situation worse as the water prefers to finger into larger pores. The viscous fingers gradually develop into macroscale channels that preferential to water flow. Afterwards, the water mainly transports through the channel from the inlet (injector) to the outlet (producer), as shown in Figures 7c and 7d. Meanwhile, the oil in smaller pores is bypassed. The core after waterflooding can be divided into two portions (Figure 7d): 1) the well-swept area (mainly the larger pores), and 2) the unswept area (mainly the smaller pores). The well-swept area is mainly composed of a bunch of larger pores and most likely acts as preferential water pathways during waterflooding. Thus, this area could be well-swept to residual oil saturation condition. The unswept area mainly consists of smaller pores that bypassed by the displacing fluid.

After switching to polymer flooding, the mobility ratio condition is improved, and the displacement becomes more stable. Though the polymer is unlikely to mobilize the residual oil in the well-swept area (larger pores) according to the capillary desaturation curve (Green & Willhite 2018; Lake et al. 2014), the previously bypassed oil left in the unswept area (smaller pores) could be displaced downstream by the viscous polymer solution. Thus, additional oil could be recovered as the consequence of sweep improvement.

The following equation was used to calculate the capillary number (N_{ca}) of all of flooding processes.

$$N_{ca} = \frac{\mu_w u}{\sigma} . \tag{1}$$

In Equation (1), μ_w is the viscosity of the displacing phase (HSW, LSW, HSP, or LSP), mPa s or cp; u is the superficial velocity, m/s; σ is the interfacial tension (IFT) between the displacing phase and the crude oil, mN/m. The IFT was measured using a Ramé-hart goniometer with the pendant-drop method. The IFT was in the range of 12-20 mN/m. The capillary number for the HSW flooding, LSW flooding, HSP flooding and LSP flooding was 2.46×10^{-7}, 2.39×10^{-7}, 12.5×10^{-6}, 16.0×10^{-6}, respectively.
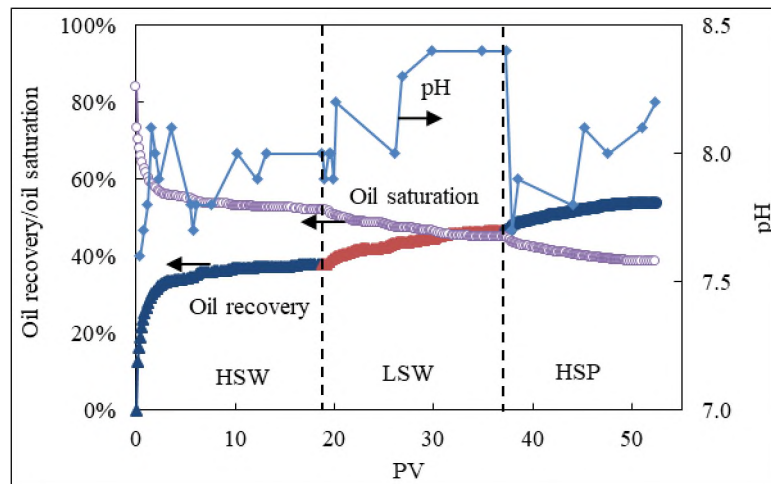
Figure 8. HSP flooding after waterflooding (Exp-3).

3.3. SECONDARY POLYMER FLOODING

In Exp-4, the HSP flooding was performed in a secondary mode, as shown in Figure 9. The results indicated a much better oil recovery performance compared with the case pre-flooded with water before implementing polymer flooding (Exp-3 and Exp-3R). After the secondary polymer flooding, the oil recovery factor was 71.2%, while in Exp-3 and Exp-3R, the oil recovery after polymer flood was 53.9% and 56.3%, respectively. The

experiment indicates that performing the polymer flood earlier can achieve a significantly better oil recovery performance.
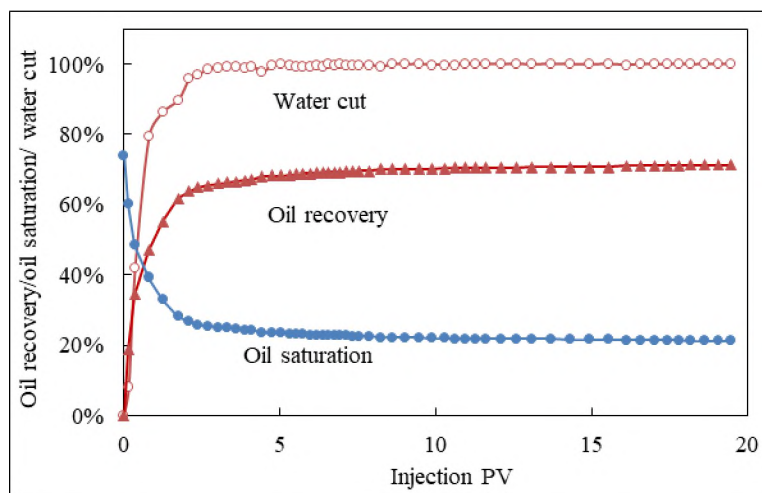
Figure 9. Secondary polymer flooding (Exp-4).

The results can be explained with Figure 7. The viscous fingers could be mitigated, and the breakthrough was delayed. The snap-off events of the oil pathways as transporting through the pore throats were weakened and delayed during a secondary polymer flooding compared with waterflooding. This interpretation can be supported by the theoretical modeling work of Huh and Pope (2008). In a secondary polymer flood, the oil is in continuous state and can be displaced downstream more uniformly. The oil pathways are more stable, and breakage into small oil drops/ganglia can be effectively delayed. The elasticity enables the oil pathways to be thinner before breakage. Most of the pore spaces could be well swept, and higher oil recovery could be achieved at the breakthrough. In Exp-4, the polymer solution broke through at 0.25 PV, which was significantly later than that in waterflooding. Also, the oil recovery at the breakthrough was about 27%, which

was nearly double of the HSW flooding in Exp-1. The water cut increased to 90% at 1.74 PV of injection and the oil recovery was 62%, indicating more stable displacement and better timing benefit of the earlier implementation of polymer flooding.

If the core has been flooded with water (e.g., in Exp-3), the oil left in the well-swept area would be present as isolated drops or ganglia, which can be trapped by capillary forces and hard to be mobilized. The mobilization of residual oil in such fashion requires a high capillary number that above a certain critical point, usually on the order of 10^{-5} (Green & Willhite 2018). However, the capillary number for a normal waterflooding is usually on the order of 10^{-7}. According to the capillary desaturation curve, the capillary number must be increased several orders of magnitudes after a normal waterflood to mobilize the residual oil and improve the displacement efficiency (Green & Willhite 2018; Lake et al. 2014). A polymer flood is insufficient to provide such a significant increase.

3.4. LSP FLOODING AFTER WATERFLOODING AND HSP FLOODING

In Exp-5, the performance of LSP flooding was investigated after extensive waterflooding and HSP flooding (Figure 10). Strikingly, even after extensive flooding with HSP, significant incremental oil was achieved when injecting LSP. Though the viscosity was almost the same with the HSP and the concentration was significantly lower, the oil recovery incremental was remarkable, 8.0% OOIP. The reproducibility was tested in Exp-5R, and 8.1% OOIP additional oil was achieved (Figure A4). The injection pressure during the LSP flooding was relatively higher than that during the HSP flooding (Figure A5). The oil recovery was increased to 64.4%. The pH was increased during the LSP flooding especially at the early stage, which synchronized well with the incremental oil recovery.

ICP (Inductively Coupled Plasma) analysis could directly give the information of ion change in the effluent. However, as the samples contained polymer and were highly viscous, the ICP test was not performed. Note that the core had already been exposure to low-salinity invading fluid during the LSW flooding process (Figure 10). The low salinity effect (e.g., ion exchange, polar component desorption and wettability alteration) had already taken effect in the pores that swept by the LSW (the well-swept area in Figure 7d). However, there was still an appreciable portion of oil left in the unswept area after the LSW flooding. Though the sweep efficiency was increased, and additional oil could be displaced out during the HSP flooding (7.4% OOIP), still the residual oil saturation could be reduced by the low salinity effect in the area previously untouched by the LSW (Figures 7b and 7d). Incremental oil recovery was achieved during the following LSP flooding (Figure 10). The results demonstrate the synergic effect of low salinity water and polymer flooding in enhancing the heavy oil recovery.

To evaluate the mechanical stability as the polymer solutions transport through the sandpacks, we monitored the viscosity of the aqueous effluent during the LSP flooding and HSP flooding. The aqueous phase was obtained by centrifuging the polymer/oil mixture effluent. Figure 11 shows the relative viscosity of the effluent versus the injected pore volumes of the HSP and LSP in Exp-5. The low value at the beginning is due to the displacement of water present in the porous media. We observed that the LSP could almost reach the injected value and the mechanical degradation was negligible. For the HSP, the effluent reached 90% of the injected value after several pore volumes of injection. It indicates the HSP went through some mechanical degradation, which was probably due to the coiled configuration of the polymer molecules.
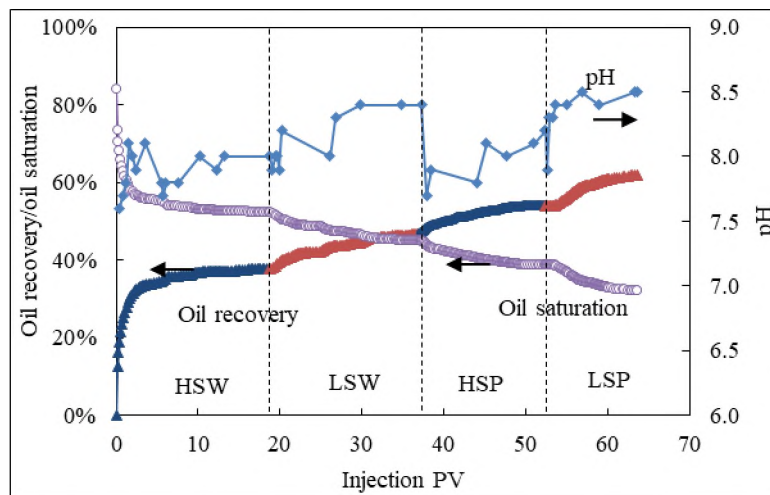
Figure 10. LSP flooding after waterflooding and HSP flooding (Exp-5).
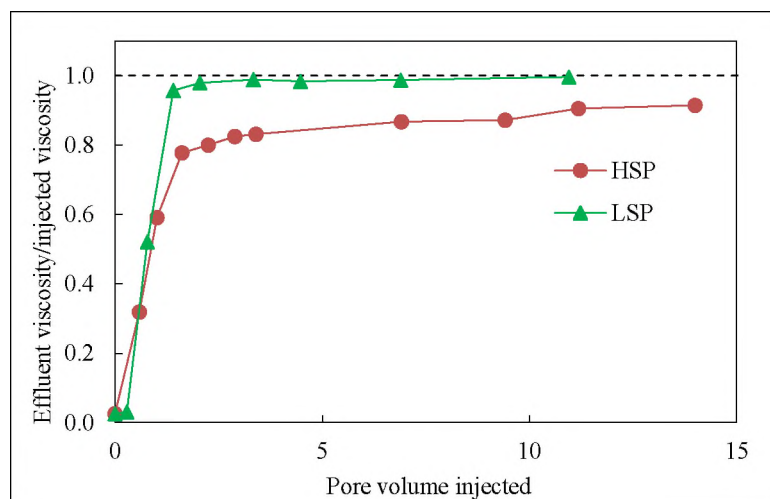
Figure 11. The relative viscosity of the effluent of HSP and LSP (Exp-5).

3.5. LSP FLOODING AFTER A SECONDARY HSP FLOODING

In Exp-6, LSP flooding was performed after the secondary PF in Exp-4. The results are shown in Figure 12. The extra oil recovery was 5.7%. The overall oil recovery was increased to 76.9% after the LSP flooding. The residual oil saturation was reduced from 0.21 to 0.17. Further discussions of the results are presented in the following subsection.

3.6. LSP FLOODING DIRECTLY AFTER WATERFLOODING

In Exp-7, the LSP flooding was performed after extensive waterflooding (including HSW flooding and LSW flooding). The results are shown in Figure 13. After the LSP flooding, 10.6% additional oil was recovered. The incremental recovery was higher than the LSP flooding after extensive waterflooding and HSP flooding (Exp-5 and Exp-5R), and was almost double that after secondary HSP flooding (Exp-6). The LSP flooding performed in this scheme was also better than the HSP flooding, as observed in Exp-3 and Exp-3R, in which the incremental recovery of HSP flooding after extensive waterflooding was 7.4% and 6.5% OOIP, respectively. Some researchers reported considerable incremental oil recovery and S_{or} reduction in a high-salinity polymer flood after a low-salinity polymer flood (Erincik et al. 2018; Qi et al. 2017). Their impressive observations may be related to the viscoelasticity effect of the polymer solution present at high shear rate condition. It may also be due to other specialized conditions associated with their experiments (e.g., core conditioning). In our experiments performed at relatively low flow velocities of ~1.2 ft/d, however, no appreciable incremental recovery was observed in the HSP flooding following the LSP flooding, indicating the injection scheme has an important impact on the oil recovery performance.

The S_{or} reduction induced by the LSE should be responsible for the improved oil recovery efficiency during the LSP flooding after secondary HSP flooding (Exp-6). The sweep efficiency in the secondary HSP flooding was higher than that in the HSW flooding and LSW flooding in Exp-7. Thus, most of the pore space in the core was well swept. Further improvement in sweep is expected to be minimal in the following LSP flooding due to the similar viscosity of the two polymer solutions. The incremental recovery was

not as significant as the case of LSP flooding after waterflooding (Exp-7). In the latter case, there was still a considerable portion in the core that was unswept after the waterflooding (mainly the smaller pores). The LSP had a better chance to achieve additional oil recovery through both sweep improvement and S_{or} reduction induced by the low salinity effect in the unswept area (Figure 7).
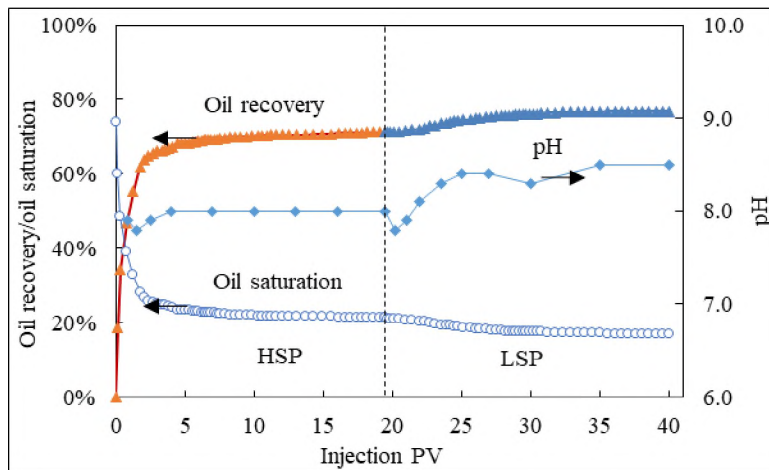
Figure 12. LSP flooding after a secondary HSP flood (Exp-6).
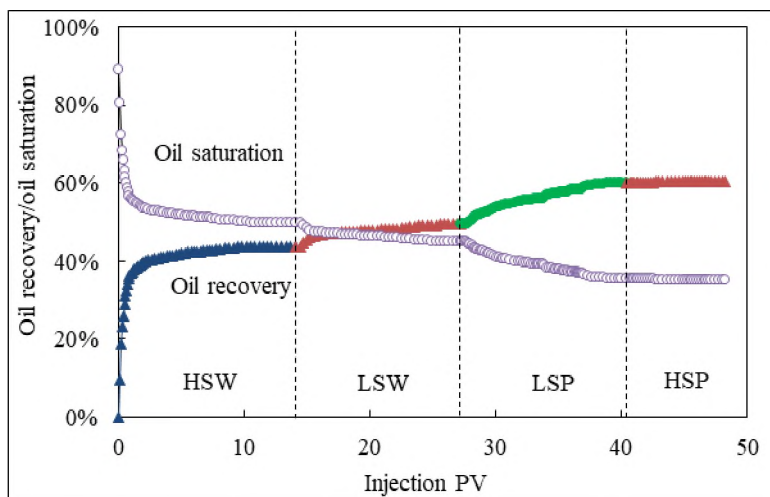
Figure 13. LSP flooding directly after waterflooding (Exp-7).

By contrast, the low-salinity-induced S_{or} reduction mechanism was absent in the HSP flooding (Exp-3 and Exp-3R), thus the oil recovery improvement was not as significant as the LSP flooding in Exp-7. Note that the sandpack had already been flooded with LSW. Further reduction of the S_{or} was unlikely in the well-swept area (mainly the larger pores). Also, the oil thread/pathway stabilization effect was favorable for the polymer to establish a lower residual oil saturation, as the oil saturation in the unswept area was higher than the S_{or} after extensive waterflooding. The mechanism was similar to a secondary polymer flood (Huh & Pope 2008).

Some researchers attribute the residual oil saturation reduction to the viscoelasticity of the polymer solution (Wang et al. 2000; Koh et al. 2018; Qi 2018; Azad & Trivedi 2020). But viscoelasticity is only significant at high shear-rate condition, as indicated by the shear thickening effect at high flux (Seright et al. 2011; Seright 2011). The linking between viscoelasticity property and the S_{or} reduction has not been well understood so far. Also, it is challenging to quantify the representative viscoelasticity property of the polymer solutions in porous media. Some review and experimental work has been reported recently (Azad & Trivedi 2019a, 2019b, 2020; Jouenne & Heurteux 2020).

We conducted rheology tests to evaluate the viscoelasticity of the LSP and HSP. Frequency sweep tests (0.1-100 rad/s) were performed to measure the storage modulus (G') and loss modulus (G") with a rheometer in the linear viscoelastic regime. The measured G' and G" of the LSP and HSP are shown in Figure 14 and Figure 15, respectively. The relaxation time of the polymer solutions were determined with the crossover point method as described in Delshad et al. (2008). The relaxation time for the LSP was 0.633 s, which was about eight times of the HSP (0.084 s). The result is consistent with the theoretical and

experimental results of polymer solutions prepared with 0.1% and 1% NaCl reported by Delshad et al. (2008) and Yuan (1981). However, more work is required to clarify the role of the viscoelasticity property in the improved oil recovery and reduced residual oil saturation during the LSP flooding performed at relatively low velocity conditions.
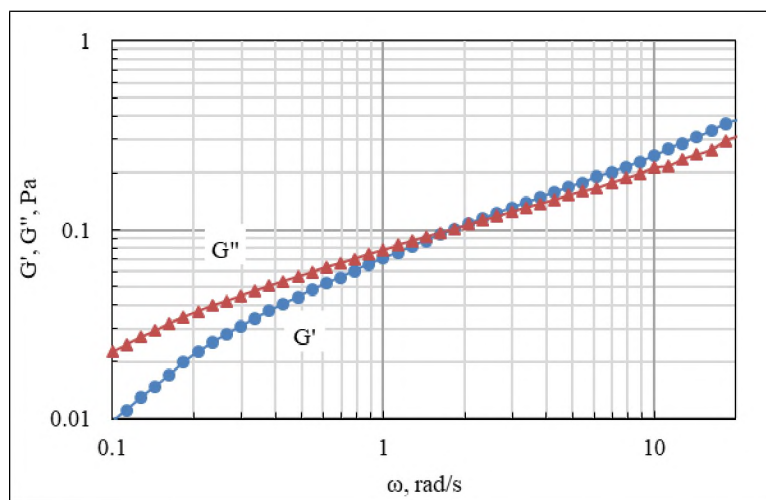
Figure 14. Rheology test results of the LSP.
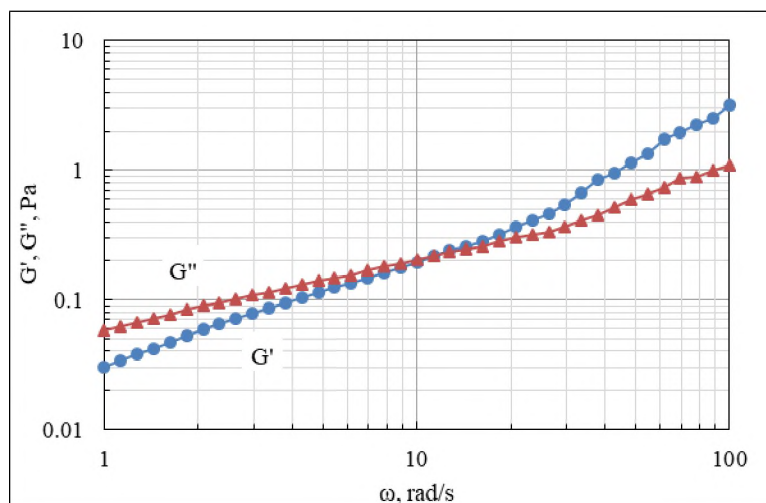
Figure 15. Rheology test results of the HSP.

Nevertheless, the results clearly demonstrate that combination of low salinity water and polymer flooding can significantly improve the oil recovery performance. The residual resistance factor (the ratio water injection pressure after and before the polymer flooding) of both LSP and HSP were below 1.5, indicating injectivity loss and formation damage were not a concern during the polymer flooding.

3.7. FIELD APPLICATION EVALUATION

The idea of combining LSW and polymer flooding has been put into practice on a pattern scale pilot test in the Milne Point field on the North Slope of Alaska. The flood pattern consists of two horizontal injection wells and two horizontal producers. Detailed field practice can be found in recent papers and publications to come (Dandekar et al. 2019, 2020; Ning et al. 2019).

The pilot test has been going on for nearly two years and the field performance up to now (May 2020) has preliminarily demonstrated the game-changing potential of low-salinity polymer flood in unlocking the enormous heavy oil resources on the Alaska's North Slope. The pilot test has shown impressive successful responses (Figures 16 and 17): the injectivity is sufficient to replace the production voidage; the water cut is reduced from 70% at the start of LSP flooding to less than 15%; no polymer breakthrough so far. Figures 16 and 17 also show that the oil rate has reversed the decline trend (as is expected during waterflood) and started to increase due to the injected polymer. Remarkable oil recovery improvement is expected from the polymer flooding compared with projected water flooding (Ning et al. 2020). Detailed field performance and benefit analysis will be presented in future publications.
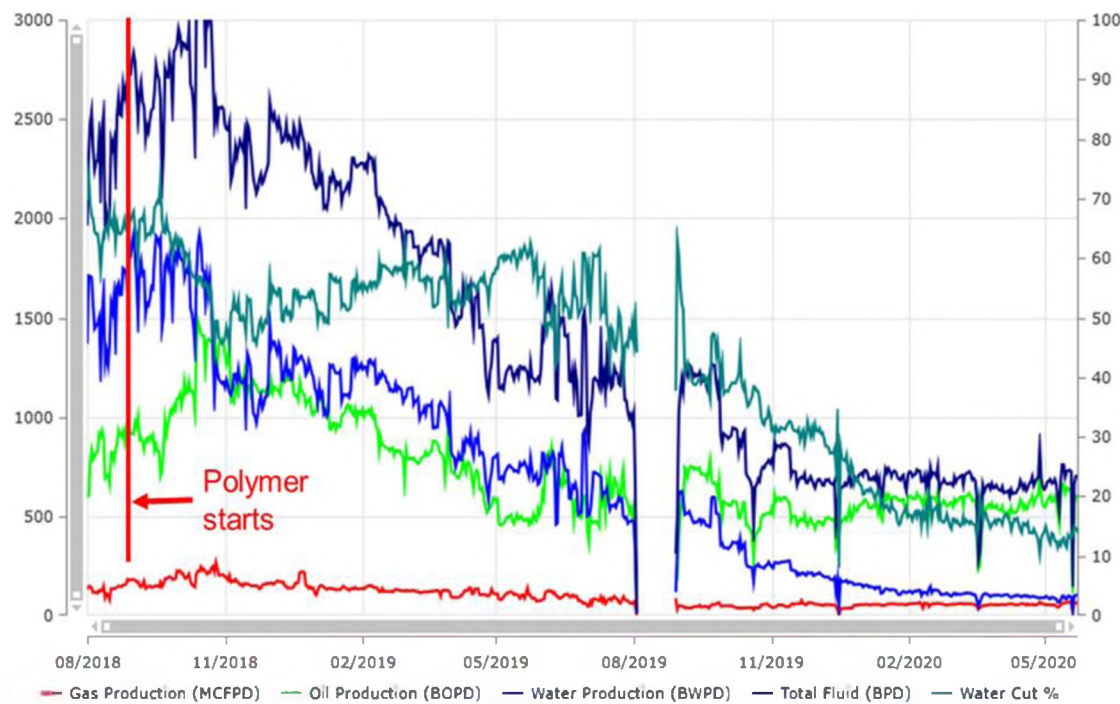
Figure 16. J-27 production performance.
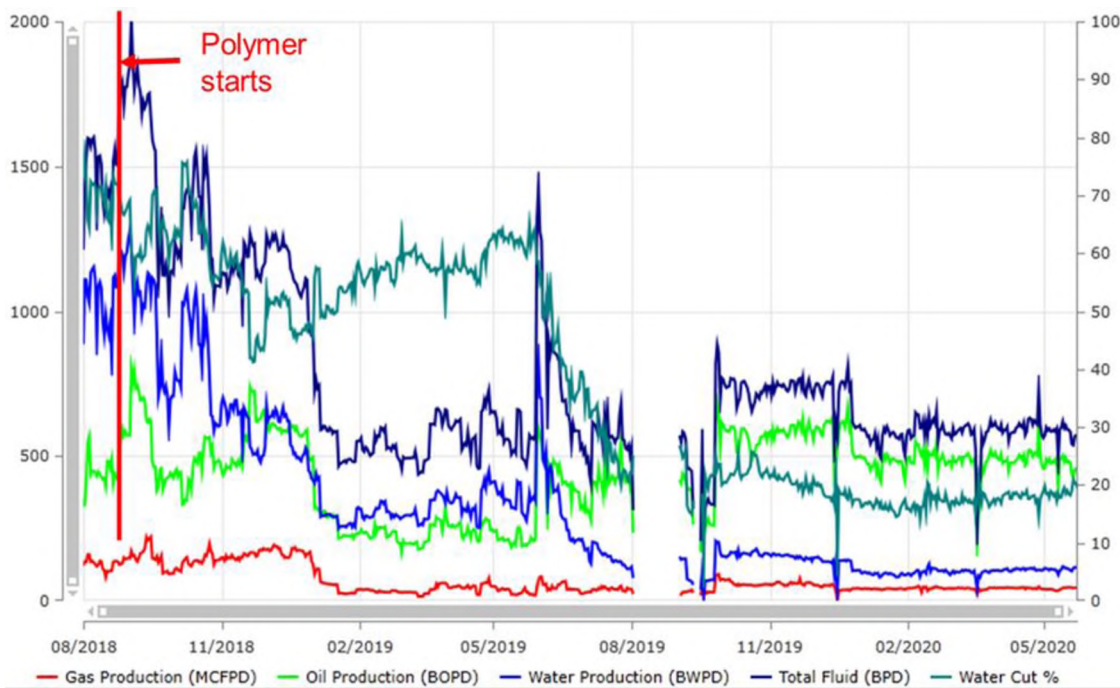
Figure 17. J-28 production performance.

3.8. DISCUSSION OF INFLUENCING FACTORS ON THE EFFECTIVENESS OF LSP FLOODING

Based on our knowledge, general working conditions required for the LSW should also be satisfied to make the LSP effective. These working conditions have been widely discussed in the literature, including: 1) The presence of polar components in the crude oil; 2) The presence of clay in the rock, especially kaolinite; 3) The presence of connate water (with relatively high salinity); 4) The presence of remarkable amount of divalent ions (Ca^{2+}, Mg^{2+}) in connate water; 5) The low-salinity injection water; 6) Relatively low pH (6-7) of the connate brine to allow adsorption of polar components onto the clay surface (Sheng, 2014). It indicates the effectiveness of the LSP is governed by multiple factors.

To demonstrate the influence of the oil properties, we performed experiments with heavy mineral oil instead of the crude oil (see Figure 18). The viscosity of the mineral oil (173 cp) was comparable with the crude oil (202 cp). Note that LSW flooding was not performed before the LSP flooding. In this circumstance, the low salinity effect during the LSP flooding was expected to be more prominent. However, the results show that no appreciable incremental oil was achieved by the LSP flooding (only 0.73% OOIP) after extensive HSP flooding. The mineral oil was composed of paraffin oil and contained no polar components. The coreflooding results indicate that the composition of the oil is an important influencing factor on the effectiveness of LSP flooding.

As for the viscosity of the oil, whether the effectiveness of LSP is selective to heavy oil or light oil? Several researchers have reported the effectiveness of LSP after limited/extensive waterflooding using crude oil with a lower viscosity (2.4-33 cp), as discussed in the Introduction. To name a few, Kozaki (2012) observed improved oil recovery performance during LSP flooding after extensive water flooding. In his

experiment, 8% more oil was achieved during LSP flooding after extensive waterflooding using aged Berea sandstone cores. Shiran and Skauge (2013) reported 5% oil recovery increase in LSP flooding after tertiary LSW flooding, and 12-17% after secondary LSW flooding in intermediate-wet Berea sandstone cores. The effectiveness of LSP after extensive HSP with the same viscosity was also reported in the literature (μ_o=25-32cp; μ_p≈4cp) (Moghadasi et al. 2019). Their experiments showed that LSP could achieve 8% additional oil after extensive HSP with the same viscosity. Our observations with heavy oil showed agreement with the reported results. Our work demonstrates that the efficiency of LSP is not unique to light oil, but it also can be achieved with heavy oil.
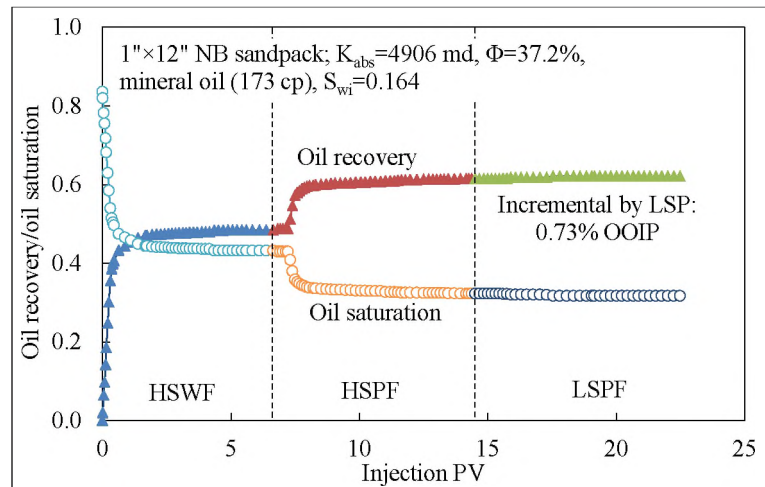
Figure 18. Coreflooding results using heavy mineral oil.

It is interesting to know whether the salinity of the LSW/LSP used in the laboratory work of this study and the pilot test is optimal. Technical and economic considerations should be taken into account in determining the optimal salinity. The salinity of the readily available low-salinity water source in the target field is about 2,500 ppm. This is the lowest

possible salinity that available without any further expensive desalination process. Further reducing the salinity requires additional facilities, and it is technically difficult in the arctic area. It is possible to obtain medium salinities between the formation salinity and source brine salinity, by mixing produced water with injection source brine. But the problem is a higher polymer concentration is required to achieve the target viscosity as the salinity is increased. Also, the LSP exhibits a better mechanical stability as shown in Figure 11. The operation at this lowest possible salinity shows no injectivity problem in the experiments or the field practice. Therefore, from technical and economic point of view, the salinity used in this paper is the optimal salinity for the given heavy oil/brine/rock system.

In this work, we only tested the 3630S polymer as used in the field pilot test. The choice of this polymer was initially based on numerical simulation, the availability and cost of the polymer products (Dandekar et al. 2019). Our project team have investigated the retention behavior of Flopaam 3430S which has a lower molecular weight of 10-12 million Daltons (Wang et al. 2020).

4. CONCLUSIONS

This study investigated oil recovery performance of combining low-salinity water and polymer flood. The following conclusions were drawn.

(1) The HSP required nearly two thirds more polymer than the LSP to achieve the same target viscosity in this study.

(2) Additional oil was recovered from LSW flooding after extensive HSW flooding (3-9% OOIP). LSW flooding performed in secondary mode could achieve a higher

recovery than that in tertiary mode. Also, the occurrence of water breakthrough was delayed in the LSW flooding compared with the HSW flooding.

(3) After extensive LSW flooding and HSP flooding, incremental oil recovery (~8% OOIP) was still achieved by LSP flooding with the same viscosity as the HSP. No appreciable incremental oil was recovered by HSP flooding performed after LSP flooding. LSP flooding performed directly after waterflooding can achieve more incremental oil recovery (~10% OOIP).

(4) The improved oil recovery performance of combining low-salinity water and polymer flooding was demonstrated under various conditions in this study. Field application practice has demonstrated remarkable success regarding water cut reduction, oil production improvement, delayed breakthrough behavior, and projected oil recovery improvement. Future work is required to further investigate the rheology behavior under reservoir conditions, polymer retention, in-situ emulsification, and the impact of wettability at varying salinity conditions.

NOMENCLATURE

Symbol	Description
ANS	Alaska's North Slope
EOR	Enhanced oil recovery
FW	Formation water, salinity=27400 ppm
HSP	High-salinity polymer, salinity=FW
HSW	High-salinity water, salinity=FW

IFT	Interfacial tension
LSE	Low salinity effect
LSP	Low salinity polymer
LSW	Low-salinity water
N_{ca}	Capillary number
OOIP	Oil originally in place
PV	Pore volume
S_{or}	Residual oil saturation
S_{wi}	Initial water saturation
u	Superficial velocity, m/s
μ_w	Viscosity of displacing phase, mPa s or cp
σ	Interfacial tension between displacing phase and crude oil, mN/m

ACKNOWLEDGMENTS

product, process, or service by trade name, trademark, manufacturer, or otherwise does not necessarily constitute or imply its endorsement, recommendation, or favoring by the United States Government or any agency thereof. The views and opinions of authors expressed herein do not necessarily state or reflect those of the United States Government or any agency thereof."

APPENDIX

The results of Exp-1R1, Exp-1R2, Exp-3R, Exp-5R and the injection pressures are shown in Figures A1 to A5.
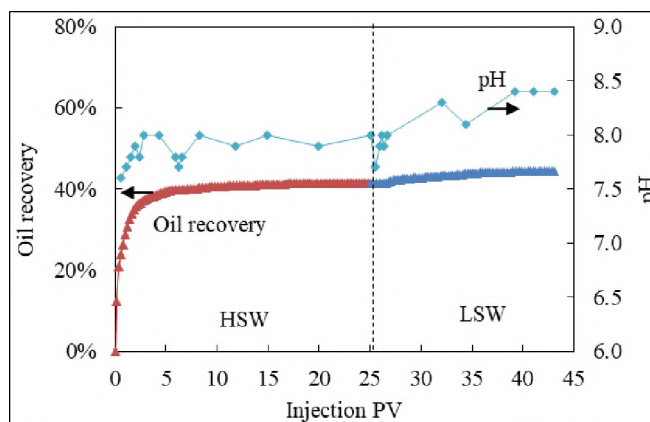
Figure A1. Tertiary LSW flooding (Exp-1R1).
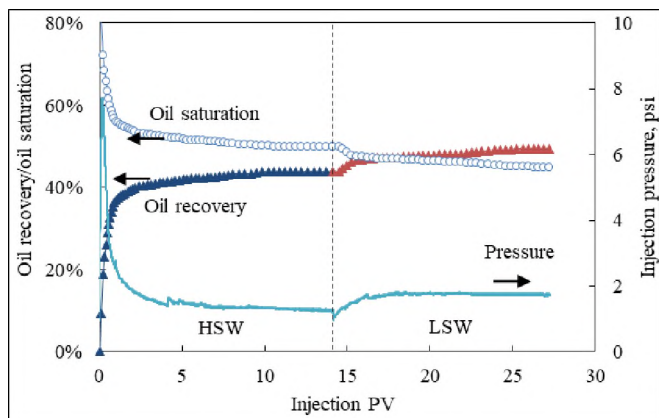
Figure A2. Tertiary LSW flooding (Exp-1R2).
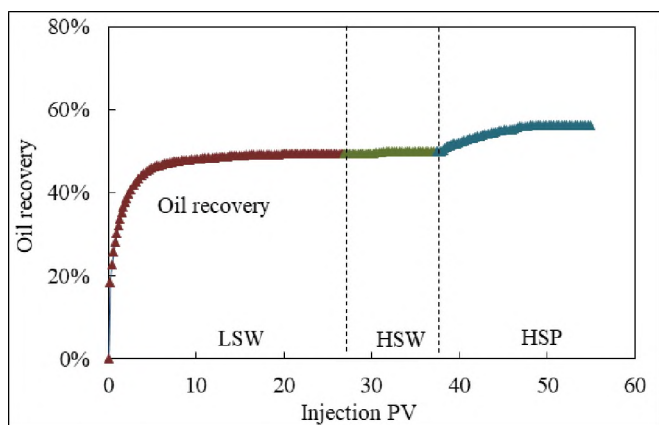
Figure A3. HSP flooding after waterflooding (Exp-3R).
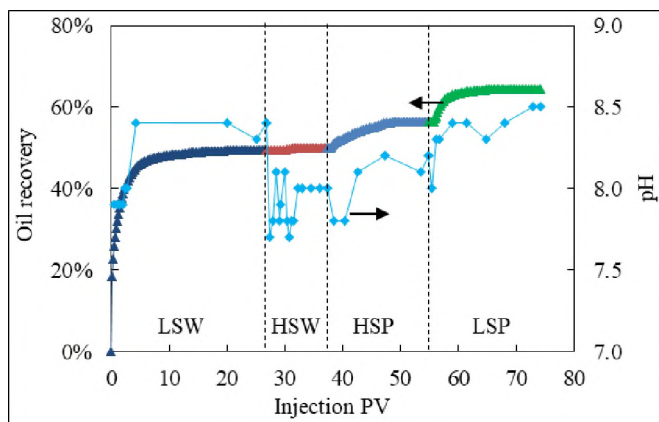
Figure A4. LSP flooding after waterflooding and HSP flooding (Exp-5R).
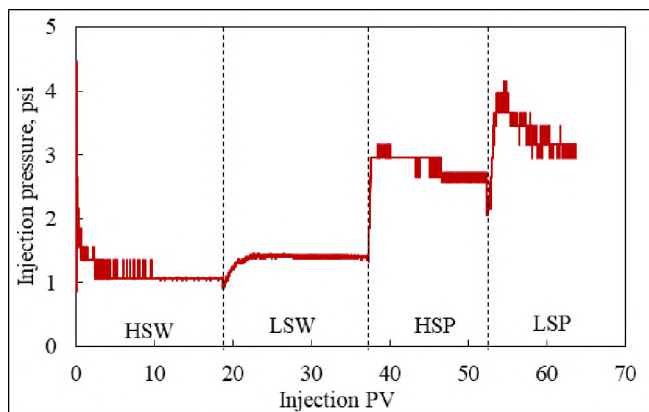
Figure A5. Injection pressures in Exp-1, Exp-3 and Exp-5.

REFERENCES

Almansour, A. O., AlQuraishi, A. A., AlHussinan, S. N., AlYami, H. Q. 2017. Efficiency of Enhanced Oil Recovery Using Polymer-Augmented Low Salinity Flooding. J Petrol Explor Prod Technol 7 (4): 1149–1158. https://doi.org/10.1007/s13202-017-0331-5.

Awolayo, A. N., Sarma, H. K., and Nghiem, L. X., 2018. Brine-Dependent Recovery Processes in Carbonate and Sandstone Petroleum Reservoirs: Review of Laboratory-Field Studies, Interfacial Mechanisms and Modeling Attempts. Energies 11 (11): 3020. https://doi.org/10.3390/en11113020.

Azad, M. S. and Trivedi, J. J. 2019a. Novel Viscoelastic Model for Predicting the Synthetic Polymer's Viscoelastic Behavior in Porous Media Using Direct Extensional Rheological Measurements. Fuel 235 (1 January): 218–226. https://doi.org/10.1016/j.fuel.2018.06.030.

Azad, M. S. and Trivedi, J. J. 2019b. Quantification of the Viscoelastic Effects during Polymer Flooding: A Critical Review. SPE J. 24 (06): 2731–2757. SPE-195687-PA. https://doi.org/10.2118/195687-PA.

Azad, M. S. and Trivedi, J. J. 2020. Does Polymer's Viscoelasticity Influence Heavy-Oil Sweep Efficiency and Injectivity at 1 ft/D? SPE Res Eval & Eng 23 (02): 446–462. SPE-193771-PA. https://doi.org/10.2118/193771-PA.

Buckley, S. E. and Leverett, M. C. 1942. Mechanism of Fluid Displacement in Sands. In Transactions of the Society of Petroleum Engineers, Vol. 146, Part I, SPE-942107-G, 107–116. Richardson, Texas, USA: Society of Petroleum Engineers.

Chavan M., Dandekar A., Patil S., Khataniar S. 2019. Low-Salinity-Based Enhanced Oil Recovery Literature Review and Associated Screening Criteria. Pet. Sci. 16 (6): 1344–1360. https://doi.org/10.1007/s12182-019-0325-7.

Cheng, Y., Czyzewski, W., Zhang, Y., Dandekar, A., Ning, S., Barnes, J. 2018. Experimental Investigation of Low Salinity Waterflooding To Improve Heavy Oil Recovery from the Schrader Bluff Reservoir on Alaska North Slope. Paper presented at the OTC Arctic Technology Conference, Houston, Texas, USA, 5–7 November. OTC-29117-MS. https://doi.org/10.4043/29117-MS.

Dandekar, A., Bai, B., Barnes, J., Cercone, D., Ciferno, J., Ning, S., Seright, R., Sheets, B., Wang, D., Zhang, Y. 2019. First Ever Polymer Flood Field Pilot—A Game Changer to Enhance the Recovery of Heavy Oils on Alaska's North Slope. Paper presented at the SPE Western Regional Meeting, San Jose, California, USA, 23–26 April. SPE-195257-MS. https://doi.org/ 10.2118/195257-MS.

Dandekar, A., Bai, B., Barnes, J., Cercone, D., Ciferno, J., Ning, S., Seright, R., Sheets, B., Wang, D., Zhang, Y. 2020. First Ever Polymer Flood Field Pilot to Enhance the Recovery of Heavy Oils on Alaska's North Slope—Pushing Ahead One Year Later. Paper presented at the SPE Western Regional Meeting, April 27-30, 2020, Bakersfield, California, USA. Note–postponed to virtual format in April 2021. SPE-200814-MS. https://doi.org/10.2118/200814-MS.

Delshad, M., Kim, D. H., Magbagbeola, O. A., Huh, C., Pope, G. A., Tarahhom, F. 2008. Mechanistic Interpretation and Utilization of Viscoelastic Behavior of Polymer Solutions for Improved Polymer-Flood Efficiency. Paper presented at SPE Symposium on Improved Oil Recovery, Tulsa, Oklahoma, USA, 20–23 April. SPE-113620-MS. https://doi.org/10.2118/113620-MS.

Erincik, M. Z., Qi, P., Balhoff, M. T., Pope, G. A. 2018. New Method to Reduce Residual Oil Saturation by Polymer Flooding. SPE J. 23 (5): 1944–1956. SPE-187230-PA. https://doi.org/10.2118/187230-PA.

Green, D. W. and Willhite, G. P. 2018. Enhanced Oil Recovery, second edition. Richardson, Texas, USA: Society of Petroleum Engineers.

Huh, C. and Pope, G. A. 2008. Residual Oil Saturation from Polymer Floods: Laboratory Measurements and Theoretical Interpretation. Paper presented at the SPE Symposium on Improved Oil Recovery, Tulsa, Oklahoma, USA, 20–23 April. SPE-113417-MS. https://doi.org/10.2118/ 113417-MS.

Jiang, J., Rui, Z., Hazlett, R., Lu, J. 2019. An Integrated Technical-Economic Model for Evaluating CO2 Enhanced Oil Recovery Development. Appl Energy 247 (1 August): 190–211. https://doi.org/10.1016/j.apenergy.2019.04.025.

Jouenne, S. and Heurteux, G. 2020. Correlation of Mobility Reduction of HPAM Solutions at High Velocity in Porous Medium with Ex-Situ Measurements of Elasticity. SPE J. 25 (1): 465–480. SPE-198899-PA. https://doi.org/10.2118/198899-PA.

Kakati, A., Kumar, G., and Sangwai, J. S. 2020. Low Salinity Polymer Flooding: Effect on Polymer Rheology, Injectivity, Retention, and Oil Recovery Efficiency. Energy Fuels 34 (5): 5715–5732. https://doi.org/10.1021/acs.energyfuels.0c00393.

Kargozarfard, Z., Riazi, M., and Ayatollahi, S. 2019. Viscous Fingering and Its Effect on Areal Sweep Efficiency during Waterflooding: An Experimental Study. Pet. Sci. 16 (1): 105–116. https://doi.org/10.1007/s12182-018-0258-6.

Koh, H., Lee, V. B., and Pope, G. A. 2018. Experimental Investigation of the Effect of Polymers on Residual Oil Saturation. SPE J. 23 (1): 1–17. SPE-179683-PA. https://doi.org/10.2118/179683-PA.

Kozaki, C. 2012. Efficiency of Low Salinity Polymer Flooding in Sandstone Cores. Master's thesis, University of Texas at Austin, Austin, Texas, USA (May 2012).

Lake, L. W., Johns, R. T., Rossen, W. R., Pope, G. 2014. Fundamentals of Enhanced Oil Recovery. Richardson, Texas, USA: Society of Petroleum Engineers.

Maini, B. 1998. Is It Futile To Measure Relative Permeability for Heavy Oil Reservoirs? J Can Pet Technol 37 (4): 56–62. PETSOC-98-04-06. https://doi.org/10.2118/98-04-06.

Moghadasi, L., Pisicchio, P., Bartosek, M., et al. 2019. Laboratory Investigation on Synergy Effect of Low Salinity-Polymer Water Injection on Sandstone Porous Media. Paper presented at the Offshore Mediterranean Conference and Exhibition, Ravenna, Italy, 27–29 March. OMC-2019-0868.

Morrow, N. R. and Buckley, J. 2011. Improved Oil Recovery by Low-Salinity Waterflooding. J Pet Technol 63 (5): 106–112. SPE-129421-JPT. https://doi.org/10.2118/129421-JPT.

Muller, G., Laine, J. P., and Fenyo, J. C. 1979. High-Molecular-Weight Hydrolyzed Polyacrylamides. I. Characterization. Effect of Salts on the Conformational Properties. J Polym Sci A Polym Chem 17 (3): 659–672. https://doi.org/10.1002/pol.1979.170170305.

Ning, S., Barnes, J., Edwards, R., Dunford, K., Eastham, K., Dandekar, A., Zhang, Y., Cercone, D., Ciferno, J. 2019. First Ever Polymer Flood Field Pilot to Enhance the Recovery of Heavy Oils on Alaska's North Slope–Polymer Injection Performance. Paper presented at the SPE/AAPG/SEG Unconventional Resources Technology Conference, Denver, Colorado, USA, 22–24 July. URTEC-2019-643-MS.

Ning, S., Barnes, J., Edwards, R., Schulpen, W., Dandekar, A., Zhang, Y., Cercone, D., and Ciferno, J. 2020. First Ever Polymer Flood Field Pilot to Enhance the Recovery of Heavy Oils on Alaska North Slope–Producer Responses and Operational Lessons Learned. Paper presented at the SPE Annual Technical Conference and Exhibition, Virtual, October 2020. doi: https://doi.org/10.2118/201279-MS.

Pope, G. A. 1980. Application of Fractional Flow Theory To Enhanced Oil Recovery. SPE J. 20 (3): 191–205. SPE-7660-PA. https://doi.org/ 10.2118/7660-PA.

Qi, P., 2018. The Effect of Polymer Viscoelasticity on Residual Oil Saturation. PhD dissertation, University of Texas at Austin, Austin, Texas, USA (May 2018).

Qi, P., Ehrenfried, D. H., Koh, H., Balhoff, M. T. 2017. Reduction of Residual Oil Saturation in Sandstone Cores by Use of Viscoelastic Polymers. SPE J. 22 (2): 447–458. SPE-179689-PA. https://doi.org/10.2118/179689-PA.

Rapoport, L. A. and Leas, W. J. 1953. Properties of Linear Waterfloods. J Pet Technol 5 (5): 139–148. SPE-213-G. https://doi.org/10.2118/213-G.

RezaeiDoust, A., Puntervold, T., and Austad, T. 2011. Chemical Verification of the EOR Mechanism by Using Low Saline/Smart Water in Sandstone. Energy Fuels 25 (5): 2151–2162. https://doi.org/10.1021/ef200215y.

Saboorian-Jooybari, H., Dejam, M., and Chen, Z. 2016. Heavy Oil Polymer Flooding from Laboratory Core Floods To Pilot Tests and Field Applications: Half-Century Studies. J Pet Sci Eng 142 (June): 85–100. https://doi.org/10.1016/j.petrol.2016.01.023.

Seright, R. S., Fan, T., Wavrik, K., De Carvaiho Balaban, R. 2011. New Insights into Polymer Rheology in Porous Media. SPE J. 16 (1): 35–42. SPE-129200-PA. https://doi.org/10.2118/129200-PA.

Seright, R. S. 2011. Use of Polymers To Recover Viscous Oil from Unconventional Reservoirs. Final scientific/technical report, DOE Award No. DE-NT0006555, US Department of Energy (October 2011).

Sheng, J. J. 2014. Critical Review of Low-Salinity Waterflooding. J Pet Sci Eng 120 (August): 216–224. https://doi.org/10.1016/j.petrol.2014.05.026.

Shiran, B. S. and Skauge, A. 2013. Enhanced Oil Recovery (EOR) by Combined Low Salinity Water/Polymer Flooding. Energy Fuels 27 (3): 1223–1235. https://doi.org/10.1021/ef301538e.

Sun, X. F., Song, Z. Y., Cai, L. F., Zhang, Y. Y., Li, P. 2020. Phase Behavior of Heavy Oil–Solvent Mixture Systems under Reservoir Conditions. Pet. Sci. 17: 1683-1698.. https://doi.org/10.1007/s12182-020-00461-x.

Tang, G.-Q. and Morrow, N. R. 1997. Salinity, Temperature, Oil Composition, and Oil Recovery by Waterflooding. SPE Res Eng 12 (4): 269–276. SPE-36680-PA. https://doi.org/10.2118/36680-PA.

Tang, G.-Q. and Morrow, N. R. 1999. Influence of Brine Composition and Fines Migration on Crude Oil/Brine/Rock Interactions and Oil Recovery. J Pet Sci Eng 24 (2–4): 99–111. https://doi.org/10.1016/S0920-4105(99)00034-0.

Torrijos, I. D. P., Puntervold, T., Strand, S., Austad, T., Bleivik, T. H., Abdullah, H. I. 2018. An Experimental Study of the Low Salinity Smart Water-Polymer Hybrid EOR Effect in Sandstone Material. J Pet Sci Eng 164 (May): 219–229. https://doi.org/10.1016/j.petrol.2018.01.031.

Vermolen, E. C. M., Pingo-Almada, M., Wassing, B. M., Ligthelm, D. J., Masalmeh, S. K. 2014. Low-Salinity Polymer Flooding: Improving Polymer Flooding Technical Feasibility and Economics by Using Low-Salinity Make-Up Brine. Paper presented at the International Petroleum Technology Conference, Doha, Qatar, 19–22 January. IPTC-17342-MS. https://doi.org/10.2523/IPTC-17342-MS.

Wang, D., Cheng, J., Yang, Q., Gong, W., Qun, L., Chen, F. 2000. Viscous-Elastic Polymer Can Increase Microscale Displacement Efficiency in Cores. Paper presented at the SPE Annual Technical Conference and Exhibition, Dallas, Texas, USA, 1–4 October. SPE-63227-MS. https://doi.org/10.2118/63227-MS.

Wang, D., Li, C., and Seright, R. S. 2020. Laboratory Evaluation of Polymer Retention in a Heavy Oil Sand for a Polymer Flooding Application on Alaska's North Slope. SPE J. 25 (4): 1842–1856. SPE-200428-PA. https://doi.org/10.2118/200428-PA.

Wassmuth, F. R., Green, K., Hodgins, L., Turta, A. T. 2007. Polymer Flood Technology for Heavy Oil Recovery. Paper presented at the Canadian International Petroleum Conference, Calgary, Alberta, Canada, 12–14 June. PETSOC-2007-182. https://doi.org/10.2118/2007-182.

Yuan, M. A Rheological Study of Polymer and Microemulsion in Porous Media. Master's thesis, University of Texas at Austin, Austin, Texas, USA (May 1981).

II. EXPERIMENTAL STUDY OF TRANSPORT BEHAVIOR OF MICROGEL PARTICLES IN SUPERPERMEABLE CHANNELS FOR CONFORMANCE CONTROL

ABSTRACT

Gel treatment is an effective way to attack excessive water production during oil development. The transport behavior of gel materials in reservoirs is of crucial importance to the effectiveness of gel treatments. This paper aimed at investigating the transport behavior of micrometer-sized preformed particle gels (microgels) through superpermeable (super-K) channels. Sandpacks with permeabilities ranging from 27 to 221 darcies were used to mimic the super-K channels. Multiple pressure sensors were applied along the sandpack models to monitor the propagation behavior of the microgels. The tested microgel particles could transport through the super-K channels, and a higher driving pressure gradient was required when the particle-to-pore matching size ratio (MSR) was larger. The pressure gradient distribution along the super-K channels was relatively uniform when the MSR was low (<1.3). However, the inlet section would show increasingly higher-pressure gradients as the MSR was increased, indicating increased difficulty in propagation. The propagation of the gel particles was significantly slower compared with the carrying fluid. The delayed propagation behavior was more pronounced when the MSR was higher. The injection pressure was much less sensitive to the injection flow rate compared with a Newtonian fluid. The gel dispersion exhibited an apparent shear thinning (pseudoplastic) behavior when transporting through the porous channels. Breakage of the gel particles was observed especially at high superficial velocities. The particle breakage was partially

responsible for the apparent shear thinning behavior. The breakage phenomenon was in favor of deep placement of the gel particles. The channel permeabilities were significantly reduced by the microgels, bringing sufficient resistance to subsequent water flooding (>99.5%). At given matching size conditions, softer gels were more likely to establish in-depth placement and uniform water-blocking capacity in the channels. The microgel particles exhibited salinity-responsive behavior to the post brine flush. The gel particles could shrink and reswell according to the salinity of the injected water. Possibilities were discussed to utilize this salinity-responsive behavior. Also, the microgels exhibit a particular disproportionate permeability reduction (DPR) effect. After gel injection, the channel permeability to water flow was reduced by more than 20-92 times of the permeability to oil flow. This work provides important support to understand the transport behavior of gel particles in super-K channels. The achievements are helpful for gel product selection and gel treatment design.

Key words: enhanced oil recovery; conformance treatment; gel treatment; preformed particle gel (PPG); microgel transport behavior

1. INTRODUCTION

A better oil recovery performance is always the pursuit of the oil & gas industry. However, many challenges are involved. One common problem plaguing many oil and gas fields around the world is the presence of high-permeability channels in the reservoirs. Generally, the channels can be divided into two categories: open fractures and porous-medium-type channels (Figure 1). The channels are beneficial and desirable in some

situations (e.g., hydraulic fractures in developing shales gases) because they largely increase the contact areas with the matrices and thus improve the injectivity/productivity. However, in many oil and gas reservoirs, the super-permeable (super-K) channels can cause fast breakthrough of the flooding fluids (water, polymer solutions, CO_2, etc.) from the injection wells to the production wells (Seright et al. 2003; Sydansk & Romero-Zeron 2011; Bai et al. 2013). A large portion of oil in the matrices is left unswept, resulting in poor sweep efficiency and unsatisfactory oil recovery performance (see Figure 1). Besides, the excessive production of the flooding fluids also brings economic and environmental concerns (Chang et al. 2020; Dhaliwal et al. 2021). Over the years, many efforts have been made to solve the unwanted channeling problem. Gel treatment has been proven an effective technique to solve the channeling issue (Bai et al. 2008, 2015; Seright et al. 2003; Kang et al. 2021; Aldhaheri et al. 2020, 2021). Different types of gel systems have been developed and applied: in-situ gels (Sydansk & Romero-Zeron, 2011), preformed bulk gels (Seright 1997), and preformed particle gels (PPGs) (Bai et al. 2007a, 2008, 2012; Pyziak & Smith 2007; Vasquez et al. 2008; Larkin & Creel 2008; Peirce et al. 2014; Targac et al. 2020).

This study focuses on the porous-medium-type channeling issue. In this scenario, the preformed bulk gels or normal millimeter-sized preformed particle gel (PPG) are unlikely to work due to low injectivity in such conditions (Seright 1999; Elsharafi & Bai 2013, 2016; Imqam et al. 2016). For example, Seright (1999) observed that an impractically high injection pressure gradient (>200 psi/ft) was required to force the preformed bulk gel [Cr(III)-acetate-HPAM] into a 28-darcy sandpack, which mimicked a proppant-filled fracture. When using in-situ gels, the water- or polymer-solution-like gelant can cause

damage to the oil zones (Seright & Brattekas 2021; Zhao et al. 2021a). Therefore, an

effective strategy is required to solve this type of channeling issue.
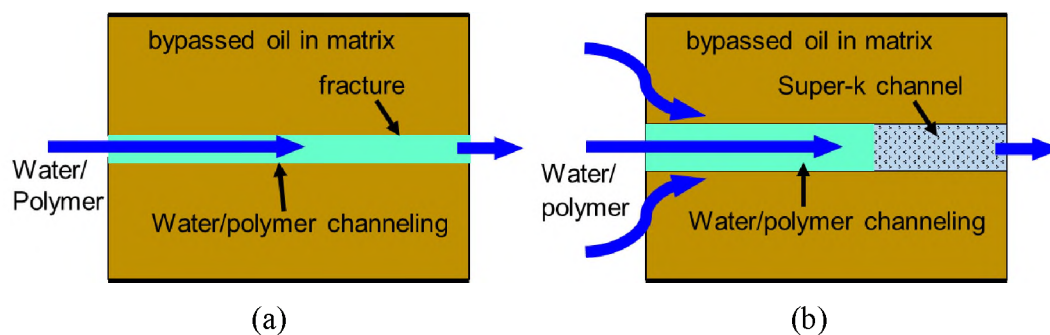
Figure 1. Open fracture type channels and porous-medium type channels in a reservoir. (a) Open fracture type channel. (b) Porous-medium type channel. This channel is composed of pore-throat structures. Preformed bulk gel and the normal millimeter-sized preformed particle gel are difficult to be injected into the channel and shut off it. Micrometer-sized gel particles (microgel) are likely to work and solve this kind of channeling problem.

In this work, we tested the feasibility of micrometer-sized PPGs in super-K channels. Due to the special properties of the microgel particles, such as elasticity (deformation), swelling, shrinking, reswelling (i.e., hydration, dehydration, rehydration), and breakage into smaller particles due to mechanical shear, the gel particles would exhibit complex behaviors when transporting through the repeated convergent-divergent flow channels in porous media. Many factors coexist and interact with each other. The factors include particle-to-pore matching size ratio, gel strength (e.g., the elastic modulus), particle size distribution, particle concentration, phase distribution in the porous medium (e.g., presence of residual oil), and surface charge conditions (for very small particles). The complex flow path geometries make the transport/retention behavior much more complicated.

A brief literature survey is summarized here to illustrate the progresses achieved over the years. Note that the survey is not exhaustive, as a thorough review is not the objective of our current work. The gel particles could directly pass through the pore throat larger than themselves due to the deformability nature of the gel particles (Bai et al. 2007b). At higher driving pressures/forces, the gel particles could shrink or even break into small pieces, and thus pass pore throats that were much smaller than themselves. For example, Bai et al. (2007b) observed that the gel particles in their study could pass through a microchannel that was only about 1/4 of the gel particle size. It was also reported that the particles could be retained in the porous media by different mechanisms. The particles could be adsorbed on the pore surfaces due to the surface charges, which was more prominent as the particles were significantly smaller than the pores (Chauveteau et al. 2003; Yao et al. 2017). For a swarm of particles, the inter-particle interactions made the system more complex. For example, the particles could block a pore throat by a bridging effect or by forming a particulate filtration layer (Yao et al. 2020).

Yao et al. (2012) observed that the particle/pore size ratio had a significant impact on the transport behavior and thus on the water-blocking efficiency of their elastic microspheres (4.3-40 μm). Relatively better water-blocking efficiency was observed at the size ratio of 1.35-1.55, which was recommended as the optimal values for conformance treatment designs. When this matching ratio was too small, effective plugging could not be established due to smooth transport and insufficient retention of the microspheres in the porous media. When the matching ratio was too high, the microspheres could hardly penetrate an appreciable depth into the porous media. Thus, the water-plugging efficiency was unsatisfactory. Three plugging mechanisms of microspheres at pore throats were

proposed: Capture-Plugging; Superposition-Plugging, and Bridge-Plugging (Yao et al. 2014). They further studied the effects of flow rate, pore-throat size, particle size, and injection concentration on transport and retention patterns (Yao et al. 2020). Five transport and retention patterns were observed in convergent−divergent microchannels: surface deposition, smooth passing, direct interception, deforming remigration, and rigid blockage. Al-Ibadi and Civan (2013) reported that the blockage mechanisms of gel particles were pore-throat plugging and pore-surface deposition. Zhao et al. (2014) proposed that the dispersed particle gel (DPG) they developed could reduce the permeability of channeling zones by adsorption, retention, trapping and bridging. They also observed the disproportionate permeability reduction phenomenon in the water and oil phases after the gel treatment. Farasat et al. (2017) performed a series of coreflooding experiments using limestone grain packs to investigate the retention (mechanical entrapment) behavior of preformed particle gels in porous media. Imqam et al. (2018) studied the effect of different factors on the transport behavior of microgels in unconsolidated sandpack cores. Four transport patterns were reported: plugging, high retention, breaking, and pass; high retention and pass; and low retention and pass.

Numerical studies help get a better understanding of the transport mechanisms of deformable gel particles in porous media. Liu et al. (2017) numerically studied the transport behavior of deformable gel particles based on size exclusion theory. Zhou et al. (2017) used an improved LBM-DEM (lattice Boltzmann method and discrete element method) simulation method to study the transport behavior of soft gel particles in porous media. They numerically investigated the effect of particle/pore size ratio and particle strength on the critical pressure gradient for a single gel particle transport through a single pore throat.

They reported an exponential relationship between the critical pressure gradient and the size ratio, and linearly correlated with the elastic modulus. For the single particle transport process, they observed that the flow rate had negligible impact on the critical pressure gradient. Goudarzi et al. (2015) reported transport behavior of preformed particle gels in fracture and sandpack models. The potential of preformed particle gels in improving the conformance and suppress excessive water production was investigated. They developed a set of models to characterize the gel rheology, adsorption, swelling ratio, resistance factor, and residual resistance factor of the PPGs in fracture and porous media (sandpacks). The models were incorporated into a reservoir simulator (UTGEL). They validated the gel transport models with experimental results. Note that in view of the complicated gel transport behavior, some assumptions were involved in the models. Some important phenomena, such as dehydration, particle breakage, and surface plugging, were not considered in the models.

Overall, though significant progresses have been achieved with the efforts of various researchers, a better understanding is still required about the deformable microgel transport in porous media, as pointed out by some recent review papers (Leng et al. 2021; Wu et al. 2021; Villone & Maffettone 2019). The first-ever polymer flooding project has been on going to tap the tremendous heavy oil resources on the Alaska's North Slope (Dandekar et al. 2019, 2020, 2021; Ning et al. 2020). Conformance control is an important issue to improve the effectiveness of polymer flooding in heavy oil reservoirs (Zhao et al. 2021a). In this study, sandpacks prepared with silica sands were used as the super-K channels to investigate the propagation behavior of microgel particles. Multiple pressure sensors were applied along the sandpack models to monitor the propagation dynamics.

Chase brines with different salinities were injected after the gel treatment to test the water-blocking performance. Crude oil was also injected to study the different blocking abilities of the microgels to water flow and to oil flow.

2. EXPERIMENTAL

2.1. MATERIALS

Brines. Two brines were prepared in lab based on the brine composition in the Milne Point oilfield on the Alaska's North Slope (Table 1). The synthetic formation brine (SFB) had a total dissolved solid (TDS) of 27500 ppm, and the synthetic injection brine (SIB) had a TDS of 2498 ppm (Zhao et al. 2021b). In the Milne Point, the injection brine was from a low-salinity water resource, and it was used in water flooding and polymer flooding. In this work, the SFB was used to saturate the sandpack models. Except otherwise noted, the SIB was used as the initial and post injection brine, as well as the carrying fluid of the microgel particles. We labeled the SIB and SFB as LSW and HSW when emphasizing the effect of salinity.

Crude oil. The crude oil was sampled in August 2018, at a wellhead in the Milne Point Field (Well #B-28, provided by Hilcorp, Alaska). The oil sample was centrifuged to remove water and solids (if any) and filtered through a 0.5-μm filter paper. The viscosity was 202 cp at reservoir temperature (71 °F), with an API gravity of 19.0° (0.940 g/ml).

Microgels. The microgels were obtained by grinding millimeter-sized preformed particle gels (Bai et al. 2007a; Zhao et al. 2021a). The microgels had a volumetric swelling ratio of 40, and 20 cm^3/cm^3 in the SIB and SFB, respectively. The swelling ratio was

defined as the ratio of swollen volume after absorbing water to the original volume of the gel. For the dry microgel particles of 170-230 mesh (63-88 μm), after fully swollen in the SIB, the gel particle sizes were in the range of 215 to 300 μm, with an average diameter of 260 μm. The sizes were 170 to 240 μm (average 206 μm) after fully swollen in the SFB. Dispersions were prepared with a microgel concentration of 1 wt% (dry weight). The two gels were labeled as softer gel and strong gel, respectively. Their storage moduli were about 820 Pa and 1370 Pa, respectively.

Table 1. Basic formation brine and injection brine.

Name	Composition (ppm)
HSW (SFB, synthetic formation brine)	Na^+: 10086.0 K^+: 80.2 Ca^{2+}: 218.5 Mg^{2+}: 281.6 Cl^-: 16834.4 TDS: 27500
LSW (SIB, synthetic injection brine)	Na^+: 859.5 K^+: 4.1 Ca^{2+}: 97.9 Mg^{2+}: 8.7 Cl^-: 1527.6 TDS=2498

Super-K Sandpack Models. Sandpacks were used as the super-K porous media, which mimicked the super-K channels present in reservoirs. The sandpack model (2.5 cm × 50 cm) had multiple pressure taps which were able to monitor the pressures at different locations in the sandpack (Figure 2). The sandpacks were prepared with silica sands with wet-packing method. Before preparing the sandpack, the sands were mixed with the SFB at a certain sand/brine ratio. The wetted sands were added into the sandpack tube at multiple times. The sandpack was vibrated with a vibration machine to ensure tight and uniform packing of the sands. Afterwards, the sandpack was vacuumed and saturated with the SFB. The absolute permeability was estimated by measuring the stable injection pressures at five different flow rates. The sandpack permeabilities ranged from 26.9 to 221 darcies. The basic information of the sandpacks was summarized in Table 2.

2.2. EXPERIMENTAL PROCEDURE

The experiment setup was shown in Figure 2. The typical experimental procedure was summarized in Figure 3. After measuring the permeability, a brine tracer test (potassium iodide) was carried out to verify the homogeneity. A typical brine tracer test curve was shown in Figure 4. The quick equilibration of the tracer concentration in the effluent indicated good homogeneity of the sandpack core.

The microgel dispersion was injected at 2 ml/min until stable injection pressures were reached at all the pressure taps. The pressure response was an indication of the gel transport dynamics in the sandpack. The moments when the pressures at different locations began to increase were recorded. The onset of pressure increase indicated the microgel bank front had arrived at that pressure tap. The gel-dispersion accumulator had a mixing

propeller mounted at the bottom to ensure the particles dispersed uniformly in the carrying fluid. In Figure 2, this accumulator was drawn upside down for simplicity. The effluent was closely monitored to capture the moment when the microgels came out from the outlet.

Table 2. Summary of basic information of the experiments.

Exp #	k, darcy	Gel size	Gel strength	MSR	Carrying fluid
1	55.4	260 (215~300)	Softer	2.35	SIB
2*	26.9	260 (215~300)	Softer	3.29	SIB
3	221	150 (100~190)	Strong	0.69	SFB
4	62.0	130 (90~170)	Strong	1.11	SFB
5	62.4	150 (100~190)	Strong	1.28	SFB
6	59.8	206 (170~240)	Strong	1.77	SFB

Note: * the dimension of this sandpack was 5 cm × 30 cm. Three internal pressure taps were evenly distributed along the model.

The effluent was also collected at different flow rates to examine the impact of flow rate on the particle size of the microgels as transporting through the porous media. At given flow rates, the effluent samples were collected at stable conditions to minimize the impact of the previous flow conditions. The size and morphology of the samples were examined with an optical microscope (HIROX Digital Microscope KH-8700). Also, the pressures in

the sandpacks at different flow rates were monitored. Stable pressures were used to calculate resistance factors (F_r) at different sections in the sandpack. Afterwards, chase water was injected at 2 ml/min until stable pressures at all locations were reached. Residual resistance factors (F_{rrw}) at different sections were calculated to evaluate whether the microgels effectively shut off the super-K channels to water flow at the in-depth regions.
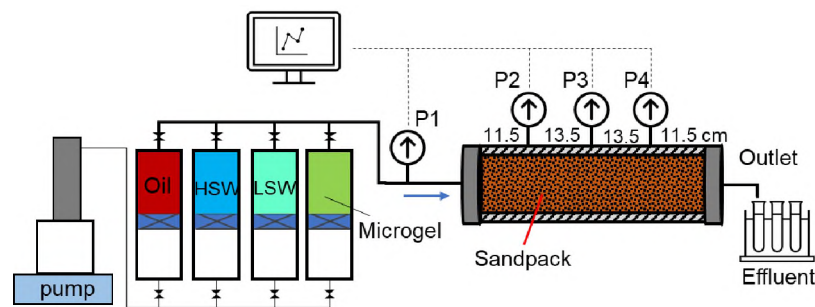
Figure 2. Experiment setup for microgel transport tests.
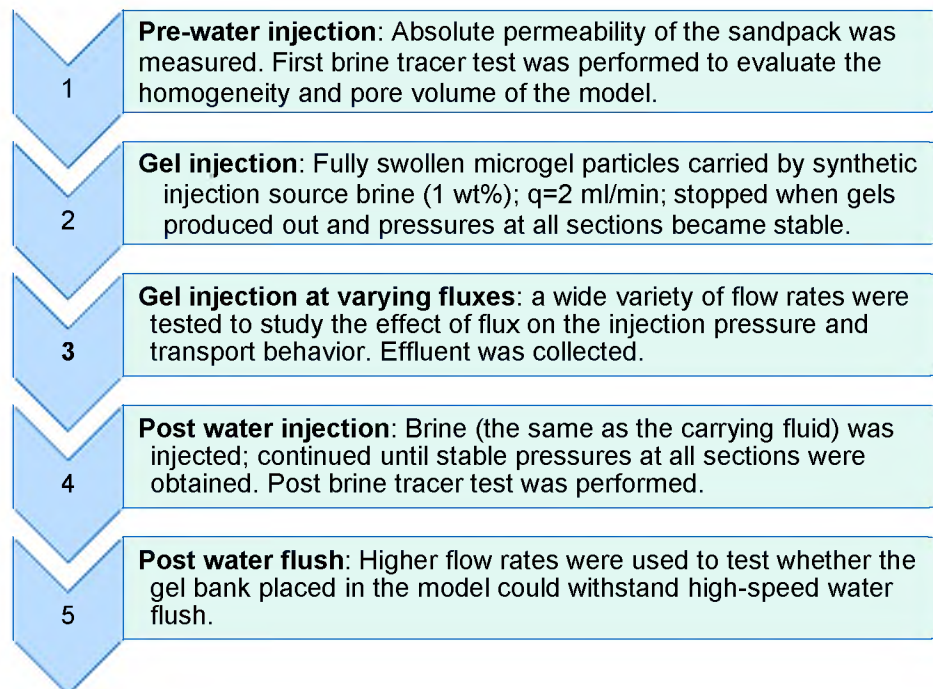
Figure 3. The typical experiment procedure.
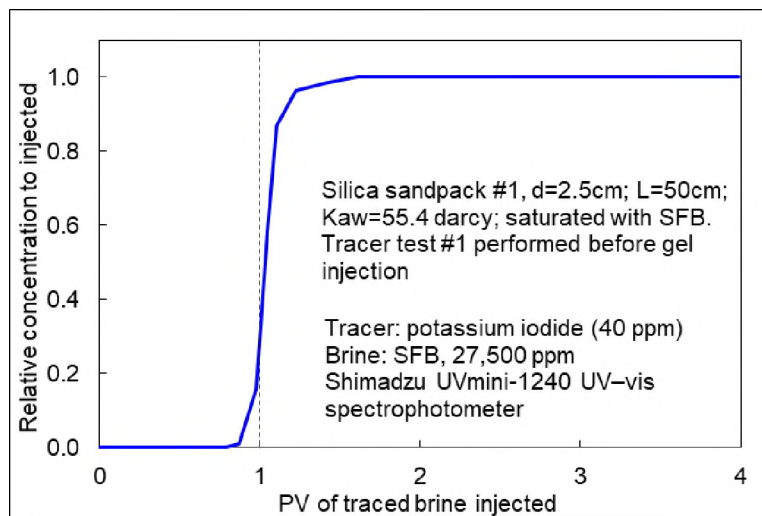
Figure 4. Result of brine tracer test (Exp #1, before gel injection).

3. RESULTS AND DISCUSSION

3.1. TRANSPORT BEHAVIOR OF MICROGELS

Figure 5 shows the pressures at different locations during the gel injection process along the super-K sandpack in Exp #1. In this experiment, the average particle-to-pore matching size ratio (MSR) in this experiment was 2.35. The specific pressure responses during gel propagation through the model were summarized in Table 3. At the beginning, the pressure at the inlet (P1) increased linearly, while the other three pressure sensors showed no change (remaining zero), as shown in Figure 5. After injecting 57.4 ml of gel dispersion, P2 started to increase, indicating the gel bank front arrived at the first internal pressure tap (P2). The injected gel dispersion corresponded to 0.72 pore volumes of the whole model, or 3.13 pore volumes of the transported section (sec 1). Meanwhile, P1 was increased to 93.9 psi (Table 3), and P2 started to increase almost linearly, following the same trend as observed in P1. The gel bank front sequentially arrived at P3 and P4 after

injecting 102.6 ml and 148.4 ml (1.29 and 1.86 PV) of gel dispersion, respectively. After injecting 193.5 ml (2.42 PV) of gel dispersion, the gel bank front broke out at the outlet. At this moment, the pressures at the four points did not reach stable conditions. Instead, they still increased as more gel dispersion was injected. The pressures at different locations gradually became stable with fluctuations around certain values (301 psi, 238 psi, 128 psi and 59 psi, respectively). In total, 317.6 ml (3.98 PV) of gel dispersion was injected. The pressure gradients in different sections of the sandpack were estimated, as shown in Figure 6. In each section, the pressure gradient first increased to a peak, then it gradually decreased and became relatively stable with fluctuation. The fluctuation was a result of repeated accumulation and release/remigration of the microgel particles in the pore-throat structures (Zhao et al. 2021a). The pressure gradients in different sections were comparable with each other. The final stable pressure gradients were in the range of 155-249 psi/ft. Due to connection malfunction of pressure sensor #3 in the early stage of gel injection, the readings of P3 were not accurate. Instead, the 2nd and 3rd sections were regarded as a whole, and P2 and P4 were used to calculate the pressure gradient in this combined section. The malfunction issue was resolved later and the late-stage P3 was used when calculating the resistance factors.

With the pressure data, we obtained the resistance factors (F_r) during the gel injection with Equation (1). The resistance factor equals to the ratio of pressure gradient during gel injection to the initial brine injection at the same flow rate. The resistance factors in the different sections were shown in Figure 7. The stable resistance factors at different sections of the sandpack are summarized in Figure 8. The resistance factors followed a similar trend as the pressure gradients during the gel injection process. The resistance

factors were relatively uniform in all the sections of the model, in the range of 2216 to 3549. No progressive surface plugging was observed during the whole process.

$$F_r = \frac{\lambda_w}{\lambda_{gel}} = \frac{\Delta P_{gel}}{\Delta P_{initial\text{-}water}}$$ (1)

Table 3. Responses during gel transport in high-permeability porous media (Exp #1, MSR=2.35).

Gel front	t, min	Dispersion injected, ml	Dispersion injected, PV	P1, psi	P2, psi	P3*, psi	P4, psi
Inlet	0	0.00	0	0	0	0	0
Arrived tap#2	28.7	57.40	0.719	93.9	0	0	0
Arrived tap#3	51.3	102.60	1.286	183.6	105.8	0	0
Arrived tap#4	74.2	148.40	1.860	280.7	203.1	15.8	0
Arrived outlet	96.8	193.50	2.424	324.7	251.5	95.6	71.1
Stable (end)	158.8	317.60	3.980	301.0	238.4	128.2	59.4

*Readings were not accurate due to sensor connection malfunction.
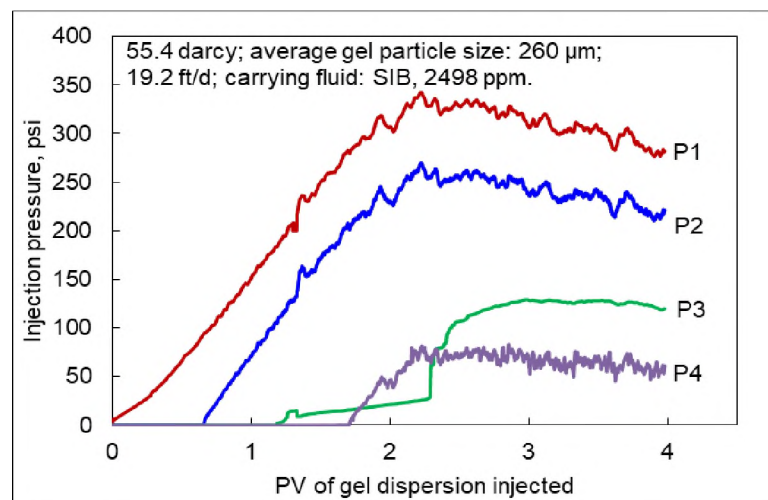
Figure 5. Pressures at different locations during gel injection (Exp #1).
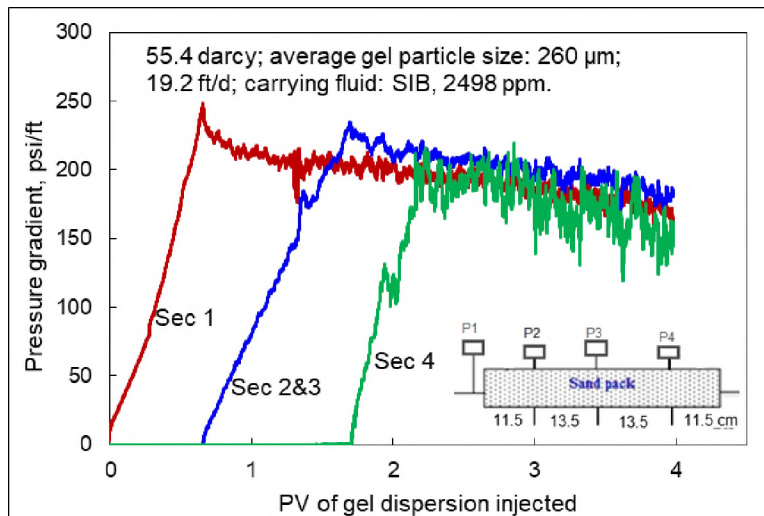
Figure 6. Pressure gradient at different sections during gel injection (Exp #1).
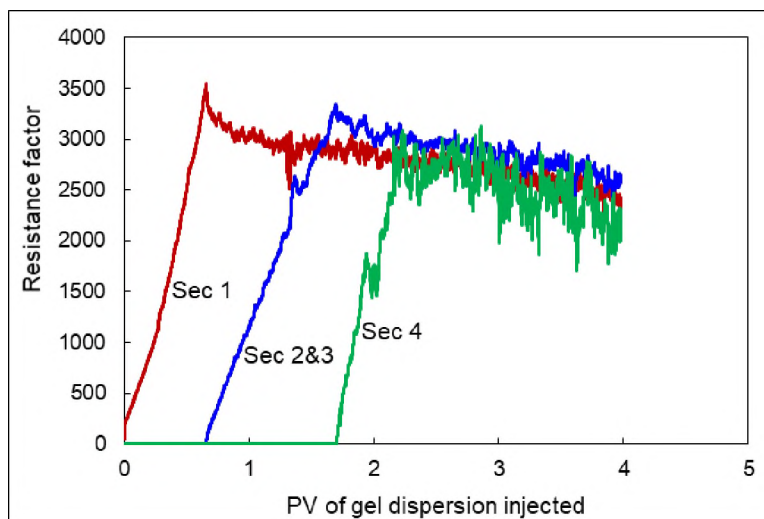
Figure 7. Resistance factor distribution (Exp #1).

In Exp #2, the MSR was 3.29. The pressures, pressure gradients and resistance factors were shown in Figures 9 to 12. The gel propagation dynamics are summarized in Table 4. In this experiment, 1.09 total PV (4.36 local PV) of gel dispersion was injected when P2 started to show response. The propagation speed of the gel particles was obviously

slower than that in Exp #1 (4.36 PV vs. 3.13 PV), indicating higher retention of the gel particles in the inlet section as the MSR was higher (3.29 vs. 2.35). In total, 770 ml (4.7 PV) of gel dispersion was injected. The stable pressures at the four locations were 361, 213, 130 and 89 psi, respectively. The first section showed a higher stable pressure gradient and resistance factor at the end of the gel injection compared with the values in the in-depth sections. The pressure gradients in the other three sections were comparable with each other. The final stable pressure gradients were in the range of 168-602 psi/ft, which were obviously higher than that in Exp #1. It was more difficult for the gel particles to transport and place in the super-K channels as the MSR was larger.
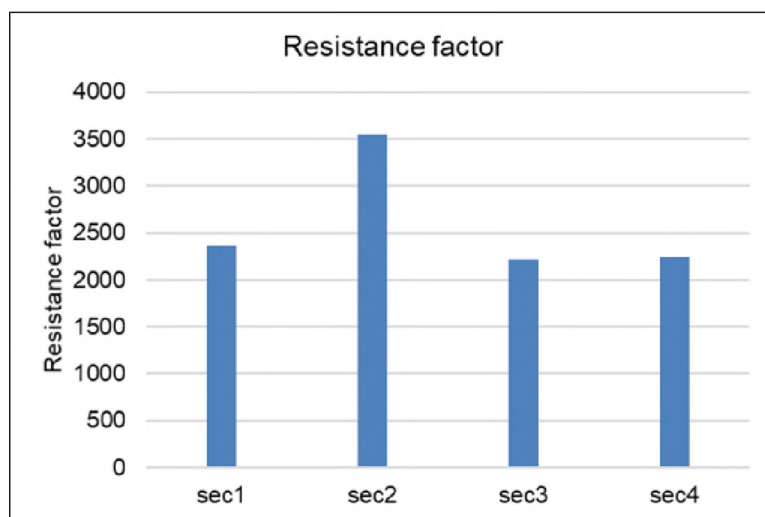
Figure 8. The stable resistance factor distribution (Exp #1).

The results indicated that though the tested 260-μm microgel particles could be injected into the in-depth sections of the sandpack with an MSR of 3.29, high pressure gradients were required. Such high pressure gradients are only available in the near wellbore regions. An MSR of 3.29 is not favorable for gel transport and placement in the

super-K porous channels. In Exp #1, the pressure gradients were also too high, though the distributions of pressure gradients and resistance factors were more uniform.

Table 4. Responses during gel transport in high-permeability porous media (Exp #2, MSR=3.29).

Gel front	t, min	Dispersion injected, ml	Dispersion injected, PV	P1, psi	P2, psi	P3, psi	P4, psi
Inlet	0	0	0	0	0	0	0
Arrived tap#2	35.9	179.25	1.09	103.2	0	0	0
Arrived tap#3	59.3	296.50	1.81	225.9	86.4	0	0
Arrived tap#4	77.9	389.33	2.37	385.9	168.3	64.5	0
Arrived outlet	103.0	455.00	2.77	348.9	180.7	100.0	28.8
Stable	217.5	672.25	4.10	352.0	207.0	127.0	89.0
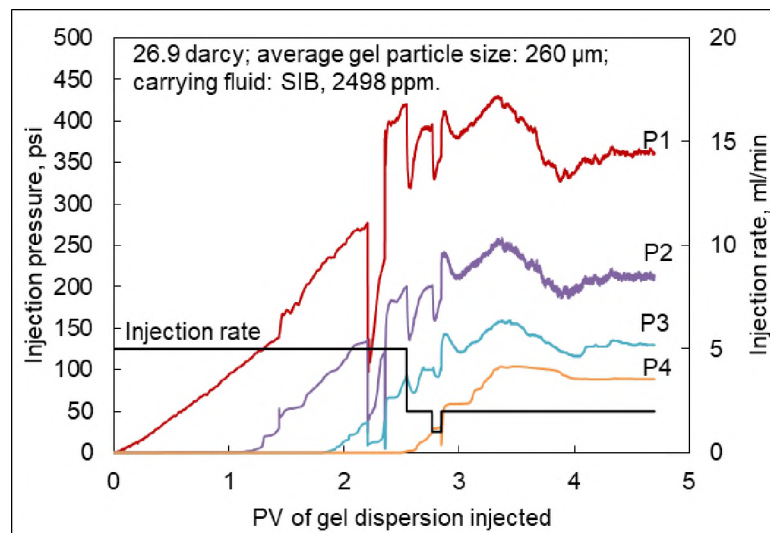
Figure 9. Injection pressure at different locations during gel injection (Exp #2).
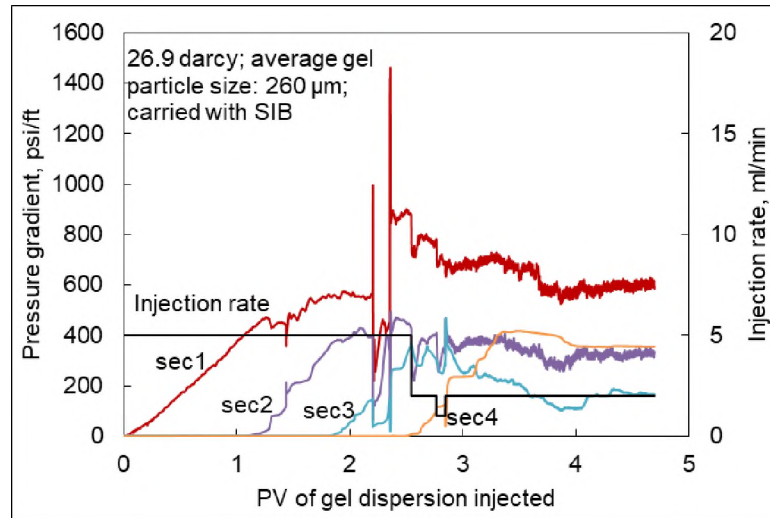
Figure 10. Pressure gradient at different sections during gel injection (Exp #2).
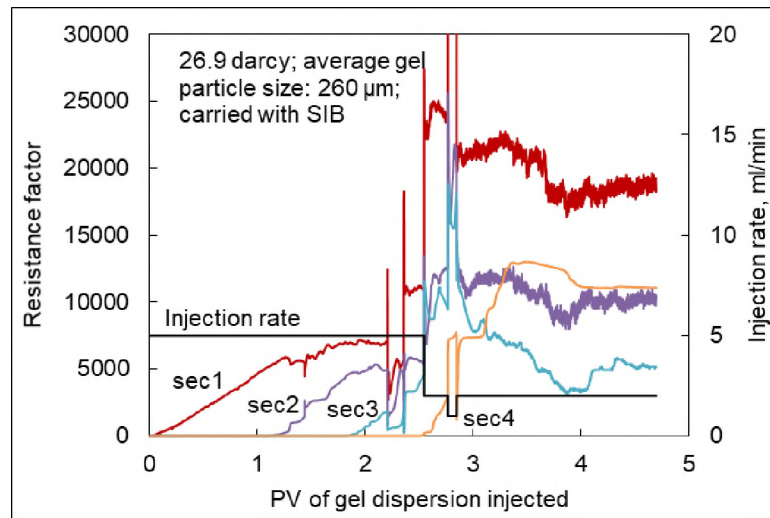
Figure 11. Resistance factor distribution (Exp #2).

Effect of MSR on Fr Distribution. More experiments were performed with lower MSRs to explore the favorable working conditions of the microgel particles. In this study, we used the Carman-Kozeny equation, Equation (2), to estimate the average pore size of the super-K sandpacks (Carman 1956; Mauran et al. 2001). In this equation, d is the average

diameter of the pores (µm), k is the permeability (µm^2) of the core, f_{CK} is the Carman-Kozeny shape factor, τ is the tortuosity, and Φ is the porosity (fraction). A value of 4.5 for the $f_{CK} \times \tau^2$ was adopted in the calculation (Carman 1956; Mauran et al. 2001).

$$d = \sqrt{\frac{16 k f_{CK} \tau^2}{\Phi}} \qquad (2)$$
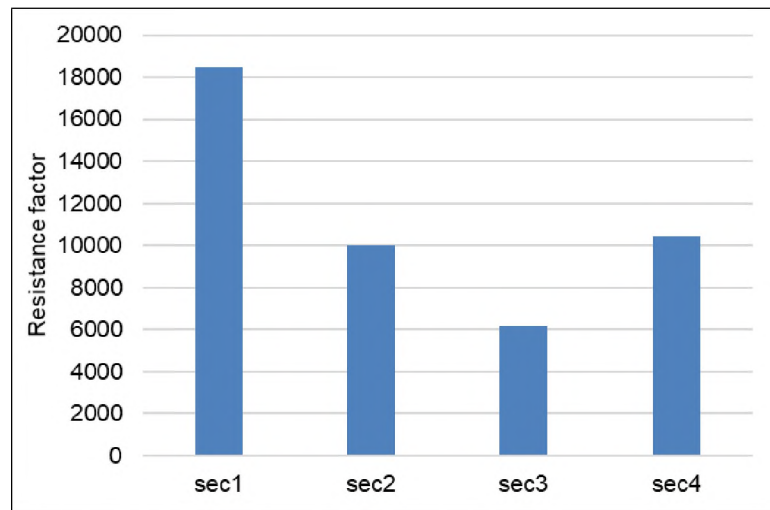
Figure 12. The stable resistance factor distribution (Exp #2).
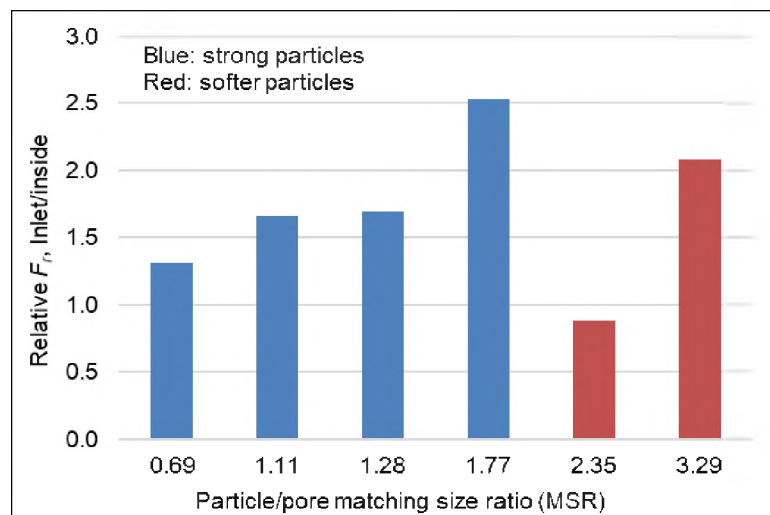
Figure 13. Resistance factor distribution at different MSRs.
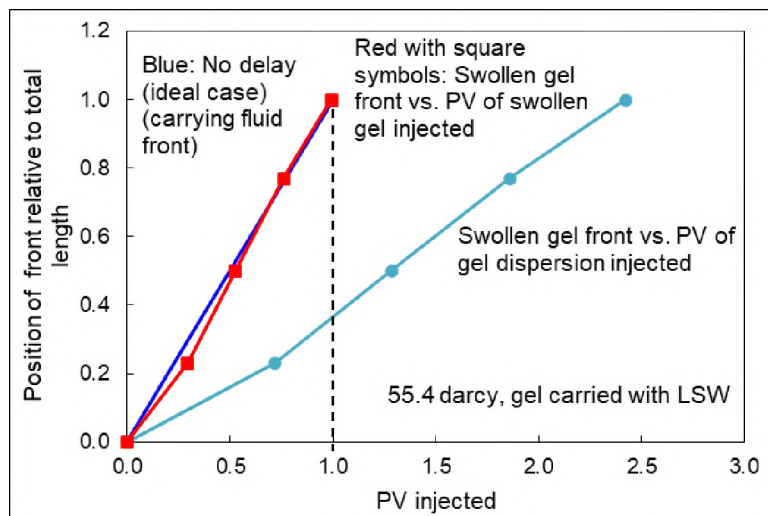
Figure 14. Transport delay (Exp #1).

A parameter termed as relative resistance factor was introduced to describe the surface retention/plugging tendency of the microgel particles in super-K channels. It was the ratio of resistance factor in the inlet section to the average value in the in-depth sections. A higher value meant a higher retention in the inlet section, thus poorer migration ability into the in-depth sections of the porous channels. In this study, the first section of the sandpacks was regarded as the inlet section. The rest segment of the sandpacks was regarded as the in-depth sections. The relative resistance factors at different MSRs were summarized in Figure 13. The results suggested that the resistance factor distribution was relatively uniform when the particle sizes were comparable or smaller than the pore throat sizes. At the same strength, this parameter increased with the MSR, indicating reduced injectivity and increased surface plugging tendency as the MSR was increased. Significant retention of the particles in the inlet section was expected, and the particles were difficult in transporting deep into the sandpacks. The strength of the gel particles also influenced

the transport and retention behavior. Softer particles were easier to transport deep into the models as indicated by the lower relative resistance factors in Figure 13.

In addition, the experiment results indicated significant delay of the gel bank front compared with the front of the carrying fluid. Figure 14 shows the position of the carrying fluid front and the position of gel bank front in Exp #1. The lag of the gel bank front against the carrying fluid front was caused by the retention of the microgel particles in the porous media. The equilibrium retention was 3180 micrograms microgels by per gram of sand based on material balance by monitoring the amount of gel injected into and produced out of the sandpack model. Note that the fully swollen gel front broke out after one pore volume of swollen gel injection, almost following the trend of the no-delay ideal case. At that time, the gel was expected to occupy all the pore spaces in the sandpack model. Note that the existence of inaccessible pore volume (IAPV) was possible to result in an earlier breakout of the gel bank front. The IAPV was the pore spaces that were too small for the gel particles to access. However, the IAPV was negligible (zero) in this case as the swollen gel front followed almost the same trend as the no-delay ideal case.

Pressure Gradients and Resistance Factors at Different Superficial Velocities. The pressure gradients and resistance factors at different injection rates (0.1-50 ml/min, equivalent to 1 to 500 ft/d) were tested. The pressure gradients were shown in Figures 15 and 16. Though the pressure gradient showed an increasing trend with the injection rate. However, the increase was much more gradual compared with the flow rate. According to the Darcy's law, for a Newtonian fluid with a constant viscosity, the pressure gradient should be proportional to the velocity (flux) with a slope of unity (angle=45°) in a log-log plot (Figure 16). However, the slope for the gel dispersion was lower compared with the

Newtonian fluid, which indicated a decreasing apparent viscosity of the gel dispersion with the increase of flow rate. Consistently, the resistance factor exhibited a decreasing trend, a behavior similar to a shear-thinning fluid.
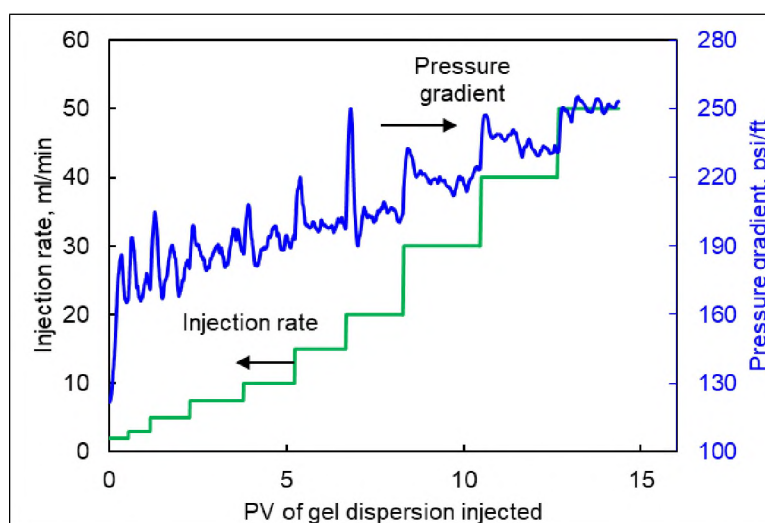
Figure 15. Pressure gradient at different flow rates.

The decreasing apparent viscosity indicated mechanical degradation was likely to occur when transporting in the porous channels. This hypothesis was supported by microscopy observation of the gel samples collected at different flow rates (see Figure 17). Smaller gel particles were observed when the flow rates were higher. The pressure responses also supported this hypothesis, as seen in Figure 15, when the flow rate increased, the pressure gradient increased at the beginning and then dropped. The changing behavior was in accordance with the breakage of gel particles. The breakage phenomenon is highly related to the significance of the shear force against the strength of the particles. More severe breakage was observed at higher flow rates for a given microgel material. Therefore, the apparent viscosity (resistance factor) would be reduced. Another possible

mechanism responsible for the apparent thinning behavior was the slippage effect between the gels and the walls of pores. The gels slipped along the pore surfaces, while there was a viscous boundary layer in the case of liquid flow. One more possible reason was the lubrication effect of the water film on the sand grains. With the assistance of the lubrication film, the gels could slip forward. Thus, the pressure gradient became less sensitive to the flow rate.

The particle breakage phenomenon was also reported by other researchers in the literature (Bai et al. 2007b; Farasat et al. 2017; Saghafi et al. 2018; Wang et al. 2017; Li et al. 2019). For instance, Li et al. (2019) observed significant particle size reduction after the microsphere particles transported through an 18-m sandstone core. The broken/pass behavior favored deep penetration of microgel particles under practical pressure gradients. The observed shear degradation (breakage) in this study can partially explain why good injectivity of PPGs were consistently observed in most field applications (Liu et al 2006; Bai et al. 2008, 2012, 2013). This explanation did not exclude other possibilities, for example, the presence of fractures/super-K channels (e.g., induced by long-term waterflood). The breakage phenomenon would benefit the injectivity of the gel dispersion. On the other hand, however, concerns may rise about the reduced water-blocking efficiency as a result of the gel breakage. From field application point of view, less water-blocking ability is required in the in-depth regions of reservoirs. That is, the water-blocking efficiency (strength) does not need to be as strong as in the near wellbore region. Therefore, the particle breakage phenomenon is not supposed to noticeably reduce the overall conformance control performance of the gel treatments.

$$u = -\frac{k}{\mu}\nabla p \Rightarrow \lg u = \lg \frac{k}{\mu} + \lg(-\nabla p)$$
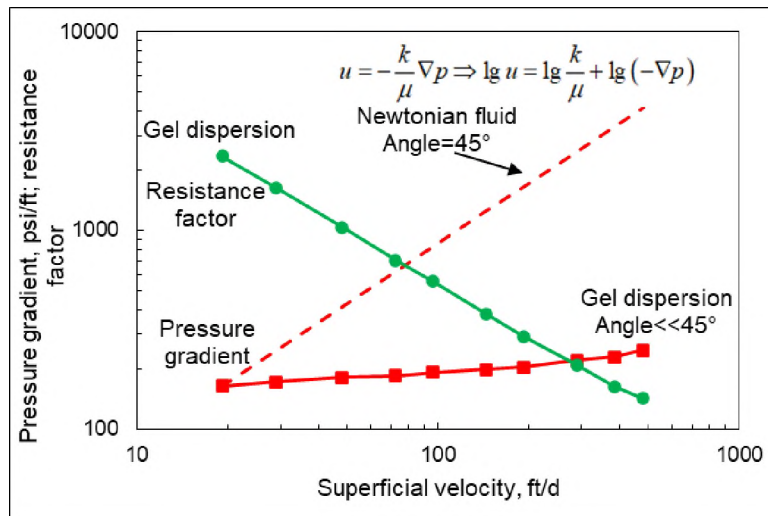
Figure 16. Pressure gradient as a function of superficial velocity.
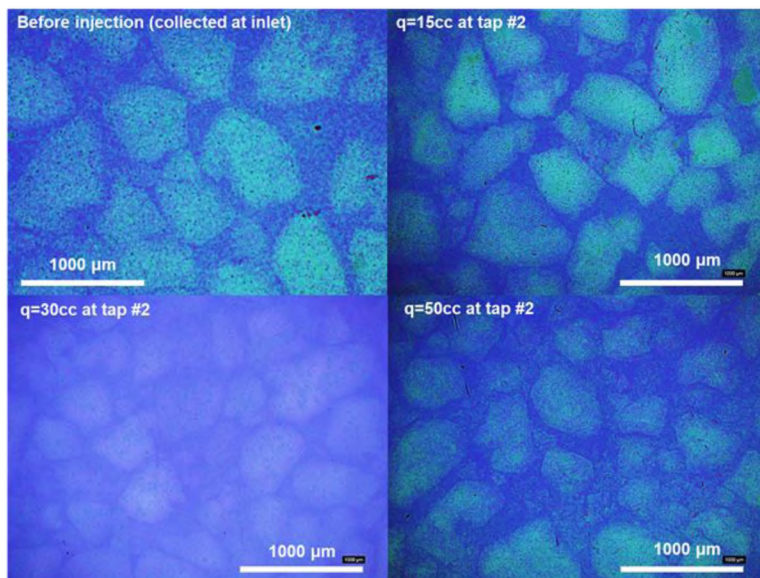
Figure 17. Microscopy examination of effluent gel samples. (Original particles were collected at inlet. Effluent samples were collected at 15, 30, and 50 ml/min.)

Transport/Pass Mechanisms. Bai et al. (2007b) reported six transport patterns of particle gels through pore throats based on micromodel experiments, including direct pass, adsorption, deform and pass, snap-off and pass, shrink and pass, and trap. The transport

patterns could be estimated based on the pressure response, effluent gel concentration and gel particle size. The direct-pass pattern was only significant when the gel particle sizes were smaller than the pore size. The adsorption mechanism was only pronounced when the particles were significantly smaller than the pores (Chauveteau et al. 2003; Yao et al. 2017). When the particles were larger than the pore throats (MSR>1), the deform/pass, shrink/pass, and break/pass patterns would co-exist. The dominant pattern(s) depended on the flow rate (or driving pressure gradient) for given gel materials. The deform/pass pattern was dominant at low flow rates, while the breakage phenomenon was more significant at high flow rates as indicated in Figure 17. Meanwhile, the retention (entrapment) of the microgels in the channels was high, 3180 µg/g in Exp #1. The retention was directly related to the water-blocking ability of the microgels.

3.2. WATER BLOCKING EFFICIENCY

The blocking efficiency of the microgels to post water flow was tested. The same brine that used to prepare the gel dispersion was injected at the same flow rate. Stable pressures were reached at the different locations in the models. The results of Exp #1 were illustrated in Figure 18. The stable pressures were used to calculate the residual resistance factors (F_{rrw}) to the post water flood at the different locations (Figure 19). The F_{rrw} was defined as the brine permeabilities ratio before and after the gel injection, as described by Equation (3). It was equal to the ratio of brine injection pressures after and before the gel injection.

$$F_{rrw} = \frac{K_{before}}{K_{after}} = \frac{\Delta P_{\text{post-water}}}{\Delta P_{\text{initial-water}}} \tag{3}$$
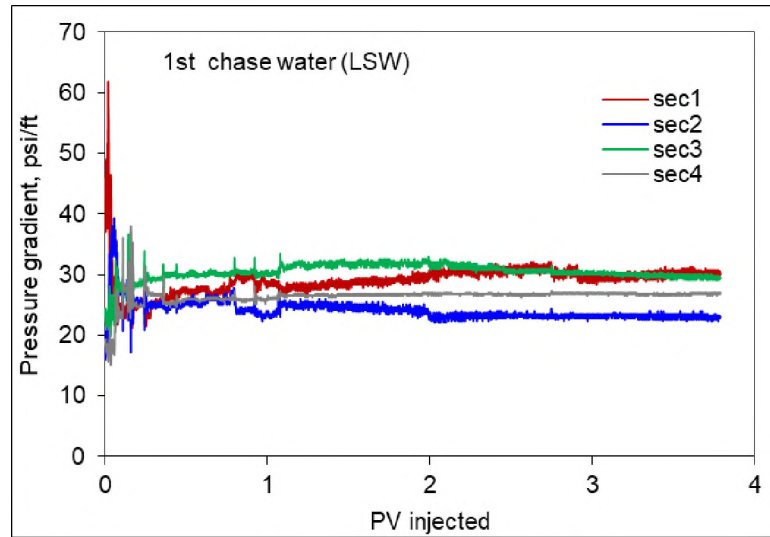
Figure 18. Pressure gradient during the first chase water flood (LSW) (Exp #1).
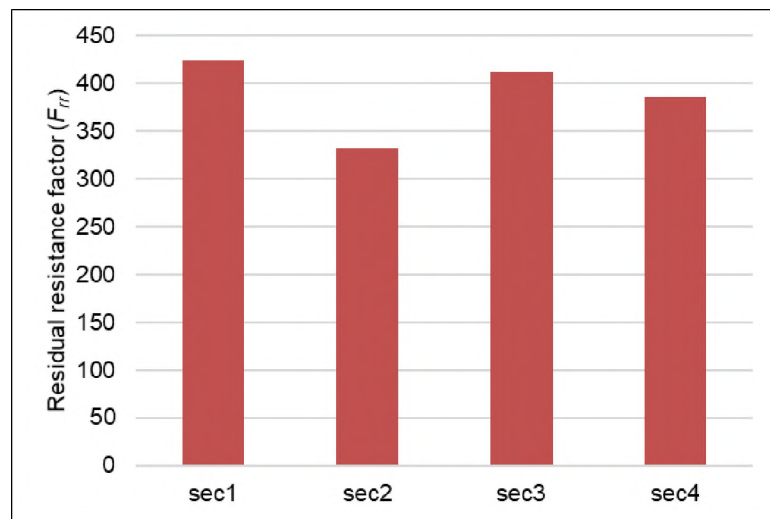
Figure 19. Distribution of residual resistance factor (Exp #1).

In Exp #1, the F_{rrw} values after gel injection were in the range of 330 to 420, and the distribution was quite uniform (Figure 19). No obvious face plugging was detected as indicated by both the F_r and F_{rrw} distributions (Figures 8 and 19). Generally, the F_{rrw} distribution was more uniform when the MSR was lower, as shown in Figure 20. The

relatively unform distribution of the F_{rrw} indicated uniform retention of the gel particles in the super-K channels. The uniform F_{rrw} distribution was a desirable merit for a deep-profile-control agent. The results demonstrated that the microgel particles were able to effectively establish water-blocking efficiency at the in-depth regions of the super-K channels. However, the performance became unsatisfactory when the MSR was higher. For example, as the MSR increased to 3.29 (Exp #2), the F_{rrw} in the inlet section was significantly higher compared with the values in the other sections (see Figure 20). This observation agreed with the gel transport behavior as discussed in the preceding subsection. The results also revealed the impact of strength of the microgels on the water-blocking performance (Figure 20). Comparing Exp #1 and Exp #6, though the MSR of the softer gels was higher than the case of strong gels (2.35 vs. 1.77), the F_{rrw} distribution was more uniform when softer particles were injected. The results suggested that at the same matching size conditions, softer gels were more likely to achieve a deep placement and unform water-blocking in the super-K channels.
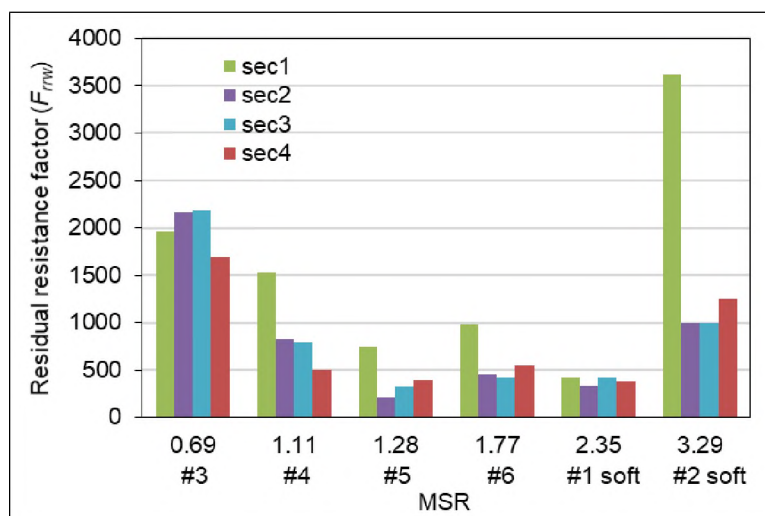
Figure 20. Summary of residual resistance factor distribution after gel treatment.

The results were consistent with our previous observations in microgel conformance control treatment during polymer flooding using channel models (Zhao et al. 2021a). We observed that the critical driving pressure that required for the microgel particles to penetrate the super-K channels followed a power-law relationship with the permeability of the channel. For the tested microgels, a much higher driving pressure was required as the channel permeability was below 30 darcy (MSR>3.5), which indicated the ineffectiveness of the microgels under these conditions. The microgels were effective when the channel permeability was above 50 darcy (MSR<2.6). Under such conditions, good injectivity, effective water-blocking performance, and significant oil recovery improvement were achieved. The results in the current study further confirmed the identified favorable working conditions of the microgels.

The water-blocking efficiency (E_{bw}) after gel treatment was estimated with Equation (4). The E_{bw} values in Exp #1 were 99.76%, 99.70%, 99.76% and 99.74% in the four sections. For all the experiments, the water-blocking efficiency in the in-depth sections was above 99.5%. The results indicated that the microgels could efficiently shut off the super-K channels. In Equation (4), K_{before} and K_{after} were the permeabilities of the sandpack to water before and after the gel injection, respectively.

$$E_{bw} = \left(1 - \frac{K_{after}}{K_{before}}\right) \times 100\% = \left(1 - \frac{1}{F_{rrw}}\right) \times 100\% \tag{4}$$

Brine tracer tests after the gel treatment also confirmed that the microgel particles effectively placed in the super-K channel and reduced the effective pore spaces to the water flow. The brine tracer tests were performed after about 20 PV chase water injection with the same flow rate as in the gel injection. As illustrated in Figure 21, the results showed

that the tracer breakthrough occurred significantly earlier after gel injection. It indicated the effective pore volume was reduced as the pore spaces were occupied by the gel particles.
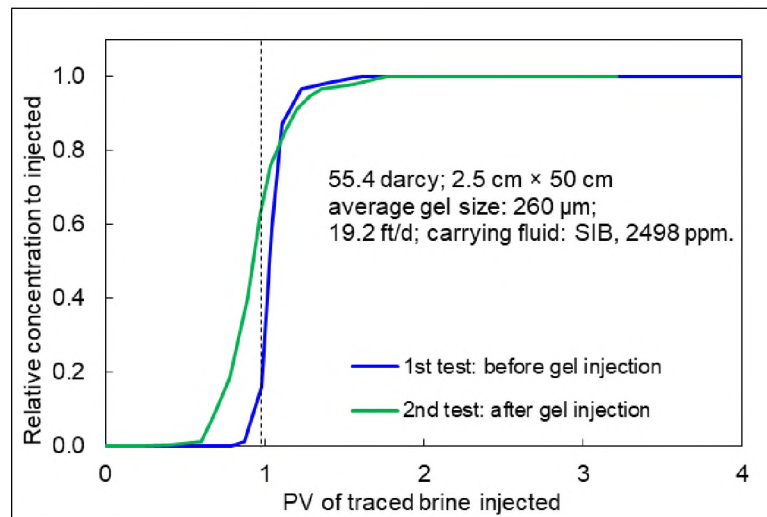
Figure 21. Results of brine tracer test after gel injection (Exp #1).

Salinity-Responsive Behavior of F_{rrw}. As the swelling behavior of the microgels was responsive to the salinity of brine, we wondered how the residual resistance factor would change when brines with different salinities were injected. A high-salinity water (HSW) slug was injected at the same flow rate following the first post low-salinity water flush to test the effect of salinity on the water blocking efficiency. We observed that the injection pressures and the residual resistance factors were significantly reduced (Figure 22 and Figure 23). Afterwards, a second low-salinity water slug (LSW, i.e., the SIB) was injected at the same flow rate. Interestingly, the pressures and residual resistance factors were recovered almost to the same level as in the first post-LSW flood, as shown in Figure 22 and Figure 23. The results suggested that the gel would shrink when the HSW was

injected. The reason was that the high concentration of ions in the HSW exerted higher compressive forces on the 3D networks and polymer chains of the gels. Consequently, the gels lost water and the volume was reduced (i.e., shrunk). The pore volume occupied by the gels was reduced, and wormholes, or microchannels were generated through the gel bank. Thus, the resistance ability to the water flow was reduced, as indicated by the lower residual resistance factors during the HSW injection in Figure 23. Our observations also demonstrated that the shrinking and swelling properties of the microgels were reversible. The stability of gel materials was not destroyed by the alternate salinity environment. After injecting the LSW again, the concentration of surrounding ions was reduced, the compression forces applied on the 3D networks of the gels were reduced, and thus the screen effect was weakened. The polymer chains and the 3D networks stretched, and more water was absorbed, thus the gels reswelled. Consequently, the wormholes and microchannels created during the HSW flush were re-sealed, and the resistance ability was recovered. The salinity-responsive behavior was also observed by Brattekås et al. (2019) for Cr(III)-HPAM gel systems.

Can this particular behavior be utilized in fields? Taking Milne Point oilfield as an example, the formation water has a high salinity of about 27500 ppm and in a normal water flood or polymer flood, the salinity is much lower, about 2500 ppm, less than one tenth of the formation brine. Therefore, if the microgel is carried with HSW, the particles placed in the formation can further swell during the post water flooding or polymer flooding. The further swelling of the gel particles can result in a reinforced water-blocking capacity in the channels and thus force the displacing fluid into the unswept zones (oil zones) to displace the previously bypassed oil. Thus, the sweep efficiency can be improved.
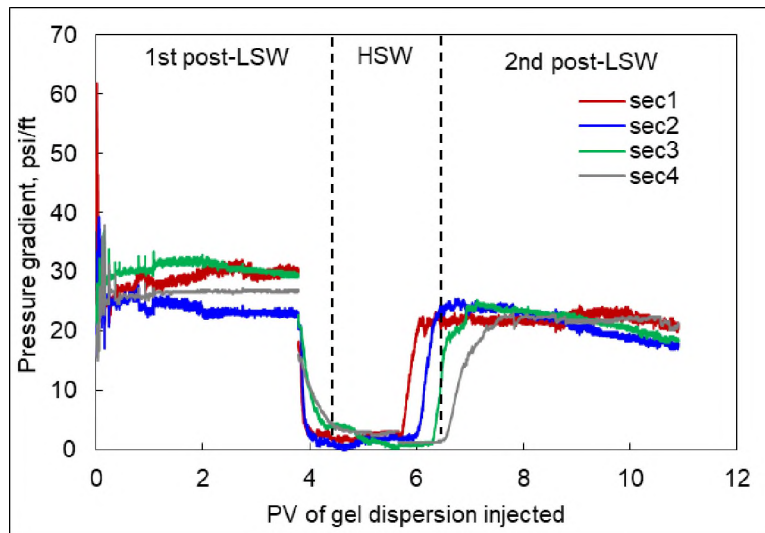
Figure 22. Pressure gradients during post water floods using brines with different salinities (Exp #1).
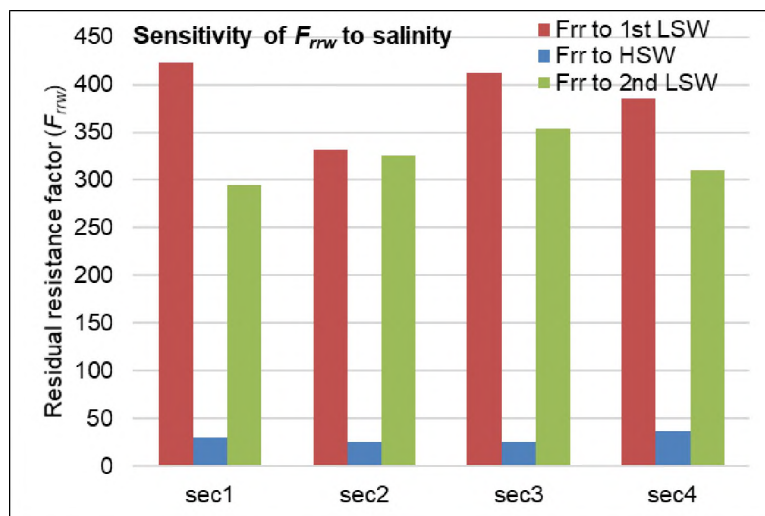
Figure 23. Salinity-responsive behavior of residual resistance factor to water after gel injection (Exp #1).

Disproportionate Permeability Reduction (DPR) Effect of the Microgels. Crude oil was injected after the post water flood to test the blocking effect of the microgel bank to oil flow. The residual resistance factors were estimated based on the stable pressures at

different locations of the sandpacks. Interestingly, the residual resistance factor to the oil

flow was much lower than the residual resistance factor to the water flow (i.e., $F_{rrw} \gg$

F_{rro}), as shown in Figure 24. That is, the microgels reduced the permeability to the water

flow much more than the permeability to the oil flow. This phenomenon was termed as

disproportionate permeability reduction (DPR) effect. The F_{rro} was in the range of 4.5 to

21, while the F_{rrw} was in the range of 330 to 420. The F_{rrw} was about 20-92 times of the

F_{rro}. The DPR effect was also observed for bulk polymer gel systems (Liang et al. 1995;

Al-Sharji et al. 1999; Willhite 2002; Seright 2009) and preformed particle gel systems

(Imqam et al. 2014). The DPR effect was also observed by Zhao et al. (2014) after

treatment with dispersed particle gels (DPG) they developed. Different mechanisms have

been proposed in the literature to interpret the special phenomenon, and a brief summary

can be found in Imqam et al. (2014).
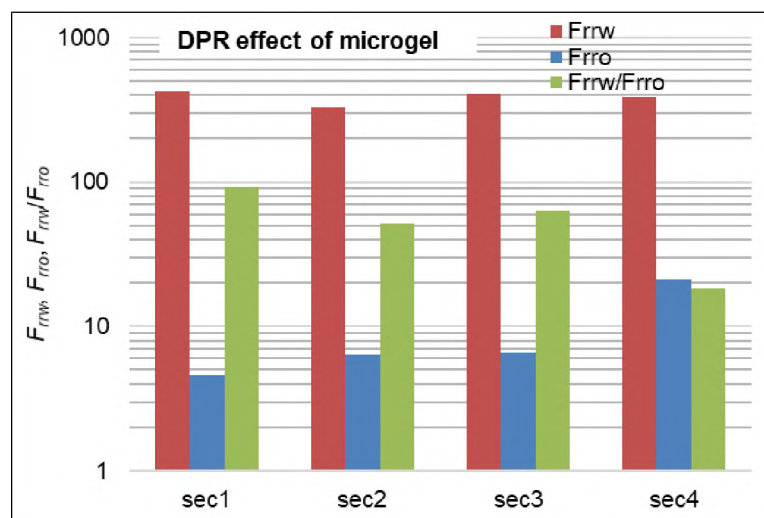
Figure 24. The disproportionate permeability reduction (DPR) effect of the microgels.
(The gels reduced the sandpack permeability to water flow much more than that to oil
flow.)

4. CONCLUSIONS

In this study, a series of experiments were carried out to investigate the transport behavior of microgels in super-K channels. Sandpacks with permeabilities ranging from 27 to 221 darcies were used to mimic the super-K channels. Multiple pressure sensors were applied along the sandpack models to monitor the propagation behavior of the microgels.

(1) The tested microgel particles could transport through the super-K channels, and a higher driving pressure gradient was required when the particle-to-pore matching size ratio (MSR) was larger. The pressure gradient distribution along the super-K channels was relatively uniform when the MSR was low (<1.3). However, the inlet section would show increasingly higher pressure gradients as the MSR was increased, indicating increased difficulty in propagation.

(2) The propagation of the gel particles was significantly slower compared with the carrying fluid. The delayed propagation behavior was more pronounced when the MSR was higher.

(3) The injection pressure was less sensitive to the injection flow rate compared with a Newtonian fluid. The gel dispersion exhibited an apparent shear thinning (pseudoplastic) behavior when transporting through the porous channels.

(4) Breakage of the gel particles was observed especially at high superficial velocities. The particle breakage was partially responsible for the apparent shear thinning behavior. The breakage phenomenon was in favor of deep placement of the gel particles.

(5) The channel permeabilities were significantly reduced by the microgels, bringing sufficient resistance to subsequent water flooding (>99.5%). At given matching

size conditions, softer gels are more likely to establish in-depth placement and uniform water-blocking capacity in the channels. The microgel particles exhibit salinity-responsive behavior to the post brine flush. It suggests that the gel particles can shrink and reswell according to the salinity of the injected water. Possibilities are discussed to utilize this salinity-responsive behavior.

(6) The microgels exhibit a particular disproportionate permeability reduction (DPR) effect. After gel injection, the channel permeability to water flow was reduced by more than 20-92 times of the permeability to oil flow.

ACKNOWLEDGEMENT

Disclaimer: "This report was prepared as an account of work sponsored by an agency of the United States Government. Neither the United States Government nor any agency thereof, nor any of their employees, makes any warranty, express or implied, or assumes any legal liability or responsibility for the accuracy, completeness, or usefulness of any information, apparatus, product, or process disclosed, or represents that its use would not infringe privately owned rights. Reference herein to any specific commercial product, process, or service by trade name, trademark, manufacturer, or otherwise does not necessarily constitute or imply its endorsement, recommendation, or favoring by the United States Government or any agency thereof. The views and opinions of authors expressed

REFERENCES

Aldhaheri, M., Wei, M., Alhuraishawy, A., Bai, B. 2021. Field Performances, Effective Times, and Economic Assessments of Polymer Gel Treatments in Controlling Excessive Water Production from Mature Oil Fields. J. Energy Resour. Technol. 143 (8): 080804. https://doi.org/10.1115/1.4049019.

Aldhaheri, M., Wei, M., Zhang, N., Bai, B. 2020. Field Design Guidelines for Gel Strengths of Profile-Control Gel Treatments Based on Reservoir Type. J Pet Sci Eng 194 (November): 107482. https://doi.org/10.1016/j.petrol.2020.107482.

Al-Ibadi, A., and Civan, F. 2013. Experimental Investigation and Correlation of Treatment in Weak and High-Permeability Formations by Use of Gel Particles. SPE Prod & Oper, 28 (04): 387-401.

Al-Sharji, H.H., Grattoni, C.A., Dawe, R.A., Zimmerman, W. R. 1999. Pore-Scale Study of the Flow of Oil and Water through Polymer Gels. Paper presented at the SPE Annual Technical Conference and Exhibition, Houston, 3–6 October. SPE-56738-MS. https://doi.org/10.2118/56738-MS.

Bai, B., Huang, F., Liu, Y., Seright, R. S., Wang, Y. 2008. Case Study on Preformed Particle Gel for in-Depth Fluid Diversion. Paper presented at the SPE Symposium on Improved Oil Recovery, Tulsa, Oklahoma, USA, 20–23 April. SPE-113997-MS. https://doi.org/10.2118/113997-MS.

Bai, B., Li, L., Liu, Y., Liu, H., Wang, Z., You, C. 2007a. Preformed Particle Gel for Conformance Control: Factors Affecting Its Properties and Applications. SPE Res Eval & Eng 10 (4): 415–422. SPE-89389-PA. https://doi.org/10.2118/89389-PA.

Bai, B., Liu, Y., Coste, J. P., Li, L. 2007b. Preformed Particle Gel for Conformance Control: Transport Mechanism Through Porous Media. SPE Res Eval & Eng 10 (2): 176–184. SPE-89468-PA. https://doi.org/10.2118/89468-PA.

Bai, B., Wei, M., and Liu, Y. 2012. Injecting Large Volumes of Preformed Particle Gel for Water Conformance Control. Oil Gas Sci. Technol.–Rev. IFP Energies Nouvelles 67 (6): 941–952. https://doi.org/10.2516/ogst/2012058.

Bai, B., Wei, M., and Liu, Y. 2013. Field and Lab Experience with a Successful Preformed Particle Gel Conformance Control Technology. Paper presented at the SPE Production and Operations Symposium, Oklahoma City, Oklahoma, USA, 23–26 March. SPE-164511-MS. https://doi.org/10.2118/ 164511-MS.

Bai, B., Zhou, J., and Yin, M. 2015. A Comprehensive Review of Polyacrylamide Polymer Gels for Conformance Control. Pet. Explor. Dev. 42 (4): 525–532. https://doi.org/10.1016/S1876-3804(15)30045-8.

Brattekås, B., Graue, A., and Seright, R. S. 2019. Low-Salinity Chase Waterfloods Improve Performance of Cr(III)-Acetate Hydrolyzed Polyacrylamide Gel in Fractured Cores. SPE Res Eval & Eng 19 (2): 331–339. SPE-173749-PA. https://doi.org/10.2118/173749-PA.

Carman, P. C. 1956. Flow of Gases Through Porous Media. London, UK: Butterworths Scientific Publications.

Chang, H., Zhang, Y., Dandekar, A., Ning, S., Barnes, J., Edwards, R., Schulpen, W., Cercone, D., Ciferno J. 2020. Experimental Investigation on Separation Behavior of Heavy-Oil Emulsion for Polymer Flooding on Alaska North Slope. SPE Prod & Oper 35 (3): 579–591. SPE-200369-PA. https://doi.org/10.2118/200369-PA.

Chauveteau, G., Tabary, R., Le Bon, C., Renard, M., Feng, Y., Omari, A. 2003. In-Depth Permeability Control by Adsorption of Weak Size- Controlled Microgels. Paper presented at the SPE European Formation Damage Conference, The Hague, 13–14 May. SPE-82228-MS. https://doi.org/10.2118/82228-MS.

Dandekar, A., Bai, B., Barnes, J., Cercone, D., Ciferno, J., Ning, S., Seright., R., Sheets, B., Wang, D., Zhang, Y. 2019. First Ever Polymer Flood Field Pilot–A Game Changer to Enhance the Recovery of Heavy Oils on Alaska's North Slope. Paper presented at the SPE Western Regional Meeting, San Jose, California, USA, 23–26 April. SPE-195257-MS. https:// doi.org/10.2118/195257-MS.

Dandekar, A., Bai, B., Barnes, J., Cercone, D., Ciferno, J., Edwards, R., Ning, S., Schulpen, W., Seright., R., Sheets, B., Wang, D., Zhang, Y. 2020. First Ever Polymer Flood Field To Enhance the Recovery of Heavy Oils on Alaska's North Slope–Pushing Ahead One Year Later. Paper presented at the SPE Western Regional Meeting, April 27-30, 2020, Bakersfield, California, USA. Note–postponed to virtual format in April 2021. SPE-200814-MS. https:// doi.org/10.2118/200814-MS.

Dandekar, A., Bai, B., Barnes, J., Cercone, D., Ciferno, J., Edwards, R., Ning, S., Schulpen, W., Seright., R., Sheets, B., Wang, D., Zhang, Y. 2021. Heavy Oil Polymer EOR in the Challenging Alaskan Arctic–It Works! Paper prepared for presentation at the Unconventional Resources Technology Conference held in Houston, Texas, USA, 26-28 July 2021. URTeC-2021-5077. https://doi.org/10.15530/urtec-2021-5077.

Dhaliwal, A., Zhang, Y., Dandekar, A., Ning, S., Barnes, J., Edwards, R., Schulpen, W., Cercone, D.P. Ciferno, J.P. 2021. Experimental Investigation of Polymer Induced Fouling of Heater Tubes in the First-Ever Polymer Flood Pilot on Alaska North Slope. SPE Prod & Oper 36 (1): 70–82. https://doi.org/10.2118/200463-PA.

Elsharafi, M. O. and Bai, B. 2013. Minimizing Formation Damage for Preformed Particle Gels in Mature Reservoirs. Paper presented at the SPE Asia Pacific Enhanced Oil Recovery Conference, Kuala Lumpur, Malaysia, 11–13 August. SPE-174645-MS. https://doi.org/10.2118/174645-MS.

Elsharafi, M. O. and Bai, B. 2016. Influence of Strong Preformed Particle Gels on Low Permeable Formations in Mature Reservoirs. Pet. Sci. 13 (1): 77–90. https://doi.org/10.1007/s12182-015-0072-3.

Farasat, A., Sefti, M.V., Sadeghnejad, S., Saghafi, H. R. 2017. Mechanical Entrapment Analysis of Enhanced Preformed Particle Gels (PPGs) in Mature Reservoirs. J Pet Sci Eng 157:441–50. https://doi.org/10.1016/j.petrol.2017.07.028.

Goudarzi, A., Zhang, H., Varavei, A., Taksaudoma, P., Hu, Y., Delshad, M., Bai, B., Sepehrnoori, K. 2015. A Laboratory and Simulation Study of Preformed Particle Gels for Water Conformance Control. Fuel 140:502–13.

Imqam, A., Aldalfag, A., Wang, Y., Bai, B. 2016. Evaluation Of Preformed Particle Gels Penetration into Matrix for a Conformance Control Treatment in Partially Open Conduits. Paper presented at the SPE Annual Technology Conference and Exhibition, Dubai, UAE. SPE-181545-MS. https://doi.org/10.2118/181545-MS.

Imqam, A., Bai, B., and Delshad, M. 2018. Micro-Particle Gel Transport Performance Through Unconsolidated Sandstone and Its Blocking to Water Flow During Conformance Control Treatments. Fuel 231 (1 November): 479–488. https://doi.org/10.1016/j.fuel.2018.05.099.

Imqam, A., Bai, B., Xiong, C., Wei, M., Delshad, M., Sepehrnoori, K. 2014. Characterizations of Disproportionate Permeability Reduction of Particle Gels through Fractures. Paper presented at the SPE Asia Pacific Oil & Gas Conference and Exhibition held in Adelaide, Australia. 14–16 October. SPE-171531-MS. https://doi.org/10.2118/171531-MS.

Kang, W., Kang, X., Lashari, Z.A., Li, Z., Zhou, B., Yang, H., Sarsenbekuly, B. Aidarova, S. 2021. Progress of Polymer Gels for Conformance Control in Oilfield. Adv Colloid Interface Sci 289 (March): 102363. https://doi.org/10.1016/j.cis.2021.102363.

Larkin, R. J. and Creel, P. G. 2008. Methodologies and Solutions to Remediate Inner-Well Communication Problems on the SACROC CO2 EOR Project: A Case Study. Paper presented at the SPE Symposium on Improved Oil Recovery, Tulsa, Oklahoma, USA, 20–23 April. SPE-113305-MS. https://doi.org/10.2118/113305-MS.

Leng, J., Wei, M., and Bai, B. 2021. Review of Transport Mechanisms and Numerical Simulation Studies of Preformed Particle Gel for Conformance Control. Journal of Petroleum Science and Engineering, 109051. (In press; published online 6 June 2021) https://doi.org/10.1016/j.petrol.2021.109051.

Liang, J.-T., Sun, H., and Seright, R.S. 1995. Why Do Gels Reduce Water Permeability More Than Oil Permeability? SPERE 10 (4): 282–286; Trans., AIME, 299. SPE-27829-PA. https://doi.org/10.2118/27829-PA.

Li, J., Niu, L., and Lu, X. 2019. Migration Characteristics and Deep Profile Control Mechanism of Polymer Microspheres in Porous Media. Energy Sci Eng 7 (5): 2026–2045. https://doi.org/10.1002/ese3.409.

Liu, Y, Bai, B., and Shuler, P.L. 2006. Application and Development of Chemical-Based Conformance Control Treatments in China Oil Fields. Paper presented at the SPE/DOE Symposium on Improved Oil Recovery, Tulsa, 22–26 April. SPE-99641-MS. https://doi.org/10.2118/99641-MS.

Liu, Y., Hou, J., Wang, Q., Liu, J., Guo, L., Yuan, F., Zhou, K. 2017. Flow of Preformed Particle Gel through Porous Media: A Numerical Simulation Study Based on the Size Exclusion Theory. Ind Eng Chem Res 56:2840–50. https://doi.org/10.1021/acs.iecr.6b03656.

Mauran, S., Rigaud, L., and Coudevylle, O. 2001. Application of the Carman-Kozeny Correlation to a High-Porosity and Anisotropic Consolidated Medium: The Compressed Expanded Natural Graphite. Transp Porous Media 43 (2): 355–376. https://doi.org/10.1023/A:1010735118136.

Ning, S., Barnes, J., Edwards, R., Schulpen, W., Dandekar, A., Zhang, Y., Cercone, D., Ciferno, J. 2020. First Ever Polymer Flood Field Pilot to Enhance the Recovery of Heavy Oils on Alaska North Slope–Producer Responses and Operational Lessons Learned. Paper presented at the SPE Annual Technical Conference and Exhibition, Virtual, 26–29 October. SPE-201279-MS. https://doi.org/10.2118/201279-MS.

Peirce, J. W., Hutcherson, M. R., Jensen, M. D., Brice, B. W., Vasquez, J. E., Woods, A. 2014. An Overview of Conformance Control Efforts for the West Sak Field on the North Slope of Alaska. Paper presented at the SPE Improved Oil Recovery Symposium, Tulsa, Oklahoma, USA, 12–16 April. SPE-169073-MS. https://doi.org/ 10.2118/169073-MS.

Pyziak, D. and Smith, D. 2007. Update on Anton Irish Conformance Effort. Paper presented at the 6th International Conference on Production Optimization-Reservoir Conformance-Profile Control-Water and Gas Shutoff, Houston, Texas, USA, 6–7 November.

Saghafi, H. R. 2018. Retention Characteristics of Enhanced Preformed Particle Gels (PPGs) in Porous Media: Conformance Control Implications. J Pet Sci Eng 166:962–8. https://doi.org/10.1016/j.petrol.2018.03.098.

Seright, R. S. 1997. Use of Preformed Gels for Conformance Control in Fractured Systems. SPE Prod Facil 12(01): 59–65. SPE-35351-PA. https://doi.org/10.2118/35351-PA.

Seright, R. S. 1999. Mechanism for Gel Propagation Through Fractures. Paper presented at the SPE Rocky Mountain Regional Meeting, Gillette, Wyoming, USA, 15–18 May. SPE-55628-MS. https://doi.org/10.2118/55628-MS.

Seright, R. S., Lane, R. H., and Sydansk, R. D. 2003. A Strategy for Attacking Excess Water Production. SPE Prod & Fac 18 (3): 158–169. SPE-84966-PA. https://doi.org/10.2118/84966-PA.

Seright, R. S. 2009. Disproportionate Permeability Reduction with Pore-Filling Gels. SPE J 14 (1): 5–13. SPE-99443-PA. http://dx.doi.org/10.2118/99443-PA.

Seright, R. S, and Brattekas, B. 2021. Water Shutoff and Conformance Improvement: An Introduction. Pet. Sci. 18, 450–478. https://doi.org/10.1007/s12182-021-00546-1.

Sydansk, R. D. and Romero-Zeron, L. 2011. Reservoir Conformance Improvement. Richardson, Texas, USA: Society of Petroleum Engineers.

Targac, G., Gallo, C., Smith, D., Huang, C. K., Autry, S., Peirce, J., Li, B. 2020. Case History of Conformance Solutions for West Sak Wormhole/Void Space Conduit with a New Reassembling Pre-Formed Particle Gel RPPG. Paper presented at the SPE Annual Technical Conference and Exhibition, Virtual, 26–29 October. SPE-201302-MS. https://doi.org/10.2118/201302-MS.

Vasquez, J. E., Dalrymple, E. D., Abbasy, I., Eoff L. S. 2008. Laboratory Evaluation of Water Swellable Materials for Fracture Shutoff. Paper presented at the SPE North Africa Technical Conference and Exhibition, Marrakech, Morocco, 12–14 March. SPE-111492-MS. https://doi.org/10.2118/111492-MS.

Villone, M. M. and Maffettone, P. L. 2019. Dynamics, Rheology, and Applications of Elastic Deformable Particle Suspensions: A Review. Rheol Acta 58 (3–4): 109–130. https://doi.org/10.1007/s00397-019-01134-2.

Wang, J., Zhang, H., Liu, H., Zhao, W., Liu, H., Yao, C., Zheng, J., Shen, Y. 2017. Quantification of Transportation of Deformable Gel Particles in Porous Media. Paper presented at the SPE Annual Technical Conference and Exhibition held in San Antonio, Texas, USA, 9-11 October. SPE-187266-MS. https://doi.org/10.2118/187266-MS.

Willhite, G. P., Zhu, H., Natarajan, D., McCool, C. S., Green, D. W. Mechanisms Causing Disproportionate Permeability in Porous Media Treated with Chromium Acetate/HPAAM Gels. SPE J. 7 (1): 100–108. SPE-77185-PA. https://doi.org/10.2118/77185-PA.

Wu, D., Zhou, K., Hou, J., An, Z., Zhai, M., Liu, W. 2021. Review of Experimental and Simulation Studies of Enhanced Oil Recovery Using Viscoelastic Particles. J Dispers Sci Technol 42(07): 956-969.

Yao, C., Lei, G., Li, L., Gao, X. 2012. Selectivity of Pore-Scale Elastic Microspheres as a Novel Profile Control and Oil Displacement Agent. Energ Fuel 26: 5092–101. https://doi.org/10.1021/ef300689c.

Yao, C., Lei, G., Cathles, L. M., Steenhuis, T. S. 2014. Pore-Scale Investigation of Micron-Size Polyacrylamide Elastic Microspheres (MPEMs) Transport and Retention in Saturated Porous Media. Environ Sci Technol 48:5329–35.

Yao, C., Wang, D., Wang, J., Hou, J., Lei, G., Steenhuis, T. S. 2017. Effect of Ionic Strength on the Transport and Retention of Polyacrylamide Microspheres in Reservoir Water Shutoff Treatment. Ind Eng Chem Res 56:8158–68. https://doi.org/10.1021/acs.iecr.7b01588.

Yao, C., Liu, B., Li, L., Zhang, K., Lei, G., Steenhuis, T. S. 2020. Transport and Retention Behaviors of Deformable Polyacrylamide Microspheres in Convergent-Divergent Microchannels. Environ Sci Technol 54:10876–84. https://doi.org/10.1021/acs.est.0c02243.

Zhao, G., Dai, C., and Zhao, M. 2014. Investigation of the Profile Control Mechanisms of Dispersed Particle Gel. PLoS One. 9, e100471.

Zhao, Y., Leng, J., Lin, B., Wei, M., Bai, B. 2021a. Experimental Study of Microgel Conformance-Control Treatment for a Polymer-Flooding Reservoir Containing Superpermeable Channels. SPE J. SPE-205486-PA (in press; posted 26 April 2021). https://doi.org/10.2118/205486-PA.

Zhao, Y., Yin, S., Seright, R. S., Ning, S., Zhang, Y., Bai, B. 2021b. Enhancing Heavy-Oil-Recovery Efficiency by Combining Low-Salinity-Water and Polymer Flooding. SPE J. 26 (03): 1535–1551. SPE-204220-PA. https://doi.org/10.2118/204220-PA.

Zhou, K., Hou, J., Sun, Q., Guo, L., Bing, S., Du, Q., Yao, C. 2017. An Efficient LBM-DEM Simulation Method for Suspensions of Deformable Preformed Particle Gels. Chem Eng Sci 167:288–96. https://doi.org/10.1016/j.ces.2017.04.026.

III. SELECTIVE PENETRATION OF MICROGELS IN SUPERPERMEABLE CHANNELS AND RESERVOIR MATRICES

ABSTRACT

Gel treatment is an effective way to attack excessive water production in many mature oilfields around the world. Selective penetration is desired for successful gel treatments. That is, the gel materials should easily penetrate the target zones (i.e., the channeling features such as superpermeable channels) without entering/damaging the nontarget zones (i.e., the matrices or oil zones). This study revealed that the presence of threshold penetration pressure (ΔP_{th}) was the underlying mechanism of selective penetration behavior of the tested microgels (micrometer-sized preformed particle gels). The concept of ΔP_{th} was utilized to figure out favorable working conditions for effective gel treatments. Microgel dispersions were injected into superpermeable (super-k) sandpacks (mimicking super-k channels in reservoirs, 60-221 darcies), heterogeneous models with super-k channels (79-230 darcies), and sandstone cores (mimicking matrices in reservoirs, 50-5000 md). The results demonstrated that a minimum differential driving pressure (i.e., the threshold penetration pressure, ΔP_{th}) was required to push the microgel particles to penetrate the channels or matrices. The critical penetration behavior was closely related to the particle-to-pore matching-size ratio (MSR). The ΔP_{th} at the inlet faces of super-k channels (60-230 darcies) was in the range of 1 to 12 psi with MSRs in the range of 0.6 to 1.8. The low ΔP_{th} was beneficial to allow easy penetration of gel materials into the channeling zones. On the contrary, the ΔP_{th} was much higher in the cores with relatively low permeabilities and high MSRs (ΔP_{th}>200 psi when MSR>6.5 for the tested gels). The

high ΔP_{th} was desirable to prevent gel materials from massively invading and damaging the matrices. Instead, the gel particles accumulated at the inlet surface, and a gel cake was gradually formed. The cake further prevented the invasion of the gels. The cake could be removed by chemical breakers to resume the injectivity/productivity of the matrices. Correlations were developed to describe the ΔP_{th}-MSR relationship. When MSR<3, the ΔP_{th} exponentially increased with the MSR. A distinct transition was identified at the MSR of about 3. When MSR>3, the ΔP_{th} became less sensitive to the MSR, but it still exponentially increased with the MSR. When MSR>20, the ΔP_{th} was higher than 1200 psi. Therefore, this study provided quantitative evidence to demonstrate the selective penetration of the tested microgels. Also, this work could help identify the favorable conditions to achieve successful gel treatments. In an effective conformance treatment, the MSR in the channel should be sufficiently low to allow easy penetration of gel materials into the channel (e.g., MSR<2 in this study). Meanwhile, the MSR in the matrix should be large enough to support a high ΔP_{th} and thus prevent massive gel invasion into the matrix.

Key words: Enhanced oil recovery; conformance control; gel treatment; preformed particle gel; microgel

1. INTRODUCTION

Excessive water production is a big challenge and is commonly encountered in oil fields around the world. Fractures and fracture-like features present in a reservoir are among the major reasons that responsible for the excessive water production. The first-ever polymer flooding project has been on going to develop the abundant heavy oil resources

on the Alaska's North Slope (Dandekar et al. 2019, 2020, 2021; Ning et al. 2020).

Conformance control is an important aspect to ensure the success of polymer flooding in

the heavy oil reservoirs, especially when channels features are present in the reservoirs

(Zhao et al. 2021a). As illustrated in Figure 1a, the flooding fluid (water, polymer solution,

etc.) would channel through the super-k channels, leaving a large portion of oil in the

matrices unswept. Gel treatment has been proven effective to block the fractures and

fracture-like features in reservoirs and improve the conformance. Different gel products

have been developed over the last several decades (Seright & Brattekas 2021; Zhu et al.

2017; Kang et al. 2021), such as in-situ gels (Sydansk & Romero-Zeron 2011), preformed

bulk gels (Seright 1997), and preformed particle gels (Bai et al. 2007a, 2008, 2012, 2013).

Each gel system has its own unique characteristics and advantages (e.g., thermal stability,

tolerance to high salinity, strength, injectivity, etc.) to accommodate different reservoir

situations (e.g., sources of excessive water production, channeling types, temperature,

salinity, well types, well completion, etc.) (Seright & Brattekas 2021; Zhu et al. 2017).

(a) A super-k channel is present in the reservoir.   (b) The channel is shut off with gels.
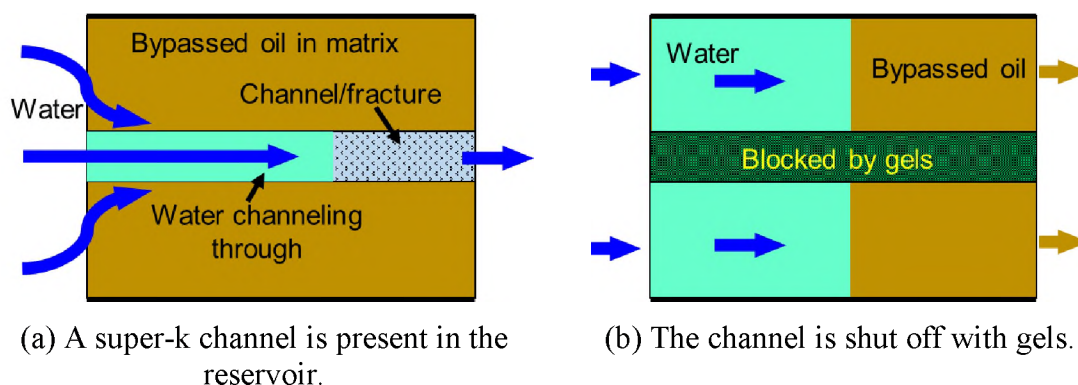
Figure 1. Gel treatment to reduce the unwanted water production and improve the effective sweep volume. (a) A super-k channel or open fracture is present in the reservoir. Water, polymer, or other flooding fluids flow through the super-k channels. The oil in the matrices is bypassed. (b) The channel is shut off with gels. The subsequent flooding fluids are forced into the matrices to displace the bypassed oil.

Selective penetration of gel materials is desired for successful gel treatments. That is, the gel materials should easily penetrate the target zones (i.e., the channeling features such as super-k channels) without entering/damaging the nontarget zones (i.e., the matrices or oil zones). In an effective gel treatment, as shown in Figure 1b, the gel materials are expected to efficiently shut off the super-k features, and thus the subsequent flooding fluid can be diverted to the matrices to displace the remaining oil previously left behind (Zhao et al. 2021a). For particulate gels, some researchers have studied the driving pressures that are required to push the viscoelastic particles to transport through pore throats on different scales. Pore-scale experimental studies (Bai et al. 2007b; Yao et al. 2014, 2020; Wang et al. 2017; Zhao et al. 2018) and numerical studies (Liu et al. 2017; Zhou et al. 2017; Lei et al. 2019) shed light on the understanding of the transport, plugging, and remigration behavior of the viscoelastic particles through pore-throat structures. Besides, studies outside the oil industry also provides insights to the transport mechanisms of microgel particles through microchannels analogous to a pore throat. Interested readers are encouraged to reach the following articles as a start for more information: Hendrickson and Lyon (2010), Zhang et al. (2018) and Villone and Maffettone (2019).

The resistance forces applied on the particle include the structural forces by the pore-throat walls, and the frictional forces by the pore-throat surfaces, while the driving force is from the drag of the carrying fluid. When the gel particle is larger than the pore throat, additional forces are required to make it deform in order to pass through the throat. The maximum resistance is believed to occur as the particle right in the middle of the throat (narrowest spot) (Yao et al. 2014; Wang et al. 2017; Zhao et al. 2018). Therefore, a minimum differential driving pressure is required to make the particle deform and

overcome the maximum resistance. Thus, the particle can pass through the throat. Different terms are used to denote this minimum differential pressure, e.g., critical pressure, threshold pressure, restarting pressure and remigration pressure. In our work, the term threshold pressure (ΔP_{th}) is adopted. Below the threshold pressure, the gel particle will be entrapped at pore throat and cannot transport downstream. This behavior is desired in the low-permeability zones (oil zones). In these zones, the threshold pressure should be sufficiently high to prevent the gel materials invading or damaging the oil zones. On the other hand, the threshold pressure in the channeling zones should be practically low to allow good injectivity and migration of the gel materials. Thus, the threshold penetration pressure is an important parameter to determine the effectiveness of a gel treatment.

In the literature, the critical migration condition is also described with the concept of critical pressure gradient, which is practically more meaningful. On the core- or reservoir-scale, a gel particle dispersion is injected into a medium with multiple pore throats, rather than a single/dispersed particle through a single pore throat. The transport behavior is a result of the statistical average of groups of particles behavior and their interactions. Bai et al. (2007b) reported that the pressure gradient increased with the strength and the diameter ratio of the particle to the pore throat size. For weak particles, the break-and-pass pattern would occur when the pressure gradient exceeded a critical value. Deform and pass pattern of microspheres through pore throats was observed by Yao et al. (2014). When the sufficient driving pressure gradient was available, the microspheres would deform and change it shape to an ellipsoid, and then pass the throat. Afterwards, the particle would quickly recover most of its original shape and size. Li et al. (2015) investigated the transport behavior of a single hydrogel particle through a single narrow

capillary with a constriction. Their study suggests that the differential driving pressure, and the dehydration degree (volume shrinkage) depended only on the confinement degree (i.e., particle/capillary size ratio) and the geometry of tapered region. They were independent of the strength (composition) of the particles, and they were also independent of the composition of the particles or the solvent. Wang et al. (2017) studied the transport behavior of gel particles using a capillary tube with a convergent-divergent structure. The gel particles they used were relatively strong (2.2, 4.8, and 6.4 kPa), and the diameter was about 1 mm. As later reported by Zhao et al. (2018), the maximum pressure drop across the capillary model was regarded as the threshold pressure [termed as restarting pressure in their subsequent work, Zhao et al. (2018)]. The superficial velocity was quite high at the throat in their experiments (~60 ft/d at the throat). They investigated the impact of particle size, pore size, particle strength, frictional coefficient, and Poisson's ratio on the restarting pressure. Lei et al. (2019) reported a power-law relationship between the critical differential pressure (i.e., ΔP_{th}) and the elastic modulus (Young's modulus) and particle/throat size ratio.

Recently, we developed sandwich-like channel models that mimicked heterogeneous reservoirs containing super-k channels (Zhao et al. 2021a). The results demonstrated that, at proper conditions, the conformance and the oil recovery performance of polymer flooding in such heterogeneous heavy oil reservoirs could be improved with microgels. The microgels did not penetrate the matrices because a gel cake built up at the matrix faces. Instead, the microgel particles selectively penetrated and shut off the superpermeable channels. The subsequent polymer solution was forced into the matrices to displace the remaining oil. It would be beneficial to figure out the underlying

mechanism(s) and favorable working conditions of the selective penetration behavior in microgel treatments.

In this work, microgel dispersions were injected into super-k sandpacks (mimicking super-k channels in reservoirs, 60-221 darcies), heterogeneous models with super-k channels (79-230 darcies), and sandstone cores (mimicking matrices in reservoirs, 50-5000 md). The threshold penetration pressures were determined. Correlations were developed to describe the relationship between the threshold penetration pressure and the particle-to-pore matching-size ratio (MSR). Favorable conditions were discussed to achieve satisfactory conformance control treatments.

2. EXPERIMENTAL AND METHODOLOGY

Microgels. The microgels were obtained by grinding dry millimeter-sized preformed particle gels into different size categories. As shown in Figure 2, the microgels had a volumetric swelling ratio of 20 cm^3/cm^3 in synthetic formation brine (SFB, TDS=27500 ppm) of the Milne Point oilfield. The brine composition of the SFB was shown in Table 1. The swelling ratio was defined as the ratio of swollen volume after absorbing water to the original volume of the gel. Microgel dispersions were prepared with the SFB with a dry gel concentration of 1 wt%. More information about the brine, microgel and other materials can be found in our recent publications (Zhao et al. 2021a, 2021b; Bai et al. 2007a).

Superpermeable Sandpacks, Channel Models, and Matrix Models. Different models were used to investigate the penetration behavior of the microgels in super-k

channels and reservoir matrices. Sandpacks were used to mimic the super-k channels present in reservoirs. Sands with different size ranges were used to prepare the sandpacks. Larger sands resulted in higher permeabilities of the sandpacks. The permeabilities were in the range of 60 to 221 darcies. Sandwich-like channel models were also used to mimic heterogeneous reservoirs containing super-k channels. A typical channel model consisted of two half-cylindrical cores (mimicking reservoir matrices) and a super-k channel between the core plugs. The channel was created by filling sand grains in the fracture space between the core plugs. Detailed preparation processes of the channel models could be found in Zhao et al. (2021a). The permeabilities of the channels were in the range of 79 to 228 darcies. Berea and Boise sandstone cores were used to mimic the reservoir matrices with relatively low permeabilities (50-5000 md). The key information of the experiments was summarized in Table 2. The average pore sizes were estimated with modified Carman-Kozeny equation (Zhao et al. 2021a). The MSRs in the different experiments were also listed in the table.

Table 1. Brine composition.

Name	Properties	Composition (ppm)
HSW (SFB, synthetic formation brine)	TDS=27500 ppm Ionic strength=0.492 Hardness: 1700 ppm	Na^+: 10086.0 K^+: 80.2 Ca^{2+}: 218.5 Mg^{2+}: 281.6 Cl^-: 16834.4

Experiment Setup and Procedures. The experiment setup was shown in Figure 3. The sandpack models had multiple pressure taps which were able to monitor the pressures at different locations in the sandpack. The microgel dispersion was injected until stable pressures were established at all the pressure taps. The pressure response was an indicator of the gel transport in the sandpack. The time when the pressures at different locations began to increase was recorded. The onset of pressure increase indicates the microgel bank front arrived at that pressure tap.
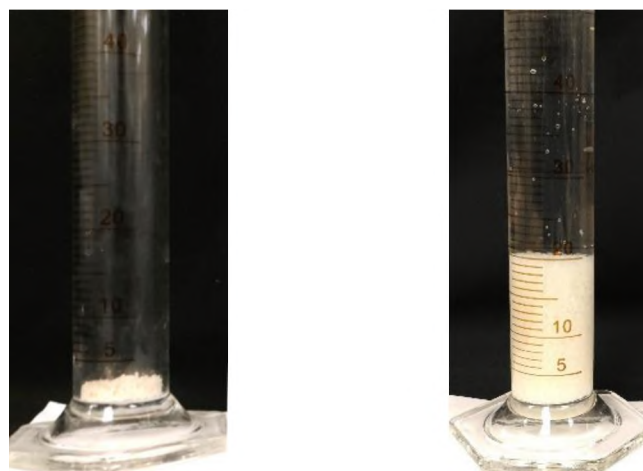
(a) Dry microgel particles.   (b) Swelling microgel in brine.

Figure 2. Dry and swollen microgels in the SFB.
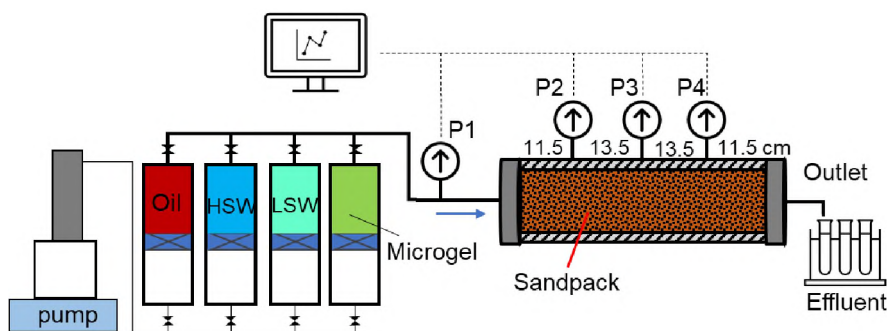
Figure 3. Experiment setup for microgel transport tests.

Table 2. Summary of basic information of the experiments.

Number	Model type	K, darcy	Average particle size D_g, µm	Average pore size D_p, µm	MSR
1	Super-k sandpack	221	150	218.90	0.69
2	Super-k sandpack	62	130	116.81	1.11
3	Super-k sandpack	62.4	150	117.18	1.28
4	Super-k sandpack	60	150	114.84	1.31
5	Super-k sandpack	59.8	205	115.51	1.77
6	Intact core	4.74	136	33.74	4.03
7	Intact core	4.00	205	31.18	6.57
8	Intact core	4.28	290	32.12	9.03
9	Intact core	0.70	136	14.35	9.48
10	Intact core	0.44	205	11.77	17.41
11	Intact core	0.69	290	14.18	20.46
12	Intact core	0.37	290	10.77	26.93
13	Intact core	0.091	205	6.01	34.13
14	Intact core	0.052	290	4.53	64.04
15	Channel model	228	136	206.11	0.66
16	Channel model	221	136	203.12	0.67
17	Channel model	87	136	127.57	1.07
18	Channel model	179	205	181.86	1.13
19	Channel model	139	205	161.11	1.27
20	Channel model	218	290	202.31	1.43
21	Channel model	212	290	200.32	1.45
22	Channel model	79	205	121.55	1.69

3. RESULTS AND DISCUSSION

3.1. THE THRESHOLD PENETRATION PRESSURES

Microgel dispersions were injected into super-k sandpacks to test the critical penetration behavior of the microgels. Exp #4 was taken as an example to show how the threshold penetration pressures of the microgel particles were determined. In this experiment, the gel dispersion was injected at constant flow rate of 2 ml/min (19.3 ft/d). The average MSR was 1.31. The pressure responses at different locations were shown in Figure 4. Obviously, the pressure at the inlet (P1) increased immediately as the gel dispersion was injected into the model. Meanwhile, the pressure readings at the other locations (P2, P3 and P4) showed no increase. As the gel dispersion was continuously injected, the other pressure sensors responded sequentially as the gel particles transported to the corresponding pressure taps. The pressure response was an indication of the transport location of the gel bank front.
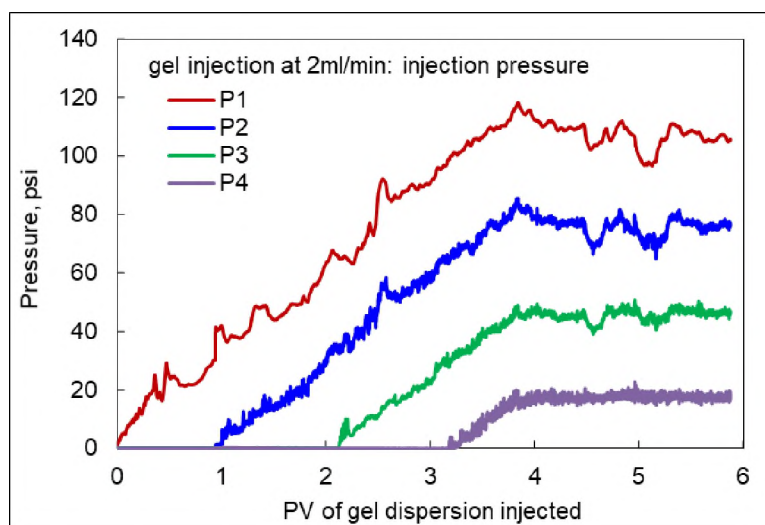
Figure 4. Pressure responses at different locations (Exp #4).

Determination of the Threshold Penetration Pressures. A close examine of the pressure response revealed that the pressures (P1 to P4) increased monotonically at the beginning (Figure 5). When exceeding certain values (e.g., 5.02 psi for P1 in this experiment), the pressures began to exhibit obvious fluctuations. The pressure fluctuations were a macroscopic reflection of the microscopic entrapment-remigration behavior of the gel particles at the pore throats near the inlet surface. As mentioned in the introduction section, the resistances acting on the particles mainly included the structural resistance by pore-throat walls, and the frictional resistance by pore-throat surfaces. The low injection pressure at the early stage was insufficient to overcome the resistances. Thus, the particle or particle groups (i.e., a particle cluster) could not pass the throats. As more particles accumulated, the injection pressure increased to a critical value that was sufficient to overcome the maximum resistance (encountered near the narrowest location of the throat). The driving pressure pushed the particle or particle cluster to pass through the narrowest spot of the throat. Afterwards, the resistances to the particle/cluster were suddenly released (reduced). Accordingly, the injection pressure would rapidly drop, which exhibited as a fluctuation in the macroscopic parameter of pressure (Figure 5). The release of the resistances has been demonstrated in pore-scale studies (Yao et al. 2020; Zhou et al. 2017; Zhao et al. 2018). For a single gel particle or a group of particles, the resistances increase as the particle approaches the middle of the throat. Once past the middle (narrowest) spot, the resistance would significantly decrease.

The pressure at the onset of fluctuation was regarded as the threshold (minimum) pressure (ΔP_{th}) for the microgel particles to penetrate the porous channels or matrices. Figure 5 shows the onsets of the pressure fluctuations and the corresponding threshold

penetration pressures at different locations in Exp #4. The ΔP_{th} had a close relationship with the particular pass/plugging patterns of the elastic gel particles in the pore throats of porous media. The flow paths in a porous medium consisted of a series of convergent-divergent structures (i.e., pore throats). The gel particles would be trapped at the pore throats when the driving differential pressure was below the threshold pressure.
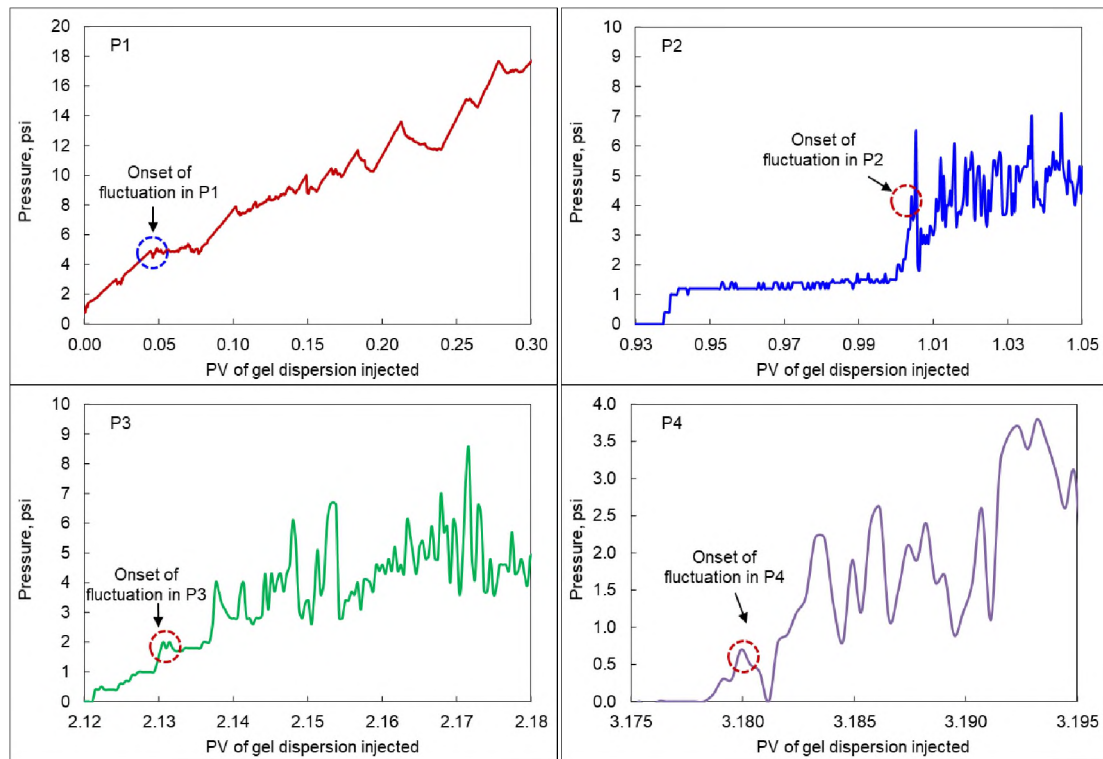
Figure 5. Threshold penetration pressures at different locations indicated by the onset of pressure fluctuation (Exp #4).

Different trapping mechanisms could contribute to the retention of the gel particles in the pore throats depending on the particle size relative to the throat size, the dispersion concentration, and other factors (Bai et al. 2007b; Yao et al. 2014, 2020). For large particles relative to the throat sizes, direct entrapment of the particles at the throat was significant.

A driving pressure was required to push the particles to pass through the pore throat. This was achieved by deforming or shrinking (i.e., compressing and dehydrating) the particles, or/and even breaking the particles into smaller pieces as observed by Bai et al. (2007b). In any pass patterns, an additional driving pressure was required. The scenario could also be explained from the energy conversion perspective. For example, in the deforming case, the deformation energy of the elastic particle was involved as the external force worked on the particle to make it deform and thus pass through the pore throat. Another plugging mechanism was related to the interactions among a group of particles at the pore throats. Some researchers further divided this type of plugging pattern into different subgroups, such as superposition plugging and bridge plugging (Yao et al. 2020). Distinguishing them on the core scale was practically difficult. Nevertheless, additional external forces (driving pressure) were required to destruct the particle clusters accumulated at the pore throat. Thus, the microgel particles could propagate through the pore throats (corresponding to the macroscopic penetration behavior at the inlet surfaces of channels or matrices).
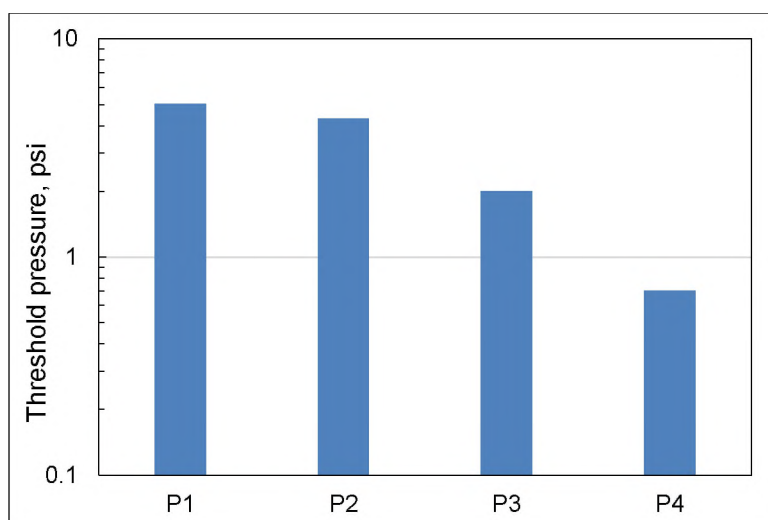
Figure 6. Threshold penetration pressures at different transport distance (Exp #4).

Lower ΔP_{th} Inside the Porous Channels. The ΔP_{th} showed a decreasing trend as the microgel particles transported deeper into the porous medium (Figure 5). The trend was more evident as shown in Figure 6. The threshold pressures at the four different locations were 5.02 psi, 4.30 psi, 2.00 psi and 0.70 psi, respectively. The inside average ΔP_{th} was 2.33 psi, which was lower than the value at the inlet face (5.02 psi). Similarly, the threshold pressures at the inlet and inside average values in the other four experiments using super-k sandpacks were obtained.

Figure 7 plots the threshold pressure as a function of the particle/pore matching size ratio (MSR). The inside threshold pressures were obtained by averaging the threshold pressures monitored at P2, P3 and P4. Generally, the threshold pressure exhibited a decreasing trend as the particles transporting deeper into the porous media. This was probably due to the breakage of the particles under the shearing effect. The particles would break into smaller particles as they transported through the porous media especially at high flow rates. Another possible reason was the adaptive behavior of the particles when transporting in the porous media. At the very beginning before entering the porous media, the particles had their original shape. Once entering the pore spaces, the viscoelasticity property made the particles adapt their geometry to the configuration of the pore-throat structures (A Newtonian fluid, e.g., water, could completely adapt to the flow pathways.). The axial dimension (in the migration direction) was increased, while the radial dimension was reduced. Thus, the gel particles were trained by the flow pathways to have a shape like an amoeba and wormhole through the porous media. Consequently, the resistances against the migration of the particle were reduced. Figure 7 also suggested that the threshold pressure increased with the MSR. That is, higher threshold pressures were required to drive

larger gel particles to penetrate the porous channels. The impact of the MSR was further studied in subsequent sections.
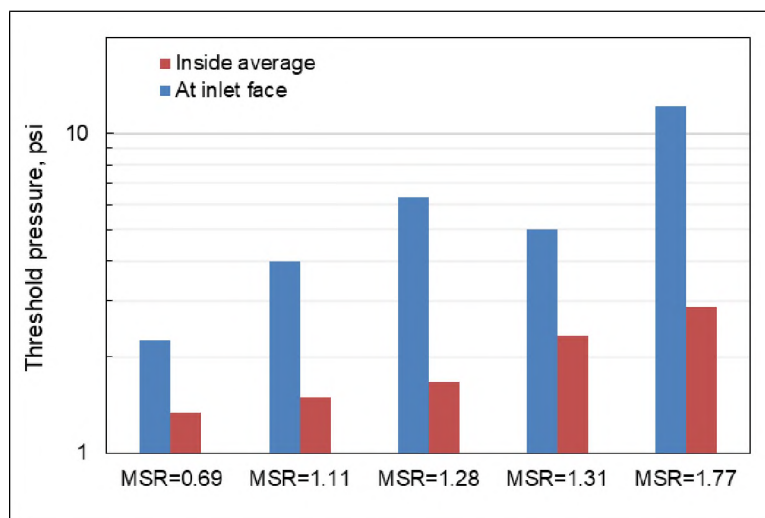
(a) Column plot.
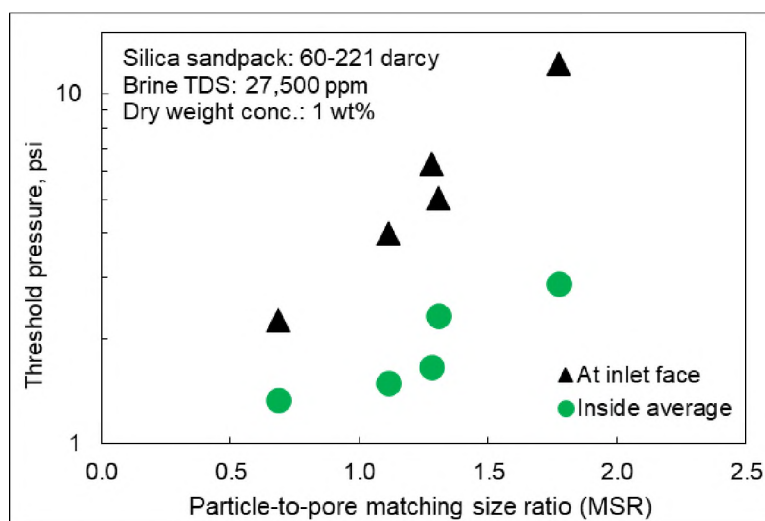
(b) Scatter plot.

Figure 7. The threshold penetration pressures at different MSRs.

Threshold Penetration Pressures in Homogeneous Cores and Channel Models. For the intact core models, which simulated the matrices in reservoirs, the gel particles were

very large relative to the pore throats (MSR>4). High threshold penetration pressures were required as shown in Figure 8. The gels were difficult in entering the cores. Instead, the gels accumulated at the inlet surfaces, and a gel cake was gradually formed (see Figure 9 as an example). The cake further prevented the gel particles from penetrating the cores. The low penetration into the matrices was desirable to avoid massive formation damage.

For the channel models, as shown in Figure 10, the gels could not enter the matrices due to the high threshold pressure. Similar as observed in the homogeneous core models, a gel cake formed at the inlet surfaces of the matrices. On the contrary, the gels could easily penetrate the channel due to the low threshold penetration pressure in the channel (5.0 psi). Consequently, the gels selectively entered and placed in the super-k channel. The selective penetration feature of the gels was favorable for successful gel treatments. Figure 8 summarizes the inlet threshold pressures in all the experiments. The results were further discussed in the next subsection.
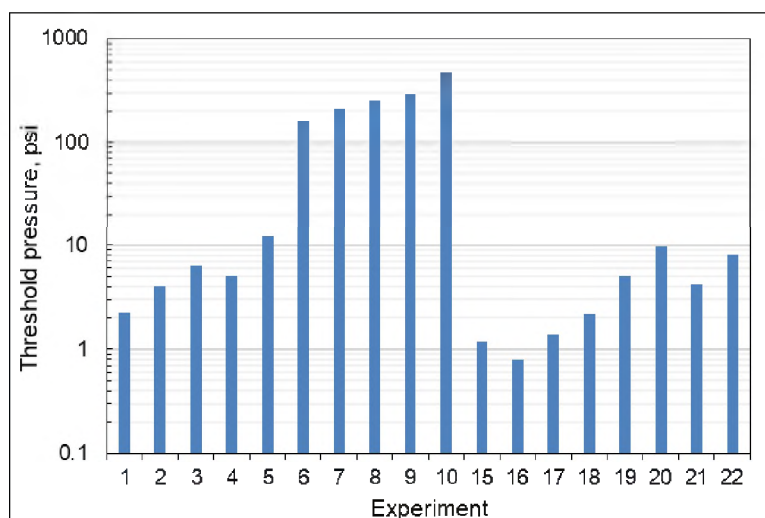
Figure 8. Summary of threshold pressures in different experiments. (In experiments #11 to #14, the values were higher than 1200 psi. However, no accurate threshold pressures were detected because the injection pressure exceeded the preset equipment limit.)

Figure 9. Gel cake formed at the inlet surface of an intact core (Exp #11, 693 md, MSR=20.46). (Due to the large gel particle sizes relative to the pore throats in the core, a high threshold penetration pressure, larger than 1200 psi, was required to drive the gel particles to invade the core. The gel particles accumulated at the inlet surface, and a gel cake was gradually formed. The gel cake further prevented the gel particles from entering the core.)

Figure 10. Gel cake formed at the inlet surface of a channel model (Exp #19, 139 darcies, MSR=1.27, matrices 167 md). [Due to the high threshold pressure at the inlet surface of the matrices, a cake formed and further prevented the gels invading into the matrices. On the other hand, the low threshold pressure in the channel (5.0 psi) allowed easy penetration of the gels into the channel. As a result, the microgels selectively penetrated and placed in super-k channel. After the gel treatment, the cake could be removed by soaking with chemical breakers to resume the injectivity of in the matrices. The selective penetration behavior was also observed in microgel treatment experiments in polymer flooding (Zhao et al. 2021a).]

3.2. IMPACT OF PARTICLE/PORE MATCHING SIZE RATIO (MSR)

The aforementioned results indicate that the MSR significantly influences the penetration behavior of gels into channels and reservoir matrices. It is important to figure out under what conditions the gels can selectively penetrate the super-k channels without massive invasion into the reservoir matrices. The threshold penetration pressures in the different experiments were plotted against the MSR, as shown in Figure 11. Correlations were developed to describe the relationship between the ΔP_{th} and the MSR. The super-k channels covered permeabilities in the range of 60-230 darcies. The MSRs ranged from 0.66 to 1.77 (Table 2). The core models (matrices) covered permeabilities in the range of 50-5000 md. The MSRs ranged from 4.03 to 64.04. When the MSRs were larger than 20 (Exp #11 to Exp #14), the threshold penetration pressures were higher than 1200 psi.
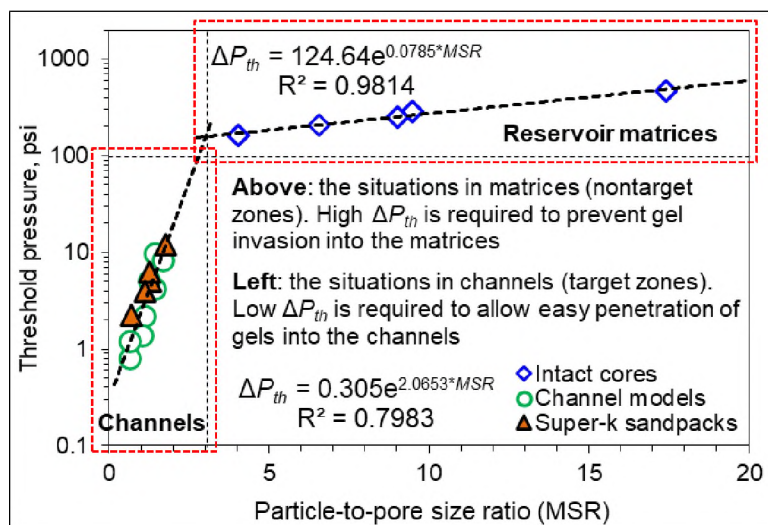
Figure 11. Relationship between the threshold penetration pressure and the MSR.

Low ΔP_{th} in Super-k Channels. Figure 11 elucidates the impact of the matching size on the threshold penetration pressure. In the super-k channels, the MSRs are relatively

low (<2). The threshold pressures are generally below 15 psi. The threshold pressure follows an exponential relationship with the MSR. Their relationship can be described quite well with Equation (1). In the equation [as well as in Equation (2)], R_r was the average MSR in the porous channels or reservoir matrices. For a given particle gel system, the matching relationship of the threshold pressure and the permeability of the channel can be easily estimated. Thus, the threshold penetration pressure in the target channel can be evaluated with the correlation [Equation (1)].

$$\Delta P_{th} = 0.305 \exp\left(2.0653 R_r\right), \ R_r < 3.$$ (1)

High ΔP_{th} in Reservoir Matrices. In the matrices, the MSRs are relatively higher (>3). As shown in Figure 11, the threshold pressures are higher than 100 psi. The threshold pressure also exponentially increases with the MSR, but the increase is much more moderate compared with the situations in the super-k channels, as indicated by the slopes of the two fitting curves (2.0653 vs. 0.0785). The ΔP_{th}-MSR can be described with Equation (2) when the MSR ranges from 3 to 20. The high penetration pressures make it hard for the gels to penetrate the reservoir matrices, which is favorable for effective gel treatments.

$$\Delta P_{th} = 124.64 \exp\left(0.0785 R_r\right), \ 3 \leq R_r < 20.$$ (2)

Interestingly, a distinct transition of the threshold pressure is identified at the MSR of about 3. The particular behavior is closely related to the penetration and retention mechanisms of the elastic gel particles in porous channels and matrices. The flow paths in the porous media consisted of a series of convergent-divergent structures (i.e., pore throats). At high MSRs (e.g., MSR>3 in this study), the direct trapping of the gel particles at the pore throats would be dominant (Bai et al. 2007b; Yao et al. 2012). The gel particles

should be deformed, dehydrated, and compressed, or/and even split into smaller pieces in order to pass through the pore throats. Under these conditions, the required driving pressures would be too high and break the particles into smaller pieces. Thus, the threshold penetration pressure would become less sensitive to the MSR. Besides, at relatively high MSRs, the amoeba effect mentioned in previous subsection can make the axial size of gel particles significantly larger than the radial size. The particles would adapt to and wormhole through the flow pathways. Therefore, the amoeba effect can also make the threshold pressure less sensitive to the relative size of the gel particles. It should be noted that some factors may influence the specific value of the transition point (MSR≈3 in this work). It may change with the strength and concentration of the gel particles. Interestingly, Wang et al. (2017) also reported that the breakage occurred when the particle/throat size ratio was larger than 3 for gel particles with different strengths. The transition point (when the breakage occurs) seems independent to the strength of the gel particles. Note that our experiment conditions (cores/sandpacks, gel particle suspensions) were substantially different with Wang et al. (2017) (single particle, single capillary tube). More work can be performed in the future to testify whether it is simply a coincidence or a universal behavior at different conditions.

The results reveal the underlying mechanism of selective penetration. In the matrices, due to the high threshold penetration pressures (Figure 11), the gel particles are difficult to penetrate the porous media. Instead, the gels accumulate at the inlet surface, and a gel cake is formed (Figure 9 and Figure 10). The cake further prevents the gels from entering the channel. On the other hand, the gels can easily penetrate the super-k channel due to the low threshold pressure in it (Figure 11). According to the relationship between

the threshold penetration pressure and the matching size ratio, favorable working conditions can be determined for effective gel treatments. The MSR in the channel should be smaller than 2 to allow easy penetration into the target zones to be treated. Meanwhile, the MSR in the matrix should be high enough to possess a high ΔP_{th} and thus prevent massive invasion into the matrix. For the tested microgels, an MSR larger than 20 can substantially suppress gel invasion into reservoir matrices.

4. CONCLUSIONS

This study investigated the critical penetration behavior of micrometer-sized preformed particle gels (microgel) into superpermeable (super-k) channels and matrices in a wide permeability range (50 md to 230 darcies). The results demonstrated the presence of threshold penetration pressure (ΔP_{th}), which was responsible for the selective penetration behavior of the tested microgels in the channels and matrices.

(1) The critical penetration behavior was closely related to the particle-to-pore matching-size ratio (MSR). The ΔP_{th} at the inlet faces of super-k channels (60-230 darcies) was in the range of 1 to 12 psi with MSRs in the range of 0.6 to 1.8. The low ΔP_{th} was beneficial to allow easy penetration of gel materials into the channeling zones.

(2) On the contrary, the ΔP_{th} was much higher in the cores with relatively low permeabilities and high MSRs (ΔP_{th}>200 psi when MSR>6.5 for the tested gels). The high ΔP_{th} was desirable to prevent the gel materials from massively invading and damaging the matrices. Instead, the gel particles accumulated at the inlet surface, and a gel cake was gradually formed. The cake further prevented the invasion of the gels.

(3) Correlations were developed to describe the ΔP_{th}-MSR relationship. When MSR<3, the ΔP_{th} exponentially increased with the MSR. A distinct transition was identified at the MSR of about 3. When MSR>3, the ΔP_{th} became much less sensitive to the MSR, but it still exponentially increased with the MSR. When MSR>20, the ΔP_{th} was higher than 1200 psi.

(4) This study provided quantitative evidence to demonstrate the selective penetration of the tested microgels. In addition, the concept of ΔP_{th} was utilized to figure out the favorable working conditions to achieve effective gel treatments. The MSR in the channel should be sufficiently low to allow easy penetration of gels into the channel (e.g., MSR<2 in this study). Meanwhile, the MSR in the matrix should be high enough to support a high ΔP_{th} and thus prevent massive invasion into the matrix.

ACKNOWLEDGEMENTS

necessarily constitute or imply its endorsement, recommendation, or favoring by the United States Government or any agency thereof. The views and opinions of authors expressed herein do not necessarily state or reflect those of the United States Government or any agency thereof."

REFERENCES

Bai, B., Huang, F., Liu, Y., Seright, R. S., Wang, Y. 2008. Case Study on Preformed Particle Gel for in-Depth Fluid Diversion. Paper presented at the SPE Symposium on Improved Oil Recovery, Tulsa, Oklahoma, USA, 20–23 April. SPE-113997-MS. https://doi.org/10.2118/113997-MS.

Bai, B., Li, L., Liu, Y., Liu, H., Wang, Z., You, C. 2007a. Preformed Particle Gel for Conformance Control: Factors Affecting Its Properties and Applications. SPE Res Eval & Eng 10 (4): 415–422. SPE-89389-PA. https://doi.org/10.2118/89389-PA.

Bai, B., Liu, Y., Coste, J. P., Li, L. 2007b. Preformed Particle Gel for Conformance Control: Transport Mechanism Through Porous Media. SPE Res Eval & Eng 10 (2): 176–184. SPE-89468-PA. https://doi.org/10.2118/89468-PA.

Bai, B., Wei, M., and Liu, Y. 2012. Injecting Large Volumes of Preformed Particle Gel for Water Conformance Control. Oil Gas Sci. Technol.–Rev. IFP Energies Nouvelles 67 (6): 941–952. https://doi.org/10.2516/ogst/2012058.

Bai, B., Wei, M., and Liu, Y. 2013. Field and Lab Experience with a Successful Preformed Particle Gel Conformance Control Technology. Paper presented at the SPE Production and Operations Symposium, Oklahoma City, Oklahoma, USA, 23–26 March. SPE-164511-MS. https://doi.org/10.2118/ 164511-MS.

Dandekar, A., Bai, B., Barnes, J., Cercone, D., Ciferno, J., Ning, S., Seright., R., Sheets, B., Wang, D., Zhang, Y. 2019. First Ever Polymer Flood Field Pilot–A Game Changer to Enhance the Recovery of Heavy Oils on Alaska's North Slope. Paper presented at the SPE Western Regional Meeting, San Jose, California, USA, 23–26 April. SPE-195257-MS. https:// doi.org/10.2118/195257-MS.

Dandekar, A., Bai, B., Barnes, J., Cercone, D., Ciferno, J., Edwards, R., Ning, S., Schulpen, W., Seright., R., Sheets, B., Wang, D., Zhang, Y. 2020. First Ever Polymer Flood Field To Enhance the Recovery of Heavy Oils on Alaska's North Slope–Pushing Ahead One Year Later. Paper presented at the SPE Western Regional Meeting, April 27-30, 2020, Bakersfield, California, USA. Note–postponed to virtual format in April 2021. SPE-200814-MS. https:// doi.org/10.2118/200814-MS.

Dandekar, A., Bai, B., Barnes, J., Cercone, D., Ciferno, J., Edwards, R., Ning, S., Schulpen, W., Seright., R., Sheets, B., Wang, D., Zhang, Y. 2021. Heavy Oil Polymer EOR in the Challenging Alaskan Arctic–It Works! Paper prepared for presentation at the Unconventional Resources Technology Conference held in Houston, Texas, USA, 26-28 July 2021. URTeC-2021-5077. https://doi.org/10.15530/urtec-2021-5077.

Hendrickson, G.R., and Lyon, L.A. 2010. Microgel Translocation through Pores under Confinement. Angew Chem Int Ed 49:2193–7. https://doi.org/10.1002/anie.200906606.

Kang, W., Kang, X., Lashari, Z.A., Li, Z., Zhou, B., Yang, H., Sarsenbekuly, B. Aidarova, S. 2021. Progress of Polymer Gels for Conformance Control in Oilfield. Adv Colloid Interface Sci 289 (March): 102363. https://doi.org/10.1016/j.cis.2021.102363.

Lei, W., Xie, C., Wu, T., Wu, X., Wang, M. 2019. Transport Mechanism of Deformable Micro-Gel Particle Through Micropores with Mechanical Properties Characterized by AFM. Sci Rep 9 :1–12. https://doi.org/10.1038/s41598-018-37270-7.

Li, Y., Sarıyer, O. S., Ramachandran, A., Panyukov, S., Rubinstein, M., Kumacheva, E. 2015. Universal Behavior of Hydrogels Confined to Narrow Capillaries. Sci. Rep. 5 (1), 17017: 1-11; https://doi.org/10.1038/srep17017.

Liu, Y., Hou, J., Wang, Q., Liu, J., Guo, L., Yuan, F., Zhou, K. 2017. Flow of Preformed Particle Gel through Porous Media: A Numerical Simulation Study Based on the Size Exclusion Theory. Ind Eng Chem Res 56:2840–50.

Ning, S., Barnes, J., Edwards, R., Schulpen, W., Dandekar, A., Zhang, Y., Cercone, D., Ciferno, J. 2020. First Ever Polymer Flood Field Pilot to Enhance the Recovery of Heavy Oils on Alaska North Slope–Producer Responses and Operational Lessons Learned. Paper presented at the SPE Annual Technical Conference and Exhibition, Virtual, 26–29 October. SPE-201279-MS. https://doi.org/10.2118/201279-MS.

Seright, R. S. 1997. Use of Preformed Gels for Conformance Control in Fractured Systems. SPE Prod Facil 12 (01): 59–65. SPE-35351-PA. https://doi.org/10.2118/35351-PA.

Seright, R. S. and Brattekas, B. 2021. Water Shutoff and Conformance Improvement: An Introduction. Pet. Sci. 18: 450–478. https://doi.org/10.1007/s12182-021-00546-1.

Sydansk, R. D. and Romero-Zeron, L. 2011. Reservoir Conformance Improvement. Richardson, Texas, USA: Society of Petroleum Engineers.

Villone, M. M. and Maffettone, P. L. 2019. Dynamics, Rheology, and Applications of Elastic Deformable Particle Suspensions: A Review. Rheol Acta 58 (3–4): 109–130. https://doi.org/10.1007/s00397-019-01134-2.

Wang, J., Zhang, H., Liu, H., Zhao, W., Liu, H., Yao, C., Zheng, J., Shen, Y. 2017. Quantification of Transportation of Deformable Gel Particles in Porous Media. Paper presented at the SPE Annual Technical Conference and Exhibition held in San Antonio, Texas, USA, 9-11 October. SPE-187266-MS. https://doi.org/10.2118/187266-MS.

Yao, C., Lei, G., Cathles, L. M., Steenhuis, T. S. 2014. Pore-Scale Investigation of Micron-Size Polyacrylamide Elastic Microspheres (MPEMs) Transport and Retention in Saturated Porous Media. Environ Sci Technol 48: 5329–35.

Yao, C., Liu, B., Li, L., Zhang, K., Lei, G., Steenhuis, T. S. 2020. Transport and Retention Behaviors of Deformable Polyacrylamide Microspheres in Convergent-Divergent Microchannels. Environ Sci Technol 54:10876–84.

Zhang, Z., Xu, J., and Drapaca, C. 2018. Particle Squeezing in Narrow Confinements. Microfluid Nanofluidics 22: 1–26. https://doi.org/10.1007/s10404-018-2129-2.

Zhao, W., Liu, H., Wang, J., Zhang, H., Yao, C., Wang, L., Qi, P. 2018. Investigation of Restarting Pressure Gradient for Preformed Particle Gel Passing Through Pore-Throat. J Pet Sci Eng, 168: 72–80. https://doi.org/10.1016/j.petrol.2018.05.005.

Zhao, Y., Leng, J., Lin, B., Wei, M., Bai, B. 2021a. Experimental Study of Microgel Conformance-Control Treatment for a Polymer-Flooding Reservoir Containing Superpermeable Channels. SPE J. SPE-205486-PA (in press; posted 26 April 2021). https://doi.org/10.2118/205486-PA.

Zhao, Y., Yin, S., Seright, R. S., Ning, S., Zhang, Y., Bai, B. 2021b. Enhancing Heavy-Oil-Recovery Efficiency by Combining Low-Salinity-Water and Polymer Flooding. SPE J. 26 (03): 1535–1551. SPE-204220-PA. https://doi.org/10.2118/204220-PA.

Zhou, K., Hou, J., Sun, Q., Guo, L., Bing, S., Du, Q., Yao, C. 2017. An Efficient LBM-DEM Simulation Method for Suspensions of Deformable Preformed Particle Gels. Chem Eng Sci 167: 288–96. https://doi.org/10.1016/j.ces.2017.04.026.

Zhu, D., Bai, B., and Hou, J. 2017. Polymer Gel Systems for Water Management in High-Temperature Petroleum Reservoirs: A Chemical Review. Energy Fuels 2017, 31 (12): 13063−13087.

IV. CRITICAL PRESSURE GRADIENTS DURING MICROGEL PROPAGATION

ABSTRACT

Gel treatment is an effective way to attack excessive water production during oil development. In an effective gel treatment, the gel materials are expected to easily propagate and place in the target places (i.e., channeling zones). In this work, we studied the propagation behavior of micrometer-sized preformed particle gels (microgels) through superpermeable channels. Microgel dispersions were injected into superpermeable channels (55-221 darcies, mimicked with sandpacks). We observed that a critical (minimum) pressure gradient (∇P_{cr}) was required to drive the gel particles to propagate through the channels. Below ∇P_{cr}, the gels could not transport in the porous channels. The existence of the ∇P_{cr} was confirmed with gel injection experiments carried out in constant-injection-pressure mode. The particle-to-pore matching size ratio (MSR) had a significant impact on the ∇P_{cr}. The ∇P_{cr} increased exponentially with the MSR at relatively low MSRs (<2). The ∇P_{cr} were lower than 60 psi/ft. A correlation was proposed to describe the ∇P_{cr}-MSR relationship in the superpermeable channels. Diagrams were developed to estimate the maximum propagation distance of the gels in channels in conceptual field applications. At low MSRs, the gel particles could transport a significant distance away from the wellbore, which was favorable for in-depth conformance treatments. At high MSRs, the transport distance of the gel particles was limited, which was favorable for near-wellbore treatments. The transport-distance diagrams can help engineers select proper gel products to address water channeling problems in reservoirs. Also, this work provides an effective

procedure to study the impact of other parameters (e.g., dispersion concentration and gel strength) on the propagation distance of gel materials.

1. INTRODUCTION

Excessive water production is a big challenge and is commonly encountered in oil fields around the world. Many field applications have proven that gel treatment is an effective way to reduce the unwanted water production and improve the effective sweep volume (Aldhaheri et al. 2020, 2021; Seright & Brattekas 2021; Bai et al. 2012, 2013, 2015; Sydansk & Romero-Zeron 2011; Leng et al. 2021). However, failed applications were also reported (Aldhaheri et al. 2020, 2021; Qiu et al. 2016; Chou et al. 1994; Portwood 1999). In an effective gel treatment, the gel materials are expected to easily propagate and place in the target places (i.e., channeling zones). Meanwhile, the invasion into the nontarget zones (i.e., the reservoir matrices, or the oil zones) should be minimum to avoid massive formation damage. In this work, we studied the propagation behavior of micrometer-sized preformed particle gels (microgels) through superpermeable channels, and the invasion behavior of the microgels in reservoir matrices.

The propagation behavior is important to determine the effectiveness of the gel treatment (Zhao et al. 2021a; Leng et al. 2021; Wu et al. 2021; Villone & Maffettone 2019). In a field application of gel treatment, the injection pressure is limited as the bottom hole pressure is usually constrained below the fracturing/parting pressure of the formation (Bai et al. 2008; Karaoguz et al. 2007; Demir et al. 2008; Portwood 1999; Seright et al. 2012). On the other hand, the gel materials should transport a certain distance away from the

wellbore to achieve a satisfactory conformance control performance. Therefore, it is crucial to know how far (from the wellbore) the gel materials can propagate through the superpermeable channels with constrained driving pressures.

The transport distance is related to the pressure gradients during gel propagation in the channels. Seright (1999, 2001, 2003) developed a method that could be used to estimate the propagation of preformed bulk gels in fractures based on the leak-off and dehydration behavior of the gels. His studies reveal that the propagation distance does not linearly correlated with the injected gel volume. For particle gels, a critical (minimum) pressure gradient that required to propagate through a porous medium has been reported. Bai et al. (2007b) observed the existence of the critical pressure gradient when gel particles transport a porous medium. The critical pressure gradient increased with the particle/throat size ratio. There was a maximum pressure gradient, above which the required pressure gradient would not increase with the particle/throat size ratio. This phenomenon was related to the breakage of the gel particles at high pressure gradients. Liu et al. (2017) numerically studied the transport behavior of deformable gel particles based on size exclusion theory. Later, Zhou et al. (2017) used an improved LBM-DEM (lattice Boltzmann method and discrete element method) simulation method to study the transport behavior of soft gel particles in porous media. They numerically investigated the effect of particle/pore size ratio and particle strength on the critical pressure gradient for a single gel particle transport through a single pore throat. They reported an exponential relationship between the critical pressure gradient and the size ratio, and linearly correlated with the elastic modulus. For the single particle transport process, they observed that the flow rate had negligible impact on the critical pressure gradient. Wang et al. (2017) regarded the critical pressure gradient

as a segmented function of the particle/pore size ratio. When the particle was smaller than the pore throat, the critical pressure gradient was assumed to increase linearly with the particle/pore size ratio, analogous to rigid particle behavior (Abrams 1977). The critical pressure gradient increased exponentially with the size ratio when the particles were larger than the pore throat sizes.

Recently, we evaluated the potential of microgels in improving the effectiveness of polymer flood in heavy reservoirs containing superpermeable channels (Zhao et al. 2021a). Unlike routine Newtonian fluids (e.g., water, oil), we observed that a minimum differential driving pressure was required for the gel particles to penetrate and transport in the superpermeable channels. The minimum differential pressure decreased with the channel permeability, following a power-law relationship. The existence of the minimum differential pressure was associated with the viscoelastic nature of the gel particles.

In this work, systematic experimental studies were carried out to investigate the propagation behavior of microgels in superpermeable channels. The existence of critical (minimum) pressure gradients was confirmed, and the impact of particle-to-pore matching size ratio (MSR) was studied. The maximum propagation distances of microgels in channels were estimated in conceptual field applications. The favorable conditions to achieve effective conformance control treatments were discussed.

2. EXPERIMENTAL AND METHODOLOGY

Microgel Particles. The microgel particles were ground from millimeter-sized dry preformed particle gels (Bai et al., 2007a). The microgel has a volumetric swelling ratio of

20 cm^3/cm^3 in synthetic formation brine of the Milne Point oilfield on Alaska's North Slope (total dissolved solids, i.e., TDS=27,500 ppm) (Zhao et al. 2021a, 2021b). The swelling ratio was defined as the ratio of swollen volume after absorbing water to the original volume of the gel.

Superpermeable Sandpacks and Channel Models. Superpermeable sandpacks were used to mimic the superpermeable channels present in heterogeneous reservoirs. The sandpacks had one pressure tap at the inlet and three internal pressure taps (see Figure 1). The multiple pressure taps were able to monitor the pressures at different locations. Silica sands with different sizes were used to prepare the sandpacks of different target permeabilities. Channel models were also used. A typical channel model was prepared by creating a lengthwise fracture in an intact core. The fracture space was filled with silica sands to make a superpermeable and porous channel in the heterogeneous model (Zhao et al. 2021a). The basic parameters of ther models were summarized in Table 1. The permeabilities ranged from 55 to 221 darcies. The MSR refers the average partice-to-pore matching size ratio.
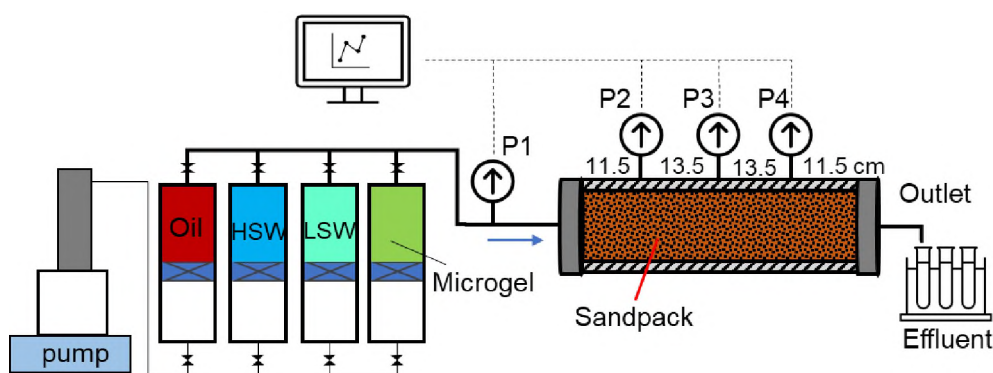
Figure 1. Experiment setup.

Figure 1 shows the experiment setup for sandpack models. For the channel models, a routine coreholder was used to hold the models. Water was injected first at different flow rates to measure the permeabilities. Afterwards, gel dispersion was injected into the models, followed by post-water injection to estimate the water-blocking performance of the gels. In some experiments, the gel dispersion was injected at constant-flow-rate mode (and changed stepwisely), and the others were performed at constant-injection-pressure mode (labeled as CP). The pressures and injection rates were recorded during the experiments, and the effluent was closely monitored to capture the moment when the microgel began to come out from the outlet.

Table 1. Summary of basic parameters of the experiments.

No.	Label*	K, darcy	Average swollen particle size (D_g), μm	Average pore size (D_p), μm	MSR
1	RE1	221	150	218.90	0.69
2	RE2	60.0	150	114.84	1.31
3	RE3	218	290	202.31	1.43
4	RE4	212	290	200.32	1.45
5	RE5	59.8	205	115.51	1.77
6	RE6	55.4	260	110.76	2.35
7	CP1	221	150	218.90	0.69
8	CP2	62.0	130	116.81	1.11
9	CP3	62.4	150	117.18	1.28

*Note: RE, rheology experiment tests; CP, constant-pressure injection experiments.

3. RESULTS AND DISCUSSION

3.1. PRESSURE GRADIENTS DURING GEL INJECTION

In experiments RE1 to RE6, the gel dispersion was injected into the sandpacks or channel models at constant flow rates. After stable pressures were established in the models, the injection flow rate was successively decreased or increased, thus the pressure gradients at different superficial velocities were obtained. Taking RE2 as an example, the permeability was 60 darcies, and the particle-to-pore matching size ratio (MSR) was 1.31. At the beginning, the gel dispersion was injected at 2 ml/min (19.2 ft/d) for about 6 pore volumes (PV).
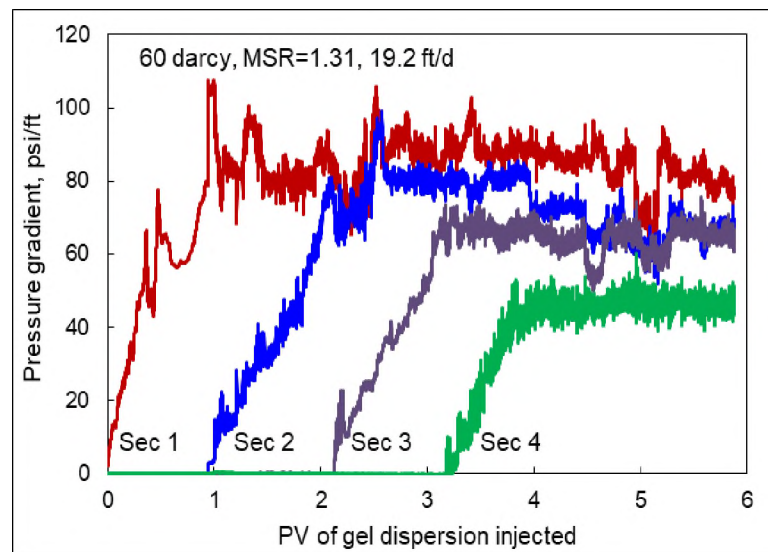
Figure 2. Pressure gradients during gel injection at constant flow rate (RE2).

As shown in Figure 2, the pressure gradients in different sections were sequentially increased and stabilized (with fluctuations). Afterwards, the flow rate was increased to 50

ml/min (481 ft/d), sequentially decreased to 1.9 ft/d, and then successively increased back to 481 ft/d. The pressure gradients in the second section (between the first and second internal pressure taps) of the sandpack were shown in Figure 3. The pressure gradient was much less sensitive to the superficial velocity of the gel dispersion compared with a Newtonian fluid. The observation was consistent with the reducing resistance factors (Figure 4). As shown in Figure 4, the gel dispersion behaved like a shear thinning (pseudoplastic) fluid when transporting through the porous channels. The slip effect and the breakage of the gel particles into smaller pieces were possible reasons responsible for the apparent shear thinning behavior.
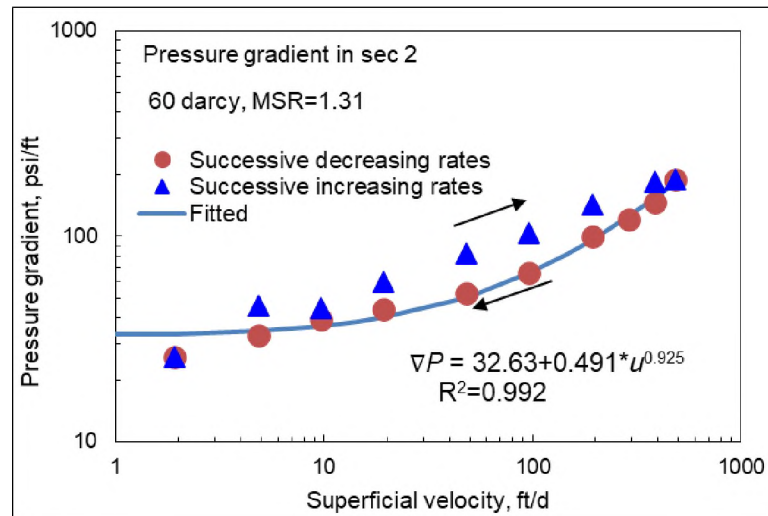
Figure 3. Pressure gradients at different superficial velocities (RE2).

The pressure gradient data was fitted with the equation in the form of Equation (1) to determine the critical pressure gradient (∇P_{cr}). The physical meaning of ∇P_{cr} was the pressure gradient at the superficial velocity of zero. It was the minimum pressure gradient

to initiate the propagation of the gel particles in the porous media. the critical pressure gradient was 32.63 psi/ft in RE2.

$$\left|\nabla P\right| = \nabla P_{cr} + a \cdot u^b .$$ (1)
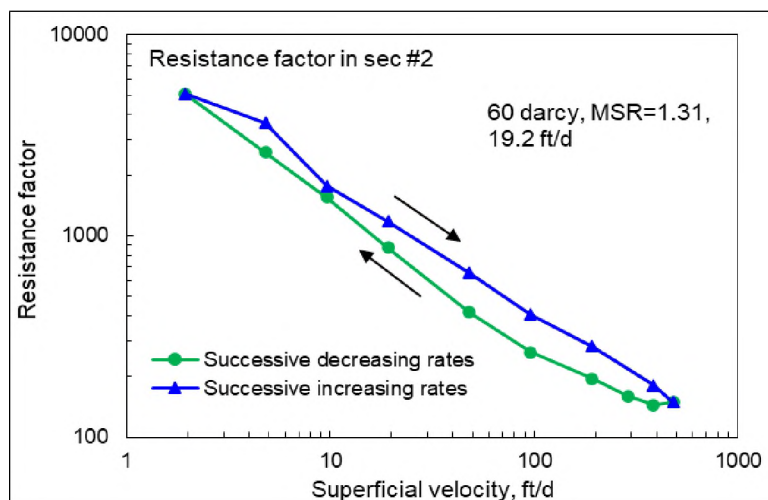
Figure 4. Resistance factor as a function of superficial velocity (RE2).

Following the similar procedure, the pressure gradients and resistance factors at different MSRs were tested. The results were summarized in Figures 5 and 6. Obviously, the pressure gradients increased with the MSR. The ∇P_{cr} under different MSRs were obtained and further discussed in subsequent sections. Figure 5 also suggested that the pressure gradient of softer particles was less sensitive to the injection flow rate compared with stronger particles. This was agreed with the observation that softer particles exhibited more significant thinning behavior (Figure 6).

Confirmation of the Existence of ∇P_{cr}. The existence of the critical pressure gradient was further confirmed with gel dispersion injection experiments carried out in constant-injection-pressure mode (CP1, CP2, CP3 in Table 1). In experiment CP1, the gel

dispersion (with an average size of 150 μm, MSR=0.69) was injected into a 221-darcy sandpack. We successively increased the injection pressure, and stable conditions were obtained at each step to test the critical pressure gradients for the gel particles to propagate in this superpermeable sandpack. The results were shown in Figures 7 to 9 and Table 2.
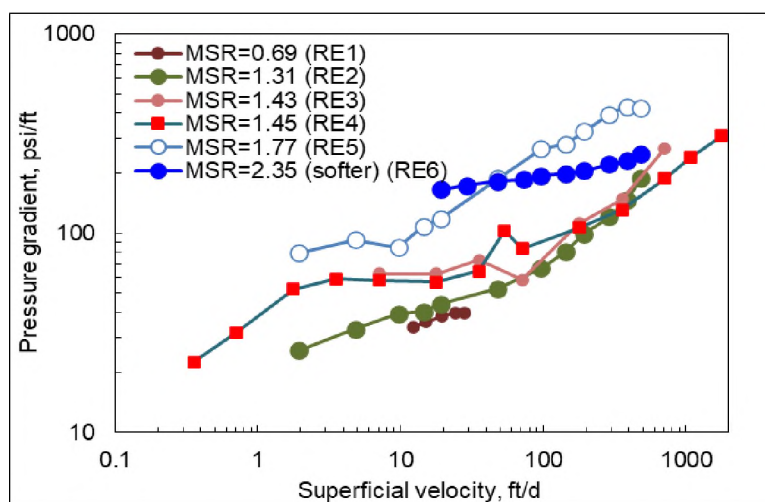
Figure 5. Pressure gradients at different MSRs and superficial velocities.

MSR	k, d	Resistance factor
0.69	221	$F_r = 28423u^{0.798}$, $R^2 = 0.9965$
1.31	60.0	$F_r = 6745.6u^{0.666}$, $R^2 = 0.9957$
1.43	218	$F_r = 36190u^{0.698}$, $R^2 = 0.9759$
1.45	212	$F_r = 53071u^{0.740}$, $R^2 = 0.9764$
1.77	59.8	$F_r = 18283u^{0.645}$, $R^2 = 0.9746$
2.35	55.4	$F_r = 31546u^{0.883}$, $R^2 = 0.9998$
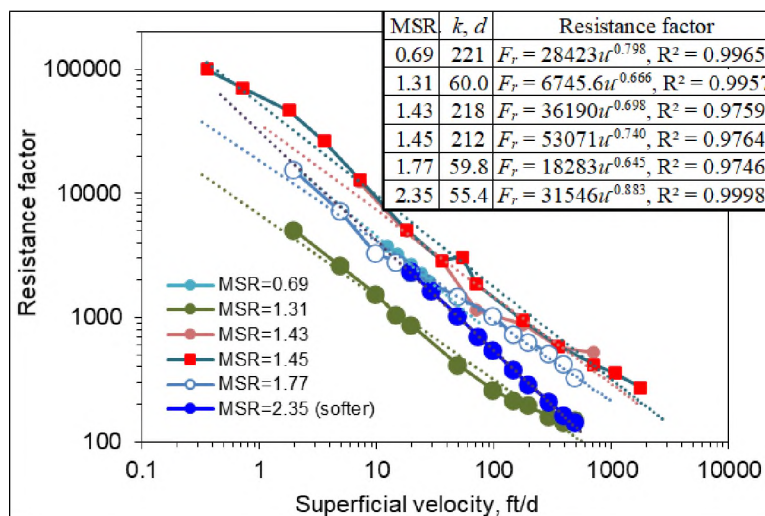
Figure 6. Resistance factors at different MSRs and superficial velocities.

Table 2. Summary of transport response in CP1 (221 darcies, MSR=0.69).

Pre-set injection pressure		Gel transport location	Distance from inlet, cm	Pressure gradient in different sections, psi/ft				Gel injected, ml	
P (pump), psi	∇P (global), psi/ft			∇P_1	∇P_2	∇P_3	∇P_4	Dispersion	Swollen gel
18	10	Inlet	0	0.00	0.00	0.00	0.00	0.00	0.00
18 (before switch)	10	Between tap #1 and #2	0~11.5	47.71	0.00	0.00	0.00	59.00	11.78
35	20	Tap #2	11.5	61.44	0.00	0.00	0.00	102.00	20.40
35 (before switch)	20	Between tap #2 and #3	11.5~25.0	68.59	20.14	0.00	0.00	171.00	34.20
50	30	Tap #3	25.0	48.66	44.34	0.00	0.00	306.00	61.20
82	50	Tap #4	38.5	41.74	70.85	59.99	0.00	356.00	71.20
82	50	Outlet	50.0	57.81	49.06	37.89	43.94	421.00	84.20
82	50	Stable	50.0	57.51	44.07	42.58	44.84	533.90	106.78

At the beginning, a low injection pressure, 18 psi, was used to test how much gel dispersion could be injected and how far the gel particles could transport in the sandpack. The injection pressure corresponded to a global pressure gradient [∇P(global)] of ~10 psi/ft, and an overall pressure gradient (∇P_1) of 48 psi/ft in the first section of the sandpack. As shown in Figures 7 and 8, the injection flow rate (dashed green curve) gradually dropped to almost zero after 40 minutes, and no more gel dispersion could be injected into the model. The second pressure sensor showed no response, indicating the gel particles did not transport to that location. Only 59.0 ml of gel dispersion was injected (containing 11.8 ml

swollen gel particles), as summarized in Table 2. In this process, only water with no gel particles was produced from the outlet. The results demonstrated that a pressure gradient of 48 psi/ft was insufficient to keep the gel particles propagating through the inlet section (11.5 cm) of the superpermeable channel. A higher pressure gradient ($>\nabla P_{cr}$) was required to push the gel particles to transport farther into the channel.
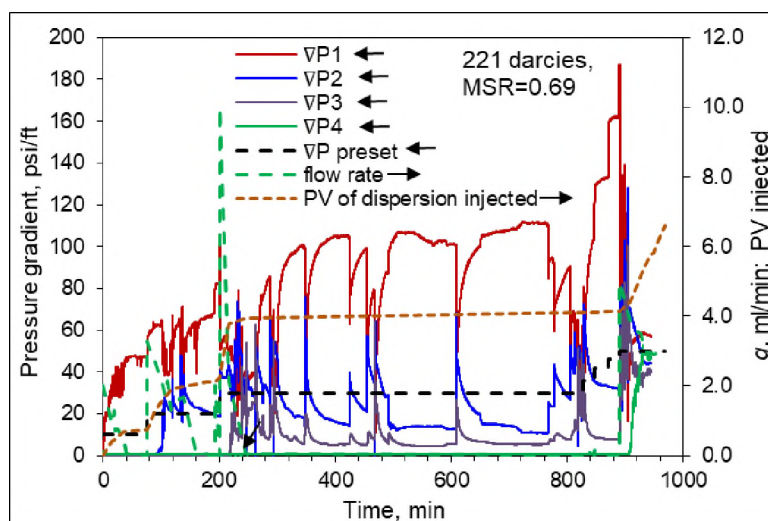
Figure 7. The responses during gel injection process (CP1).

The global injection pressure gradient was then increased to 20 psi/ft (P_1=35 psi). The microgel particles could transport to the second pressure tap as P_2 began to increase (Figure 9). The average pressure gradient in the first section was 61 psi/ft, which was sufficient to drive the microgel particles to propagate through this section. Thus, the critical pressure gradient in the first section was in the range of 48 psi/ft to 61 psi/ft. The injection flow rate would gradually drop (with fluctuation) to zero. Consequently, no more gel dispersion could be injected. The gel particles propagated to a certain location between tap #2 and tap #3, and could not transport farther inside the superpermeable channel. The

cumulative injection volume of the gel dispersion was 171 ml (containing 34.2 ml swollen gel particles). No gel particles were detected in the effluent. The overall pressure gradient in the second section (between pressure tap #2 and tap #3) was about 20 psi/ft, which was lower than the critical pressure gradient in this section.
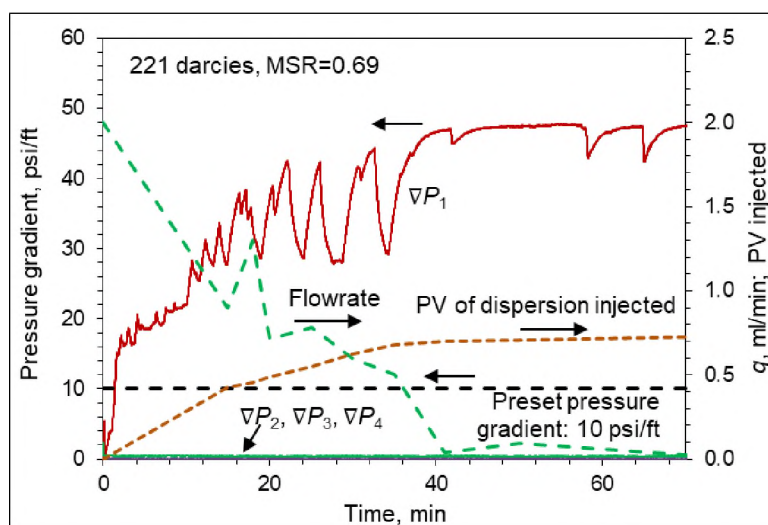
Figure 8. The responses in the early stage (CP1).
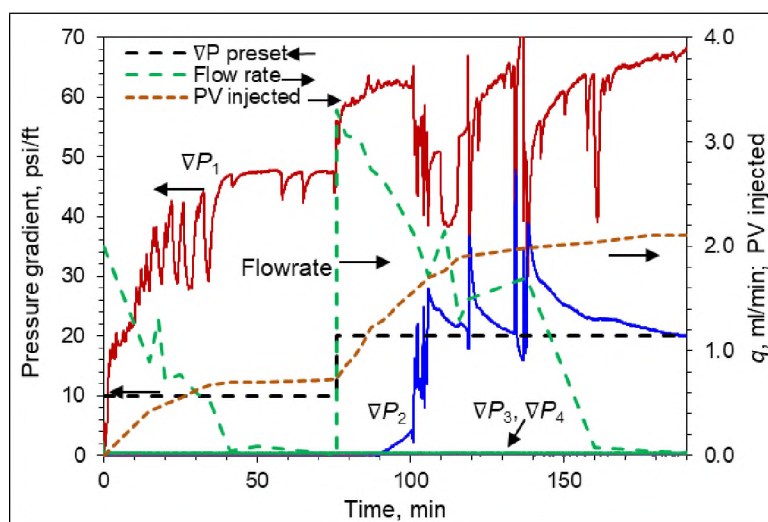
Figure 9. The responses at increased injection pressure gradients (CP1).

Afterwards, the global injection pressure gradient was sequentially increased to 30, 36, 42, 48 and 50 psi/ft. As seen in Figure 7 and Table 2, the gel particles propagated deeper into the channel, and P_3 and P_4 sequentially began to increase. Gel particles were then produced from the outlet. At the global pressure gradient of 50 psi/ft, the injection process became relatively stable, as illustrated in Figure 7. At the equilibrium condition, the pressure gradients in the four sections were stabilized (with fluctuation) at 57.5, 44.1, 42.6, and 44.8 psi/ft, respectively (Figures 7 to 9 and Table 2). These values were not the minimum (critical) pressure gradients as the propagation of the microgel particles was not at the critical status (i.e., the flow rate close to zero). The injection flow rate was stabilized at about 3.0 ml/min (~30 ft/d). In these processes, the critical pressure gradients in each section were determined based on whether the gel particles could propagate under the given pressure gradients. The average critical pressure gradient was about 29 psi/ft, with a relatively higher value in the range of 48-61 psi/ft in the inlet section and 10-30 psi/ft in the in-depth region of the sandpack.

Following the similar procedures, another two experiments were performed. In CP2, the gel particles with an average size of 120 µm were injected through a 62-darcy sandpack (MSR=1.11). The results were shown in Figures 10 and 11. The dynamic propagation responses were summarized in Table 3 and Table 4. The overall critical pressure gradient in the sandpack model was about 37 psi/ft. In CP3, the gel dispersion was injected into a 60-darcy sandpack in constant-pressure mode (MSR=1.28). The pressure gradient results were shown in Figures 12 and 13. The critical pressure gradient in the inlet section was in the range of 60.7-62.6 psi/ft, and it was 30-40 psi/ft in the in-depth sections. The overall critical pressure gradient in the entire sandpack model was about 45 psi/ft.

Table 3. Summary of transport response in CP2 (62.0 darcies, MSR=1.11).

Pre-set injection pressure		Gel transport location	Distance from inlet, cm	Pressure gradient in different sections, psi/ft				Gel injected, ml	
P (pump), psi	∇P (global), psi/ft			∇P1	∇P2	∇P3	∇P4	Dispersion	Swollen gel
50	30	Tap #1	0	0.00	0.00	0.00	0.00	0.00	0.00
50	30	Tap #2	11.5	70.24	0.00	0.00	0.00	90.00	18.00
50 (before switch)	30	Between tap #2 and #3	11.5~25	111.05	24.84	0.00	0.00	180.10	36.02
65	40	Tap #3	25.0	83.49	58.02	6.10	0.00	190.00	38.00
65	40	Tap #4	38.5	62.82	44.70	41.32	0.53	250.00	50.00
65	40	Outlet	50.0	52.74	33.19	48.54	24.91	344.60	68.92
65	40	Stable	50.0	54.60	32.51	44.48	21.73	480.10	96.02
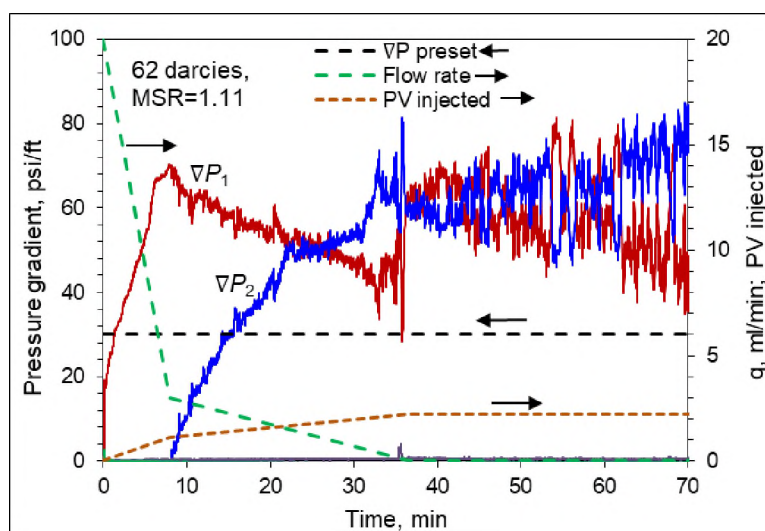
Figure 10. The responses in the early stage (CP2).
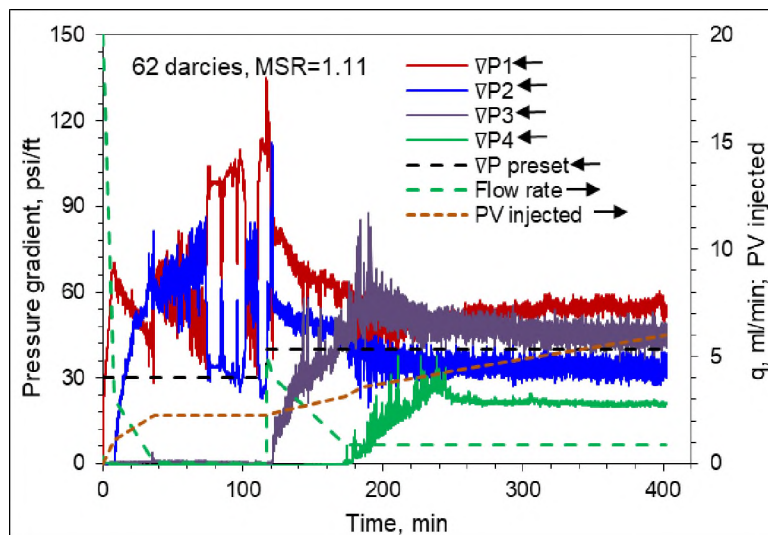
Figure 11. The responses at increased injection pressure gradients (CP2).

Table 4. Summary of transport response in CP3 (62.4 darcies, MSR=1.28).

Pre-set injection pressure		Gel transport location	Distance from inlet, cm	Pressure gradient in different sections, psi/ft				Gel injected, ml	
P (pump), psi	∇P, psi/ft			∇P1	∇P2	∇P3	∇P4	Dispersion	Swollen gel
25	15	Tap #1	0	0.13	0.00	0.00	0.00	0.00	0.00
25 (before switch)	15	Between tap #1 and #2	0~11.5	60.69	0.00	0.00	0.00	36.41	6.62
70	43	Tap #2	11.5	114.76	0.00	0.00	0.00	55.00	10.00
70	43	Tap #3	25	77.66	39.51	0.00	0.00	120.80	21.96
70	43	Tap #4	38.5	68.65	34.77	53.06	0.00	223.50	40.64
70	43	Outlet	50	53.54	29.58	44.70	40.55	288.50	52.45
70	43	Stable	50	62.55	30.48	41.54	38.96	805.00	146.36
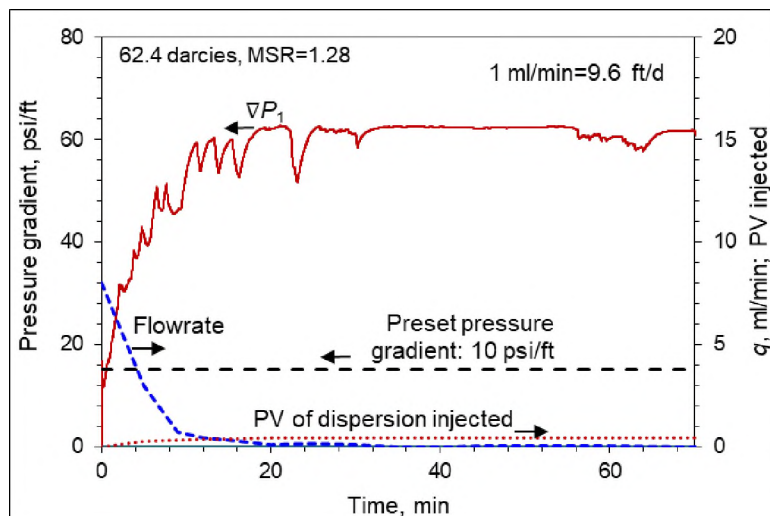
Figure 12. The responses in the early stage (CP3).
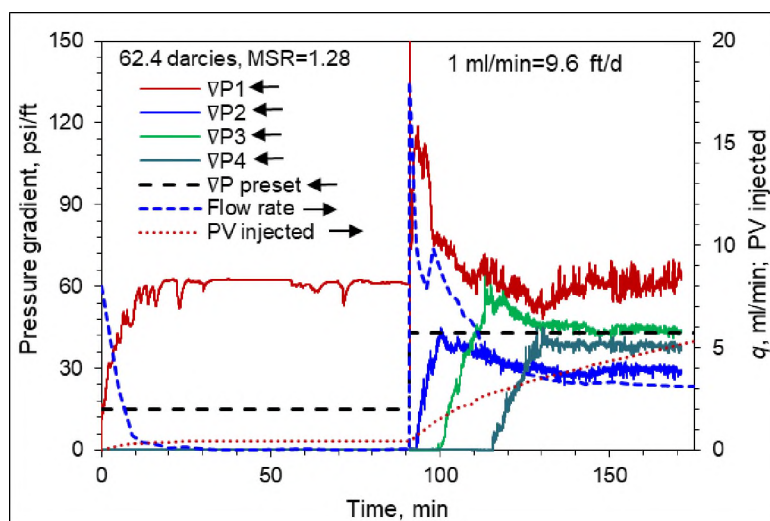
Figure 13. The responses at increased injection pressure gradients (CP3).

In sum, these three experiments confirmed the existence of the critical pressure gradient. The inlet section generally exhibited higher pressure gradients compared with that in the in-depth sections. Also, the results suggested that the critical pressure gradient increased with the MSR.

3.2. IMPACT OF MSR ON THE CRITICAL PRESSURE GRADIENT

In the previous subsection, we observed that the MSR had a significant impact on the critical pressure gradient. As the matching size of the gel particles was a crucial design parameter for gel treatment in field applications, it was practically meaningful to carry out more investigations to elucidate the impact of the particle size on the critical pressure gradient. In Figure 14, the critical pressure gradients during gel injection were plotted against the MSR. The experimental data covers the MSR in the range from 0.67 to 1.77.
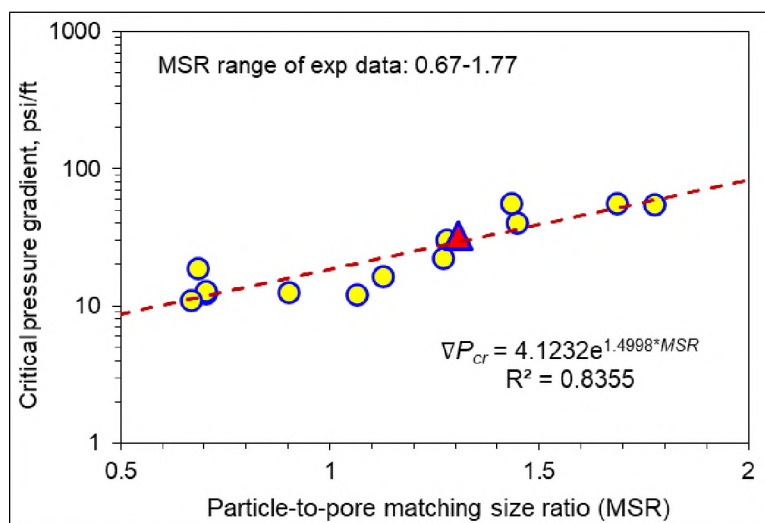
Figure 14. Correlating the critical pressure gradient with the MSR.

As shown in Figure 14, the critical pressure gradient followed an exponential relationship with the MSR. The critical pressure gradients were generally below 60 psi/ft as the MSRs were below 2. When the MSRs were lower than 1, that is, the particles were smaller than the pore throats, the critical pressure gradients were roughly below 20 psi/ft. The low MSRs represented the desired situations in the channels to be treated. Low pressure gradients were necessary to allow easy propagation and placement of the gels in

the channels. The critical pressure data could be described quite well with an exponential equation [Equation (2)].

$$\nabla P_{cr} = 4.1232 \exp\left(1.4998 R_r\right), R_r < 2.$$ (2)

In the equation, R_r was the MSR. The correlation could predict the critical pressure gradients of the microgels at other matching size conditions in the validated range.

3.3. IMPLICATIONS TO GEL TREATMENT FIELD APPLICATIONS

As aforementioned, it is usually required that the bottom hole pressure in the wellbore below the fracturing/parting pressure of the formation in a gel treatment. Therefore, it is important to know how far (from the wellbore) the gel particles can propagate through the superpermeable channels constrained injection pressure gradient is applied. On the other hand, in many field applications, an important gel treatment design criterion is the treatment distance. That is, in a gel treatment, it is usually required that the gel materials be placed to a certain distance away from the wellbore to achieve a satisfactory conformance control performance in the reservoir. For vertical wells in particular, it is also termed as the treatment radius (Bai et al. 2013; Qiu et al. 2016; Aldhaheri et al. 2020, 2021). Why is a certain treatment distance required? As the working philosophy of the gel treatment is to shut off (partially or totally) the channeling zone and to force the subsequent displacing fluid to the oil zones previously bypassed. If the treatment distance is too small, the fluid can flow back into the channels from the matrices. If the treatment distance is too large, the injectivity and/or the productivity can be damaged. The optimal treatment distance varies case by case, depending on many factors like the size, orientation and conductivity of the channels, the oil viscosity (or mobility ratio

between the displacing fluid and the oil), and the wellbore conditions (horizontal versus vertical, open hole versus cased hole, etc.) (Bai et al. 2013; Goudarzi et al. 2017; Imqam et al. 2015; Qiu et al. 2016; Seright et al. 2003; Sydansk & Romero-Zeron 2011). The optimal treatment distance can be determined through numerical reservoir simulation based on the breakthrough time, water cut, sweep efficiency, and overall oil recovery improvement performance (Imqam et al. 2015; Goudarzi et al. 2017; Qiu et al. 2016).

On the contrary, gel invasion into the reservoir matrices should be avoided. When the invasion distance is small, or only a surface cake is formed at the sand faces, the damage can be effectively remediated through some extra efforts, such as reperforation or soaking with chemical breakers.

The correlation developed in this work could be used to estimate the maximum possible propagation distance of gels in the channels. The basic principle was that the gel particles would stop propagating when the driving pressure gradient at the frontal section was insufficient to overcome the required critical pressure gradient. The procedure was illustrated with a simple schematic horizontal injector-producer pair (Figure 15). A superpermeable channel connected the horizontal injector and the producer. As a base case, assume the maximum allowable bottom hole pressure in the injector was 2500 psi, and the average reservoir pressure was 1750 psi. Thus, the maximum allowable driving differential pressure was 750 psi. As the channel had superhigh permeabilities compared with the matrices (see Table 5), in the conceptual simulation, we assumed linear flow in the super-k channel, and the near-wellbore radial flow was neglected.

The basic parameters in the conceptual simulation were summarized in Table 5. Based on the relationship between the critical pressure gradient and the MSR [Equation

(2)], the transport distances of the microgel particles at different MSRs were obtained, as shown in Figure 16. Figure 17 illustrate the maximum transport distances at different allowable driving pressures. The bond blue curve represented the base case.
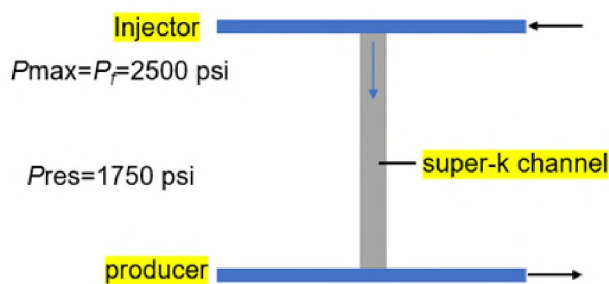
Figure 15. Schematic diagram of the horizontal pair and super-k channel.

Table 5. Basic parameters of the horizontal well pair.

Item	Value
Depth, ft	3,000-4,000
Layer thickness, ft	10-50
Well type	Horizontal well
Length of the horizontal section, ft	1,000-10,000
Well distance, ft	500-5,000
Reservoir permeability, md	200-10,000
Channel permeability, darcies	30-300
Channel width, ft	10-100
Channel height, ft	Same as layer thickness
MSR in the channel	0.1-2.0
Gel dispersion concentration, wt%	1
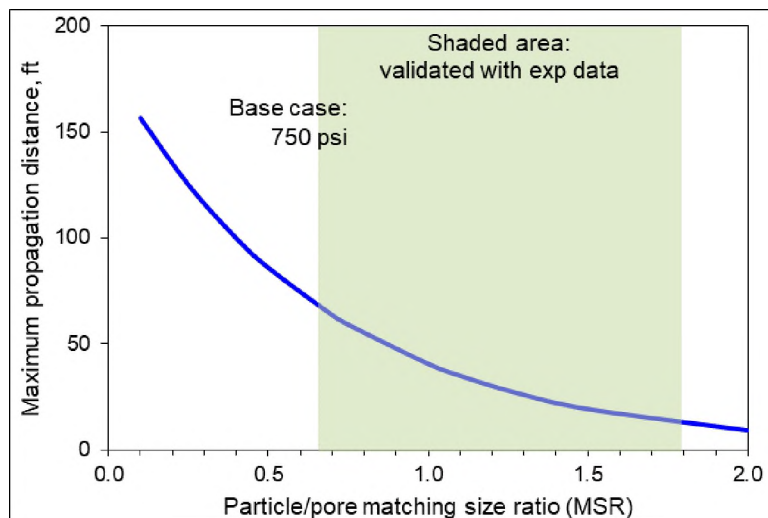
Figure 16. Diagram of the maximum transport distances in superpermeable channels (base case).
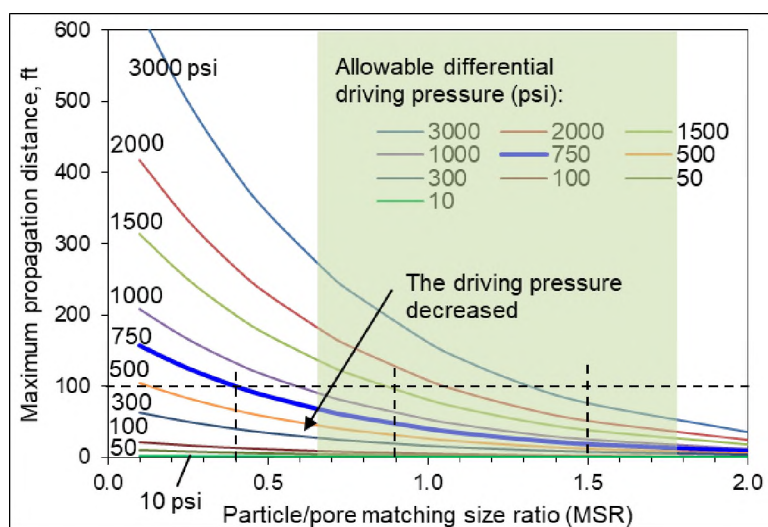
Figure 17. Diagram of the maximum transport distances in superpermeable channels at different allowable differential driving pressures.

As seen in Figure 16, it was straightforward that the propagation distance decreased

with the MSR at a given differential driving pressure. The propagation distance was limited

when the MSR was too high. For example, the propagation distance was less than 100 ft

when the MSR was above 0.4 in the base case. Figure 17 demonstrated the transport distances at different allowable differential driving pressures. Obviously, the gels transported farther through the channel away from the wellbore when a higher injection pressure was available. On the contrary, the treatment distances would be limited when the allowable driving pressures were low. In these situations, the gel particles could only transport a small distance away from the wellbore. This was undesirable when pursuing an in-depth conformance treatment. However, this behavior was favorable in some circumstances, for example, when pursuing a near-wellbore conformance treatment. The selection of the MSR was crucial in a conformance treatment. For example, the transport distance was less than 100 ft even under a very high driving pressure (3000 psi) as the MSR was above 1.5. In other words, the in-depth gel placement was hard to achieve even with very high injection pressures when the gel particles were too large.

The diagrams can help engineers to select proper gel materials to achieve a desired conformance treatment performance. For example, if a treatment distance of 100 ft is required and the allowable driving pressure is 1500 psi, the possible gel materials that are able to fulfill the desired treatment distance can be determined. It is required that the MSR is lower than 0.9. Otherwise, the gel materials cannot reach the target treatment distance. For a given gel product, the MSR decreases with the permeability of the channel. Therefore, the penetration distance increases with the channel permeability. This behavior is appreciable because as the channel becomes more permeable, and the heterogeneity issue is more severe. Thus, more of the channel should be shut off to achieve a satisfactory conformance improvement. Following the procedure proposed in this work, diagrams similar to Figures 16 and 17 can be obtained to illustrate the impact of dispersion

concentration, gel strength and other factors. For softer particles, the curves in the diagrams are expected to shift toward the upper right direction. That is, at the same MSR and driving pressure, the gels could transport a larger distance into the channels.

Note that the shaded areas in Figure 16 and Figure 17 indicate the MSR range of the experiments. The unshaded areas are the results based on simple extension of the validated region. The transport behaviors can be very different when the MSRs are much smaller (e.g., MSR<0.5). The critical pressure gradient may follow a substantially different trend compared with the situations in this study. The propagation is expected to be much easier for the smaller gel particles. In the future, it is meaningful to perform more experiments at lower MSRs.

4. CONCLUSIONS

In this study, we carried out systematic studies to explore the critical pressure gradients and transport distances of micrometer-sized preformed particle gels (microgels) through superpermeable porous channels.

(1) We observed that a critical (minimum) pressure gradient (∇P_{cr}) was required to drive the microgel particles to propagate the superpermeable porous channels. Below ∇P_{cr}, the microgel particles could not transport in the porous channels. The existence of the ∇P_{cr} was confirmed with gel injection experiments carried out in constant-injection-pressure mode.

(2) The particle-to-pore matching size ratio (MSR) had a significant impact on the ∇P_{cr}. The ∇P_{cr} increased exponentially with the MSR at relatively low MSRs (<2). The

∇P_{cr} was lower than 60 psi/ft at the low MSRs. The low MSRs represented the desired situations in channels to be treated.

(3) A simple correlation was developed to describe the relationship between the critical pressure gradient and the MSR in the superpermeable channels. A procedure was developed to estimate the maximum transport (treatment) distance of the gel particles in reservoirs based on the critical pressure gradient.

(4) At low MSRs, the gel particles could transport a significant distance away from the wellbore, which was favorable for in-depth conformance treatments. At high MSRs, the transport distance of the gel particles was limited, which was favorable for near-wellbore treatments.

(5) The transport-distance diagrams can help engineers select proper gel products to address water channeling problems in reservoirs. Also, this work provides an effective procedure to study the impact of other parameters (e.g., dispersion concentration and gel strength) on the propagation distance of gel materials.

ACKNOWLEDGEMENTS

of any information, apparatus, product, or process disclosed, or represents that its use would not infringe privately owned rights. Reference herein to any specific commercial product, process, or service by trade name, trademark, manufacturer, or otherwise does not necessarily constitute or imply its endorsement, recommendation, or favoring by the United States Government or any agency thereof. The views and opinions of authors expressed herein do not necessarily state or reflect those of the United States Government or any agency thereof."

REFERENCES

Abrams, A. 1977. Mud Design to Minimize Rock Impairment Due to Particle Invasion. J Pet Technol. 29: 586–592.

Aldhaheri, M., Wei, M., Alhuraishawy, A., Bai, B. 2021. Field Performances, Effective Times, and Economic Assessments of Polymer Gel Treatments in Controlling Excessive Water Production from Mature Oil Fields. J. Energy Resour. Technol. 143 (8): 080804. https://doi.org/10.1115/1.4049019.

Aldhaheri, M., Wei, M., Zhang, N., Bai, B. 2020. Field Design Guidelines for Gel Strengths of Profile-Control Gel Treatments Based on Reservoir Type. J Pet Sci Eng 194 (November): 107482. https://doi.org/10.1016/j.petrol.2020.107482.

Bai, B., Huang, F., Liu, Y., Seright, R. S., Wang, Y. 2008. Case Study on Preformed Particle Gel for in-Depth Fluid Diversion. Paper presented at the SPE Symposium on Improved Oil Recovery, Tulsa, Oklahoma, USA, 20–23 April. SPE-113997-MS. https://doi.org/10.2118/113997-MS.

Bai, B., Li, L., Liu, Y., Liu, H., Wang, Z., You, C. 2007a. Preformed Particle Gel for Conformance Control: Factors Affecting Its Properties and Applications. SPE Res Eval & Eng 10 (4): 415–422. SPE-89389-PA. https://doi.org/10.2118/89389-PA.

Bai, B., Liu, Y., Coste, J. P., Li, L. 2007b. Preformed Particle Gel for Conformance Control: Transport Mechanism Through Porous Media. SPE Res Eval & Eng 10 (2): 176–184. SPE-89468-PA. https://doi.org/10.2118/89468-PA.

Bai, B., Wei, M., and Liu, Y. 2012. Injecting Large Volumes of Preformed Particle Gel for Water Conformance Control. Oil Gas Sci. Technol.–Rev. IFP Energies Nouvelles 67 (6): 941–952. https://doi.org/10.2516/ogst/2012058.

Bai, B., Wei, M., and Liu, Y. 2013. Field and Lab Experience with a Successful Preformed Particle Gel Conformance Control Technology. Paper presented at the SPE Production and Operations Symposium, Oklahoma City, Oklahoma, USA, 23–26 March. SPE-164511-MS. https://doi.org/10.2118/ 164511-MS.

Bai, B., Zhou, J., and Yin, M. 2015. A Comprehensive Review of Polyacrylamide Polymer Gels for Conformance Control. Pet. Explor. Dev. 42 (4): 525–532. https://doi.org/10.1016/S1876-3804(15)30045-8.

Chou, S. I., Bae, J. H., and Dolan, J. D. 1994. Development of Optimal Water Control Strategies. Paper SPE 28571 Presented at the SPE Annual Technical Conference and Exhibition in New Orleans, LA, U.S.A. https://doi.org/10.2118/28571-MS.

Demir, M., Topguder, N. N. S., Yilmaz, M., Ince, Y., Karabakal, U., Gould, J. H., 2008. Water Shutoff Gels Improved Oil Recovery in Naturally Fractured Raman Heavy Oilfield. Paper presented at the SPE Russian Oil and Gas Technical Conference and Exhibition, Moscow, Russia, October. https://doi.org/10.2118/116878-MS.

Goudarzi, A., Almohsin, A., Varavei, A., Taksaudom, P., Hosseini, S. A., Delshad, M., Bai, B., Sepehrnoori, K. 2017. New Laboratory Study and Transport Model Implementation of Microgels for Conformance and Mobility Control Purposes. Fuel 192: 158–68. https://doi.org/10.1016/j.fuel.2016.11.111.

Imqam, A., Goudarzi, A., Delshad, M., Bai, B. 2015. Development of a Mechanistic Numerical Simulator for Preformed Particle Gel Applications in Non-Crossflow Heterogeneous Reservoirs. Paper presented at the SPE Annual Technical Conference and Exhibition held in Houston, Texas, USA, 28-30 September. SPE-175058-MS. https://doi.org/10.2118/175058-MS.

Imqam, A., Wang, Z., and Bai, B., 2017. The Plugging Performance of Preformed Particle Gel to Water Flow Through Large Opening Void Space Conduits. J Pet Sci Eng 156: 51-61.

Karaoguz, O. K., Topguder, N. N. S., Lane, R. H., Kalfa, U., Celebioglu, D. 2007. Improved Sweep in Bati Raman Heavy-Oil CO2 Flood: Bullhead Flowing Gel Treatments Plug Natural Fractures. SPE Res Eval & Eng, 10 (02), 164-175. https://doi.org/10.2118/89400-PA.

Leng, J., Wei, M., and Bai, B. 2021. Review of Transport Mechanisms and Numerical Simulation Studies of Preformed Particle Gel for Conformance Control. J Pet Sci Eng 109051. (In press; published online 6 June 2021) https://doi.org/10.1016/j.petrol.2021.109051.

Liu, Y., Hou, J., Wang, Q., Liu, J., Guo, L., Yuan, F., Zhou, K. 2017. Flow of Preformed Particle Gel through Porous Media: A Numerical Simulation Study Based on the Size Exclusion Theory. Ind Eng Chem Res 56:2840–50. https://doi.org/10.1021/acs.iecr.6b03656.

Portwood, J. T. 1999. Lessons Learnt from Over 300 Producing Water Shutoff Gel Treatment, Paper SPE 52127 presented At SPE Mid-Continent Operations Symposium in Oklahoma, U.S.A. https://doi.org/10.2118/52127-MS.

Qiu, Y., Wei, M., Geng, J. Wu, F. 2016. Successful Field Application of Microgel Treatment in High Temperature High Salinity Reservoir in China. Paper presented at the SPE Improved Oil Recovery Conference, Tulsa, Oklahoma, USA, 11–13 April. SPE-179693-MS. https://doi.org/10.2118/179693-MS.

Seright, R. S. 1999. Polymer Gel Dehydration During Extrusion Through Fractures. SPE Prod Facil 14 (02): 110–116. SPE-56126-PA. https://doi.org/10.2118/56126-PA.

Seright, R. S. 2001. Gel Propagation Through Fractures. SPE Prod Facil 16(04): 225–31. SPE-74602-PA. https://doi.org/10.2118/74602-PA.

Seright, R. S. 2003. An Alternative View of Filter-Cake Formation in Fractures Inspired by Cr(III)-Acetate-HPAM Gel Extrusion. SPE Prod & Fac 18 (1): 65–72. SPE-81829-PA. http://dx.doi.org/10.2118/ 81829-PA.

Seright, R. S., Lane, R. H., and Sydansk, R. D. 2003. A Strategy for Attacking Excess Water Production. SPE Prod & Fac 18 (3): 158–169. SPE-84966-PA. https://doi.org/10.2118/84966-PA.

Seright, R. and Brattekas, B. 2021. Water Shutoff and Conformance Improvement: An Introduction. Pet. Sci. 18: 450–478. https://doi.org/10.1007/s12182-021-00546-1.

Seright, R., Zhang, G., Akanni, O., Wang, D. 2012. A Comparison of Polymer Flooding with In-Depth Profile Modification. J Can Pet Technol 51: 393–402. SPE-146087-PA. https://doi.org/10.2118/146087-PA.

Sydansk, R. D. and Romero-Zeron, L. 2011. Reservoir Conformance Improvement. Richardson, Texas, USA: Society of Petroleum Engineers.

Villone, M. M. and Maffettone, P. L. 2019. Dynamics, Rheology, and Applications of Elastic Deformable Particle Suspensions: A Review. Rheol Acta 58 (3–4): 109–130. https://doi.org/10.1007/s00397-019-01134-2.

Wang, J., Liu, H. Q., Zhang, H. L., Sepehrnoori, K. 2017. Simulation of Deformable Preformed Particle Gel Propagation in Porous Media. AIChE J 63: 4628–4641. https://doi.org/10.1002/aic.

Wu, D., Zhou, K., Hou, J., An, Z., Zhai, M., Liu, W. 2021. Review of Experimental and Simulation Studies of Enhanced Oil Recovery Using Viscoelastic Particles. J Dispers Sci Technol 42 (07): 956-969.

Zhao, Y., Leng, J., Lin, B., Wei, M., Bai, B. 2021a. Experimental Study of Microgel Conformance-Control Treatment for a Polymer-Flooding Reservoir Containing Superpermeable Channels. SPE J. SPE-204220-PA (in press; posted 26 April 2021). https://doi.org/10.2118/205486-PA.

Zhao, Y., Yin, S., Seright, R. S., Ning, S., Zhang, Y., Bai, B. 2021b. Enhancing Heavy-Oil-Recovery Efficiency by Combining Low-Salinity-Water and Polymer Flooding. SPE J. 26 (03): 1535–1551. https://doi.org/10.2118/204220-PA.

Zhou, K., Hou, J., Sun, Q., Guo, L., Bing, S., Du, Q., Yao, C. 2017. An Efficient LBM-DEM Simulation Method for Suspensions of Deformable Preformed Particle Gels. Chem Eng Sci 167: 288–296. https://doi.org/10.1016/j.ces.2017.04.026.

V. A COMPREHENSIVE LABORATORY METHOD TO EVALUATE MICROGEL CONFORMANCE CONTROL PERFORMANCE USING SANDWICH-LIKE CHANNEL MODELS

ABSTRACT

It is crucial to perform proper and comprehensive evaluations of gel products and/or an enhanced oil recovery processes before deploying them in field. In this work, a particular sandwich-like physical model and a set of comprehensive evaluation techniques were developed. The model, together with the proposed evaluation methodology, is able to identify and assess both positive and negative effects of a gel product or an EOR process from various aspects. The model consists of low-permeability matrices and a superpermeable porous channel. The characteristic properties of the model (kc, km, channel size, etc.) could be adjusted to represent the reservoir conditions of interest. The model overcame some drawbacks associated with commonly used conventional parallel coreflooding models. The design allowed crossflows between the matrices and the channel, and it was more representative of real channeling problems in reservoirs. The comprehensive evaluations included but were not limited to: 1) selective penetration/placement behavior, 2) sweep efficiency improvement (and fluid diversion) performance, 3) water-blocking efficiency, 4) damage effect to matrices, and 5) potential oil recovery improvement.

The evaluation methodology was elaborated upon using case studies. Under the conditions of the case studies, the results suggested that the tested microgel particles can selectively penetrate and be placed in the superpermeable channel of the reservoir. A cake

formed at the matrix inlet faces and prevented gel particles from further penetrating and damaging the matrix. The damage at the matrix inlet faces were effectively removed with a chemical breaker. The subsequent water was diverted to the matrices. Thus, the swept volume was significantly increased (e.g., 0.35 PV vs. 0.06 PV at breakthrough). The results also indicated that the water cut was effectively reduced after the gel treatment, thus the oil recovery performance was improved.

Above all, this study helps industry researchers and engineers gain better and more comprehensive understandings of the transport and placement behaviors of gel particles in superpermeable channels. The channel model and the comprehensive evaluation methodology developed in this work can serve as a useful tool in designing a conformance treatment.

Key words: conformance control; gel treatment; enhanced oil recovery (EOR); sweep efficiency; in-depth profile control

1. INTRODUCTION

Presence of high-permeability channels in a reservoir can result in early breakthrough of the injected fluids and excessive water production. As a result, a large portion of the oil in place is left unswept (Bai et al. 2013). The channels can be shut off with gel materials and the subsequent flooding fluids can be forced to the oil zones that have relatively low permeabilities (Seright & Brattekas 2021). There are different types of channels that cause excessive water production, such as open fractures, partial open fractures, high-permeability layers, and conduits (Sydansk & Romero-Zeron 2011; Seright

& Brattekas 2021; Bai et al. 2013). This study focused on excessive water production caused by superpermeable porous channels. These channels have super-high permeabilities (ten to several hundred darcies) compared with the matrices that hold most of the oil in place (Zhao et al. 2021a). Such superpermeable channels can also result in severe circulation loss of drilling fluids, especially in weak formations (Wang et al. 2008). The flow pathways in this type of channel are composed of large pore throat structures. The gel materials' transport mechanisms in such porous channels are substantially different with that in open fractures. Systematic studies are required to establish a better understanding of the transport behavior in such situations (Wu et al. 2021; Zhao et al. 2021a; Imqam et al. 2018).

Numerous applications have proven that gel treatment is effective to overcome the excessive water production problem, yet not all the applications were successful (Qiu et al. 2016; Aldhaheri et al. 2020, 2021). Gel treatment effectiveness is largely controlled by transport and placement behavior of the gel materials in the reservoirs/wells of interest (Bai et al. 2007b, 2008, 2012, 2013, 2015; Sydansk & Romero-Zeron 2011; Seright & Brattekas 2021). One important lesson can be learned from past practices is that proper and comprehensive evaluations of a gel product in the target well/reservoir are crucial to pursue a successful conformance control treatment. Various gel products were developed with intentions to achieve an in-depth profile control (Zhu et al. 2017; Kang et al. 2021; Seright & Brattekas 2021). In this scenario, the gel materials were injected quite a distance (rather than only the near-wellbore regions) into the channeling zones.

Breakout (production) of the injected gel materials at the outlet of a sandpack (core, conduit, or other models) were widely observed. However, the breakout of the gel materials

alone was insufficient to prove that the gel materials had good (deep) injectivity/migration abilities. At this stage, it cannot be claimed that the gel materials achieved in-depth profile control. Note that the pressure gradient used to force the gel materials through the model with a limited length (less than 1 m in most reported cases). An unrealistic high injection pressure was required if the model length was on the order of hundred meters. The distributions of the resistance factor (a measure of injectivity) and residual resistance factor (a measure of plugging efficiency) were also key considerations. The distributions should be unform along the model within a limited length. A significantly higher value at the inlet section was actually an indication of poor injectivity (surface plugging) and ineffective in-depth placement (plugging).

Several crucial issues should be evaluated prior to a gel treatment, including: 1) how the gel materials transport and place in the reservoirs to be treated, 2) whether the gel materials can selectively go into the target locations (i.e., the channeling/thief zones) without causing uncontrollable damage to the oil zones (matrices, or low-permeability zones), 3) whether the gel can effectively block the thief layer to the subsequent water flow (or other flooding fluids) and withstand extensive post-water flush, 4) whether the subsequent water can be significantly diverted to the oil zones and thus the sweep efficiency can be substantially improved, 5) how much oil recovery improvement can be achieved after the gel treatment, and 6) how to quickly screen a compatible gel product for a specific well/reservoir.

To address these concerns, representative physical models should be used to make comprehensive evaluations of the performance of the candidate gel materials, which provides the basis for selecting the proper gel materials to solve the excessive water

production problems in a given well/reservoir. Probably more importantly, especially for operators, the model and the comprehensive evaluation procedures established in this study can help identify both the positive and negative effects of the gel products from various aspects that address the concerned issues as discussed above. The evaluations should include penetration and placement behavior, sweep improvement, water-blocking efficiency, damage to matrices, and oil recovery improvements. Linear parallel models are commonly used for the evaluations. These models consist of two or more separated cores/sandpacks. However, some drawbacks are associated with these models, making the results sometimes misleading. The drawbacks include experimental artifacts, the differences between radial and linear flow, absence of communication between the channeling zones and the matrices, and the effects of diffusion and dispersion (Seright & Brattekas 2021). Some negative effects of the gel materials can be overlooked when using such models. The gel materials may actually cause damages to the reservoirs/wells, rather than contribute an improvement (Seright & Brattekas 2021).

To address the aforementioned concerns, a particular sandwich-like channel model was developed in this study. The model overcame the drawbacks associated with the commonly used conventional parallel coreflooding models. On the basis of the channel model, we developed a set of guidelines to perform comprehensive evaluations to test the conformance improvement potential of gel materials in heterogeneous reservoirs to be treated. The comprehensive evaluations include: 1) selective penetration/placement in the target location, 2) sweep efficiency improvement (and fluid diversion) after the gel treatment, 3) water-blocking efficiency, 4) damage to matrices, and 5) potential for improving oil recovery.

2. FABRICATION OF THE SANDWICH-LIKE CHANNEL MODELS

Heterogeneous models were fabricated to mimic reservoirs containing superpermeable channels. The model had a sandwich-like structure (Figure 1): two semicylindrical core plugs and a sand-filled fracture between them. The core plugs had relatively low permeabilities and acted as reservoir matrices. The sand-filled fracture was also a porous medium, but it was much more permeable than the matrices. The permeability could be adjusted by using sands of different grain size distributions.

(1) An intact core plug cut into halves. Supporting strips used to ensure a fracture space.
(2) Sands filled into the fracture space. The sands tightly packed to avoid movement and repacking during flooding and gel injection.
(3) The model is assembled. Gaps between strips and fracture faces are sealed with epoxy to ensure the gels do not migrate along these gaps.
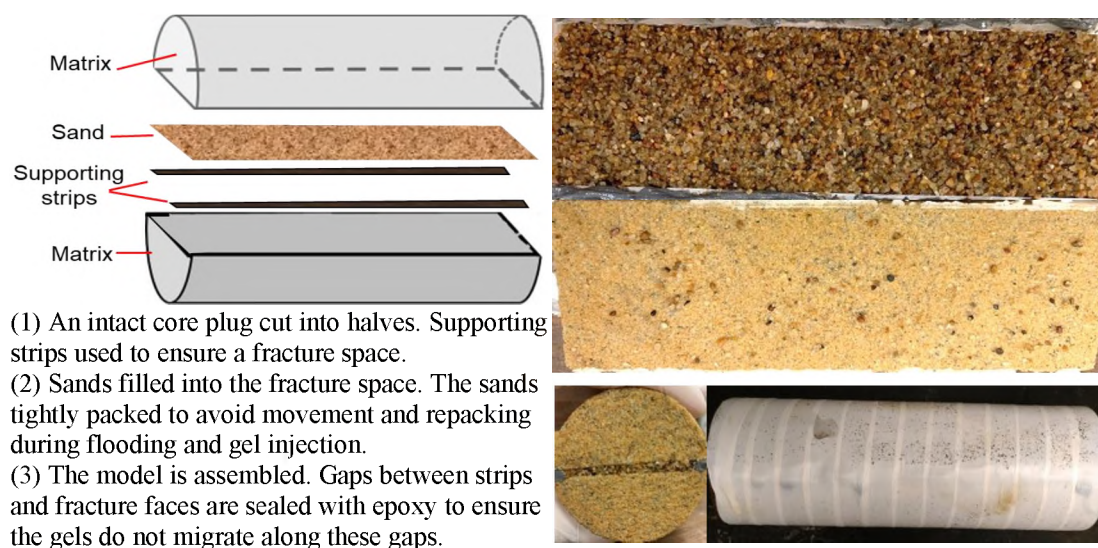
Figure 1. Fabrication of the sandwich-like channel model.
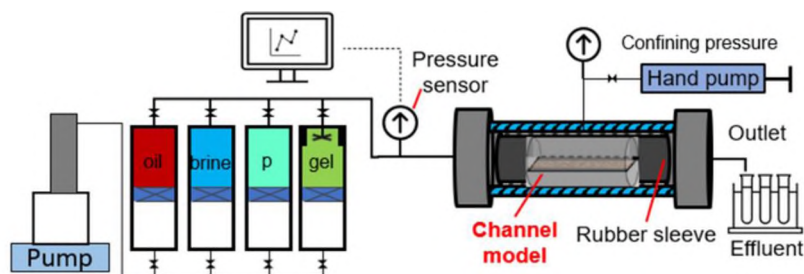
Figure 2. Experiment setup.

Table 1. Key parameters of a single-phase channel model.

Category	Parameter	Value	Note
Matrix	Length, L (cm)	13.90	/
	Diameter, d (cm)	5.07	/
	A (cm^2)	20.21	Original cross-sectional area of matrix before cut
	Porosity	0.294	Porosity of matrix
	Permeability, k_m (darcy)	4.8	Permeability of matrix
	MPV1 (cm^3)	82.50	Original matrix pore volume before cut
	MPV2 (cm^3)	75.93	Matrix pore volume after cut
Channel	Thickness, δ (cm)	0.32	Channel thickness
	Width (cm)	4.15	10/20 mesh sand
	CPV (cm^3)	7.04	PV of channel
	Total PV$_t$ (cm^3)	82.97	Total PV of matrix and channel
	Permeability, k_c (darcy)	212	Permeability of channel
Saturation (single phase, no oil)	OOIP	0	Original oil in place
	S_{oi}	0	/
	S_{wi}	1	/
Gel	Microgel, mesh	120/170	88-125 μm (average 290 μm after swollen in SFB)
	Swelling ratio	20	In SFB (synthetic formation brine of the Milne Point reservoir on Alaska's North Slope)
	Dispersion	1 wt%	Dry weight

Fabrication Procedures. The fabrication processes for the channel model are shown in Figure 1. In the demonstrative case studies, the cores used were 2-inch Berea or Boise Buff cores with permeabilities in the range of 100 md to 5,000 md. The key parameters of the model are shown in Table 1. As shown in Figure 1, the cores were cut into two half plugs. A 0.3-cm fracture was created between the two half parts. The fracture was filled with coarse sand with a specific range of mesh sizes. The channel had a higher permeability when filled with larger sand, and therefore, the permeability contrast between the channel and matrix became larger and the heterogeneity of the model became more pronounced.

According to whether the experiments involve oil recovery processes, the models can be divided into two categories: single-phase models and two-phase models. In the first category, the models are only saturated with brine before injecting the gel materials. In the latter case, initial oil saturation condition is established in the models (Zhao et al. 2021a). The preparation procedures for a single-phase channel model are summarized as follows:

(1) Prepare the intact core plug following standard processes (cut, clean, dry, vacuum, and saturate with brine). The synthetic formation brine (SFB) of the Milne Point oilfield on the Alaska's North Slope was used to saturate the core plug. In this step, the pore volume (MPV1 in Table 1) and porosity of the intact core were routinely measured through mass balance.

(2) Measure the matrix permeability and perform tracer test #1. The core was placed in a coreholder, and a confining pressure (also called overburden) was applied (Figure 2). The permeability was measured (km). The first brine tracer test was performed to provide a comparative baseline to the second tracer test after a channel was created and the third tracer test after the gel treatment (see next section). Before a tracer test, the fluid in the

flowline before the inlet of the coreholder was replaced with the traced brine. Otherwise, the fluid originally in the flowline (i.e., brine with no tracer) could lead to distortion of the tracer responses. Also, after the test, the flowline was cleaned with non-traced brine, and a large volume of the non-traced brine (>20 PV) was injected to flush out the tracer left in the model, thus eliminating interference in the next tracer test.

(3) Cut the core into two semi-cylindrical core plugs. In this process, a small volume of the core was lost as cuttings. The volume was estimated and subtracted from the total bulk volume of the core. Thus, the effective pore volume (MPV2 in Table 1) can be obtained accordingly.

(4) Fill the fracture with sands. Two supporting strips were mounted along the edges of the fracture to ensure a constant thickness of the fracture space between the two core plugs (Figure 1). The fracture space was filled with silica sands. The sands were pre-saturated with formation brine. The sands were tightly packed to avoid movement or repacking during brine flush and gel injection. The pore volume of the channel (CPV in Table 1) was estimated based on mass balance. Also, the total pore volume of the model (PVt) was determined.

(5) Seal the gaps and assemble the model. The gaps between the strips and the fracture faces were sealed with epoxy. This ensured that the gel did not migrate along these gaps and ensured the microgels went into the target zone (the channel). The whole model was wrapped with Teflon tape at the side surface to enhance integrity of the model (Figure 1). The inlet and outlet faces were left open.

(6) Estimate the permeabilities. The channel model was placed into the coreholder, and a confining pressure was applied on the model. The total permeability of the channel

model was measured (kt). Accordingly, the permeability of the channel (kc) was easily estimated with Darcy's law of multi-layer porous media based on kt, km, and the cross-sectional areas of the matrices and the channel.

(7) Perform the second brine tracer test. The second tracer test was carried out to measure the breakthrough and transport behaviors of the tracer. The results could be used to estimate the heterogeneity and channeling severity of the model. The model was then flushed with sufficient non-traced brine to displace out the tracer left in the model. Afterwards, gel treatment was performed. The tracer test procedures and results were discussed in the next section.

Features of the Channel Model. The sandwich-like channel model possessed several advantages. The design allowed for a confining pressure to be applied on the packed sand, thereby avoiding repacking or channeling along the matrix/channel interface. One may wonder whether it was applicable to drill a smaller hole inside the core and pack the hole with sand to mimic the channel. One problem with this kind of design was that the confining pressure cannot be applied on the packed sand. The fluid could channel along the internal wall. Likely, the sand would be repacked by the fluid or the injected gels. The characteristic parameters of the model were adjustable in quite a wide range. For example, different core plugs can be used to match the different permeabilities of the reservoirs of interest. Sands of different sizes can be used to mimic the channels of different permeabilities. Also, the size (thickness, width, extension degree into the matrices, etc.) of the channel relative to the matrices can be adjusted.

The channel model allows free crossflow between the matrices and the channel. It is usually the case in real reservoirs. However, for the conventional parallel coreflooding

models, the two parallel core models are separated from each other, and there is no crossflow between them. The channel model improves the representativeness over the traditional parallel models. The inlet faces of the matrices and the channel are close to each other, while the inlet faces of the conventional parallel models are separate from each other. The flow rates in the flowlines leading to the low-permeability core and high-permeability core are substantially different. This issue is possible to result in misleading observations of the gel penetration into the two cores (Seright & Brattekas 2021). The channel model developed in this study can avoid such experimental defects.

With some modifications to the end plug of the coreholder (e.g., adding separate effluent flowlines to the channel and matrix end faces), the fractional flow from the channel and matrices can be quantified. The possible dehydration and leak-off during the gel injection can also be monitored. The information can help estimate the extent of dehydration and gel propagation in scaled-up applications, analogous to the cases of gel propagation in open fracture systems (Seright 1999, 2001, 2003). Multiple pressure sensors can be connected to the model to monitor the pressures at different locations along the model.

Overall, the sandwich-like channel model overcame some key drawbacks of the conventional parallel coreflooding experiments. The distinct features discussed above enabled comprehensive and systematic evaluations of the conformance improvement potential of a gel material in reservoirs to be treated. The evaluations included but were not limited to: 1) selective penetration/placement in the target location, 2) sweep efficiency improvement after the gel treatment, 3) water-blocking efficiency, 4) damage to matrices, and 5) potential for improving oil recovery.

3. EVALUATION OF PENETRATION/PLACEMENT AND SWEEP IMPROVEMENT

3.1. SELECTIVE PENETRATION/PLACEMENT OF THE GEL PARTICLES

A basic requirement for a good conformance control treatment is that the gel materials penetrate and place in the target locations (e.g., the thief channels) without uncontrollable damage to the matrices (i.e., the oil zones). The channel model developed in this study evaluated the selective penetration/placement behavior of the gel materials. A case study was introduced to illustrate the methodology.
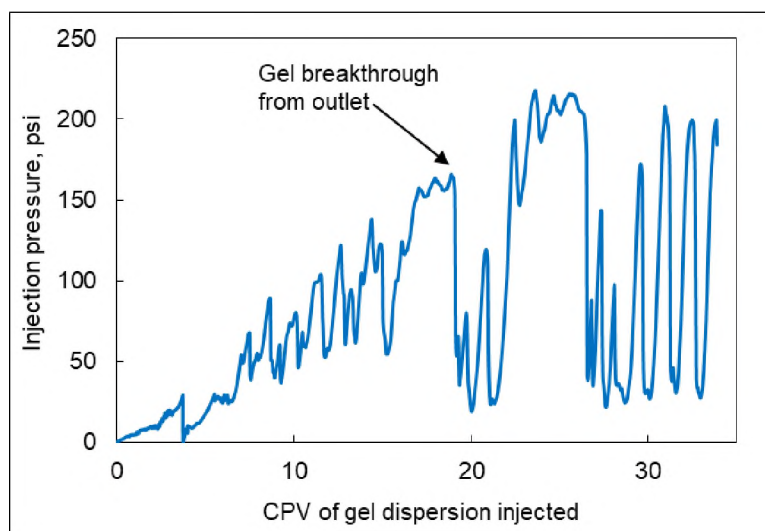
Figure 3. Injection pressure during gel injection. (It was also the differential pressure along the channel model.)

In the case study, microgel dispersion was injected into a channel model with a constant flow rate of 1 ml/min (equivalent to a superficial velocity of ~35 ft/d in the superpermeable channel). The permeability of the channel and the matrix was 212 and 4.8 darcies, respectively (Table 1). Thus, the permeability contrast between the channel and

the matrix was 45. The thickness of the channel was 3 mm. The concentration of the dispersion was 1 wt% (dry weight). The sizes of the dry gel particles were in the range of 88 to 125 μm, and the sizes were 240 to 340 μm (average 290 μm) after fully swollen in the formation brine. More detailed material information can be found in our previous publications (Zhao et al. 2021a; Bai et al. 2007a). The average particle-to-pore matching size ratio in the channel was 1.45, and the average size ratio in the matrices was 8.50. The dispersion was dyed with purple ink to help examine the placement of the microgel particles in the channel model.
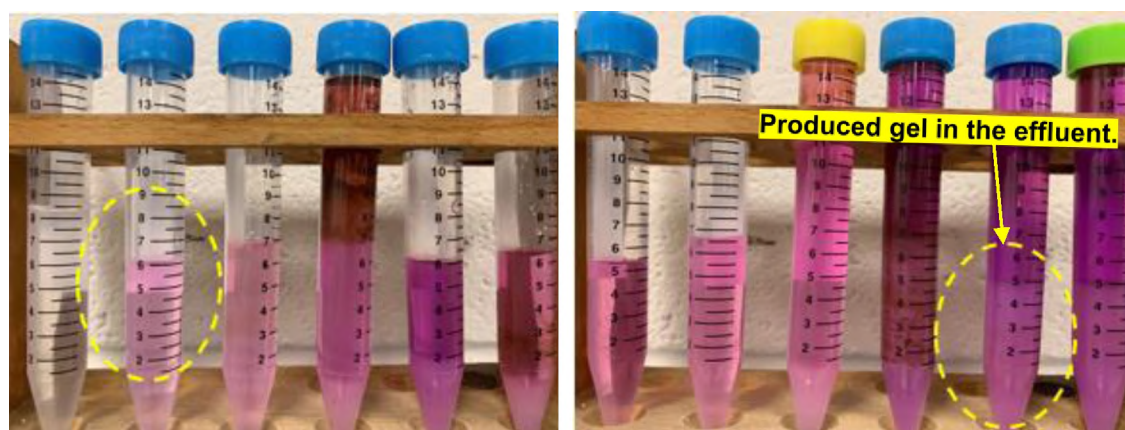
(a) Carrying fluid broke through.   (b) Gel particles broke through.

Figure 4. Breakthrough of the carrying fluid and the gel particles.

Gel particles were produced from the outlet after injecting 20 CPV of gel dispersion (Figure 3 and Figure 4). A total of about 34 CPV of gel dispersion was injected. Fluctuation in the injection was observed, which was a reflection of the viscoelastic nature of the gel particles transporting through a porous medium. The magnitude of the fluctuation can be mitigated by adjusting the concentration, strength, and/or particle size (Imqam et al. 2018).

After the gel treatment, a gel cake was formed at the inlet face of the matrices, as shown in Figure 5. The cake was a result of leak-off at the matrix face. The gel particles could not penetrate the matrices due to their too-large sizes relative to the pore throat sizes (8.5:1). Consequently, the gel particles accumulated at the face and formed a filter cake. The cake further prevented the gel particles from entering the matrices. Instead, the gel particles were transported into the superpermeable channel and were partially retained in the pore spaces of the channel. Therefore, the gel particles were selectively placed in the channel. The placement of the gel particles in the channel is shown in Figure 6. The sand/gel mixture at different locations could be collected to further evaluate the retention, dehydration, and re-swelling behavior of the gels. As a result of the selective placement behavior, the permeability contrast between the channel and the matrices were substantially reduced, and the effective sweep efficiency was improved.

Figure 5. Photo of the surface gel cake.
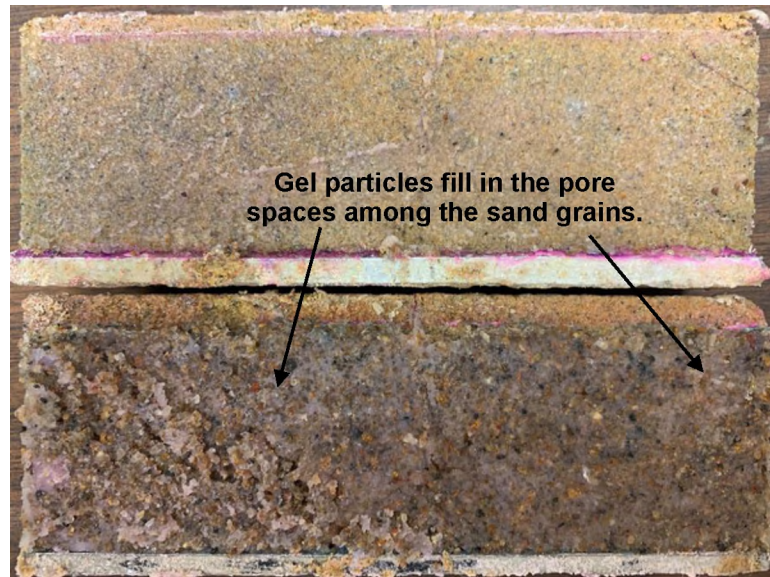
Figure 6. Gel placement in the channel.

3.2. EVALUATION OF SWEEP IMPROVEMENT

A procedure was established to evaluate the potential sweep improvement after the gel treatment. This was achieved by comparing the brine tracer test responses after and before the gel treatment. The procedure was detailed using the case study.

The tracer used was potassium iodide (anhydrous, ACS reagent, $\geq$99%, Sigma-Aldrich). The potassium iodide (KI) was dissolved in the formation brine. A spectrophotometer (UVmini-1240, Shimadzu) was used to test the absorbance of the tracer at a wavelength of approximately 230 nm. To obtain the relationship between the tracer concentration and the absorbance, a series of brine with known tracer concentration ranging from 0.11 ppm to 40 ppm were tested. The absorbance as a function of the tracer concentration is shown in Figure 7. The results suggested a good linear relationship between the concentration and the absorbance. The standard curve (Figure 7) provided the basis to measure the tracer concentration from the effluent of the channel model. Note that

the absorbance-concentration relationship was influenced by various factors, including the solvent (e.g., organic, inorganic), salinity, ion composition, pH of the solvent, etc. A standard reference curve should be obtained first in any specific applications.
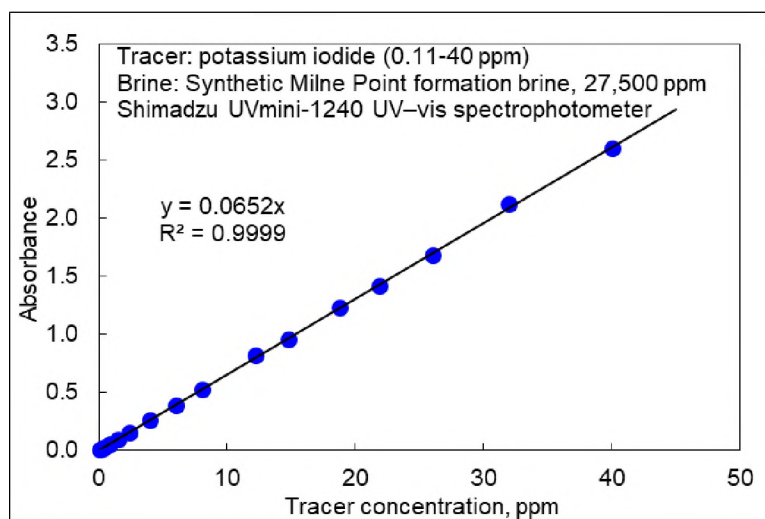
Figure 7. Standard absorbance-concentration curve.
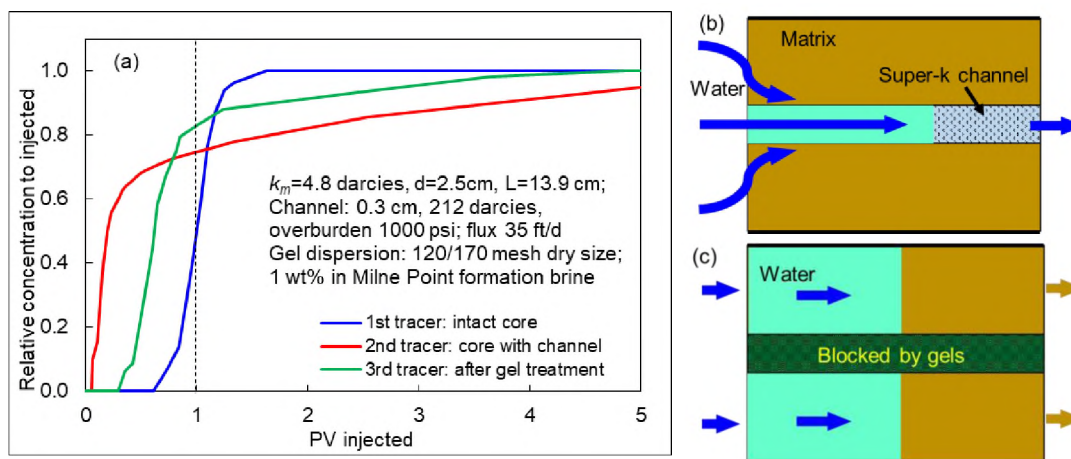
Figure 8. Fluid diversion and sweep efficiency improvement after gel treatment. (a) Tracer tests before and after the gel treatment. (b) Before gel treatment. (c) After gel treatment. (Breakthrough of the tracer after the gel treatment was delayed, indicating the fluid was diverted to the matrices. Therefore, the sweep efficiency was improved.)

As aforementioned, three tracer tests were performed. The injected brine contained 40 ppm tracer. The third test was carried out after the gel treatment. Before the test, the filter cake at the matrix face was removed with breaker (Wang et al. 2019). The model was flooded with non-traced brine to remove possible interference in the tracer test. Afterwards, the traced brine was injected, and the effluent was collected every 3-5 ml at the beginning, and the sample sizes were larger after 2 PV_t of brine was injected. The absorbances of the effluent samples were measured, and the tracer concentrations were determined with the assistance of the standard curve.

The brine tracer test results from the case study are summarized in Figure 8a. In the intact core, the tracer broke through (first sight of tracer in effluent) after 0.67 PV of brine injection (the blue curve). The tracer concentration of the effluent reached the original injected value quite quickly. In the channel model before the gel treatment, the tracer broke through almost immediately after injecting the traced brine (the red curve). Specifically, the breakthrough occurred at 0.06 PV_t of brine injection. It corresponded to 0.60 pore volume of the channel (CPV). The quick tracer breakthrough indicates that most of the injected brine only flowed through the superpermeable channel, instead of going into the matrices (see Figure 8b). Additionally, the effluent tracer concentration could not reach its injected value after several pore volumes of flooding. The sweep efficiency after 1 pore volume of injection was only 33% (the area above the curve in Figure 8a). The effective sweep volume was very limited.

After the gel treatment, the injected brine broke through at 0.35 PV_t, which was significantly delayed compared with the situations before the gel treatment. As the permeability of the channel was considerably reduced by the gels, the injected fluid was

diverted into the matrices to displace the fluid there, rather than only flowing through the channel (see Figure 8c). The tracer test results clearly demonstrate that the effective sweep volume was substantially increased after the gel treatment (0.62 PV_t vs. 0.33 PV_t after 1 pore volume of flood). Another indication of the fluid diversion and sweep improvement was the recovery of additional oil after the gel treatment (discussed later).

4. EVALUATION OF WATER-BLOCKING EFFICIENCY

The water-blocking efficiency in the channel is an important criterion to assess the effectiveness of the gel product. With the assistance of the channel model, a procedure was developed to directly evaluate the water-blocking efficiency. This new technique overcame some drawbacks of the existing commonly used methods. The water-blocking efficiency is related with the residual resistance factor (F_{rr}, i.e., permeability reduction after the gel treatment). The residual resistance factor (F_{rr}) and the water-blocking efficiency (E_{bw}) in the channel were estimated with Equation (1) and (2).

$$F_{rr} = \frac{(k_c)_b}{(k_c)_a} = \frac{(\Delta P/q)_a}{(\Delta P/q)_b}. \tag{1}$$

$$E_{bw} = \left(1 - \frac{(k_c)_a}{(k_c)_b}\right) \times 100\% = \left(1 - \frac{1}{F_{rr}}\right) \times 100\%. \tag{2}$$

One frequently used method is to measure the permeability of the channel model by injecting brine into the model after the gel treatment. However, the measured value is the overall permeability of the entire model (k_t), rather than the permeability of the channel (k_c). The Darcy's equation of multilayer reservoirs was not applicable here because both

the k_c and k_m (matrix permeability) were unknown. The k_m was unknown due to possible damage to the matrices caused by the gel materials as discussed in the next section.

Another common practice is to inject the same gel dispersion into a homogeneous sandpack of petrophysical properties comparable with the channel. Then the permeability after the gel injection is measured with brine to estimate the residual resistance factor (F_{rr}) and the water-blocking efficiency. However, the retention behavior is different in the two models, and the extra step is also time consuming. In the channel model, due to the pressure difference between the channel and matrices, water leaked off into the matrices. The gels were dehydrated and concentrated, and a higher retention was expected in this situation.
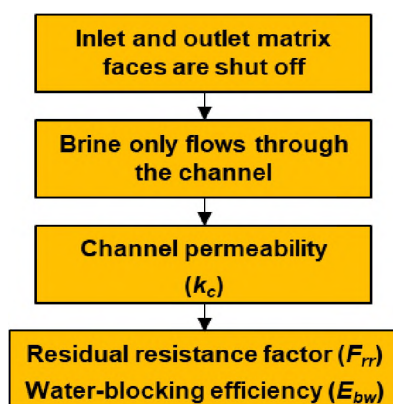
Figure 9. The procedure to evaluate water-blocking efficiency of the gel in the channel.
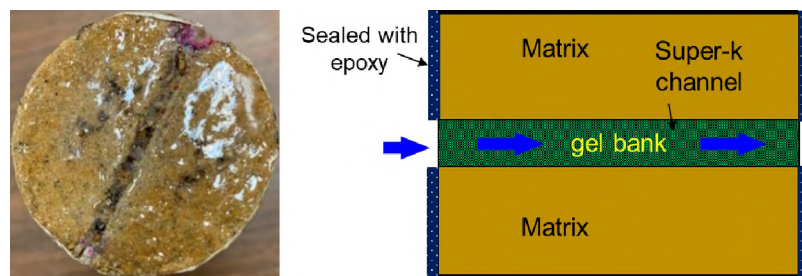
Figure 10. The inlet and outlet faces were sealed with epoxy.
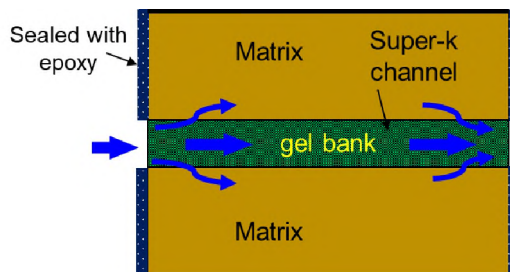
Figure 11. Possible crossflow into the matrix and back to the channel. [The crossflow leads to underestimation of the water-blocking efficiency in channel (i.e., the measured k_c is higher than the actual k_c).]

To have a reliable estimation of the water-blocking efficiency in the channel, a new direct test procedure was developed in this study (Figure 9). In this test, the inlet and the outlet faces of the matrix were shut off with epoxy (Figure 10). Only the inlet and outlet of the channel were kept open. In this situation, the injected fluid was expected to flow only through the channel. Therefore, the channel permeability (k_c) after the gel treatment was directly measured, and the F_{rr} and E_{bw} were estimated using Equation (1) and (2).

One may be concerned that the injected fluid is still possible to crossflow into the matrix somewhere (e.g., near the inlet), transport through the matrix, and flow back to the channel somewhere (e.g., near the outlet), as shown in Figure 11. If the crossflow does occur, it is practical to neglect it in the evaluation process. It may result in underestimation of the water-blocking efficiency in the channel (as the measured k_c may be higher than the actual k_c). This was acceptable because, at least, it did not lead to overestimation and/or overoptimism but rather results in a conservative water-blocking ability of the gel product.

In the case study, stable pressures at several different flow rates were measured to estimate the effective permeability of the channel. The k_c after the gel treatment was 610 md, thus the residual resistance factor (F_{rr}) was 348, that is, the permeability of the super-

k channel was reduced by 348 times. The permeability contrast (k_c/k_m) was reduced from 45 to 0.14. The water-blocking efficiency was 99.7%. The channel was effectively blocked with the gel particles. The subsequent flooding fluid was diverted into the matrices to increase the sweep volume.

5. EVALUATION OF DAMAGE TO MATRICES (INJECTIVITY LOSS)

The injectivity loss in the low-permeability zones (i.e., the oil zones) is always a crucial issue that should be considered whenever performing a gel treatment. The effective injectivity (E_I) of the matrices after the gel treatment relative to the original value can be estimated with Equation (3).

$$E_I = \frac{I_a}{I_b} \times 100\% = \frac{\left(q/\Delta P\right)_a}{\left(q/\Delta P\right)_b} \times 100\% = \frac{\left(k_m\right)_a}{\left(k_m\right)_b} \times 100\% . \tag{3}$$

In the equation, I, q, ΔP and k_m is the injectivity index, flow rate, pressure drop, and matrix permeability, respectively. The subscripts, a and b, denote after and before the gel treatment.

Smooth injectivity may be observed after resuming the injection. However, such observation does not necessarily mean the gel materials had no damage to the oil zones. The good injectivity after the gel treatment may be due to the poor placement or insufficient water-blocking ability of the gel materials in the fractures/channels. That is, the fractures/channels were still quite permeable after the gel treatment. Without a proper evaluation process, the negative effect may be misled by the seemingly good injectivity after the gel treatment. It may lead to underestimation of the damage to the matrices.
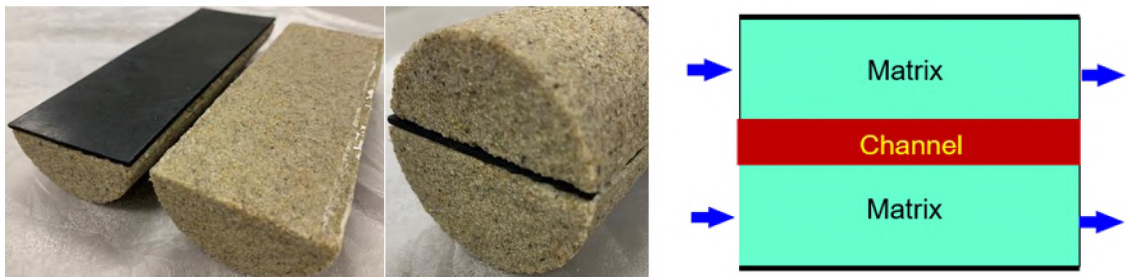
Figure 12. The channel is totally shut off with epoxy and a rubber gasket. (Red color means the channel is totally shut off with epoxy and a rubber gasket.)

On the basis of the channel model, we developed an approach to directly measure the matrix permeability (k_m) and evaluate the damage (injectivity loss) in the matrices after the gel treatment. In this test, the sand/gel mixture in the channel was removed. A rubber gasket the same size as the channel was placed in the fracture space (Figure 12). Both sides of the sleeve sheet were covered with epoxy to achieve good sealing at the matrix faces. The epoxy sealings at the inlet and outlet faces were removed. Brine was injected to measure the permeability of the matrix. The results were used to estimate permeability (injectivity) loss (i.e., damage) of the matrix after the gel treatment.

In the case study, stable pressures at different flow rates were measured to estimate the effective matrix permeability. The matrix permeability was 4340 md after the gel treatment. Note that the gel cake at the inlet surface was removed with a chemical breaker (Wang et al. 2019). After breaker soaking, the possible damage in the near-surface region in the matrices were also removed. The matrix retained 91.3% of its original injectivity.

One may wonder whether it is reliable to estimate the k_m (and injectivity loss) on the basis of k_t and k_c with Darcy's equation. Although, this approach can give a quick estimation, the accuracy can be influenced by the flow behavior in the channel model. The

gels may not be evenly packed in the channel. The gel particles may be packed more tightly near the inlet section, while it is not that tight near the outlet section. There was likely complex crossflow between the channel and the matrices when injecting brine. Therefore, a more reliable approach to estimate the k_m and the effective injectivity is directly measuring them, as discussed previously.

Another approach was to inject the same gel dispersion into a similar and intact core (with no fractures/channels) at the same loading pressure. Then brine was injected to measure the permeability after the gel injection and remediation processes to estimate the damage (injectivity loss). This approach is simple and straightforward to get an idea of the possible negative effects of the gel products (Elsharafi & Bai 2013, 2016; Imqam et al. 2016). Still, the simple approach was unable to account for some particular transport behaviors in the channel model. For example, during the gel injection process, some small gel particles or less-crosslinked materials may crossflow into the matrices through the matrix-channel interfaces. Therefore, it was still helpful to directly measure the k_m, and we present a practical approach to perform the direct measurement.

6. EVALUATION OF OIL RECOVERY IMPROVEMENT

The model can be used to evaluate the potential of oil recovery improvement by conformance treatment and/or other enhanced oil recovery (EOR) strategies (e.g., polymer flooding) (Zhao et al. 2021a). The model preparation procedure was similar except for the following: 1) the core was saturated with crude oil to establish the initial oil saturation condition, 2) the model was re-saturated with crude oil after the channel is created, and 3)

different oil recovery processes (e.g., water flood and polymer flood) were carried out before/after the gel treatment depending on the research objectives. The evaluation methodology was demonstrated with a case study.

The permeabilities of the matrix and the channel in the case study were 0.49 darcies and 237 darcies, respectively. Thus, the permeability contrast was 484. The brines and crude oil were from Milne Point oilfield on the Alaska's North Slope. Two brines were used in this case study. The synthetic formation brine (SFB) was used to saturate the model. The synthetic injection brine (SIB) was used as the flooding fluid, the makeup water to prepare polymer solutions, and the carrying fluid for the gel particles. The polymer used was Flopaam® (S.P.C.M. SA, Andrezieux-Boutheon, France) 3630S with a viscosity of approximately 45 cp at 7.3 s^{-1} at 71 °F (reservoir temperature). The crude oil had a viscosity of 202 cp. More information about the materials used can be found in previous works (Zhao et al. 2021a, 2021b). The information about the pilot polymer flood in the Milne Point oilfield can be found in Dandekar et al. (2019, 2020, 2021) and Ning et al. (2020).

After establishing the initial water saturation condition, waterflooding and polymer flooding were performed before a microgel treatment was implemented. The initial waterflooding was run until the water cut increased to 80%, which is comparable to the starting conditions of the ongoing polymer pilot (Dandekar et al. 2019; Ning et al. 2020). Polymer flooding was then performed until no oil was produced and the injection pressure became stable. Microgel dispersion (dry size: 170/230 mesh; concentration: 1 wt% in SIB) was injected until the gel particles were observed at the outlet (if possible) and the injection pressure became stable (if possible). After the gel treatment, post polymer flooding and waterflooding were performed sequentially.

Figure 13. Gel placement in the channel (sand size=10/20 mesh).
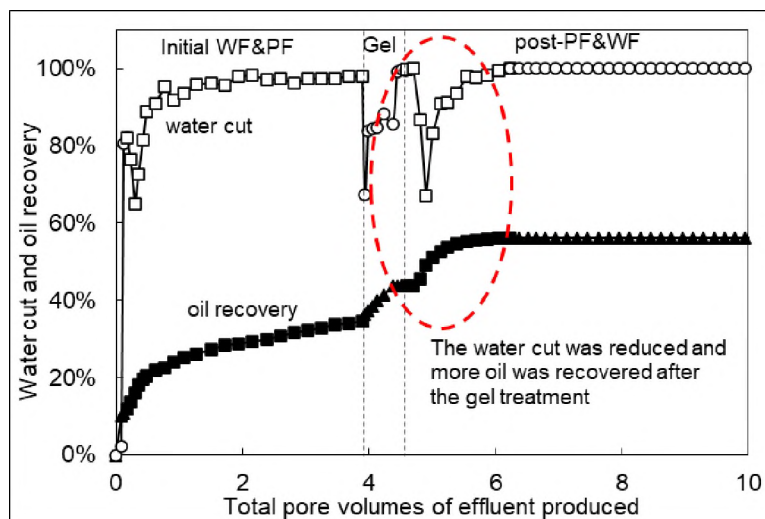
Figure 14. Water cut and oil recovery responses before and after the gel treatment.

The gel placement in the channel is shown in Figure 13. The water cut was effectively reduced after the gel treatment (from 100% to 63%), and additional oil was recovered (Figure 14). The oil recovery efficiency was increased by 21.4% of oil originally

in place (OOIP). The results suggest the subsequent polymer solution and brine were diverted to the matrices to displace the remaining oil previously left behind in the matrices. Therefore, the sweep efficiency was increased after the gel treatment, which agreed with the tracer tests in the single-phase case study mentioned previously.

The aforementioned case studies demonstrate that the sandwich-like channel model is a useful tool to evaluate the oil recovery improvement potential of a gel product or EOR process. By changing the parameters of the model (e.g., k_c, k_m, channel size), the favorable working conditions to achieve the best performance can be identified. Meanwhile, the effects of the various factors can be elucidated, e.g., the effect of gel particle size, particle size distribution, gel strength, concentration of the dispersion, channel and matrix permeabilities, salinity, and temperature. The injectivity, migration ability, placement behavior, water-blocking efficiency, profile control ability, and damage effect can be estimated. Besides, probably more importantly, especially for operators, the model and the comprehensive evaluation procedures established in this study can help identify both the positive and negative effects of a gel product or an EOR process from various aspects that address the most critical issues as discussed in the introduction part.

Based on the comprehensive evaluations, the favorable matching relationship between the gel properties and the reservoirs can be established. The appropriate gel materials and the associated properties (size, strength, etc.) can be selected for the reservoirs of interest. In addition, the channel model and the established comprehensive evaluation methodology can be used to test the feasibility of new gel products, such as the recently reported gels that have a secondary crosslinking ability (e.g., recrosslinkable PPG) (Pu et al. 2019).

7. CONCLUSIONS

In this paper, a particular sandwich-like physical model was developed. The model consists of low-permeability matrices and a superpermeable porous channel. The characteristic properties of the model (k_c, k_m, channel size, etc.) can be adjusted to represent the reservoir conditions of interest. The model overcomes some drawbacks associated with the commonly used conventional parallel coreflooding model. The special design allows crossflow between the matrices and the channel, and it is more representative of the real channeling problems in reservoirs.

On the basis of the particular channel model, we developed a set of guidelines to perform comprehensive evaluations to test the conformance improvement potential of a gel material in reservoirs to be treated. The evaluations include: selective penetration and placement in target locations, fluid diversion and sweep improvement, water-blocking efficiency, matrix damage, and oil recovery improvement.

The evaluation methodology was elaborated upon using case studies. The results suggest that the tested microgel particles can selectively penetrate and place in the superpermeable channel of the reservoir. A cake forms at the matrix inlet faces and prevents gel particles from further penetrating and damaging the matrix. The damage at the matrix inlet faces can be effectively removed with a chemical breaker. The subsequent water can be diverted to the matrices and thus the sweep volume is significantly increased (e.g., 0.35 PV vs. 0.06 PV at breakthrough). The water cut can be effectively reduced after the gel treatment, and thus the oil recovery performance is improved. Note that these specific results are pertaining to the experimental conditions in this study.

Above all, this study supports relevant researchers and engineers to gain a better and more comprehensive understanding of the transport and placement behaviors of gel particles in the superpermeable channels. The channel model and the comprehensive evaluation methodology developed in this work can serve as a useful tool in designing a conformance treatment.

NOMENCLATURE

Symbol	Description
CPV	Pore volume of channel
E_{bw}	Water-blocking efficiency
E_I	Effective relative injectivity after the gel treatment, percent
F_{rr}	Residual resistance factor
I_a	Injectivity after gel treatment
I_b	Injectivity before gel treatment
k_c	Permeability of channel, md
k_m	Permeability of matrices, md
k_t	Overall permeability of the channel model
MPV	Pore volume of matrix
MSR	Particle-to-throat matching size ratio
OOIP	Oil originally in place
ΔP	Differential pressure between the injector and the producer, psi
PPG	Preformed Particle Gel

PV_t	Total pore volume of channel model
q	Injection flow rate, ml/min
S_{oi}	Initial oil saturation, fraction
S_{wi}	Initial water saturation, fraction

ACKNOWLEDGEMENTS

herein do not necessarily state or reflect those of the United States Government or any agency thereof."

REFERENCES

Aldhaheri, M., Wei, M., Alhuraishawy, A., Bai, B. 2021. Field Performances, Effective Times, and Economic Assessments of Polymer Gel Treatments in Controlling Excessive Water Production from Mature Oil Fields. J. Energy Resour. Technol. 143 (8): 080804. https://doi.org/10.1115/1.4049019.

Aldhaheri, M., Wei, M., Zhang, N., Bai, B. 2020. Field Design Guidelines for Gel Strengths of Profile-Control Gel Treatments Based on Reservoir Type. J Pet Sci Eng 194 (November): 107482. https://doi.org/10.1016/j.petrol.2020.107482.

Bai, B., Huang, F., Liu, Y., Seright, R. S., Wang, Y. 2008. Case Study on Preformed Particle Gel for in-Depth Fluid Diversion. Paper presented at the SPE Symposium on Improved Oil Recovery, Tulsa, Oklahoma, USA, 20–23 April. SPE-113997-MS. https://doi.org/10.2118/113997-MS.

Bai, B., Li, L., Liu, Y., Liu, H., Wang, Z., You, C. 2007a. Preformed Particle Gel for Conformance Control: Factors Affecting Its Properties and Applications. SPE Res Eval & Eng 10 (4): 415–422. SPE-89389-PA. https://doi.org/10.2118/89389-PA.

Bai, B., Liu, Y., Coste, J. P., Li, L. 2007b. Preformed Particle Gel for Conformance Control: Transport Mechanism Through Porous Media. SPE Res Eval & Eng 10 (2): 176–184. SPE-89468-PA. https://doi.org/10.2118/89468-PA.

Bai, B., Wei, M., and Liu, Y. 2012. Injecting Large Volumes of Preformed Particle Gel for Water Conformance Control. Oil Gas Sci. Technol.–Rev. IFP Energies Nouvelles 67 (6): 941–952. https://doi.org/10.2516/ogst/2012058.

Bai, B., Wei, M., and Liu, Y. 2013. Field and Lab Experience with a Successful Preformed Particle Gel Conformance Control Technology. Paper presented at the SPE Production and Operations Symposium, Oklahoma City, Oklahoma, USA, 23–26 March. SPE-164511-MS. https://doi.org/10.2118/ 164511-MS.

Bai, B., Zhou, J., and Yin, M. 2015. A Comprehensive Review of Polyacrylamide Polymer Gels for Conformance Control. Pet. Explor. Dev. 42 (4): 525–532. https://doi.org/10.1016/S1876-3804(15)30045-8.

Dandekar, A., Bai, B., Barnes, J., Cercone, D., Ciferno, J., Ning, S., Seright., R., Sheets, B., Wang, D., Zhang, Y. 2019. First Ever Polymer Flood Field Pilot–A Game Changer to Enhance the Recovery of Heavy Oils on Alaska's North Slope. Paper presented at the SPE Western Regional Meeting, San Jose, California, USA, 23–26 April. SPE-195257-MS. https:// doi.org/10.2118/195257-MS.

Dandekar, A., Bai, B., Barnes, J., Cercone, D., Ciferno, J., Edwards, R., Ning, S., Schulpen, W., Seright., R., Sheets, B., Wang, D., Zhang, Y. 2020. First Ever Polymer Flood Field To Enhance the Recovery of Heavy Oils on Alaska's North Slope–Pushing Ahead One Year Later. Paper presented at the SPE Western Regional Meeting, April 27-30, 2020, Bakersfield, California, USA. Note–postponed to virtual format in April 2021. SPE-200814-MS. https:// doi.org/10.2118/200814-MS.

Dandekar, A., Bai, B., Barnes, J., Cercone, D., Ciferno, J., Edwards, R., Ning, S., Schulpen, W., Seright., R., Sheets, B., Wang, D., Zhang, Y. 2021. Heavy Oil Polymer EOR in the Challenging Alaskan Arctic–It Works! Paper prepared for presentation at the Unconventional Resources Technology Conference held in Houston, Texas, USA, 26-28 July 2021. URTeC-2021-5077. https://doi.org/10.15530/urtec-2021-5077.

Elsharafi, M. O. and Bai, B. 2013. Minimizing Formation Damage for Preformed Particle Gels in Mature Reservoirs. Paper presented at the SPE Asia Pacific Enhanced Oil Recovery Conference, Kuala Lumpur, Malaysia, 11–13 August. SPE-174645-MS. https://doi.org/10.2118/174645-MS.

Elsharafi, M. O. and Bai, B. 2016. Influence of Strong Preformed Particle Gels on Low Permeable Formations in Mature Reservoirs. Pet. Sci. 13 (1): 77–90. https://doi.org/10.1007/s12182-015-0072-3.

Imqam, A., Bai, B., and Delshad, M. 2018. Micro-Particle Gel Transport Performance Through Unconsolidated Sandstone and Its Blocking to Water Flow During Conformance Control Treatments. Fuel 231 (1 November): 479–488. https://doi.org/10.1016/j.fuel.2018.05.099.

Imqam A, Aldalfag A, Wang Y, Bai B. 2016. Evaluation Of Preformed Particle Gels Penetration into Matrix for a Conformance Control Treatment in Partially Open Conduits. Paper presented at the SPE Annual Technology Conference and Exhibition, Dubai, UAE. SPE-181545-MS. https://doi.org/10.2118/181545-MS.

Kang, W., Kang, X., Lashari, Z.A., Li, Z., Zhou, B., Yang, H., Sarsenbekuly, B. Aidarova, S. 2021. Progress of Polymer Gels for Conformance Control in Oilfield. Adv Colloid Interface Sci 289 (March): 102363. https://doi.org/10.1016/j.cis.2021.102363.

Ning, S., Barnes, J., Edwards, R., Schulpen, W., Dandekar, A., Zhang, Y., Cercone, D., Ciferno, J. 2020. First Ever Polymer Flood Field Pilot to Enhance the Recovery of Heavy Oils on Alaska North Slope–Producer Responses and Operational Lessons Learned. Paper presented at the SPE Annual Technical Conference and Exhibition, Virtual, 26–29 October. SPE-201279-MS. https://doi.org/10.2118/201279-MS.

Qiu, Y., Wei, M., Geng, J. Wu, F. 2016. Successful Field Application of Microgel Treatment in High Temperature High Salinity Reservoir in China. Paper presented at the SPE Improved Oil Recovery Conference, Tulsa, Oklahoma, USA, 11–13 April. SPE-179693-MS. https://doi.org/10.2118/179693-MS.

Pu, J., Bai, B., Alhuraishawy, A., Schuman, T., Chen, Y., Sun, X. 2019. A Recrosslinkable Preformed Particle Gel for Conformance Control in Heterogeneous Reservoirs Containing Linear-Flow Features. SPE J. 24 (04): 1714–1725. SPE-191697-PA. https://doi.org/10.2118/191697-PA.

Seright, R. S. 1999. Polymer Gel Dehydration During Extrusion Through Fractures. SPE Prod Facil 14 (02): 110–116. SPE-56126-PA. https://doi.org/10.2118/56126-PA.

Seright, R. S. 2001. Gel Propagation Through Fractures. SPE Prod Facil 16 (04): 225–231. SPE-74602-PA. https://doi.org/10.2118/74602-PA.

Seright, R. S. 2003. An Alternative View of Filter-Cake Formation in Fractures Inspired by Cr(III)-Acetate-HPAM Gel Extrusion. SPE Prod & Fac 18 (01): 65–72. SPE-81829-PA. http://dx.doi.org/10.2118/ 81829-PA.

Seright, R. S and Brattekas, B. 2021. Water Shutoff and Conformance Improvement: An Introduction. Pet. Sci. 18: 450–478. https://doi.org/10.1007/s12182-021-00546-1.

Sydansk, R. D. and Romero-Zeron, L. 2011. Reservoir Conformance Improvement. Richardson, Texas, USA: Society of Petroleum Engineers.

Wang, H., Sweatman, R., Engelman, B., Deeg, W. F., Whitfill, D. L., Soliman, M. Y., Towler, B. F. 2008. Best Practice in Understanding and Managing Lost Circulation Challenges. SPE Drill & Compl 23 (2): 168–175. SPE-95895-PA. http://dx.doi.org/10.2118/95895-PA.

Wang, Z., Bai, B., Zhou, E., Pu, J., Schuman, T. 2019. Experimental Evaluation of Oxidizing Breakers for a Polyacrylamide-Based Re-Crosslinkable Preformed Particle Gel. Energy Fuels 33 (6): 5001–5010. https://doi.org/10.1021/acs.energyfuels.9b00709.

Wu, D., Zhou, K., Hou, J., An, Z., Zhai, M., Liu, W. 2021. Review of Experimental and Simulation Studies of Enhanced Oil Recovery Using Viscoelastic Particles. J Dispers Sci Technol 42 (07): 956-969.

Zhao, Y., Leng, J., Lin, B., Wei, M., Bai, B. 2021a. Experimental Study of Microgel Conformance-Control Treatment for a Polymer-Flooding Reservoir Containing Superpermeable Channels. SPE J. SPE-205486-PA (in press; posted 26 April 2021). https://doi.org/10.2118/205486-PA.

Zhao, Y., Yin, S., Seright, R. S., Ning, S., Zhang, Y., Bai, B. 2021b. Enhancing Heavy-Oil-Recovery Efficiency by Combining Low-Salinity-Water and Polymer Flooding. SPE J. 26 (03): 1535–1551. SPE-204220-PA. https://doi.org/10.2118/204220-PA.

Zhu, D., Bai, B., and Hou, J. 2017. Polymer Gel Systems for Water Management in High-Temperature Petroleum Reservoirs: A Chemical Review. Energy Fuels, 31 (12): 13063-13087.

VI. TRANSPORT, PLACEMENT, FLUID DIVERSION AND MATRIX DAMAGE BEHAVIOR OF MICROGELS FOR CONFORMANCE CONTROL IN RESERVOIRS CONTAINING SUPERPERMEABLE CHANNELS

ABSTRACT

Gel treatment has been proven an effective method to attack excessive water production in many mature oilfields. However, not all the application projects have successful stories. The effectiveness of a gel treatment largely depends on the transport and placement behavior of gel materials in the reservoirs to be treated. In this work, we carried out systematic studies to investigate the transport, placement, water-blocking ability, fluid diversion and sweep improvement, and matrix damage effect of micrometer-sized preformed particle gels (microgels) in reservoirs containing superpermeable (super-K) channels. The impact of the channel/matrix permeability contrast, the particle/pore size ratio in the channels, and the particle/pore size ratio in the matrices were studied. The favorable conditions of the gel treatment were identified. The results show that the microgel particles selectively penetrate, place in, and effectively shut off the super-K channels under proper conditions. Delayed breakthrough of the gel particles was observed, which was partially resulted from the dehydration of the gel particles in the channel and the buildup of a filter cake at the inlet face of the matrices. The sweep improvement after the gel treatment was evaluated by chemical tracer tests. The results clearly demonstrate delayed breakthrough, fluid diversion, and increased swept volume of the subsequent flooding fluid. In the experiments, the sweep improvement was in the range of 0.25-0.43 total pore volumes (PV_t). A higher sweep improvement was achieved as the permeability

contrast was higher (i.e., the reservoir was more heterogeneous). To achieve both good injectivity and water-blocking efficiency for the tested microgels, the matching size ratio in the channel (MSR_c) should be below 2. Meanwhile, the MSR in the matrices (MSR_m) should be kept above 5 to avoid significant damage to the matrices. The results of this study provide support for gel product selection, and successful gel treatment designs & implementations.

Key words: conformance control; gel treatment; preformed particle gel (PPG); enhanced oil recovery (EOR); water control; gel transport and placement

1. INTRODUCTION

Gel treatment has been proven an effective method to attack excessive water/polymer production in many mature oilfields (Bai et al. 2008, 2012, 2013, 2015; Sydansk and Romero-Zeron 2011; Qiu et al. 2016; Aldhaheri et al. 2020, 2021). However, not all the application projects are successful (Qiu et al. 2016; Aldhaheri et al. 2020, 2021). The effectiveness of a gel treatment largely depends on the transport and placement behavior of the gel materials in the reservoirs to be treated (Seright & Brattekas 2021).

Due to the complexity, the transport and placement behavior of gel materials in porous-medium-type super-K channels are still not clearly understood (Leng et al. 2021; Wu et al. 2021; Villone & Maffettone 2019). Bai et al. (2007b) studied the transport mechanisms of PPGs at microscopic and macroscopic scales. Six patterns were identified at the microscopic scale: direct pass, adsorption, deform and pass, snap-off and pass, shrink and pass, and trap. Three transport patterns were proposed to describe the macroscopic

propagation behavior: pass, broken and pass, and plug. The size ratio of the swollen PPG particles and the pore throat, the gel strength and the driving force were regarded as the dominant factors on the transport patterns.

Yao et al. (2012, 2013) investigated the transport behavior of microspheres (~20 µm) through homogeneous and heterogeneous sandpacks with relatively high permeabilities. They further studied the effects of flow rate, pore-throat size, particle size, and injection concentration on transport and retention patterns (Yao et al., 2020). Five transport and retention patterns were observed in experiments using microchannels: surface deposition, smooth passing, direct interception, deforming remigration, and rigid blockage. Dupuis et al. (2016) investigated the effect of concentration of 2-µm microgels on the transport behavior in sandstone cores. Their results indicated that the resistance factor and residual resistance factor increased with the microgel concentration. Imqam et al. (2018) studied the effect of concentration, salinity, gel size and permeability on the transport behavior of microgel in sandpacks. The microgels was able to transport deep into high-permeability sandpacks, but the inlet section showed a much higher pressure drop due to microgel retention. The results also indicated the transport was more sensitive to the strength of the microgel compared with the particle size. Al-Ibadi and Civan (2013) noticed that the particle size distribution was changed after transporting through the sandpacks. The fraction of large particles in the effluent was reduced compared with the injected particles. It was an indication of entrapment or surface deposition in the sandpacks. They observed wavy-shape pressure response during gel suspension injection, which was regarded as a result of the repeated plugging and remigration of the elastic gel particles in the porous media.

The matching relationship between the gel properties (size, strength, concentration, etc.) and the reservoir parameters (permeability, pore size, etc.) plays a crucial role in an effective gel treatment. Different optimal matching parameters were reported to achieve the satisfactory plugging and sweep improvement performance (Yao et al. 2012, 2013; Dai et al. 2017, 2018; Yuan et al. 2020; Wang et al. 2021).

Yao et al. (2012, 2013) reported that the favorable matching factor (particle-to-pore size ratio) for their microspheres was in the range of 1.35-1.55 (with an optimal value around 1.45) according to the water-blocking performance. Dai et al. (2017, 2018) reported that for the dispersed particle gels (DPG) they developed, the optimal matching factor was in the range of 0.21-0.29 to achieve both good injectivity and profile control. Yuan et al. (2020) studied the transport and plugging behavior of microgel particles (~10 µm) in cores with relatively low permeabilities (20-900 md) at high-temperature and high-salinity conditions. Three matching parameters were proposed to account for the effect of size distribution of the gel particles on the transport and plugging behavior. Wang et al. (2021) studied the plugging–matching relationship between the gel particles (labeled as DBR elastic particles) and pore throats of reservoirs. They proposed an interesting equation to quantify the optimal plugging matching conditions. In the equation, they incorporated the more established matching relationship of rigid particles through a parameter of elastic deformation coefficient. The best plugging-matching fell in the range of 0.21 to 1.10 in a wide range of concentration, particle size and permeability conditions.

Attention should be paid to the potential damage effect to matrices (oil zones) when performing a gel treatment. Elsharafi & Bai (2012, 2013, 2016) performed filtration tests to study the invasion of weak and strong preformed particle gels into low-permeability

matrices with relatively low permeabilities (4-320 md). They tested the impact of particle size, salinity (gel strength), permeability, and loading pressure on the damage effect. Imqam et al. (2016a) studied the damage of the preformed particle gels to matrix using core plugs with permeabilities in the range of 3 to 1650 md. They studied the effect of loading pressure, permeability, particle size, particle strength on the damage depth and damage degree (injectivity/permeability loss). The damage was small, and the invasion depth was limited when the particle-to pore size ratio was high (>500). Wang et al. (2019) tested different formulas of chemical breakers to degrade gel materials in bulk conditions.

The above brief review indicates that significant discrepancies still exist on the favorable conditions for effective gel treatments. Besides, homogenous single sandpack/core or separated parallel sandpack/core models were frequently used to investigate the injectivity, plugging, fluid diversion, and/or oil recovery improvement performance. However, the parallel models lack connectivity between the channeling layer and the matrices. the transport and placement behaviors are different in heterogeneous models compared with that in homogeneous models.

To make the experimental conditions more representative, we recently developed a sandwich-like channel model to study the transport and placement behavior of gel materials in super-K channels (Zhao et al., 2021c). The model had good connectivity between the matrices and the channel, which overcame some drawbacks of the conventional parallel models. A set of comprehensive evaluation methodologies were developed to assess the fluid diversion and oil recovery performance of microgels in heterogeneous reservoirs containing super-K channels (Zhao et al. 2021a, 2021c).

This study intended to investigate the transport, placement, water-blocking ability, sweep improvement, and matrix damage effect of microgel particles in reservoirs containing super-K channels. The impact of the channel/matrix permeability contrast, the particle/pore size ratio in the channels, the particle/pore size ratio in the matrices, and other factors were explored. The favorable working conditions for the gel treatment were identified. The important implications to field applications were discussed. The results can provide support for successful particle gel treatment design and implementations.

2. METHODOLOGY

Micrometer-sized preformed particle gels (PPG) (Bai et al. 2007a; Zhao et al. 2021a) were used with the swelling ratio around 20 in the synthetic Milne Point formation brine (SFB). The SFB had a total dissolved solid (TDS) of 27500 ppm (Zhao et al., 2021a, 2021b). The microgel particles were carried with the SFB with a dry weight concentration of 1 wt%.

The experiment setup is shown in Figure 1. An accumulator equipped with a blending rotor was used to store the gel dispersion (also called suspension). The dispersion was injected while being stirred to avoid gravitational segregation of the gel particles and the carrying fluid.

Sandpacks, channel models, and intact sandstone cores were used to investigate the transport, placement, water-blocking efficiency, sweep improvement, and possible matrix damage effect of the microgels. The channel models (Figure 1) had a sandwich-like structure, which consisted of two semi-cylindrical core plugs (i.e., the matrices) and a 0.3-

cm sand-filled fracture (i.e., the super-K channel) between the plugs. The cores had a diameter of 2 inches and a length of around 15 cm. The experiments were performed at single phase conditions. The intact cores and the entire channel models were not saturated with crude oil. The fabrication processes of the channel model and detailed experimental procedures can be found in Zhao et al. (2021c).

The experiments performed with channel models are summarized in Table 1. The table gives the matrix permeability, channel permeability, permeability contrast, average particle-to-pore matching size ratio (MSR), and average gel particle sizes. Three brine tracer tests were performed to evaluate the sweep efficiency before and after the gel treatment. The channel permeability (k_c) was directly measured to estimate the water-blocking efficiency in the channel. In this process, we only kept the inlet and outlet of the channel open. The inlet and outlet faces of the matrices were shut off. The matrix permeability (k_m) was directly measured after the gel treatment to evaluate the damage in the matrix. In this test process, only the matrices were kept open, and the channel was totally shut off.
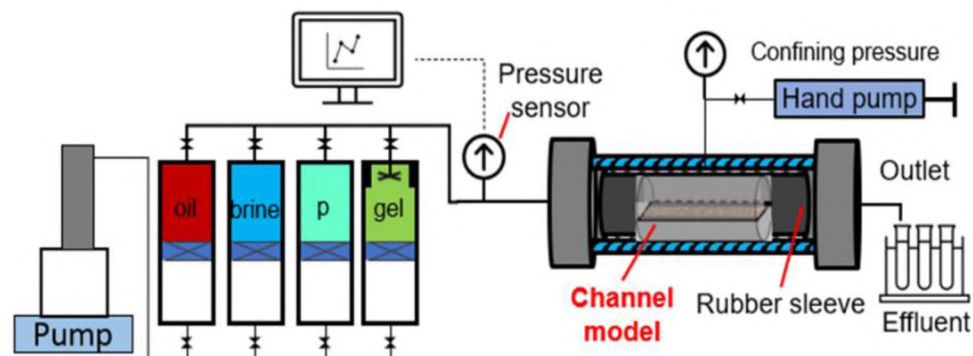
Figure 1. Experiment setup.

Table 1. Summary of experiments performed with channel models.

Exp #.	Matrix permeability (k_m), darcies	Channel permeability (k_c), darcies	Dry gel size, mesh	Average swollen gel size, μm	k_c/k_m	MSR_c (channel)	MSR_m (matrix)
S1	4.75	212	120/170	290	45	1.45	8.50
S2	7.83	218	120/170	290	28	1.43	6.72
S3	4.74	179	170/230	205	38	1.13	6.10
S4	0.17	139	170/230	205	833	1.27	26.42
S5	10.46	79	170/230	205	7.6	1.69	4.11
S6	4.83	221	230/400	136	46	0.67	4.02
S7	9.94	87	230/400	136	8.8	1.07	2.79

3. TRANSPORT AND PLACEMENT BEHAVIOR

The transport and placement behavior of the microgels under different conditions were studied. Taking Exp S4 as an example, the gel dispersion was injected into the model at 1 ml/min (equivalent to a superficial velocity of 35.6 ft/d in the channel). The matrices had a permeability of 0.17 darcies, and the channel-to-matrix permeability contrast was 833. The MSR in the channel (MSR_c) was 1.27 and it was 26.4 in the matrices (MSR_m). The average pore sizes of the matrices and the porous channels were estimated with the modified Carman-Kozeny equation, Equation (1) (Mauran et al., 2001; Carman, 1956).

$$d = \sqrt{\frac{16 k f_{CK} \tau^2}{\varPhi}} . \tag{1}$$

Figure 2 presents the injection pressures, pressure gradients, and resistance factors during gel injection. The resistance factor was calculated as the ratio of the gel injection pressure to the initial brine injection pressure at the same flow rate. As shown in Figure 2, the pressure exhibited a steady increase at the beginning and started to exhibit fluctuation after the pressure reached about 5 psi. The injection pressure became stable around 30 psi (balanced pressure) with fluctuation after about 9.5 CPV (channel pore volume) of gel dispersion was injected. Following the similar procedures, more experiments were performed to investigate the transport and placement behavior of microgel particles at different conditions (see Table 1).
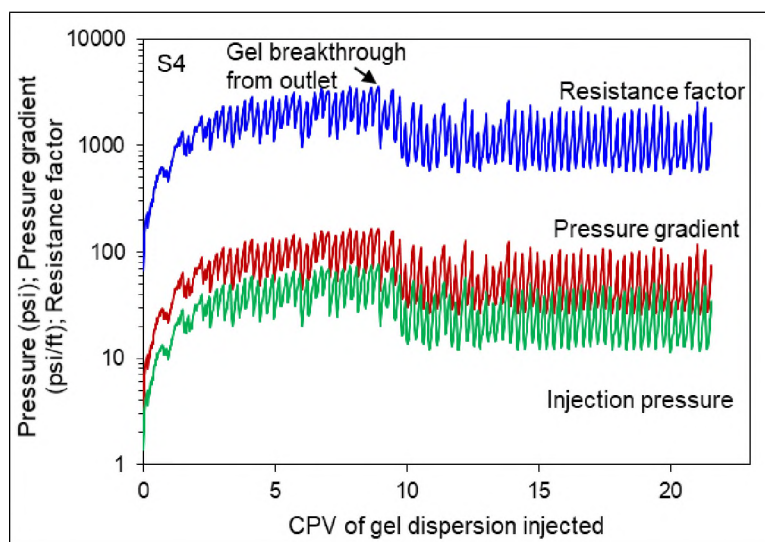
Figure 2. The injection pressure, pressure gradient and resistance factor during gel injection (Exp S4).

Figures 3 to 5 respectively summarize the injection pressures, pressure gradients, and resistance factors of the experiments. More detailed results of each experiment are presented in the Appendix (Figures A1 to A6). Figure 6 plots the balanced values against

the MSR_c. Generally, the injection pressure, pressure gradient and resistance factor increased with the MSR_c. Larger particles were more difficult to transport through the superpermeable channels.
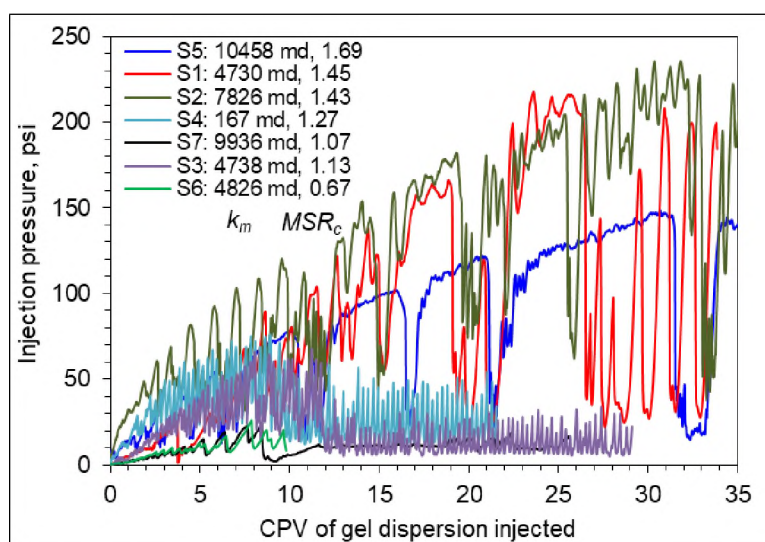
Figure 3. Summary of the injection pressures in different experiments.
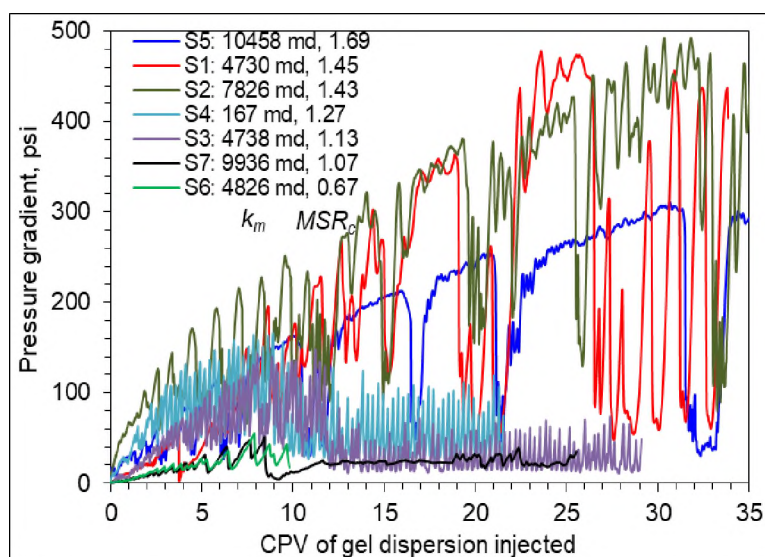
Figure 4. Summary of the injection pressure gradients during gel injection.
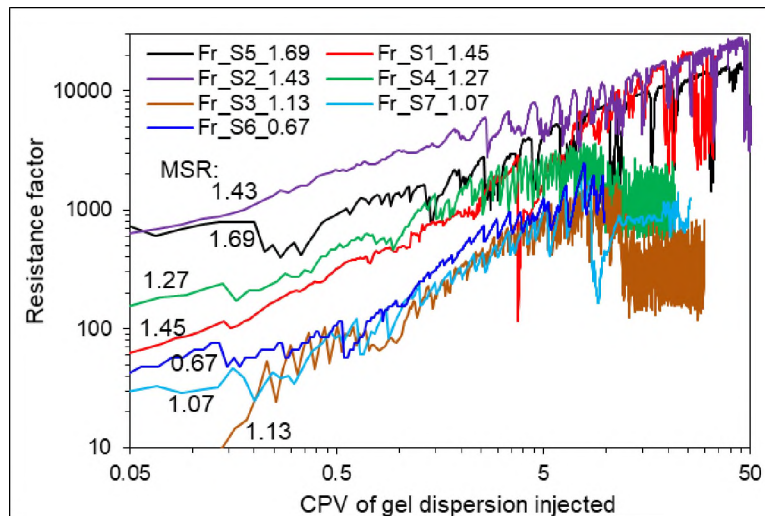
Figure 5. Summary of the resistance factors.
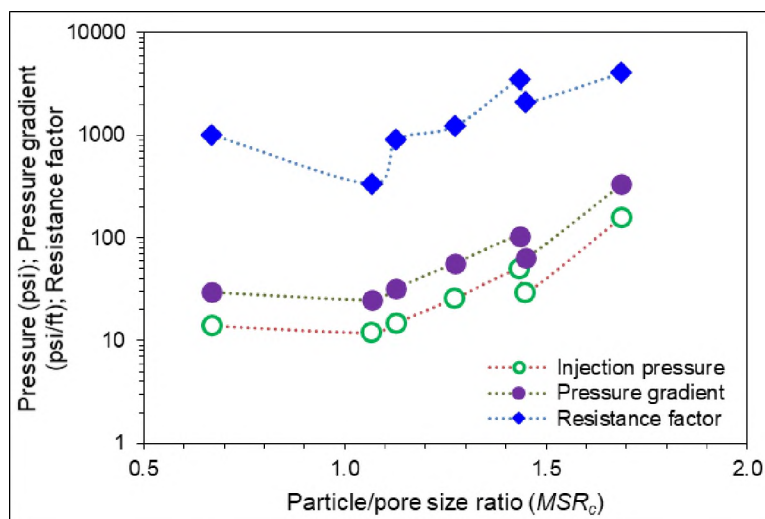
Figure 6. The injection pressure, pressure gradient, and resistance factor as a function of MSR_c.

Delayed Propagation and Breakthrough Time of the Gel Particles. The gel particles could penetrate and transport through the super-K channel. However, significantly delayed propagation of the gel particles was observed compared with the carrying fluid. In S4, gel particles in the effluent were detected after injecting about 9.5 CPV of gel dispersion, while

the carrying fluid broke out at about 1 CPV. The impact of different parameters on the breakthrough time (in terms of CPV) was checked to identify the influential factors, as shown in Figure 7. Among the tested parameters, the breakthrough time showed the strongest correlation with the MSR_c, followed by the matrix permeability (k_m) (Figure 7a and Figure 7b). On the contrary, its correlation with the permeability contrast (k_c/k_m) and MSR_c was weak, as shown in Figure 7c and Figure 7d. The breakthrough occurred later as the MSR_c was increased, which was reasonable as it was more difficult for the gel particles to transport through the channel as the MSR_c was larger.

The impact of the matrix permeability on the breakthrough time was related to the leak-off phenomenon at the inlet face of the matrices. After taking the model out of the coreholder, we observed a gel cake formed at the inlet face of the matrices (Figure 8). It indicated that leak-off took place at the face of the channel model during gel injection. The carrying fluid leaked off into the matrices, while the gel particles were left behind at the inlet surface of the channel model. As more gel particles accumulated at the surface, a cake was formed.

When the matrices were more permeable, the brine was easier to leak off into the matrices. More gel particles were required to build up the surface cake. The delayed breakthrough phenomenon was also observed for preformed bulk gels transporting through open fractures (Seright 1999, 2001). The breakthrough of the gels through open fractures was dominated by the injection flow rates and fracture width (conductivity) (Seright 1999, 2001). However, a fixed flow rate and channel size were used in all the experiments of our study. Still, the breakthrough times of the gels were very different in the different experiments (Figure 7).

(a) Effect of MSR_c.　　　　　　　　　　(b) Effect of k_m.

(c) Effect of k_c/k_m.　　　　　　　　　　(d) Effect of MSR_c.
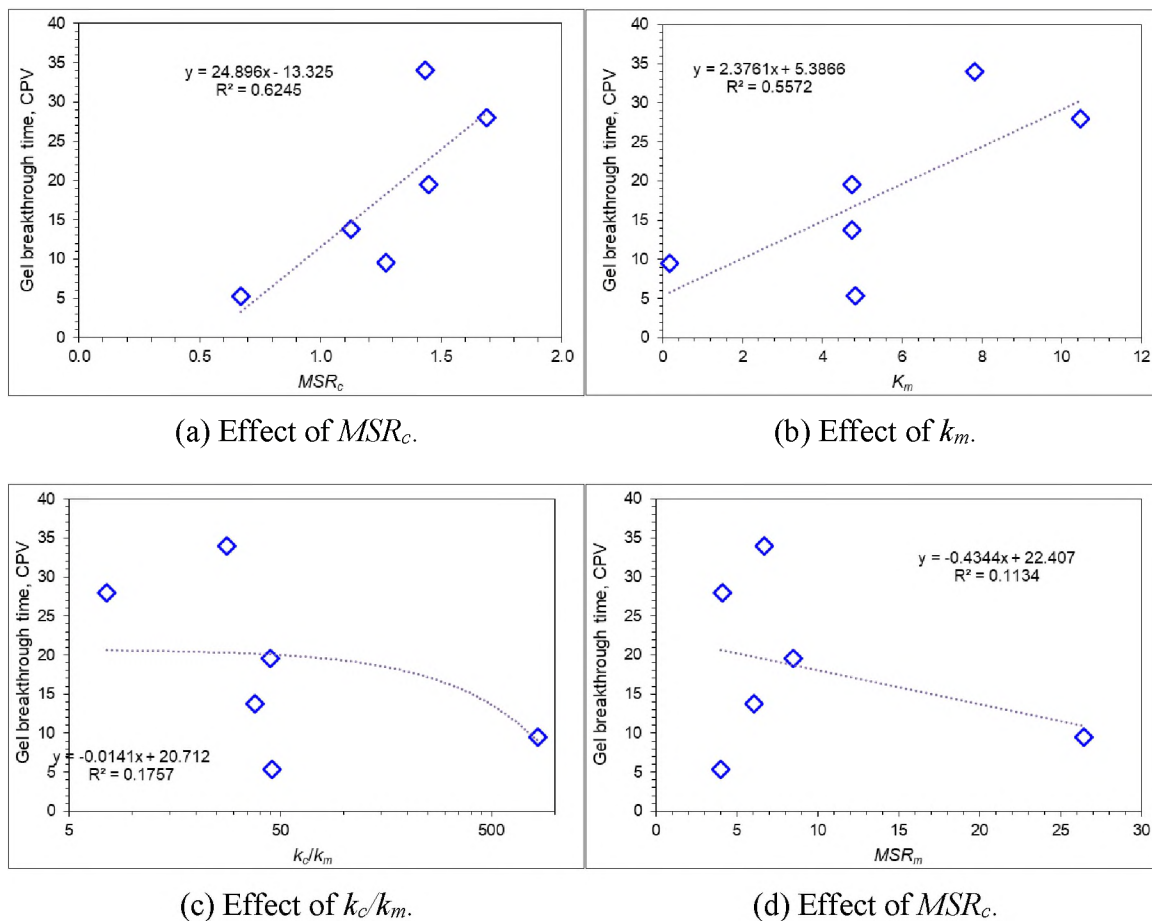
Figure 7. Impact of different factors on the breakthrough time of the gel particles through the channel. (The strongest correlation was detected with the MSRc, followed by the matrix permeability.)

Figure 8. Surface cake at the inlet face.
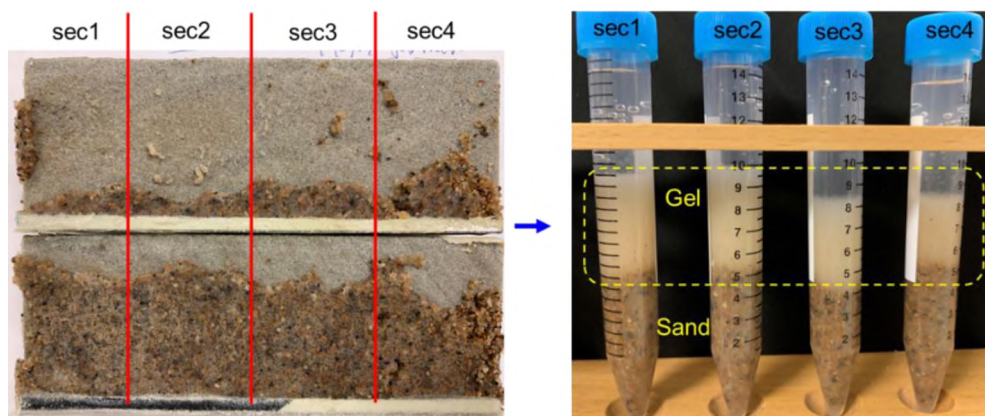
Figure 9. Placement of gels in the superpermeable channel. Left: Pore spaces among the sand grains in the channel were filled with gels. Right: the gel/sand mixture in different sections were collected, re-hydrated, centrifuged, and separated.

The delayed breakthrough of gels was related to the dehydration and retention of gels in the channels. As shown in Figure 9, the retained gels filled the pore spaces among the sand grains in the channel. The channel was equally divided into four sections in the lengthwise direction (sec1 to sec4), and the sand/gel mixtures in the different sections were collected, re-hydrated, and centrifuged. Thus, the gels were separated from the mixture.
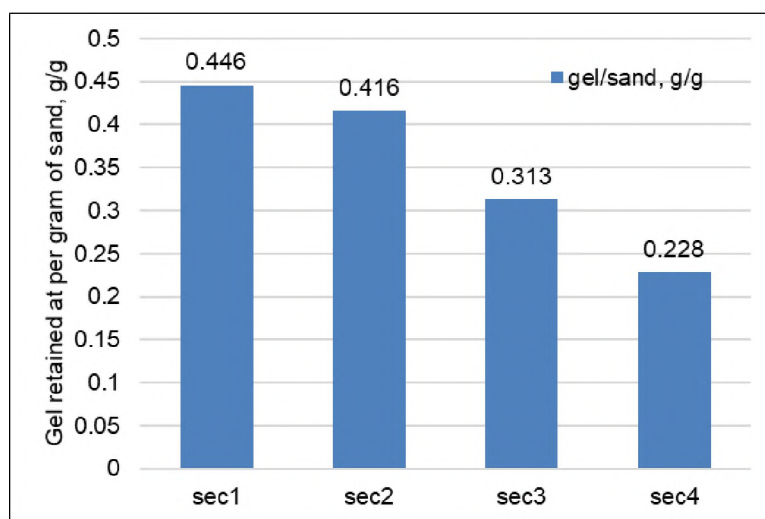
Figure 10. Gel retention in the channel (Exp S4).
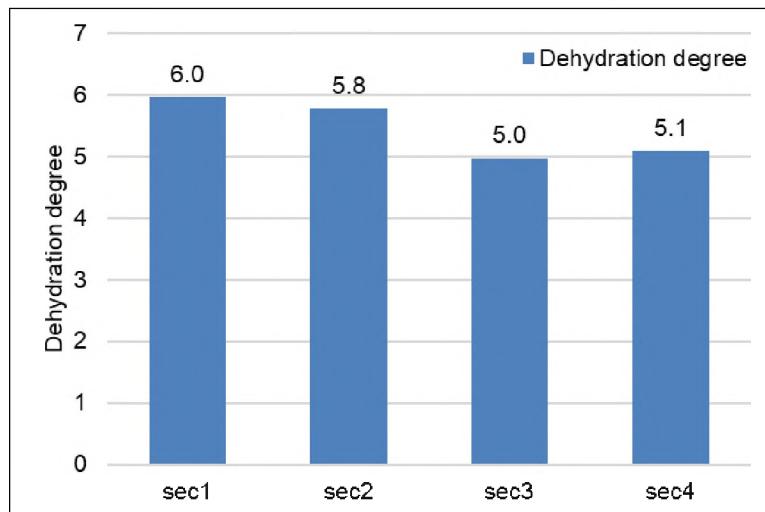
Figure 11. Dehydration degree of the gel retained in the channel (Exp S4).

The retention (grams of gels by per gram of sand) and dehydration degree of the gels at different locations were estimated with Equation (2) and Equation (3). In the equations, SR was the swelling ratio of the gels retained in the pore spaces of the channels. The results are shown in Figures 10 and 11. Figure 10 shows the gel retentions in the channel at different locations. The results revealed a higher gel retention in the inlet section and a decreasing trend towards the outlet. The gels were dehydrated (concentrated) by 5-6 times after being placed in the channel (Figure 11). Leak-off across the channel walls was possible to contribute to dehydration of the gels. While propagation through the channel, the microgels may lose water under the differential pressures between the channel and the matrices. The lost water leaked off into the matrices. Meanwhile, the gels were dehydrated. The dehydration phenomenon partially explained the delayed breakthrough behavior of the gel particles (at ~9.5 CPV). Besides the dehydration, another reason that caused the gel frontal delay was the formation of the gel cake at the inlet face of the matrices (Figure 8). One important implication of the delayed breakthrough was that the transport distance of

the gels did not linearly correlate with the volume injected (Seright 1999, 2001). The results also demonstrated that the channel model was able to take account for leak-off phenomenon across the channel walls (and the associated dehydration behavior) of the gels when transporting in the channel, which was an advantage over conventional separated parallel models. Thus, the results are expected to more representative of the real conditions in a reservoir.

$$\text{Gel retention} = \frac{M_{gel}}{M_{sand}}. \tag{2}$$

$$\text{Dehydration degree} = \frac{SR}{\text{Full SR}} = \frac{\left[M_{gel}\right] / \left[M_{gel}(\text{dry})\right]}{\text{Full SR}}. \tag{3}$$

Selective Penetration and Placement. As the gel cake was built up at the inlet face of the matrices, the injection pressure climbed up. The cake continued to grow stronger and temporarily plugged the matrices. Consequently, the gels could not penetrate the matrices. The gel cake was removed by soaking with a chemical breaker after the gel treatment to resume the subsequent flooding (Zhao et al., 2021c; Wang et al., 2019). The low penetration into the matrices was desirable for successful gel treatments. Otherwise, the matrices would be significantly damaged if the gel particles invaded a significant depth.

On the other hand, the pore spaces in the super-K channel were filled with gel particles, as shown in Figure 9. It suggested that the gel particles selectively penetrated and placed in the channel as the pore size was large enough for the gel particles to pass through. Pressure fluctuation (Figure 2) was observed during the gel placement process. The pressure fluctuation was a result of the repeated accumulation and remigration of the gel particles in the channel. In this process, a gel bank was gradually formed and propagated

downstream. The peak pressure was increased as the gel bank became larger. The front of the gel bank advanced towards the outlet, and gel particles were produced as the front arrived at the outlet. After breakthrough at 9.5 CPV, the accumulation/remigration of the gel particles would reach a dynamic equilibrium status as indicated by the fluctuated pressure around a relatively constant level (~30 psi in Exp S4). The selective placement of the gels was expected to significantly reduce the permeability of the channel and thus the subsequent flooding fluids (water, polymer solutions, etc.) were diverted to the matrices to displace the remaining oil previously bypassed.

The water-blocking efficiency in the super-K channels after the gel treatment were measured. The water-blocking efficiency was quantified with two parameters: residual resistance factor (F_{rr}), and water-blocking efficiency (E_{bw}). The following Equation (4) and Equation (5) were used to calculate the F_{rr} and E_{bw}. The two parameters were estimated by directly measuring the channel permeability after the gel treatment (Zhao et al., 2021c). In the test process, the inlet and outlet faces were shut off with epoxy, and only the entrance and the outlet of the channel were kept open (Figure 12).

$$F_{rr} = \frac{(k_c)_b}{(k_c)_a} = \frac{(\Delta P/q)_a}{(\Delta P/q)_b} . \tag{4}$$

$$E_{bw} = \left(1 - \frac{(k_c)_a}{(k_c)_b}\right) \times 100\% = \left(1 - \frac{1}{F_{rr}}\right) \times 100\% . \tag{5}$$

Brine was injected at different flow rates, and the stable injection pressure was obtained at each flow rate to estimate the effective permeability of the channels. In Exp S4, the channel permeability after the gel treatment was 481 md, and the residual resistance factor was 289. That is, the permeability of the super-k channel was reduced by 289 times.

The water-blocking efficiency was 99.65%. Therefore, the flow capacity of the super-k channel was substantially reduced after the gel treatment. The results also suggested that the gels did not totally shut off the super-k channel. Instead, the gel bank was still partially permeable. Imqam and Bai (2015) also reported partial permeable gel packs. Nevertheless, the channeling problem was substantially mitigated. Consequently, the displacing profile and sweep efficiency were improved, as discussed in the next section.
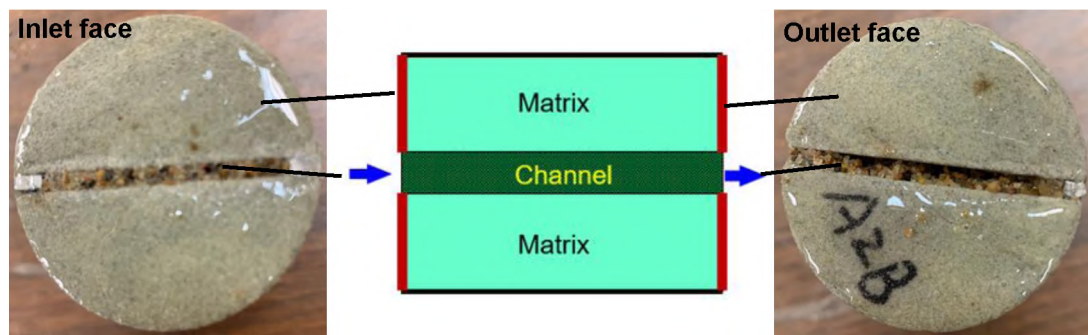
Figure 12. The outlet inlet faces matrix are sealed off with epoxy.

4. SWEEP IMPROVEMENT AFTER GEL TREATMENTS

As the superpermeable channels were shut off by the microgel materials under proper conditions, the subsequent flooding fluids would be forced into the matrices. Therefore, the displacing profile and the effective sweep volume (sweep efficiency) could be improved. The sweep improvement after the microgel treatment was estimated by chemical tracer tests. Figure 13 shows the tracer test results of the experiments. In each experiment, three tracer tests were performed respectively on the intact core model, the channel model before the microgel treatment, and the channel model after the microgel

treatment. Since the tracer responses before the microgel treatment were basically close to each other in different experiments, the results of Exp S1 were plotted in Figure 13 to represent the pre-gel-treatment situation in all experiments.

When a superpermeable channel was present in the model, the tracer broke out from the outlet almost immediately (at 0.06 total pore volumes, equivalent to 0.7 CPV) after injecting the traced brine. It indicated the injected fluid quickly flowed through the channel (Figure 14a), and the matrix was not effectively swept by the displacing fluid. The effluent tracer could not reach its injected value after five pore volumes of flooding. It could be inferred that the sweep efficiency would be poorer when the matrices were saturated with viscous/heavy oil as the mobility ratio situation was more unfavorable. The breakthrough of the traced brine slug was significantly delayed after the gel treatment. For example, in Exp S4, the breakthrough occurred after 0.41 PV_t of traced brine was injected. The results proved that the channeling was suppressed as the channel permeability was reduced by the gel materials. The subsequent flooding fluid was diverted into the matrices (Figure 14b).
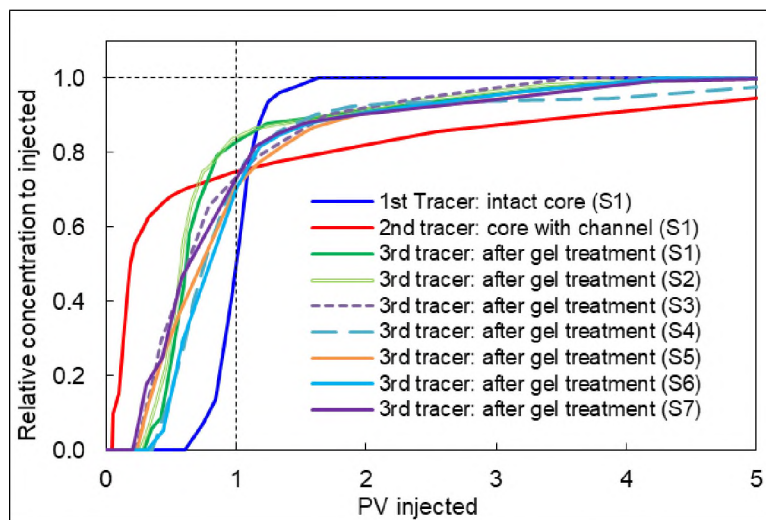
Figure 13. Sweep improvement demonstrated by tracer tests after gel treatments.

(a) Before gel treatment.

(b) After gel treatment.

(c) Insufficient gel placement.
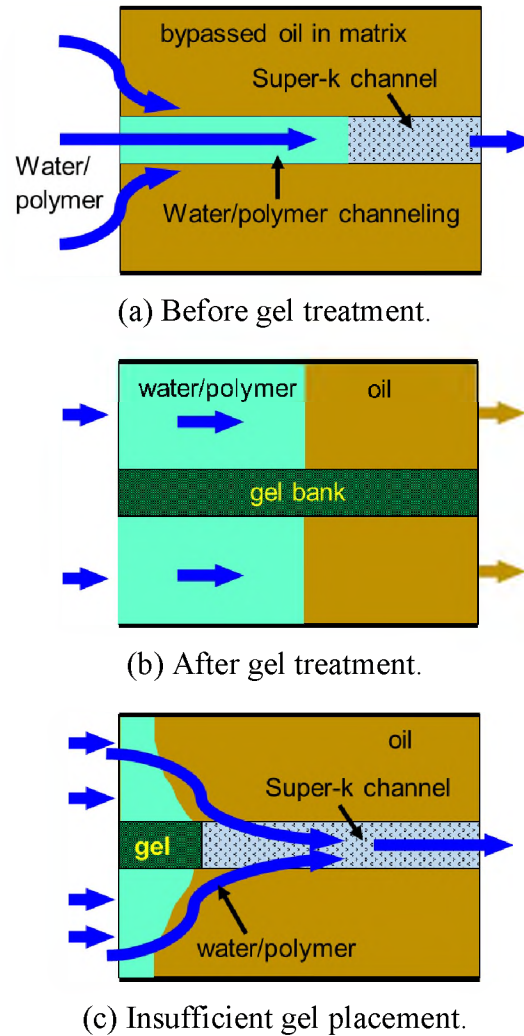
Figure 14. Sweep efficiency improvement after gel treatment.

The delayed breakthrough of the subsequent flooding fluid was an indication of sweep improvement. The sweep improvements in the different experiments were plotted against different parameters to identify the influential factors (see Figure 15). After the gel treatments, the sweep efficiency was improved by 0.25-0.43 PV_t, equivalent to an incremental oil recovery of 36-61% OOIP (oil original in place) assuming an initial oil saturation of 0.7. The results demonstrated the effectiveness of microgel particles in improving the conformance.

The results were consistent with the remarkable oil recovery improvement (~20% OOIP) during post-gel-treatment polymer flooding in some of our previous experiments (Zhao et al., 2021a). In that work, we studied the effectiveness of microgel particles in improving the sweep efficiency in reservoirs containing superpermeable channels during polymer flooding. Without additional conformance control efforts, the oil recovery was still unsatisfactory even after extensive polymer flooding (>5 PV). In other words, polymer flood alone was insufficient to overcome the adverse impact of the channeling issue. After the gel treatment, significant extra oil was recovered when the channels were highly permeable (>50 darcies). The recovery of additional oil was a clear evidence of sweep improvement after the gel treatment.

Figure 15 illustrates that the sweep improvement performance had a good correlation with the permeability contrast (k_c/k_m) between the channel and the matrices, followed by the matrix permeability. On the contrary, the sweep improvement did not exhibit a good correlation with the MSR_c or the channel permeability. The results suggested that the gel treatment was more likely to achieve a greater conformance improvement in the reservoirs where the channeling problem was more severe (i.e., higher k_c/k_m), while the benefit was reduced as the reservoir was more permeable. The gels had a better chance to place in the in-depth section of the channel as the reservoir was more heterogeneous. Otherwise, the gel particles mainly placed in the inlet section of the channel and resulted in insufficient placement of the gel materials, as shown in Figure 14c. The internal sections were not effectively shut off. Consequently, the subsequent fluid may be diverted to the matrices near the entrance, but it would quickly crossflow back to the channel. A large portion of the matrices was still left unswept.

(a) Effect of permeability contrast (k_c/k_m).

(b) Effect of matrix permeability (k_m).

(c) Effect of channel permeability (k_c).

(d) Effect of MSR_c.
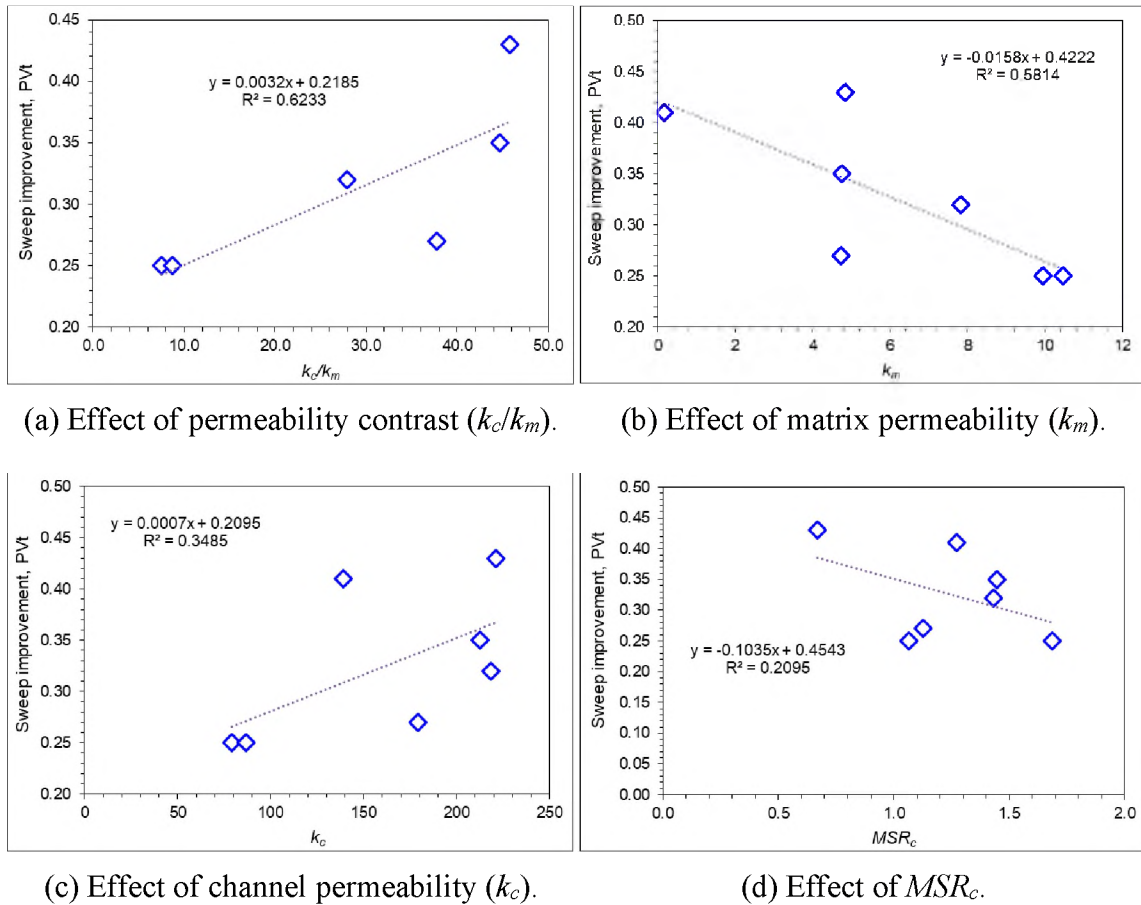
Figure 15. The effect of different parameters on the sweep improvement after gel treatment.

5. EVALUATION OF MATRIX DAMAGE

The gel materials were expected to place in and shut off the channeling zones (i.e., the target zones). However, it was also possible that the gel materials penetrate and damage the matrices in some circumstances. Thus, it was important to evaluate the matrix damage effect of the gel materials in order to minimize the negative impact. In this study, the damage of the gel materials to the matrices was assessed by directly measuring the matrix permeabilities after the gel treatment. In the tests, the channel was completely blocked off

and only the matrices were kept open (Figure 16). The subsequent fluid could only flow through the matrices. The permeability was directly obtained, and the effective injectivity (E_I) of the matrices after the gel treatment relative to the original value was estimated with Equation (6). More detailed experimental procedures can be found in Zhao et al. (2021c).

$$E_I = \frac{I_a}{I_b} \times 100\% = \frac{(q/\Delta P)_a}{(q/\Delta P)_b} \times 100\% = \frac{(k_m)_a}{(k_m)_b} \times 100\% \,. \tag{6}$$

For experiment S4, the matrix permeability after the gel treatment and chemical remediation was 134 md, which was 80.2% of its original permeability (167 md) prior to the gel treatment. The result indicated a 20% injectivity loss after the gel treatment in this experiment. The matrix damage under various conditions were investigated and the results are summarized in Figure 17. The effective injectivity retained after the gel treatment was relatively low when the MSR_m had a low value. As shown in Figure 17, when the MSR_m was below 5 (smaller particles or/and more permeable matrices), the particles could penetrate a significant depth into the matrices. Even after a mechanical or chemical remediation, the injectivity loss was still considerably high and could not be ignored. For instance, in experiment S5, the matrix was much more permeable (10458 md), and thus the MSR_m was relatively low (MSR_m=4.11). After the gel treatment and the remediation process, the matrix still lost significant injectivity (71%), which was much higher than that in S4. When the gel particles were sufficiently large relative to the pore sizes of the matrices (e.g., MSR_m>5 in this study), a higher critical pressure gradient was required to force the gel particles into the matrices. Therefore, it would be difficult for the particles to penetrate a noticeable distance into the matrices and cause serious formation damage. The injectivity could be substantially recovered after removing the surface filter cake.
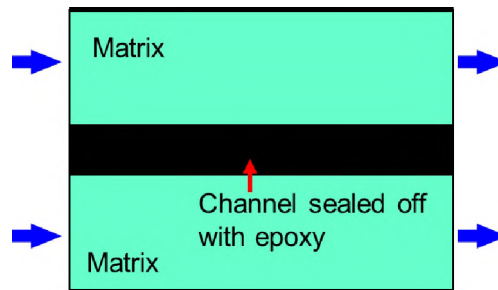
Figure 16. Evaluation of matrix damage after gel treatment.
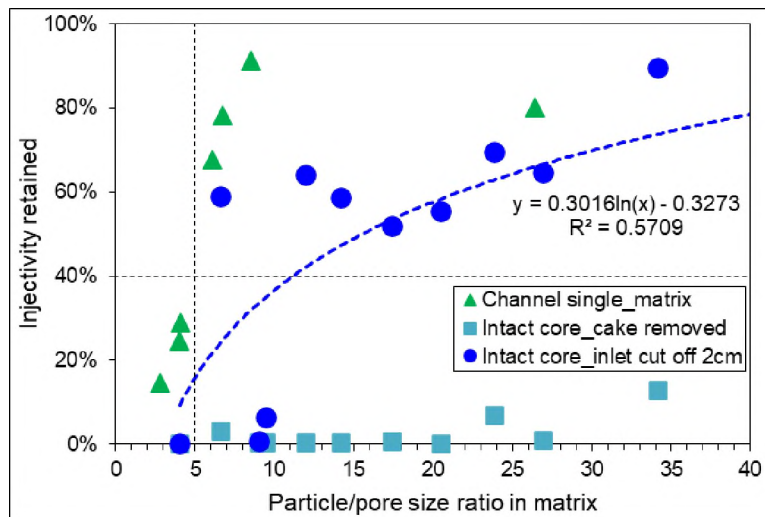
Figure 17. Impact of MSR_m on matrix damage.

The matrix damage is always an important consideration in a gel treatment. Two strategies can be adopted to deal with the potential damage: the preventive method (such as zonal isolation), and the remediation method (e.g., mechanical/chemical remediation).

When possible, zonal isolation is recommended to avoid the damage to the matrices. This fashion can help get rid of the requirement of remediation efforts after the gel treatment. Imqam et al. (2016b) investigated the performance of hydrochloric acid in removing damage caused by gels. Wang et al. (2019) tested different formulas of breakers to degrade gel materials. The results of this study can help to identify the favorable working conditions of the microgels. The gel particles should be small enough (e.g., MSR_c<2) to ensure good injectivity and placement in the target zones to be treated (the channels), and big enough (MSR_m>5) to prevent invasion into the low-permeability zones (the oil zones).

6. CONCLUSIONS

In this paper, we investigated the transport, placement, water-blocking ability, fluid diversion and sweep improvement, and matrix damage effect of microgel particles in reservoirs containing super-K channels. The impact of the channel/matrix permeability contrast, the particle/pore size ratio to the channels, the particle/pore size ratio to the matrices were studied. The favorable conditions of the tested microgels were identified. The results are expected to provide crucial support for successful gel treatment design and implementations.

(1) The microgel particles selectively penetrate and place in the porous super-K channels. The pressure gradient during gel injection increased with the particle-to-pore matching size ratio. The pores in the channels were filled with the gel particles. The channel permeabilities were significantly reduced after microgel treatments. The channels were effectively blocked by the microgels.

(2) Delayed breakthrough of the gel particles was observed, which was partially resulted from the dehydration and retention of the gel particles in the channel, and the buildup of a filter cake at the inlet face of the matrices.

(3) Sweep improvement after gel treatments was evaluated by chemical tracer tests. The results clearly demonstrate delayed breakthrough, fluid diversion, and increased swept volume of the subsequent flooding fluid. In the experiments, the sweep improvement was in the range of 0.25-0.43 PV_t. A higher sweep improvement was achieved as the permeability contrast was higher (i.e., the reservoir was more heterogeneous).

(4) The effectiveness of the gel treatment is related to the quality of the gel placement in the channels. Better sweep improvement can be achieved when the gel particles have good injectivity and the gel particles can be placed at the in-depth sections of the channels. Insufficient placement of the gel materials can result in unsatisfactory sweep improvement.

(5) The damage of the gel materials to the matrices was evaluated by directly measuring matrix permeabilities after the gel treatment. A gel cake could be formed at the inlet faces of the matrices during treatment, but the cake could be removed with chemical breakers. The injectivity of the matrices was effectively recovered.

NOMENCLATURE

Symbol	Description
d	Average diameter of the pores, μm
E_{bw}	Water-blocking efficiency

E_I	Effective relative injectivity after the gel treatment, percent
f_{CK}	Carman-Kozeny factor
F_{rr}	Residual resistance factor
I_b, I_a	Injectivity before and after the gel treatment
k_c	Permeability of channel, md
k_m	Permeability of matrices, md
k_t	Overall permeability of the channel model, md
MSR	Particle-to-pore matching size ratio
ΔP	Differential pressure between the injector and the producer, psi
PV_t	Total pore volume of the channel model
q	Injection flow rate, ml/min
S_{wi}	Initial water saturation, fraction
Φ	Porosity, fraction
τ	Tortuosity, dimensionless

ACKNOWLEDGEMENTS

agency thereof, nor any of their employees, makes any warranty, express or implied, or assumes any legal liability or responsibility for the accuracy, completeness, or usefulness of any information, apparatus, product, or process disclosed, or represents that its use would not infringe privately owned rights. Reference herein to any specific commercial product, process, or service by trade name, trademark, manufacturer, or otherwise does not necessarily constitute or imply its endorsement, recommendation, or favoring by the United States Government or any agency thereof. The views and opinions of authors expressed herein do not necessarily state or reflect those of the United States Government or any agency thereof."

APPENDIX

The injection pressure, pressure gradient, and resistance factor during gel injection in the experiments (except for S4) are presented in Figures A1 to A6.
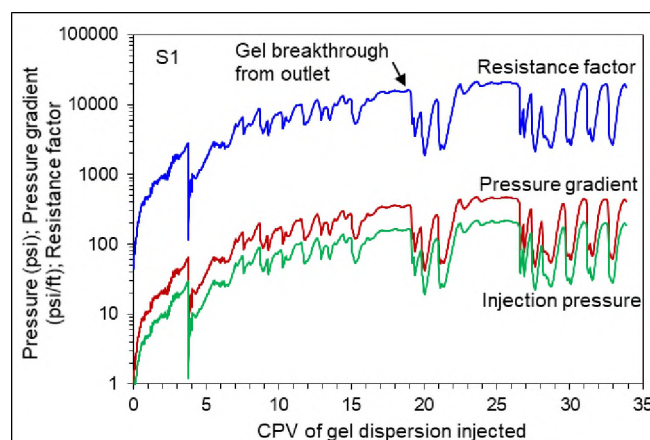
Figure A1. The pressure responses during gel injection in Exp S1.
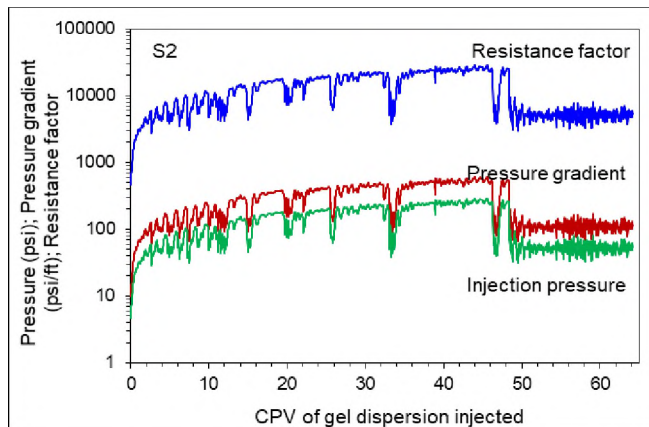
Figure A2. The pressure responses during gel injection in Exp S2.
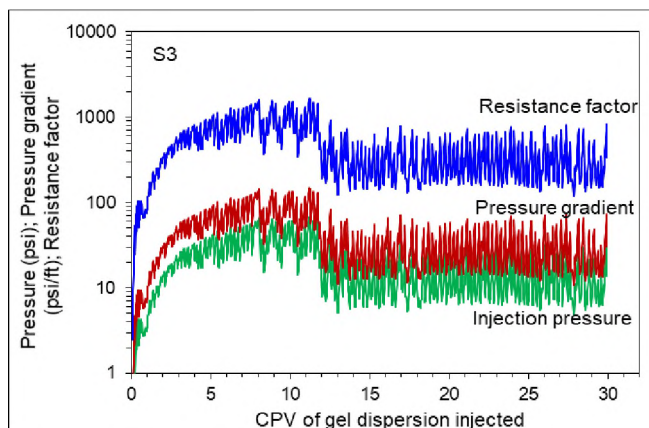
Figure A3. The pressure responses during gel injection in Exp S3.
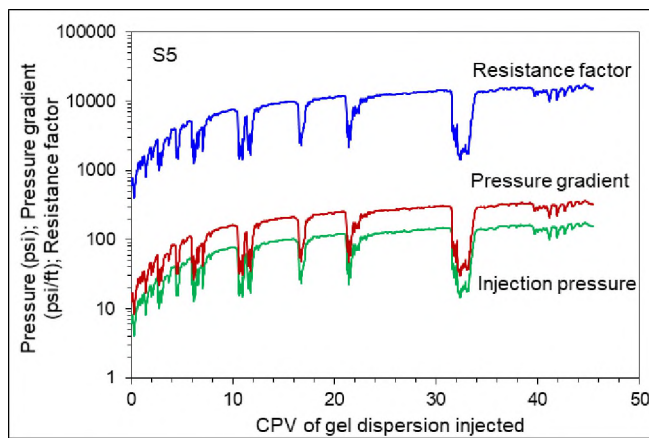
Figure A4. The pressure responses during gel injection in Exp S5.
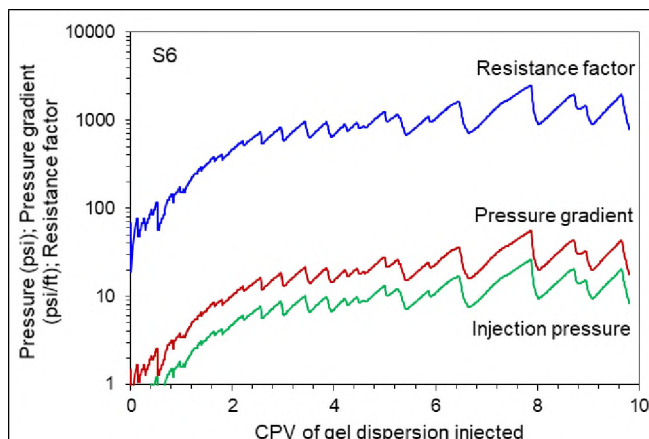
Figure A5. The pressure responses during gel injection in Exp S6.
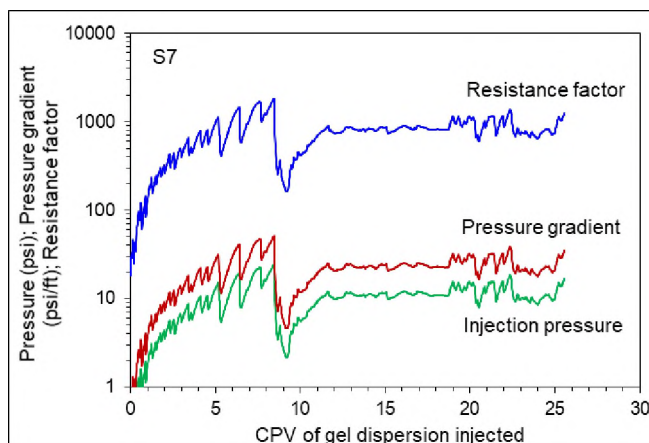
Figure A6. The pressure responses during gel injection in Exp S7.

REFERENCES

Aldhaheri, M., Wei, M., Alhuraishawy, A., Bai, B. 2021. Field Performances, Effective Times, and Economic Assessments of Polymer Gel Treatments in Controlling Excessive Water Production from Mature Oil Fields. J. Energy Resour. Technol. 143 (8): 080804. https://doi.org/10.1115/1.4049019.

Aldhaheri, M., Wei, M., Zhang, N., Bai, B. 2020. Field Design Guidelines for Gel Strengths of Profile-Control Gel Treatments Based on Reservoir Type. J Pet Sci Eng 194 (November): 107482. https://doi.org/10.1016/j.petrol.2020.107482.

Al-Ibadi, A., and Civan, F. 2013. Experimental Investigation and Correlation of Treatment in Weak and High-Permeability Formations by Use of Gel Particles. SPE Prod & Oper, 28 (04): 387-401.

Bai, B., Huang, F., Liu, Y., Seright, R. S., Wang, Y. 2008. Case Study on Preformed Particle Gel for in-Depth Fluid Diversion. Paper presented at the SPE Symposium on Improved Oil Recovery, Tulsa, Oklahoma, USA, 20–23 April. SPE-113997-MS. https://doi.org/10.2118/113997-MS.

Bai, B., Li, L., Liu, Y., Liu, H., Wang, Z., You, C. 2007a. Preformed Particle Gel for Conformance Control: Factors Affecting Its Properties and Applications. SPE Res Eval & Eng 10 (4): 415–422. SPE-89389-PA. https://doi.org/10.2118/89389-PA.

Bai, B., Liu, Y., Coste, J. P., Li, L. 2007b. Preformed Particle Gel for Conformance Control: Transport Mechanism Through Porous Media. SPE Res Eval & Eng 10 (2): 176–184. SPE-89468-PA. https://doi.org/10.2118/89468-PA.

Bai, B., Wei, M., and Liu, Y. 2012. Injecting Large Volumes of Preformed Particle Gel for Water Conformance Control. Oil Gas Sci. Technol.–Rev. IFP Energies Nouvelles 67 (6): 941–952. https://doi.org/10.2516/ogst/2012058.

Bai, B., Wei, M., and Liu, Y. 2013. Field and Lab Experience with a Successful Preformed Particle Gel Conformance Control Technology. Paper presented at the SPE Production and Operations Symposium, Oklahoma City, Oklahoma, USA, 23–26 March. SPE-164511-MS. https://doi.org/10.2118/ 164511-MS.

Bai, B., Zhou, J., and Yin, M. 2015. A Comprehensive Review of Polyacrylamide Polymer Gels for Conformance Control. Pet. Explor. Dev. 42 (4): 525–532.

Carman, P. C. 1956. Flow of Gases Through Porous Media. London, UK: Butterworths Scientific Publications.

Dai, C., Liu, Y., Zou, C., You, Q., Yang, S., Zhao, M., Zhao, G., Wu, Y., Sun, Y. 2017. Investigation on Matching Relationship between Dispersed Particle Gel (DPG) and Reservoir Pore-Throats for In-Depth Profile Control. Fuel 207: 109–120.

Dai, C., Zou, C., Liu, Y., You, Q., Tong, Y., Wu, C., Shan, C. 2018. Matching Principle and in-Depth Profile Control Mechanism between Elastic Dispersed Particle Gel and Pore Throat. Acta Petrolei Sinica 39: 427–434.

Dandekar, A., Bai, B., Barnes, J., Cercone, D., Ciferno, J., Ning, S., Seright., R., Sheets, B., Wang, D., Zhang, Y. 2019. First Ever Polymer Flood Field Pilot–A Game Changer to Enhance the Recovery of Heavy Oils on Alaska's North Slope. Paper presented at the SPE Western Regional Meeting, San Jose, California, USA, 23–26 April. SPE-195257-MS. https:// doi.org/10.2118/195257-MS.

Dandekar, A., Bai, B., Barnes, J., Cercone, D., Ciferno, J., Edwards, R., Ning, S., Schulpen, W., Seright., R., Sheets, B., Wang, D., Zhang, Y. 2020. First Ever Polymer Flood Field To Enhance the Recovery of Heavy Oils on Alaska's North Slope–Pushing Ahead One Year Later. Paper presented at the SPE Western Regional Meeting, April 27-30, 2020, Bakersfield, California, USA. Note–postponed to virtual format in April 2021. SPE-200814-MS. https:// doi.org/10.2118/200814-MS.

Dandekar, A., Bai, B., Barnes, J., Cercone, D., Ciferno, J., Edwards, R., Ning, S., Schulpen, W., Seright., R., Sheets, B., Wang, D., Zhang, Y. 2021. Heavy Oil Polymer EOR in the Challenging Alaskan Arctic–It Works! Paper prepared for presentation at the Unconventional Resources Technology Conference held in Houston, Texas, USA, 26-28 July 2021. URTeC-2021-5077. https://doi.org/10.15530/urtec-2021-5077.

Dupuis, G., Lesuffleur, T., Desbois, M., Bouillot, J., Zaitoun, A. 2016. Water Conformance Treatment Using SMG Microgels: A Successful Field Case. Paper presented at the SPE EOR Conference at Oil and Gas West Asia, March 21–23. SPE-179765-MS. https://doi.org/10.2118/179765-MS.

Elsharafi, M. O. and Bai, B. 2012. Effect of Weak Preformed Particle Gel on Unswept Oil Zones/Areas During Conformance Control Treatments. Ind Eng Chem Res 51: 11547–54. https://doi.org/10.1021/ie3007227.

Elsharafi, M. O. and Bai, B. 2013. Minimizing Formation Damage for Preformed Particle Gels in Mature Reservoirs. Paper presented at the SPE Asia Pacific Enhanced Oil Recovery Conference, Kuala Lumpur, Malaysia, 11–13 August. SPE-174645-MS. https://doi.org/10.2118/174645-MS.

Elsharafi, M. O. and Bai, B. 2016. Influence of Strong Preformed Particle Gels on Low Permeable Formations in Mature Reservoirs. Pet. Sci. 13 (1): 77–90. https://doi.org/10.1007/s12182-015-0072-3.

Imqam, A., Aldalfag, A., Wang, Y., Bai, B. 2016a. Evaluation of Preformed Particle Gels Penetration into Matrix for a Conformance Control Treatment in Partially Open Conduits. Paper presented at the SPE Annual Technology Conference and Exhibition, Dubai, UAE. SPE-181545-MS. https://doi.org/10.2118/181545-MS.

Imqam, A., and Bai, B. 2015. Optimizing the Strength and Size of Preformed Particle Gels for Better Conformance Control Treatment. Fuel 148: 178–85. https://doi.org/10.1016/j.fuel.2015.01.022.

Imqam, A., Bai, B., and Delshad, M. 2018. Micro-Particle Gel Transport Performance Through Unconsolidated Sandstone and Its Blocking to Water Flow During Conformance Control Treatments. Fuel 231 (1 November): 479–488. https://doi.org/10.1016/j.fuel.2018.05.099.

Imqam, A., Bai, B., Wei, M., Elue, H., Muhammed, F. A. 2016b. Use of Hydrochloric Acid to Remove Filter-Cake Damage from Preformed Particle Gel During Conformance-Control Treatments. SPE Prod & Oper 31 (3): 247–257. SPE-172352-PA. https://doi.org/10.2118/172352-PA.

Leng, J., Wei, M., and Bai, B. 2021. Review of Transport Mechanisms and Numerical Simulation Studies of Preformed Particle Gel for Conformance Control. J Petro Sci Eng 109051 (In press; published online 6 June 2021) https://doi.org/10.1016/j.petrol.2021.109051.

Mauran, S., Rigaud, L., and Coudevylle, O. 2001. Application of the Carman-Kozeny Correlation to a High-Porosity and Anisotropic Consolidated Medium: The Compressed Expanded Natural Graphite. Transp Porous Media 43 (2): 355–376. https://doi.org/10.1023/A:1010735118136.

Ning, S., Barnes, J., Edwards, R., Schulpen, W., Dandekar, A., Zhang, Y., Cercone, D., Ciferno, J. 2020. First Ever Polymer Flood Field Pilot to Enhance the Recovery of Heavy Oils on Alaska North Slope–Producer Responses and Operational Lessons Learned. Paper presented at the SPE Annual Technical Conference and Exhibition, Virtual, 26–29 October. SPE-201279-MS. https://doi.org/10.2118/201279-MS.

Qiu, Y., Wei, M., Geng, J. Wu, F. 2016. Successful Field Application of Microgel Treatment in High Temperature High Salinity Reservoir in China. Paper presented at the SPE Improved Oil Recovery Conference, Tulsa, Oklahoma, USA, 11–13 April. SPE-179693-MS. https://doi.org/10.2118/179693-MS.

Seright, R. S. 1999. Polymer Gel Dehydration During Extrusion Through Fractures. SPE Prod Facil 14 (02): 110–6. SPE-56126-PA. https://doi.org/10.2118/56126-PA.

Seright, R. S. 2001. Gel Propagation Through Fractures. SPE Prod Facil 16(04): 225–31. SPE-74602-PA. https://doi.org/10.2118/74602-PA.

Seright, R. S and Brattekas, B. 2021. Water Shutoff and Conformance Improvement: An Introduction. Pet. Sci. 18: 450–478. https://doi.org/10.1007/s12182-021-00546-1.

Sydansk, R. D. and Romero-Zeron, L. 2011. Reservoir Conformance Improvement. Richardson, Texas, USA: Society of Petroleum Engineers.

Villone, M. M. and Maffettone, P. L. 2019. Dynamics, Rheology, and Applications of Elastic Deformable Particle Suspensions: A Review. Rheol Acta 58 (3–4): 109–130. https://doi.org/10.1007/s00397-019-01134-2.

Wang, Z., Bai, B., Zhou, E., Pu, J., Schuman, T. 2019. Experimental Evaluation of Oxidizing Breakers for a Polyacrylamide-Based Re-Crosslinkable Preformed Particle Gel. Energy Fuels 33 (6): 5001–5010.

Wang, Z., Li, Z., Fu, S., He, H., Chen, A., Zhai, D. 2021. Experimental Study of the Plugging–Matching Relationship Between Elastic Particles and Formation Pore Throats. J Dispers Sci Technol 42: 190–205. https://doi.org/10.1080/01932691.2019.1667819.

Wu, D., Zhou, K., Hou, J., An, Z., Zhai, M., Liu, W. 2021. Review of Experimental and Simulation Studies of Enhanced Oil Recovery Using Viscoelastic Particles. J Dispers Sci Technol 42 (07): 956-969.

Yao, C., Lei, G., Gao, X., Li, L. 2013. Controllable Preparation, Rheology, and Plugging Property of Micron-Grade Polyacrylamide Microspheres as a Novel Profile Control and Flooding Agent. J Appl Polym Sci 130: 1124–1130. https://doi.org/10.1002/app.39283.

Yao, C., Lei, G., Li, L., Gao, X. 2012. Selectivity of Pore-Scale Elastic Microspheres as a Novel Profile Control and Oil Displacement Agent. Energ Fuel 26: 5092–101.

Yao, C., Liu, B., Li, L., Zhang, K., Lei, G., Steenhuis, T. S. 2020. Transport and Retention Behaviors of Deformable Polyacrylamide Microspheres in Convergent-Divergent Microchannels. Environ Sci Technol 54: 10876–10884. https://doi.org/10.1021/acs.est.0c02243.

Yuan, C., Pu, W., Varfolomeev., M.A., Wei, J., Zhao, S., Cao, L. 2020. Deformable Micro-gel for EOR in High-Temperature and Ultra-High-Salinity Reservoirs: How to Design the Particle Size of Micro-gel to Achieve its Optimal Match with Pore Throat of Porous Media. SPE J. SPE 197804-PA (in press; published online 02 December 2020). https://doi.org/10.2118/197804-PA.

Zhao, Y., Leng, J., Lin, B., Wei, M., Bai, B. 2021a. Experimental Study of Microgel Conformance-Control Treatment for a Polymer-Flooding Reservoir Containing Superpermeable Channels. SPE J. SPE-205486-PA (in press; posted 26 April 2021). https://doi.org/10.2118/205486-PA.

Zhao, Y., Yin, S., Seright, R. S., Ning, S., Zhang, Y., Bai, B. 2021b. Enhancing Heavy-Oil-Recovery Efficiency by Combining Low-Salinity-Water and Polymer Flooding. SPE J. 26 (03): 1535–1551. https://doi.org/10.2118/204220-PA.

Zhao, Y., and Bai, B. 2021c. A Comprehensive Laboratory Method to Evaluate Microgel Conformance Control Performance Using Sandwich-like Channel Models. Under review.

VII. EXPERIMENTAL STUDY OF MICROGEL CONFORMANCE-CONTROL TREATMENT FOR A POLYMER-FLOODING RESERVOIR CONTAINING SUPERPERMEABLE CHANNELS

ABSTRACT

Polymer flooding has been widely used to improve oil recovery. However, its effectiveness would be diminished when channels (e.g., fractures, fracture-like channels, void-space conduits) are present in a reservoir. In this study, we designed a series of particular sandwich-like channel models and tested the effectiveness and applicable conditions of micrometer-sized preformed particle gels (PPGs, or microgels) in improving the polymer-flooding efficiency. We studied the selective penetration and placement of the microgel particles, and their abilities for fluid diversion and oil-recovery improvement. The results suggest that polymer flooding alone would be inefficient to achieve a satisfactory oil recovery as the heterogeneity of the reservoir becomes more serious (e.g., permeability contrast $k_c/k_m>50$). The polymer solution would vainly flow through the channels and leave the majority of oil in the matrices behind. Additional conformance- treatment efforts are required. We tried to inject microgels in an attempt to shut off the channels. After the microgel treatment, impressive improvement of the polymer-flooding performance was observed in some of our experiments. The water cut could be reduced significantly by as high as nearly 40%, and the sweep efficiency and overall oil recovery of the polymer flood were improved. The conditions under which the microgel-treatment strategy was effective were further explored. We observed that the microgels form an external impermeable cake

at the very beginning of microgel injection and prevent the gel particles from entering the matrices. Instead, the microgel particles could selectively penetrate and shut off the superpermeable channels under proper conditions. Our results suggest that the 260-mm microgel particles tested in this study are effective to attack the excessive-water-production problem and improve the oil recovery when the channel has a high permeability (>50 darcies). The gels are unlikely to be effective for channels that are less than 30 darcies because of the penetration/transport difficulties. After the gels effectively penetrate and shut off the superpermeable channel, the subsequent polymer solution is diverted to the matrices (i.e., the unswept oil zones) to displace the bypassed oil. Overall, this study provides important insights to help achieve successful polymer-flooding applications in reservoirs with superpermeable channels.

1. INTRODUCTION

Fast water breakthrough and excessive water production are commonly encountered in oil fields around the world. Local and large-scale heterogeneities (e.g., fractures, channels, conduits, and so forth) present in a reservoir act as preferential water pathways from injection wells to production wells (Bai et al. 2013; Sun & Bai 2017). Polymer flood, although effective in reducing the mobility ratio between the water phase and the oil phase, might be insufficient to overcome the adverse effect caused by the heterogeneities and achieve satisfac- tory oil recovery. Various factors (e.g., the fracture inclination, dimension, spacing and intensity) can greatly affect the performance of polymer flooding (Shedid 2006; SayedAkram & Mamora 2011; Abedi et al. 2012; Abedi

& Kharrat 2016). Considering the relatively high cost of the flooding fluid and the processing difficulties of the produced water (Chang et al. 2020; Dhaliwal et al. 2021), the exces- sive water production during polymer flooding is more undesirable compared with the issue encountered during waterflooding. Conformance-control treatment can help improve the polymer-flooding performance and suppress the excessive water/polymer production. Numerical forecasts of the Buffalo Coulee heavy-oil reservoir by Baker et al. (2014) suggest that a remarkable synergistic per- formance could be achieved if gel treatments were conducted right before the polymer flooding, compared with polymer flooding alone (10 to 15% vs. 5 to 8%). They emphasized the importance of shutting off the preferential water channels created by extensive waterflooding before implementing a tertiary enhanced-oil-recovery process (e.g., polymer flooding). Similarly, numerical studies by Abu-Shiekah et al. (2014) suggest that although polymer flooding itself could improve the overall sweep efficiency over waterflooding, it was insufficient to overcome the effect of abnormal highly conductive channels and long extended fractures. Hatzignatiou et al. (2016) performed coreflooding experiments to study the performance of polymer flooding in naturally fractured chalk reservoirs. Their results indicate that polymer flood could not achieve a better recovery performance, and conformance treatments were beneficial to improve both the oil-recovery rate and the sweep efficiency. Coreflooding experiments aided with nuclear-magnetic-resonance measurements were performed by Alshehri et al. (2019) to compare the potential of gel treatment and polymer flooding in fractured carbon- ate reservoirs. They reported that a gel treatment would make the production process more efficient. Gel treatment has proved to be effective to block fractures and fracture-like features in reservoirs and improve the conformance (Bai et al.

2008, 2015; Seright et al. 2003; Aldhaheri et al. 2020, 2021; Kang et al. 2021). According to where the gels form, the gel systems can be divided into two categories: in-situ gel and preformed gel (Bai et al. 2012). For the in-situ gel, a water-like or polymer-solution- like gelant is injected into a reservoir, and the gel is formed after a gelation process in the reservoir (Sydansk & Romero-Zeron 2011). To overcome some drawbacks inherent with the in-situ gel (e.g., damage to oil zones, sensitivity to reservoir temperature, salinity, and so forth), PPG has been developed in a variety of size series (Bai et al. 2015). Successful applications by Chinese companies (Bai et al. 2008, 2012), Occidental Petroleum (Pyziak & Smith 2007), Halliburton (Vasquez et al. 2008), Kinder-Morgan (Larkin & Creel 2008), and ConocoPhillips (Peirce et al. 2014; Targac et al. 2020) have demonstrated the effectiveness of this type of gel system.

Superpermeable channels can exist in a reservoir and result in early breakthrough of the polymer fluid and/or excessive water-production issues. For the target block where the Department of Energy–funded first-ever heavy-oil/polymer-flood pilot on Alaska's North Slope is taking place (Dandekar et al. 2019), production-history data indicate that no direct fractures are present in the reservoir. However, preliminary history-matching studies suggest that channels with super-high permeabilities of ten to several hundred darcies might exist in the reservoir (Ning et al. 2020; Dandekar et al. 2020). Compared with fracture-type problems, the porous-medium-type superpermeable channels are more challenging (Seright et al. 2003). As shown in Figure 1, such channels are much more permeable than the matrices, and water, polymer, or other flooding fluids will preferentially flow through the superpermeable channels, leaving a large amount of oil in the matrices unswept. Preformed bulk gels (Seright 1999) and millimeter-sized PPGs (Elsharafi & Bai

2013, 2016) have serious injectivity difficulties for the porous-medium-type superpermeable channels. Water/polymer-like gelant can cause severe damage to the oil zones without a proper zonal isolation for such reservoirs without open fractures or conduits. Even if zonal isolation measures are taken during the injection process, the gelant might still crossflow into the oil zones from the channels and result in damage.
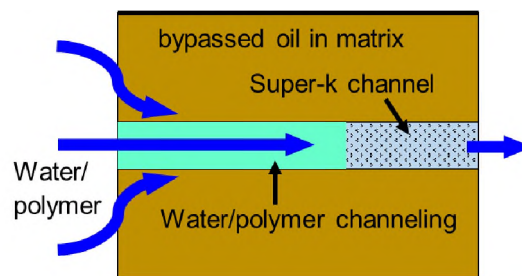
Figure 1. Impact of super-k channels in a reservoir. (Water, polymer, or other flooding fluids flow through the super-k channels. Oil in matrices is bypassed.)

In this study, micrometer-sized PPGs (microgels) were tested to solve the excessive-water-production problem caused by superpermeable channels during polymer flooding. In the literature, there have been some studies that focused on the transport behavior of microgels in high-permeability porous media, which mimic the high-permeability channels in a reservoir (Bai et al. 2007b; Yao et al. 2012; Imqam et al. 2018; Villone & Maffettone 2019; Wu et al. 2021). The elasticity and deformability enable the microgel particles to pass through pore throats that are significantly smaller than their own sizes, which is distinctly different from the transport behavior of rigid particles (Bai et al. 2007b; Yao et al. 2012; Imqam et al. 2018). The microgel particles could have the ability of selective penetration (Imqam et al. 2018; Villone & Maffettone 2019). That is, the particles cannot penetrate the low-permeability matrices (oil zones) because of the size-

exclusion effect. Instead, the particles can selectively enter and shut off the superpermeable channels. However, in the literature, the selective penetration of particle gels is frequently claimed in the use of parallel linear coreflooding experiments, in which a gel-injection flowline is connected to two or more separate cores or sandpacks. However, some drawbacks are associated with the conventional parallel linear coreflood models (Seright & Brattekas 2021). One example is the absence of crossflow between the parallel cores, while there is usually free crossflow between channels and matrices.

Above all, considering the wide applications of polymer flooding and the commonly encountered channeling issue (especially after long-term waterflood), it is valuable to explore appropriate strategies to conquer the channeling problem and improve the efficiency of the polymer flooding. However, to the knowledge of the authors, the study of the application of microgels in polymer flooding is seldom reported so far. The effectiveness and applicable conditions of microgel treatment in improving the polymer-flooding performance in channeled reservoirs need to be investigated.

This study focuses on the excessive-water-production caused by superpermeable channels (ten to several hundred darcies) during polymer flooding. To improve the experiment representativeness over the conventional parallel models, we constructed a particular heterogeneous model to study the selective-penetration, water-blocking, and oil-recovery-improvement performance of microgel particles. With the special channel model, we performed a series of experiments to examine whether polymer flooding alone is sufficient to overcome the adverse effect of the superpermeable channels and achieve satisfactory oil recovery, to test the selective-penetration behavior of the microgels in the channel models, to identify the appropriate conditions under which the microgels can

effectively penetrate and shut off the superpermeable channels, to evaluate the water-blocking efficiency in the superpermeable channels, to estimate the potential damage to the oil zones, and to investigate the potential of microgel treatment in reducing the water cut and improving the sweep efficiency and oil-recovery performance.

2. EXPERIMENTAL

2.1. MATERIALS

Brines. Two brines were used in this study: synthetic formation brine [total dissolved solids (TDS)=27,500 ppm], and synthetic injection brine (SIB) (TDS=2,498 ppm). The information of the brines is summarized in Table 1. The injection brine has a relatively low salinity, and it is used for waterflooding and polymer flooding in the field (Milne Point Unit on Alaska's North Slope). The synthetic formation brine and SIB were prepared according to the corresponding brine compositions in Milne Point Unit.

Polymer. Flopaam® (S.P.C.M. SA, Andre´zieux-Boutheon, France) 3630S (the same as used in the polymer-flood pilot in the Milne Point oilfield), with a concentration of 1,400 ppm in SIB, was used. The molecular weight was 18 to 20×10^6 daltons with a hydrolysis degree of 25 to 30%. Before adding polymer powder, the brine was deoxygenated with argon. The desired amount of polymer powder was slowly added into the brine being stirred with a magnetic bar. The solution was stirred at 300 rev/min at room temperature for approximately 24 hours until all the polymer powders were well-dissolved. The polymer solution was filtered through a 1.2-mm filter paper. The polymer solution had a viscosity of 45 cp at 7.3 s^{-1} measured with a DV3T Brookfield viscometer.

Table 1. Basic formation brine and injection brine.

Name	Properties (Measured at 71 °F)	Composition (ppm)
HSW (SFB, synthetic formation brine)	pH=7.30 μ=1.15 cp TDS=27500 ppm Ionic strength=0.492 Hardness: 1700 ppm	Na^+: 10086.0 K^+: 80.2 Ca^{2+}: 218.5 Mg^{2+}: 281.6 Cl^-: 16834.4
LSW (SIB, synthetic injection brine)	pH=7.50 μ=1.07 cp TDS=2498 ppm Ionic strength=0.046 Hardness: 280 ppm	Na^+: 859.5 K^+: 4.1 Ca^{2+}: 97.9 Mg^{2+}: 8.7 Cl^-: 1527.6

Crude Oil. The crude oil was sampled in August 2018, at a wellhead in the Milne Point Oil Field (Well B-28). The oil sample was centrifuged to remove water and solids (if any) and filtered through a 0.5-mm filter paper. The viscosity was 202 cp at reservoir tempera- ture (71°F), with a gravity of 19.0 °API (0.940 g/cm^3).

Microgels. Microgel particles were used as the conformance-treatment agent. The microgel was ground from millimeter-sized PPG. The PPG was synthesized through polymerization using monomer (acrylamide), crosslinker (N, N'-methylenebisacrylamide), initiator (peroxyldisulfate), and some other additives. More information can be found in our previous publications (Bai et al. 2007a). The gel had an average elastic modulus (G') of 820 Pa, derived from three tests of the gel. The tests were performed with a HAAKE

MARS III rheometer. The G' was measured as a function of time at a frequency of 1 Hz and controlled strain of 1%. The PP35L Ti L spindle was used with a gap of 1mm. Free water was removed from the full swollen gels when performing the tests. The microgels had a full swelling ratio of approximately 40 in the SIB. Figure 2 shows the microgels before and after swelling in the SIB. The size of the fully swollen gel particles was 215-300 mm, with an average diameter of 260 mm. The gel was carried by the SIB with a microgel concentration of 1 wt% (dry weight).
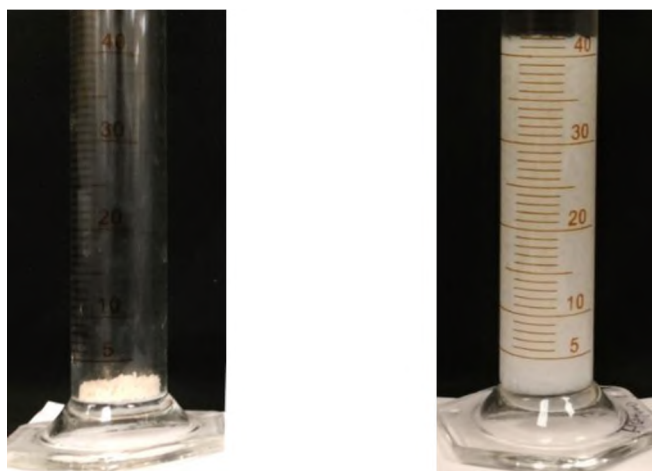
(a) Dry microgel particles.   (b) Swelling microgel in brine.

Figure 2. Dry and swollen microgels.

Channel Models. A typical channel model in our study was composed of matrices (core plugs) and a sand-filled channel, thus, the channel model had a sandwich-like structure (Figure 3). The cores used were 2-inch Berea cores with a length of about 15 cm and a permeability of about 500 md. The key parameters of the model are shown in Table 2. As shown in Figure 3, after measuring the absolute permeability with SFB and establishing the initial water saturation (S_{wi}) conditions, the permeability to oil (Km) at Swi

was measured by injecting the crude oil. The cores were then cut into two halves. A 0.3-cm fracture was created between the two half parts. Two stainless-steel supporting strips were placed along the lengthwise edges of the fracture to ensure a constant thickness of the facture (Figures 3a and 3b). The fracture was filled with NB sands (formation sand from the target Milne Point oilfield) with a specific range of mesh sizes. The sands were tightly packed to avoid movement and repacking during the gel injection process. The gaps between the supporting strips and the fracture faces were sealed with epoxy. This was to make sure the gel particles do not migrate along these gaps and ensure the microgel go into the target zone, i.e., the channel. Sands with different sizes (10/20, 20/30, 30/60 and 60/80 mesh) were used to fill the fracture and make the channel with different permeabilities (k_c). The resulted permeabilities increased as larger sands were used. Therefore, the permeability contrast (k_c/k_m) between the channel and matrix became larger and the heterogeneity of the model became more serious. Additional experiments were performed using a homogeneous Berea core with a comparable permeability for comparison purpose. Note that the k_c was estimated using Darcy's law of multi-layer porous media, Equation (1).

$$k_c = \frac{k_t \left(A_c + A_m \right) - k_m A_m}{A_c}.$$

(1)

where K_t is the overall permeability of the channel model, determined by injecting oil into the channel model at initial water saturation condition. A_c and A_m are the cross-sectional area of the channel and the matrices, respectively. The design can overcome some distinct drawbacks associated with the conventional parallel coreflooding experiments. The channel models ensure free crossflow between the super-k channels and the matrices,

which is usually the case in a real reservoir. During gel injection, the gel dispersion arrives at the inlet faces of the channels and the matrices at the same time. This feature overcomes the possible experimental artefacts (e.g., water filled in the injection flowline, and dispersion/diffusion effect) associated with the slow flow in the flowline leading to the low-permeability core in the conventional parallel coreflooding (Seright and Brattekas 2021). Note that it is still linear flow in our channel models, which simulate the linear flow between horizontal injector-producer pairs in the target oilfield. Overall, the design is expected to be more representative to the target channeling issue.

(a) An intact core plug is cut into two halves. A pair of supporting strips are placed to ensure a fracture space between the half plugs.

(b) The model before filling sand in the fracture space.

(c) Sand is filled into the fracture space. The sand should be tightly packed to avoid movement and repacking during flooding and gel injection process.

(d) Model is assembled. Gaps between strips and fracture faces are sealed with epoxy to prevent gels migrating along the gaps.

Figure 3. Construction of the sandwich-like channel model.

Table 2. Key parameters of a typical channel model.

Exp #4	Parameter	Value	Note
Matrix	L, cm	14.52	/
	d, cm	5.07	/
	A, cm^2	20.21	Original before cutting
	Porosity	0.226	Porosity of matrix
	MPV, cm^3	67.62	Original matrix pore volume
	MPV, cm^3	62.91	Matrix pore volume after cut
Channel	Thickness (δ), cm	0.3	Channel thickness
	Width (b), cm	4.10	20/30 mesh sand
	CPV, cm^3	9.12	PV of channel
	Total PV$_t$, cm^3	72.03	Matrix +channel
Saturation	OOIP	61.39	Matrix +channel
	S_{oi}	0.852	Matrix +channel
	S_{wi}	0.148	Matrix +channel
Gel	Microgel, mesh	170-230	63-88 μm (averaged 260 μm after swollen)
	Swelling ratio	40	In SIB
	Dispersion	1 wt%	Dry weight

2.2. EXPERIMENTAL PROCEDURE

Figure 4 shows the experimental setup used in this study. The accumulator had a mixing propeller mounted at the bottom to ensure the microgel particles dispersed uniformly in the carrying fluid. The procedure of the experiments is shown in Figure 5.

After establishing initial water saturation condition, water flooding and polymer flooding were performed before a microgel treatment was implemented. The effluent was collected, and the injection pressure was recorded at a proper frequency with a digital data acquisition system. The initial waterflooding was run until the water cut increased to 80%, as comparable to the pilot situation (Dandekar et al. 2019). Polymer flooding was then performed until no oil produced and the injection pressure became stable.

Microgel dispersion was injected until the gel was observed at the outlet (if possible) and the injection pressure became stable (if possible). For a gel treatment project, the gel slug was usually injected at very high flow rates. However, to avoid the impact of the increased flow rates on the oil recovery, high injection rates of the gel dispersion were not adopted in this study. Instead, the gel dispersion was injected at the same flow rate as the polymer flooding. After the gel treatment, the possible gel cake at the inlet surface was removed with breaker, 5% HCl (Imqam et al. 2016; Wang et al. 2019). Afterwards, post polymer flooding and water flooding were performed sequentially. The oil recovery improvement was estimated compared with that before the gel treatment.
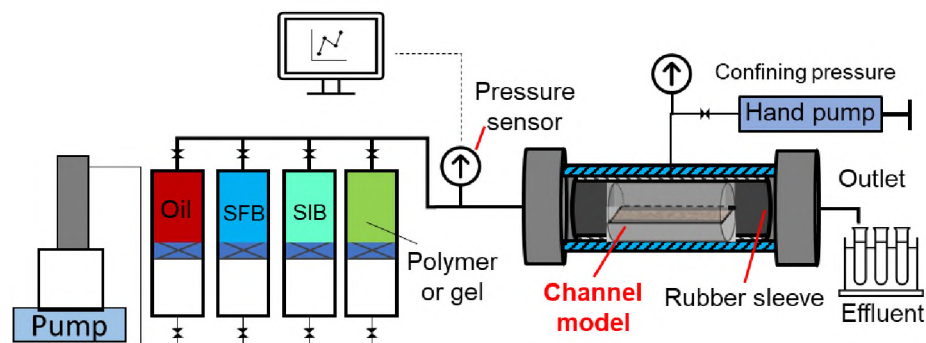
Figure 4. Experiment setup.
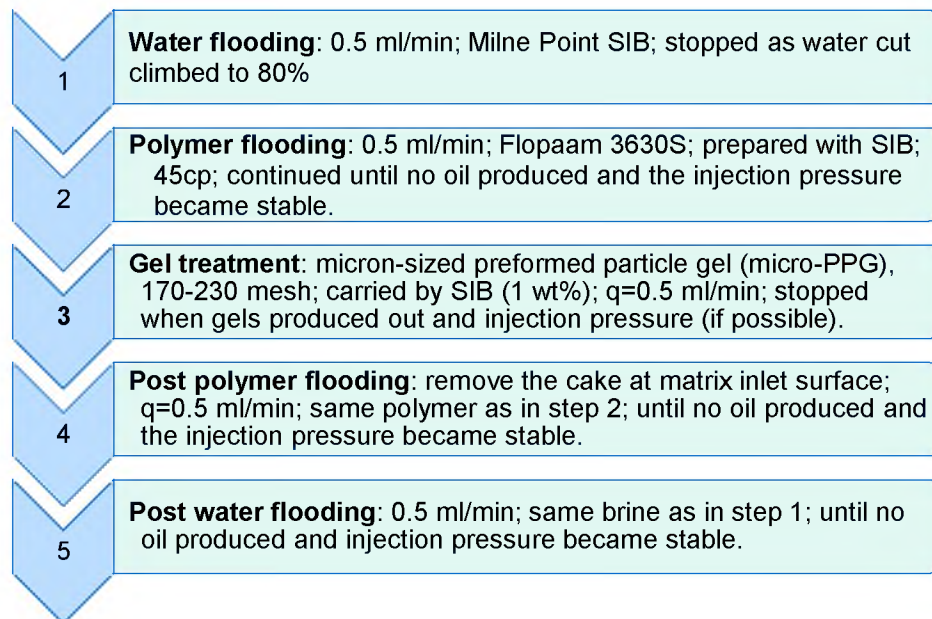
Figure 5. The typical experiment procedure.

3. RESULTS AND DISCUSSION

3.1. OIL RECOVERY PERFORMANCE

3.1.1. Before Gel Treatment. Table 3 summarizes the basic conditions and key results of the experiments. As a base case, the results obtained from the model with the channel filled with 20/30 mesh (0.60-0.84 mm) sand are discussed in detail (Exp #4). In this experiment, the permeability of the channel and the matrix was 57 darcy and 0.50 darcy, respectively. Another experiment was carried out using homogeneous core with a comparable permeability (Exp #1). In this study, we use the permeability contrast (Kc/Km) between the channel and the matrix to quantify the heterogeneity severity of the model. Another parameter, R_{FC}, is also introduced to estimate the heterogeneity severity of the model. The R_{FC} is defined as the flow capacity ratio of the channel to that of the matrix,

Equation (2). A higher R_{FC} indicates more flooding fluid would vainly flow through the channel, rather than through the matrix to effectively displace the majority remaining oil there. For the channel model, the permeability contrast (k_c/k_m) was 114 and the flow capacity ratio, R_{FC}, was 7.4, while $k_c/k_m=1$ and $R_{FC}=0$ for the homogeneous model.

$$R_{FC} = \frac{K_c A_c}{K_m A_m} .$$
(2)

Figure 6 shows the oil recovery performance of water flooding and extensive polymer flooding. Compared with the homogeneous model, the water breakthrough in the channel model occurred much earlier (0.10 PV versus 0.24 PV), and the secondary recovery from waterflooding was much lower (16.7% versus 49.0%). Note that the pore volume of the channel (CPV) was about 13% of the total pore volume. It indicates most of the injected water transported through the super-k channel and most of the recovered oil was from the channel. The majority oil in the matrix was bypassed.

Table 3. Summary of the experiment results.

Exp #	Sand	k_m, D	k_c, D	k_c/k_m	R_{FC}	Water breakthrough, PV_t	Oil recovery (% OOIP)		
							WF at f_w=80%	PF	Overall
1	Homo	0.86	0.86	/	/	0.24	49.0	22.7	72.9
2	60-80	0.52	19.6	38	2.6	0.20	29.3	36.7	67.7
3	30-60	0.64	31.0	48	3.2	0.11	19.0	32.1	58.4
4	20-30	0.50	57.0	114	7.4	0.10	16.7	32.1	48.9
5	10-20	0.49	237	484	30.0	0.09	10.8	22.7	34.7
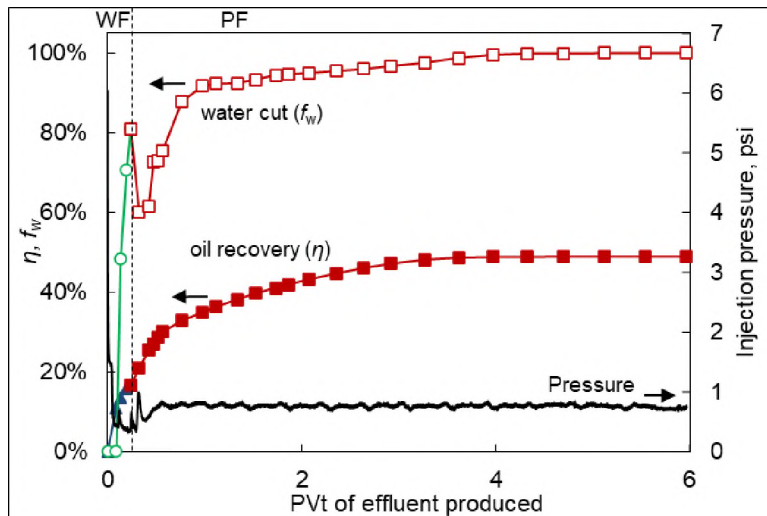
(a) Oil recovery performance in channel model before gel treatment (Exp #4).
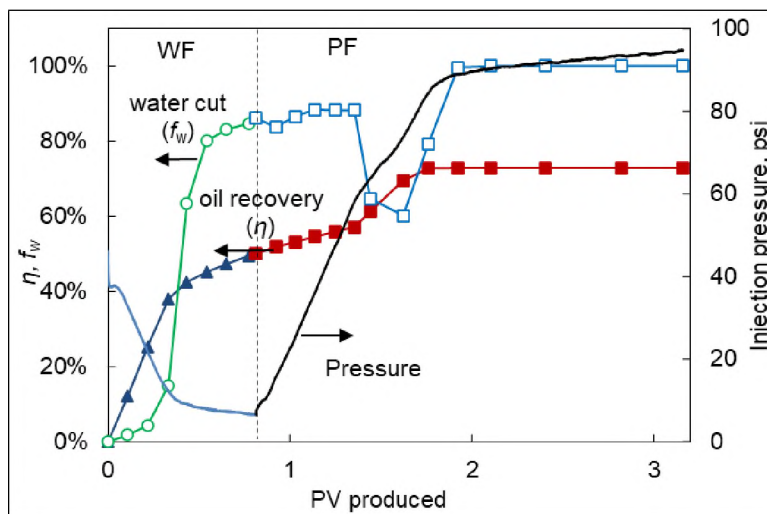
(b) Oil recovery performance in homogeneous model (Exp #1).

Figure 6. Comparison of oil recovery performance in channel model and homogeneous model.

In the following polymer flooding process, the pressure buildup was much lower in the channel model. Though significant incremental oil was recovered from both models (32.1% and 22.7%), substantial difference was observed after a closer examination. As shown in Figure 6, the incremental oil was recovered gradually over quite a long period of

polymer flooding (more than 4 PV) in the channel model. Note that after switching to polymer flooding, though the water cut declined, it would quickly increase back to a high level, making the production process uneconomical. The channel model would reach a water cut of 90% after 0.64 PV of polymer flood, and the oil recovery factor was only 34.0%. In contrast, the homogeneous model would achieve an overall oil recovery factor of 70.5% when the water cut rose to 90%. Our previous coreflooding experiments using reservoir sand materials also demonstrated the effectiveness of polymer flooding in improving the oil recovery of the heavy oil with a viscosity of more than 200 cp (Zhao et al. 2021). Combining the polymer flood with low salinity water could further improve the performance. Three more experiments were carried out to test the performance in reservoirs with different heterogeneity severities. The superpermeable channel was filled with 10/20, 30/60, and 60/80 mesh sands, respectively. The results are summarized in Table 3 and Figure 7.

Generally, the overall oil recovery would be unfavorable as the permeability contrast was over 50:1. For the worst case (Exp #5, Figure 7d), the super-k channel had a permeability of 237 darcy, and the permeability contrast to the matrices was 484:1. The flow capacity ratio was about 30, and the heterogeneity was more serious. As expected, the recovery performance of water flooding and polymer flooding was very unsatisfactory before the gel treatment.

Clearly, the unsatisfactory recovery performance in the channel model indicates that the oil bank generated by the polymer flood was much less concentrated, and the oil production rate was much slower. Therefore, the impact of heterogeneity was significant and polymer flood alone was insufficient to attack the excessive water production and

achieve a satisfactory oil recovery performance. Additional conformance treatment efforts were required to shut off the superpermeable channels and force the displacing fluid into the matrices to displace the bypassed oil.
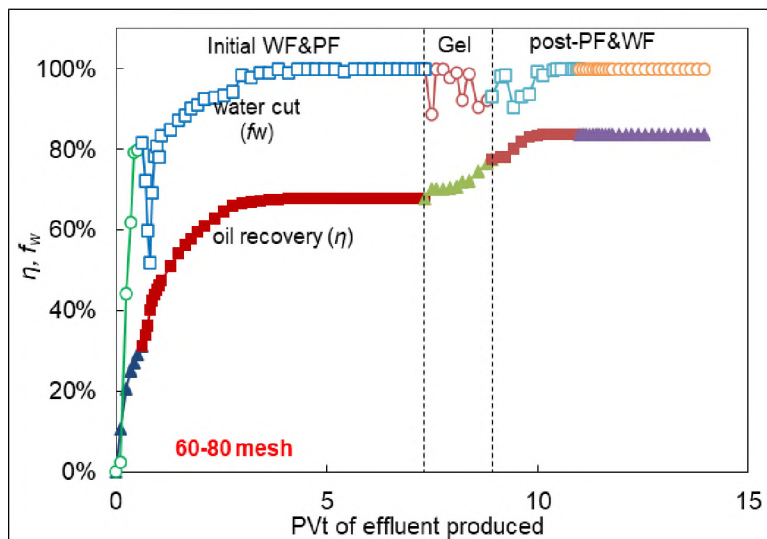
(a) Experiment 2 (Kc/Km=38; MSR=4.5).
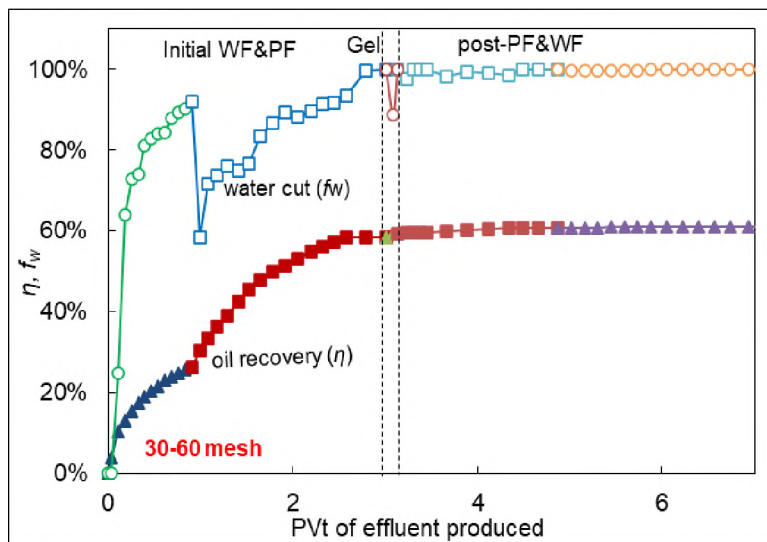
(b) Experiment 3 (Kc/Km=48; MSR=3.5).

Figure 7. Water cut reduction and oil recovery performance after gel treatment.
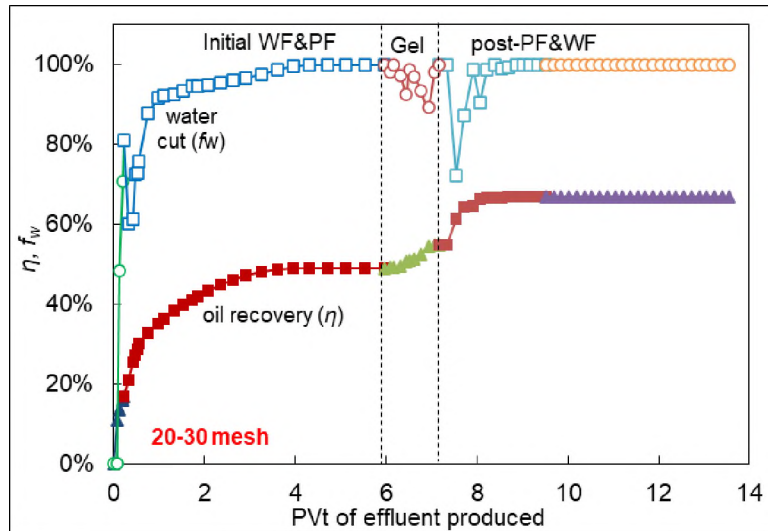
(c) Experiment 4 (Kc/Km=114; MSR=2.6).
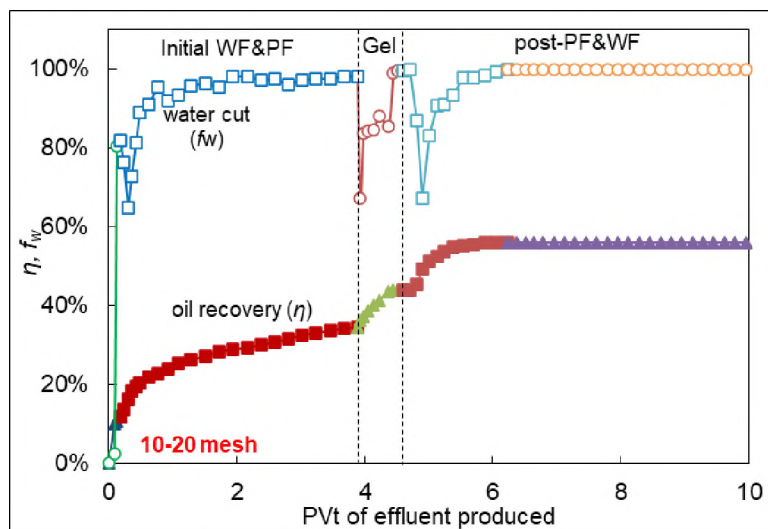
(d) Experiment 5 (Kc/Km=484; MSR=1.2).

Figure 7. Water cut reduction and oil recovery performance after gel treatment (continued).

3.1.2. After Gel Treatment. The oil recovery performance after gel treatment is shown in Figure 7. In the base case (Exp #4), the water cut was significantly reduced (from 100% to 70%). Also, the water cut could be maintained at a relatively low level for an

appreciably long period of flooding (~1 PV with water cut below 98%). Thehe sweep efficiency and overall oil recovery were improved. The improvement after gel treatment was 18.0% OOIP. The noticeable improvement indicates the subsequent flooding fluid was diverted into the matrices to displace the previously bypassed oil, as shown in Figure 8. For the worst case (Exp #5, Figure 7d), after the gel treatment, the water cut was reduced to 63%, and the oil recovery factor was increased from 34.7% to 56.1%. The results demonstrate the effectiveness of the tested microgels under proper conditions.

For the case of 30/60-mesh-sand-filled model (Exp #3, Figure 7b), the overall improvement was quite limited, only 2.7% OOIP. The injected gel volume was insufficient, and no gel was produced out. The gel was not successfully injected into the channel and a gel bank was not formed. Consequently, the water cut first reduced and then rapidly increased after a short period during the post polymer flooding. In the first 0.1 PV, the polymer was forced into the matrix at the front section of the model. This is because the gel packed tightly and form an effective resistance to the chasing fluid. After transporting for a distance, the polymer solution would crossflow back into the channel as the gel was not tightly packed in that section. Instead, the gel bank there was much looser, and was insufficient to establish an effective resistance to the polymer or water flow.

For the case of 60/80-mesh-sand-filled model (Exp #2, Figure 7a), the channel had a lower permeability of 19.6 darcy. The heterogeneity was not as serious as the other models. The overall oil recovery performance before the gel treatment was comparable with the homogeneous model (Figure 6b). However, in the latter case, the oil bank established during the tertiary polymer flooding was more concentrated and exhibited a better timing effect. During the gel treatment, the microgel particles were harder to

penetrate the channel, and higher injection pressures were required. A total of 11.4 CPV of gel dispersion was injected with no gel particles produced out at the outlet. The gel injection was stopped as the injection pressure reached the equipment limit. Still, we observed appreciable incremental recovery, 15.9% OOIP, after the gel treatment, resulting in an overall recovery factor even higher than in the homogeneous model. This is not surprising as the injection pressure was much higher in this experiment. The high injection pressures indicate the difficulty of the gels in transporting in the channels with lower permeabilities.

(a) Before gel treatment.   (b) After gel treatment.
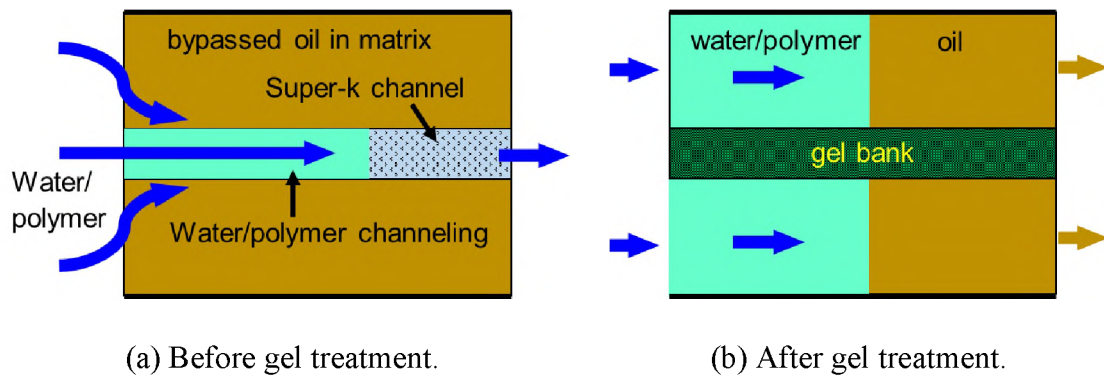
Figure 8. Sweep efficiency improvement after gel treatment.

3.2. MICROGEL TRANSPORT BEHAVIOR

Microgel (170/230 mesh, 63-88 μm) dispersion with a concentration of 1 wt% was injected into the channel model. The injection pressure during the gel treatment process is shown in Figure 9. According to the pressure behavior, the gel injection process exhibited three different stages. In the first stage, the injection pressure steadily increased with no fluctuation. In the second stage, wild pressure fluctuation was observed with an upward trend. Afterwards, the gel would break out at the outlet, and the pressure would jump around a relatively constant value, 240 psi.

3.2.1. Selective Penetration. At the beginning, leak-off took place at the face of the channel model. The carrying fluid leaked off into the matrices, while the gel particles would be left behind at the surface. As more gel particles accumulate at the surface (Figure 9b), a cake would be formed, and the injection pressure would climb up. The cake would continue to grow stronger as the injection pressure increased. A check of the channel model showed that a sticky filter cake was formed at the inlet face. Figure 10a shows the photo of the cake formed at the inlet face, which confirms the occurrence of leak-off during gel injection. The leak-off and formation of the cake are further illustrated in Figure 9b.
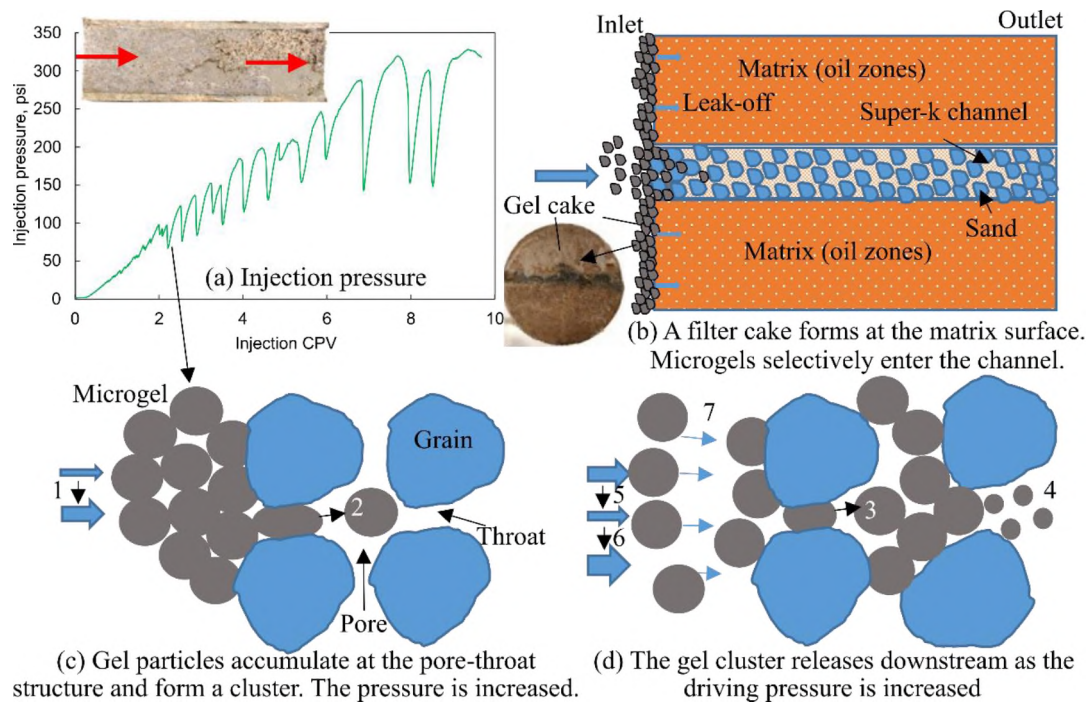
Figure 9. Injection pressure and schematic diagram of gel transport behavior. (Note: 1. Pressure buildup as particles accumulate. 2. Deform and pass. 3. Shrink/deform and pass. 4. Break and pass. This occurs at high pressure gradients/shear forces. 5. Pressure released as gel clusters break out downstream. 6. Pressure buildup as released particles re-accumulate and upstream particles arrive and accumulate. 7. Upstream particles occupy the vacancy left by released particles. Size of the bold blue arrows in (c) and (d) denotes magnitude of pressures. The repeated particle accumulation/release are in accordance with the pressure fluctuations.)

(a) Filter cake at matrix surface.
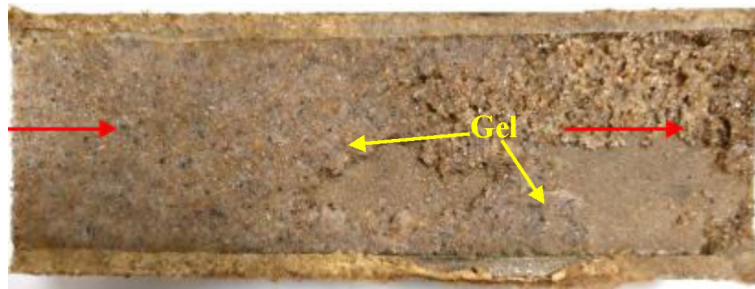
(b) Gel placement in the super-k channel. (The gels filled in the inter-grain pore spaces. The gels are still discernible, especially compared with pure sand grains in Figure 3c.)
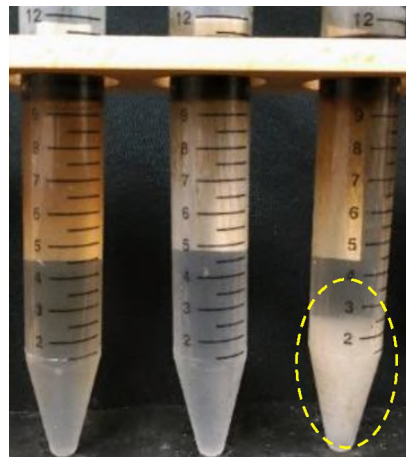
(c) Gel produced in effluent (white material in the 3rd tube).

Figure 10. Filter cake at inlet surface and gel placement in the super-k channel (Exp #4).

The critical pressure for the microgel particles to penetrate the channel can also be estimated from the pressure response (Figure 9a). The injection pressure when the process

transited from the first stage to the second stage (the first peak pressure during fluctuation) can be regarded as the critical pressure. At that time, the pressure at the inlet surface would exceed the critical pressure for the microgel particles to penetrate the super-k channel. The particles accumulated at inlet of the channel would break out downstream, and the injection pressure would suddenly decline, as shown in Figure 9a. The critical pressure will be further discussed.

The cake would prevent the gel particle from penetrating the matrices (oil zones). The gel cake can be easily removed by soaking with breaker after the gel treatment to resume the production. Otherwise, the oil zones would be catastrophically damaged if gel particles penetrate a significant distance into the oil zones. Meanwhile, as the pore size was large enough for the gel particles to pass through the super-k channel. The classic Carman-Kozeny correlation, Equation (3), was used to calculate the average pore throat size of the channels and the matrices (Carman 1956; Mauran et al. 2001).

$$d = \sqrt{\frac{16 k f_{CK} \tau^2}{\Phi}} \,. \tag{3}$$

where d is the average diameter of the pores (μm), k is the permeability (μm^2) of the core, f_{CK} is the Carman-Kozeny shape factor, τ is the tortuosity, and Φ is the porosity (fraction). A value of 4.5 for the $f_{CK} \times \tau^2$ was adopted in our calculation (Carman 1956; Mauran et al. 2001). The matching size ratio (MSR, average particle diameter/pore diameter) between the microgels and the channel was 2.6, while the MSR between the microgels and the matrices was 20.7.

The results indicate that the microgel particles possess the ability to temporarily block and protect the matrices (i.e., the oil zones). Also, the cake grew stronger during the

gel injection process and thus could withstand an increasing injection pressure. Therefore, the microgels can smartly enter the super-k channel without damaging the oil zones.

3.2.2. Pressure Fluctuation and Transport/Retention Patterns. The pressure fluctuation is a result of the repeated accumulation and breakout to downstream of the gel particles in the super-k channel (Figures 9c and 9d). The microgel particles would accumulate at the pore-throat structures. As the injection pressure increased, the gel would deform, shrink, or even break into smaller pieces and then passed through the pore-throat structures (Bai et al. 2007b). The injection pressure would sharply drop down as the gel clusters broke out downstream. The gel again accumulated at the downstream pore-throat structures. Consequently, the injection pressure was built up, the newly formed gel clusters were broken out, and the pressure was sharply released. The gel particles coming from upstream occupy the vacancy left by the released gel cluster. With the repeated accumulation/breakout of the microgel particles, a gel bank was gradually formed and grew in the channel from the inlet towards the outlet. Note that the injection pressure required for the breakout to occur was increased as the gel bank became larger, as shown in Figure 9a. The front of the gel bank advanced towards the producer (outlet), and gel particles would be produced out (Figure 10). The gel came out at 9.7 CPV. The accumulation/release of the gel particles would reach a dynamic equilibrium status as indicated by the fluctuated pressure around a relatively constant level, 240 psi.

The transport/retention pattern of deformable particles in porous media is governed by multiple factors, including the MSR, particle size distribution, particle strength, particle shape, the charge conditions of the particles and the pore surfaces, as well as the driving

differential pressure. The pressure behavior in Figure 9 reveals the dominant transport/retention pattern of the gel particles through the super-k channel.

The MSR is one of the key parameters that determines the transport/retention pattern of the particles. The MSR for our channel model was 2.6. The swollen particles were significantly larger than the average pore throat size. A schematic diagram in Figure 9 shows the transport/retention behavior of the microgel particles. The particles would deform or even shrink (by losing water, i.e., dehydration/syneresis) in order to pass the pore throats. After passing the throat configuration, the shape would recover because of the elasticity and reswelling property of the gel particles. In some cases, as the driving pressure increased, the particles would break into smaller pieces and transport downstream. The broken/pass behavior was also observed by Bai et al. (2007b) in etched glass micromodels and sandpacks models. Li et al. (2019) observed reduced size of the microgel particles after flowing through a core. As the MSR of 2.6 is significantly greater than one for the channel model, the major retention mechanism should be direct capture plugging, and the dominant transport mechanisms are deforming/shrinking/breaking and passing.

3.2.3. Evaluation of Plugging Efficiency to the Super-k Channels. The residual resistance factor (Frr) of the channel after gel treatment was evaluated using a sandpack model with three internal pressure taps. The sandpack model (d×L=2.5×50 cm) was divided into four sections by the internal pressure taps. The same sand/microgel/brine materials were used. The Frr distribution was quite uniform after the gel treatment, in the range of 330-420 (Figure 11). Therefore, the permeability of the super-k channel is expected to be reduced to 0.14-0.17 darcy, even lower than the absolute permeability of the matrices (~0.5 darcy). Note that the oil saturation in the matrices was much higher than

in the channel, thus considering the relationship between the relative permeabilities and phase saturation, a lower-than-matrix channel permeability is beneficial. The water blocking efficiency (E_{bw}) defined by Equation (4) was estimated to be 99.7-99.8%. The results indicate the superpermeable channel was efficiently shut off by the microgels. In Equation (4), K_{cwi} and K_{cw} are the permeabilities of the channel to water before and after the gel treatment, respectively.

$$E_{bw} = \left(1 - \frac{K_{cw}}{K_{cwi}}\right) \times 100\% = \left(1 - \frac{1}{F_{rrw}}\right) \times 100\% .$$
(4)

For a gel treatment, the damage to the oil zones (the matrices of the channel model) is always a key concern. The damage can be minimized in two ways: 1) zonal isolation (Seright et al. 2003; Bai et al. 2012, 2013), and 2) chemical remediation with breaker (Imqam et al. 2016; Wang et al. 2019). As aforementioned, the protective cake at the matrix surface would prevent further penetration of the microgels into the matrices. After removing the cake, the injectivity into the matrices is expected to be recovered to the same level as before the gel treatment. To testify this expectation, the injectivity reduction (J_b/J_a) of the matrix after the gel treatment was calculated to evaluate the potential damage (if any) caused by gel injection to the matrix. A high J_b/J_a value (>>1) indicates significant injectivity reduction and damage to the oil zones. The J_b/J_a is estimated by Equation (5).

$$(J_b / J_a)_p = \frac{q_m / \Delta P_{pb}}{q_m / \Delta P_{pa}} .$$
(5a)

$$(J_b / J_a)_{w1} = \frac{q_m / \Delta P_{wb}}{q_m / \Delta P_{wa}} .$$
(5b)

$$(J_b / J_a)_{w2} = \frac{(Jb / Ja)_{w1}}{1.5} .$$
(5c)

In these equations, J_b and J_a is the injectivity before and after the gel treatment, respectively; q_m is the flow rate in the matrices; and ΔP is the differential pressure between the injector and the producer. The subscripts p and w denote the polymer flooding and water flooding, respectively, and b and a mean before and after the gel treatment, respectively. $(J_b/J_a)_p$ is the injectivity ratio of polymer flood before and after gel treatment. $(J_b/J_a)_{w1}$ includes both the residual resistance by polymer retention (F_{rr}) and damage caused by microgel. For the homogeneous model, the F_{rr} is only caused by polymer retention, $F_{rr}=1.50$. $(J_b/J_a)_{w2}$ excludes the impact of polymer retention. The $(J_b/J_a)_p$ and $(J_b/J_a)_{w2}$ in this study was 1.06 and 1.02, respectively. That is, the injectivity loss to the polymer flooding and to the water flooding was only 5.7% and 2.0%, respectively.
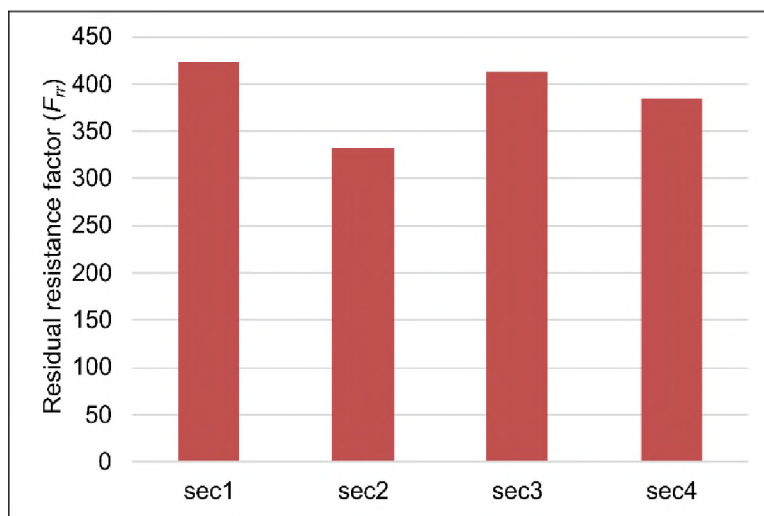
Figure 11. Residual resistance factor distribution after the gel injection.

3.3. DISCUSSION OF APPLICABLE CONDITIONS

Following the same procedure as used for Exp #4 discussed above, we obtained the critical pressure for the different experiments. The relationship between the critical

pressure and the channel permeability is plotted in Figure 12. For the microgels tested in this study, Equation (6) can be used to describe the critical pressure required for the gel particles to penetrate the pore spaces of the channel.

$$P_{cr} = 79937 K_c^{-1.964}.$$ (6)
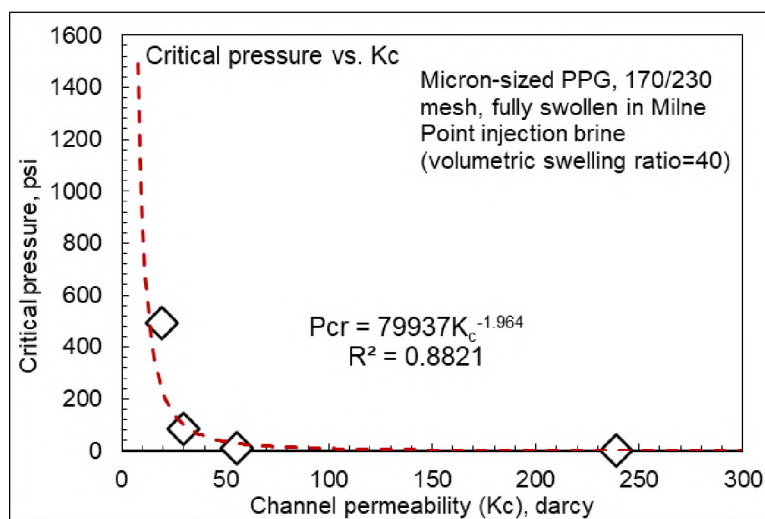
Figure 12. The relationship between critical pressure and channel permeability (K_c).

The results suggest that when the channel is not very permeable (<30 darcy), the required critical pressure gradient would increase sharply as the channel becomes less permeable, indicating a poorer injectivity of the gel. When the channel has a relatively high permeability (>50 darcy), much lower driving pressures are required to force the gel particles into the channel. Therefore, a good injectivity is expected as the channel becomes very permeable. However, on the other hand, concerns may be raised as whether the gel can still establish a sufficient block efficiency to such channels. Our experimental results indicate that, for a channel with a permeability as high as 237 darcy, the tested microgel can still effectively shut off the channel, reduce the water cut, and increase the sweep

efficiency. More studies will be carried out to further study the transport behavior of the gel particles. In general, our results suggest that:

(1) The 260-μm microgel particles are effective to attack the excessive water production problem and improve the oil recovery when the channel has a much higher permeability (>50 darcy). The oil recovery improvement was noticeably greater when the model was more heterogeneous. For the case with the most serious heterogeneity problem in this study (Exp #5), the water cut was effectively reduced as low as 63% from 100%, and the incremental oil recovery was 24.1% OOIP.

(2) The 260-μm microgel we tested is ineffective for channels below 30 darcy due to the penetration/transport difficulties, as observed in Exp #2 and Exp #3. These observations also explain why the tested gel particles did not enter the matrix, as the particle size was much larger than the pore size of the matrix.

This work is not suggesting the microgel is overwhelming over the polymer flood or a replacement of it. The role of the microgel is to help improve the effectiveness of the polymer flood when the severe channeling issue exists in the reservoir. As discussed above, this work demonstrates that under some proper conditions, the microgel is a good candidate to solve the problem. The essential principles for the microgel to work include: 1) the microgels are effectively placed in the channels to prevent the flooding agent (water, polymer, etc.) from channeling vainly through such channels; 2) the microgels should not damage the matrix (or the low-k zones) where the majority of the remaining oil present; and 3) the subsequent flooding fluid can be diverted to the matrix to displace the bypassed remaining oil. These principles should be kept in mind when designing a gel treatment work. More information about how to design and perform a gel treatment in field

applications can be found in the literature (Seright et al. 2003; Bai et al. 2008, 2012, 2013; Qiu et al. 2016; Aldhaheri et al. 2020, 2021; Seright & Brattekas 2021).

4. CONCLUSIONS

In this study, we designed a series of particular sandwich-like channel models and tested the effectiveness and applicable conditions of micron-sized preformed particle gels (microgels) in improving the polymer flooding efficiency.

(1) Polymer flooding alone would be insufficient to achieve a satisfactory oil recovery as the heterogeneity of the reservoir becomes more serious (e.g., permeability contrast $K_c/K_m > 50$). Additional conformance treatment efforts are required.

(2) The microgel forms an external impermeable cake and prevent the gel particles from entering the matrices. Instead, the microgel particles could selectively penetrate and shut off the superpermeable channels under proper conditions.

(3) Our results suggest that the 260-μm microgel particles tested in this study are effective to attack the excessive water production problem and improve the oil recovery when the channel has a much higher permeability (>50 darcy). The gels are unlikely effective for channels below 30 darcy due to the penetration/transport difficulties.

(4) After the gels effectively penetrate and shut off the superpermeable channel, the subsequent flooding fluid is diverted to the matrices (i.e., the unswept oil zones) to displace the bypassed oil. The water cut can be significantly reduced by as high as nearly 40 percentage units in our study, and the sweep efficiency and overall oil recovery are improved.

251

Overall, the results demonstrate the effectiveness of microgel particles in attacking the excessive water production issue caused by super-k channels under appropriate conditions. The essential principles to keep in mind when designing a gel treatment work include: 1) the microgels are effectively placed in the channels to prevent the flooding agent (water, polymer, etc.) from channeling vainly through such channels; 2) the microgels should not damage the matrix (or the low-k zones) where the majority of the remaining oil present; and 3) the subsequent flooding fluid can be diverted to the matrix to displace the bypassed remaining oil.

NOMENCLATURE

Symbol	Description
A_c	Cross-sectional area of channel, cm^2
A_m	Cross-sectional area of matrices, cm^2
d	Average diameter of the pores, μm
E_{bw}	Water blocking efficiency
f_{CK}	Carman-Kozeny factor
Frr	Residual resistance factor
f_w	Water cut, $f_w = q_w/(q_w + q_o)$
J_b, J_a	Injectivity before and after the gel treatment
K_c	Initial permeability of channel, md
K_{cw}	Permeability of the channel to water after the gel treatment, md
K_{cwi}	Permeability of the channel to water before the gel treatment, md

K_m	Initial (absolute) permeability of matrices, md
K_t	Overall permeability of the channel model
MSR	Particle-to-pore matching size ratio
P_{cr}	Critical pressure, psi
ΔP	Differential pressure between the injector and the producer, psi
q_m	Flow rate in the matrices, ml/min
S_{or}	Residual oil saturation, fraction
S_{wi}	Initial water saturation, fraction
Φ	Porosity, fraction
η	Oil recovery factor
τ	Tortuosity, dimensionless

ACKNOWLEDGEMENT

necessarily constitute or imply its endorsement, recommendation, or favoring by the United States Government or any agency thereof. The views and opinions of authors expressed herein do not necessarily state or reflect those of the United States Government or any agency thereof."

REFERENCES

Abedi, B., Ghazanfari, M. H., and Kharrat, R. 2012. Experimental Study of Polymer Flooding in Fractured Systems Using Five-Spot Glass Micromodel: The Role of Fracture Geometrical Properties. Energy Explor. Exploit. 30 (5): 689–705. https://doi.org/10.1260%2F0144-5987.30.5.689.

Abedi, B. and Kharrat, R. 2016. Study the Effect of Fracture Inclination, Spacing and Intensity on Polymer Flooding Efficiency. J Nat Gas Sci Eng 34 (August): 645–649. https://doi.org/10.1016/j.jngse.2016.07.007.

Abu-Shiekah, I., Glasbergen, G., Balushi, S., Wunnik, J. 2014. Conformance Control Treatments for Water and Chemical Flooding: Opportunity and Risk Evaluation. Paper presented at the SPE EOR Conference at Oil and Gas West Asia, Muscat, Oman, 31 March–2 April. SPE-169665-MS. https://doi.org/ 10.2118/169665-MS.

Aldhaheri, M., Wei, M., Alhuraishawy, A., Bai, B. 2021. Field Performances, Effective Times, and Economic Assessments of Polymer Gel Treatments in Controlling Excessive Water Production from Mature Oil Fields. J. Energy Resour. Technol. 143 (8): 080804. https://doi.org/10.1115/1.4049019.

Aldhaheri, M., Wei, M., Zhang, N., Bai, B. 2020. Field Design Guidelines for Gel Strengths of Profile-Control Gel Treatments Based on Reservoir Type. J Pet Sci Eng 194 (November): 107482. https://doi.org/10.1016/j.petrol.2020.107482.

Alshehri, A. J., Wang, J., Kwak, H. T., AlSofi, A. M. 2019. A Closer Look on Viscosity and Divergence Effects of Gel Treatments in Fractured Systems. Paper presented at the SPE Middle East Oil and Gas Show and Conference, Manama, Bahrain, 18–21 March. SPE-194964-MS. https://doi.org/10.2118/ 194964-MS.

Bai, B., Huang, F., Liu, Y., Seright, R. S., Wang, Y. 2008. Case Study on Preformed Particle Gel for in-Depth Fluid Diversion. Paper presented at the SPE Symposium on Improved Oil Recovery, Tulsa, Oklahoma, USA, 20–23 April. SPE-113997-MS. https://doi.org/10.2118/113997-MS.

Bai, B., Li, L., Liu, Y., Liu, H., Wang, Z., You, C. 2007a. Preformed Particle Gel for Conformance Control: Factors Affecting Its Properties and Applications. SPE Res Eval & Eng 10 (4): 415–422. SPE-89389-PA. https://doi.org/10.2118/89389-PA.

Bai, B., Liu, Y., Coste, J. P., Li, L. 2007b. Preformed Particle Gel for Conformance Control: Transport Mechanism Through Porous Media. SPE Res Eval & Eng 10 (2): 176–184. SPE-89468-PA. https://doi.org/10.2118/89468-PA.

Bai, B., Wei, M., and Liu, Y. 2012. Injecting Large Volumes of Preformed Particle Gel for Water Conformance Control. Oil Gas Sci. Technol.–Rev. IFP Energies Nouvelles 67 (6): 941–952. https://doi.org/10.2516/ogst/2012058.

Bai, B., Wei, M., and Liu, Y. 2013. Field and Lab Experience with a Successful Preformed Particle Gel Conformance Control Technology. Paper presented at the SPE Production and Operations Symposium, Oklahoma City, Oklahoma, USA, 23–26 March. SPE-164511-MS. https://doi.org/10.2118/ 164511-MS.

Bai, B., Zhou, J., and Yin, M. 2015. A Comprehensive Review of Polyacrylamide Polymer Gels for Conformance Control. Pet. Explor. Dev. 42 (4): 525–532. https://doi.org/10.1016/S1876-3804(15)30045-8.

Baker, R., Lok, C., Stephenson, T., Weghorn, S. 2014. Combining Conformance Treatment with Mobility Control Increases Enhanced Recovery Factor. Paper presented at the SPE Improved Oil Recovery Symposium, Tulsa, Oklahoma, USA, 12–16 April. SPE-169046-MS. https://doi.org/10.2118/169046-MS.

Carman, P. C. 1956. Flow of Gases Through Porous Media. London, UK: Butterworths Scientific Publications.

Chang, H., Zhang, Y., Dandekar, A., Ning, S., Barnes, J., Edwards, R., Schulpen, W., Cercone, D., Ciferno J. 2020. Experimental Investigation on Separation Behavior of Heavy-Oil Emulsion for Polymer Flooding on Alaska North Slope. SPE Prod & Oper 35 (3): 579–591. SPE-200369-PA. https://doi.org/10.2118/200369-PA.

Dandekar, A., Bai, B., Barnes, J., Cercone, D., Ciferno, J., Ning, S., Seright., R., Sheets, B., Wang, D., Zhang, Y. 2019. First Ever Polymer Flood Field Pilot–A Game Changer to Enhance the Recovery of Heavy Oils on Alaska's North Slope. Paper presented at the SPE Western Regional Meeting, San Jose, California, USA, 23–26 April. SPE-195257-MS. https:// doi.org/10.2118/195257-MS.

Dandekar, A., Bai, B., Barnes, J., Cercone, D., Ciferno, J., Edwards, R., Ning, S., Schulpen, W., Seright., R., Sheets, B., Wang, D., Zhang, Y. 2020. First Ever Polymer Flood Field To Enhance the Recovery of Heavy Oils on Alaska's North Slope–Pushing Ahead One Year Later. Paper presented at the SPE Western Regional Meeting, April 27-30, 2020, Bakersfield, California, USA. Note–postponed to virtual format in April 2021. SPE-200814-MS. https:// doi.org/10.2118/200814-MS.

Dhaliwal, A., Zhang, Y., Dandekar, A., Ning, S., Barnes, J., Edwards, R., Schulpen, W., Cercone, D.P. Ciferno, J.P. 2021. Experimental Investigation of Polymer Induced Fouling of Heater Tubes in the First-Ever Polymer Flood Pilot on Alaska North Slope. SPE Prod & Oper 36 (1): 70–82. https://doi.org/10.2118/200463-PA.

Elsharafi, M. O. and Bai, B. 2013. Minimizing Formation Damage for Preformed Particle Gels in Mature Reservoirs. Paper presented at the SPE Asia Pacific Enhanced Oil Recovery Conference, Kuala Lumpur, Malaysia, 11–13 August. SPE-174645-MS. https://doi.org/10.2118/174645-MS.

Elsharafi, M. O. and Bai, B. 2016. Influence of Strong Preformed Particle Gels on Low Permeable Formations in Mature Reservoirs. Pet. Sci. 13 (1): 77–90. https://doi.org/10.1007/s12182-015-0072-3.

Hatzignatiou, G. D., Giske, H. N., and Stavland, A. 2016. Polymers and Polymer-Based Gelants for Improved Oil Recovery and Water Control Applications in Naturally Fractured Chalk Formations. Paper presented at the SPE Bergen One Day Seminar, Bergen, Norway, 20 April. SPE-180024-MS. https://doi.org/10.2118/180024-MS.

Imqam, A., Bai, B., and Delshad, M. 2018. Micro-Particle Gel Transport Performance Through Unconsolidated Sandstone and Its Blocking to Water Flow During Conformance Control Treatments. Fuel 231 (1 November): 479–488. https://doi.org/10.1016/j.fuel.2018.05.099.

Imqam, A., Bai, B., Wei, M., Elue, H., Muhammed, F. A. 2016. Use of Hydrochloric Acid To Remove Filter-Cake Damage from Preformed Particle Gel During Conformance-Control Treatments. SPE Prod & Oper 31 (3): 247–257. SPE-172352-PA. https://doi.org/10.2118/172352-PA.

Kang, W., Kang, X., Lashari, Z.A., Li, Z., Zhou, B., Yang, H., Sarsenbekuly, B. Aidarova, S. 2021. Progress of Polymer Gels for Conformance Control in Oilfield. Adv Colloid Interface Sci 289 (March): 102363.

Larkin, R. J. and Creel, P. G. 2008. Methodologies and Solutions To Remediate Inner-Well Communication Problems on the SACROC CO2 EOR Project: A Case Study. Paper presented at the SPE Symposium on Improved Oil Recovery, Tulsa, Oklahoma, USA, 20–23 April. SPE-113305-MS. https://doi.org/10.2118/113305-MS.

Li, J., Niu, L., and Lu, X. 2019. Migration Characteristics and Deep Profile Control Mechanism of Polymer Microspheres in Porous Media. Energy Sci Eng 7 (5): 2026–2045. https://doi.org/10.1002/ese3.409.

Mauran, S., Rigaud, L., and Coudevylle, O. 2001. Application of the Carman-Kozeny Correlation to a High-Porosity and Anisotropic Consolidated Medium: The Compressed Expanded Natural Graphite. Transp Porous Media 43 (2): 355–376. https://doi.org/10.1023/A:1010735118136.

Ning, S., Barnes, J., Edwards, R., Schulpen, W., Dandekar, A., Zhang, Y., Cercone, D., Ciferno, J. 2020. First Ever Polymer Flood Field Pilot To Enhance the Recovery of Heavy Oils on Alaska North Slope–Producer Responses and Operational Lessons Learned. Paper presented at the SPE Annual Technical Conference and Exhibition, Virtual, 26–29 October. SPE-201279-MS. https://doi.org/10.2118/201279-MS.

Peirce, J. W., Hutcherson, M. R., Jensen, M. D., Brice, B. W., Vasquez, J. E., Woods, A. 2014. An Overview of Conformance Control Efforts for the West Sak Field on the North Slope of Alaska. Paper presented at the SPE Improved Oil Recovery Symposium, Tulsa, Oklahoma, USA, 12–16 April. SPE-169073-MS. https://doi.org/ 10.2118/169073-MS.

Pyziak, D. and Smith, D. 2007. Update on Anton Irish Conformance Effort. Paper presented at the 6th International Conference on Production Optimization-Reservoir Conformance-Profile Control-Water and Gas Shutoff, Houston, Texas, USA, 6–7 November.

Qiu, Y., Wei, M., Geng, J., Wu, F. 2016. Successful Field Application ofMicrogel Treatment in High Temperature High Salinity Reservoir in China. Paper presented at the SPE Improved Oil Recovery Conference, Tulsa, Oklahoma, USA, 11–13 April. SPE-179693-MS. https://doi.org/10.2118/179693-MS.

SayedAkram, N. I. and Mamora, D. 2011. Simulation Study on Surfactant-Polymer Flood Performance in Fractured Carbonate Reservoir. Paper presented at the SPE Saudi Arabia Section Technical Symposium and Exhibition, Al-Khobar, Saudi Arabia, 15–18 May. SPE-149106-MS. https:// doi.org/10.2118/149106-MS.

Seright, R. S. 1999. Mechanism for Gel Propagation Through Fractures. Paper presented at the SPE Rocky Mountain Regional Meeting, Gillette, Wyoming, USA, 15–18 May. SPE-55628-MS. https://doi.org/10.2118/55628-MS.

Seright, R. S, and Brattekas, B. 2021. Water Shutoff and Conformance Improvement: An Introduction. Pet. Sci. 18: 450–478. https://doi.org/10.1007/s12182-021-00546-1.

Seright, R. S., Lane, R. H., and Sydansk, R. D. 2003. A Strategy for Attacking Excess Water Production. SPE Prod & Fac 18 (3): 158–169. SPE-84966-PA. https://doi.org/10.2118/84966-PA.

Shedid, S. A. 2006. Influences of Fracture Orientation on Oil Recovery by Water and Polymer Flooding Processes: An Experimental Approach. J Pet Sci Eng 50 (3–4): 285–292. https://doi.org/10.1016/j.petrol.2005.12.002.

Sun, X. and Bai, B. 2017. Comprehensive Review of Water Shutoff Methods for Horizontal Wells. Pet. Explor. Dev. 44 (6): 1022–1029. https://doi.org/10.1016/S1876-3804(17)30115-5.

Sydansk, R. D. and Romero-Zeron, L. 2011. Reservoir Conformance Improvement. Richardson, Texas, USA: Society of Petroleum Engineers.

Targac, G., Gallo, C., Smith, D., Huang, C. K., Autry, S., Peirce, J., Li, B. 2020. Case History of Conformance Solutions for West Sak Wormhole/Void Space Conduit with a New Reassem- bling Pre-Formed Particle Gel RPPG. Paper presented at the SPE Annual Technical Conference and Exhibition, Virtual, 26–29 October. SPE-201302-MS. https://doi.org/10.2118/201302-MS.

Vasquez, J. E., Dalrymple, E. D., Abbasy, I., Eoff L. S. 2008. Laboratory Evaluation of Water Swellable Materials for Fracture Shutoff. Paper presented at the SPE North Africa Technical Conference and Exhibition, Marrakech, Morocco, 12–14 March. SPE-111492-MS. https://doi.org/10.2118/111492-MS.

Villone, M. M. and Maffettone, P. L. 2019. Dynamics, Rheology, and Applications of Elastic Deformable Particle Suspensions: A Review. Rheol Acta 58 (3–4): 109–130. https://doi.org/10.1007/s00397-019-01134-2.

Wang, Z., Bai, B., Zhou, E., Pu, J., Schuman, T. 2019. Experimental Evaluation of Oxidizing Breakers for a Polyacrylamide-Based Re-Crosslinkable Preformed Particle Gel. Energy Fuels 33 (6): 5001–5010.

Wu, D., Zhou, K., Hou, J., An, Z., Zhai, M., Liu, W. 2021. Review of Experimental and Simulation Studies of Enhanced Oil Recovery Using Viscoelastic Particles. J Dispers Sci Technol 42 (07): 956-969.

Yao, C., Lei, G., Li, L., Gao, X. 2012. Selectivity of Pore-Scale Elastic Microspheres as a Novel Profile Control and Oil Displacement Agent. Energy Fuels 26 (08): 5092–5101. https://doi.org/10.1021/ef300689c.

Zhao, Y., Yin, S., Seright, R. S., Ning, S., Zhang, Y., Bai, B. 2021. Enhancing Heavy-Oil-Recovery Efficiency by Combining Low-Salinity-Water and Polymer Flooding. SPE J. 26 (03): 1535–1551. SPE-204220-PA. https://doi.org/10.2118/204220-PA.

SECTION

2. CONCLUSIONS AND RECOMMENDATIONS

2.1. MAJOR CONTRIBUTIONS AND CONCLUSIONS

(1) Advantages of low-salinity polymer (LSP) over high-salinity polymer (HSP) were demonstrated through systematic coreflood experiments using Schrader Bluff viscous oil/brine/rock materials in Milne Point Unit on Alaska's North Slope. Less polymer was required to achieve the target viscosity. LSP could recover more oil after HSP flood. No additional oil was recovered by HSP after LSP flood. Field application showed remarkable success regarding water cut reduction, oil production increase, delayed breakthrough, and projected oil recovery improvement.

(2) Microgels were attempted to shut off super-k channels (27-221 darcies) in reservoirs. The transport and water-blocking behavior were studied using sandpacks with multiple pressure sensors. The gels could penetrate, place in, and shut off the channels under proper conditions. The gels exhibited frontal delay, shear-thinning, salinity-responsive, and disproportionate permeability reduction (DPR) behaviors. The particle-to-pore matching size ratio (MSR) significantly impacted the effectiveness of the gels.

(3) A threshold penetration pressure (ΔP_{th}) was required to push the gels to penetrate the superpermeable porous channels. The ΔP_{th} revealed the underlying mechanism of selective penetration behavior of microgels in heterogeneous reservoirs. Correlations were developed to describe the relationship between ΔP_{th} and MSR. Favorable working conditions were identified for effective gel treatments, in which the gels

could easily penetrate the target zones (channels) without massive invasion into the reservoir matrices.

(4) A critical (minimum) pressure gradient (∇P_{cr}) was required to drive the microgel particles to propagate through porous channels. A correlation was developed to describe the ∇P_{cr}-MSR relationship in the superpermeable channels. Diagrams were developed to estimate the maximum possible propagation distances of the gels in channels in conceptual field applications.

(5) A particular sandwich-like physical model and a set of comprehensive evaluation techniques were developed. The model overcame some drawbacks associated with commonly used conventional parallel coreflooding models. The design allowed crossflows between the matrices and the channel. The comprehensive evaluations included but were not limited to selective penetration/placement, sweep efficiency improvement, water-blocking efficiency, matrix damage, and oil recovery improvement.

(6) The microgels could selectively place in, and effectively shut off the superpermeable channels under proper conditions. After gel treatments, tracer tests demonstrated remarkable sweep improvement (0.25-0.43 total pore volumes). To achieve both good injectivity and water-blocking efficiency for the tested microgels, the MSR in the channel should be below 2. Meanwhile, the MSR in the matrices should be above 5 to minimize matrix damage.

(7) Polymer flood alone is insufficient to achieve a satisfactory oil recovery as the reservoirs are very heterogeneous (e.g., $k_c/k_m > 50$). Microgel conformance treatments can improve the effectiveness of polymer flood by reducing water cut and increasing oil recovery. Favorable working conditions for the microgels were identified.

2.2. SPECIFIC CONCLUSIONS

In Paper I, the enhanced oil recovery performance of low-salinity HPAM polymer flooding in heavy oil reservoirs were systematically studied. The following conclusions were drawn based on the experimental results.

(1) The HSP required nearly two thirds more polymer than the LSP to achieve the same target viscosity in this study.

(2) Additional oil was recovered from LSW flooding after extensive HSW flooding (3-9% OOIP). LSW flooding performed in secondary mode could achieve a higher recovery than that in tertiary mode. Also, the occurrence of water breakthrough was delayed in the LSW flooding compared with the HSW flooding.

(3) After extensive LSW flooding and HSP flooding, incremental oil recovery (~8% OOIP) was still achieved by LSP flooding with the same viscosity as the HSP. No appreciable incremental oil was recovered by HSP flooding performed after LSP flooding. LSP flooding performed directly after waterflooding can achieve more incremental oil recovery (~10% OOIP).

(4) The synergy of combining low-salinity water and polymer flooding has been demonstrated under various conditions in this study. Field application practice has demonstrated remarkable success regarding water cut reduction, oil production improvement, delayed breakthrough behavior, and projected oil recovery improvement.

In Paper II, a series of experiments were carried out to investigate the transport behavior of microgels in super-k channels. Sandpacks with permeabilities ranging from 27 to 221 darcies were used to mimic the super-k channels. Multiple pressure sensors were applied along the sandpack models to monitor the propagation behavior of the microgels.

(1) The tested microgel particles could transport through the super-k channels, and a higher driving pressure gradient was required when the particle-to-pore matching size ratio (MSR) was larger. The pressure gradient distribution along the super-k channels was relatively uniform when the MSR was low (<1.3). However, the inlet section would show increasingly higher pressure gradients as the MSR was increased, indicating increased difficulty in propagation.

(2) The propagation of the microgel particles was significantly slower compared with the carrying fluids. The delay behavior was more pronounced when the MSR was larger.

(3) The injection pressure was less sensitive to the injection flow rate compared with a Newtonian fluid. The gel dispersion exhibited an apparent shear thinning (pseudoplastic) behavior when transporting through the porous channels.

(4) Breakage of the microgel particles was observed especially at high superficial velocities. The particle breakage was partially responsible for the apparent shear thinning behavior during gel propagation in superpermeable porous channels. The breakage phenomenon was in favor of deep placement of the microgel particles.

(5) The channel permeabilities were significantly reduced by the microgels, bringing sufficient resistance to subsequent water flooding (>99.5%). At given matching size conditions, softer gels are more likely to establish in-depth placement and uniform water-blocking capacity in the channels. The microgel particles exhibit salinity-responsive behavior to the post brine flush. It suggests that the gel particles can shrink and reswell according to the salinity of the injected water. Possibilities are discussed to utilize this salinity-responsive behavior.

(6) The microgels exhibit a particular disproportionate permeability reduction (DPR) effect. After gel injection, the channel permeability to water flow was reduced by more than 20-92 times of the permeability to oil flow.

In Paper III, experiments were conducted to investigate the critical penetration behavior of microgels into channels and matrices (50 md to 230 darcies). The results demonstrated the presence of threshold penetration pressure (ΔP_{th}), which was responsible for the selective penetration behavior of the microgels in the channels and matrices.

(1) The critical penetration behavior was closely related to the MSR. The ΔP_{th} at the inlet faces of super-k channels (60-230 darcies) was in the range of 1 to 12 psi with MSRs in the range of 0.6 to 1.8. The low ΔP_{th} was beneficial to allow easy penetration of gel materials into the channeling zones.

(2) On the contrary, the ΔP_{th} was much higher in the cores with relatively low permeabilities and high MSRs (ΔP_{th}>200 psi when MSR>6.5 for the tested gels). The high ΔP_{th} was desirable to prevent the gel materials from massively invading and damaging the matrices. Instead, the gel particles accumulated at the inlet surface, and a gel cake was gradually formed. The cake further prevented the invasion of the gels.

(3) Correlations were developed to describe the ΔP_{th}-MSR relationship. When MSR<3, the ΔP_{th} exponentially increased with the MSR. When MSR>3, the ΔP_{th} became less sensitive to the MSR, but it still exponentially increased with the MSR. When MSR>20, the ΔP_{th} was higher than 1200 psi.

(4) This study provided quantitative evidence to demonstrate the selective penetration of the tested microgels. In addition, the concept of ΔP_{th} was utilized to figure out the favorable working conditions to achieve effective gel treatments. The MSR in the

channel should be sufficiently low to allow easy penetration of gels into the channel (e.g., MSR<2 in this study). Meanwhile, the MSR in the matrix should be high enough to support a high ΔP_{th} and thus prevent massive invasion into the matrix.

In Paper IV, systematic studies were carried out to explore the critical pressure gradients and transport distances of microgels in channels and matrices.

(1) A critical (minimum) pressure gradient (∇P_{cr}) was required to drive the microgel particles to propagate the superpermeable porous channels. Below ∇P_{cr}, the gel particles could not transport in the porous channels. The existence of the ∇P_{cr} was confirmed with gel injection experiments carried out in constant-injection-pressure mode.

(2) The particle-to-pore matching size ratio (MSR) had a significant impact on the ∇P_{cr}. The ∇P_{cr} increased exponentially with the MSR at relatively low MSRs (<2). The ∇P_{cr} was lower than 60 psi/ft at the low MSRs. The low MSRs represented the desired situations in channels to be treated.

(3) A simple correlation was developed to describe the relationship between the critical pressure gradient and the MSR in the superpermeable channels. A procedure was developed to estimate the maximum transport (treatment) distance of the gel particles in reservoirs based on the critical pressure gradient.

(4) At low MSRs, the gel particles could transport a significant distance away from the wellbore, which was favorable for in-depth conformance treatments.

(5) The transport-distance diagrams can help engineers select proper gel products to address water channeling problems in reservoirs. Also, this work provides an effective procedure to study the impact of other parameters (e.g., dispersion concentration and gel strength) on the propagation distance of gel materials.

In Paper V, a particular sandwich-like physical model was developed. The model consisted of low-permeability matrices and a superpermeable porous channel. The characteristic properties of the model (k_c, k_m, channel size, etc.) could be adjusted to represent the reservoir conditions of interest. The model allowed crossflow between the matrices and the channel, and it was more representative of the real channeling problems in reservoirs.

On the basis of the particular channel model, we developed a set of guidelines to perform comprehensive evaluations to test the conformance improvement potential of a gel material in a given reservoir to be treated. The evaluations included: selective penetration/placement behaviors, sweep efficiency improvement, water-blocking efficiency, matrix damage, and oil recovery improvement.

The evaluation methodology was elaborated upon using case studies. The results suggested that the tested microgel particles could selectively penetrate and place in the superpermeable channel of the reservoir. A cake formed at the matrix inlet faces and prevented gel particles from further penetrating and damaging the matrix. The damage at the matrix inlet faces could be effectively removed with a chemical breaker. The subsequent water was diverted to the matrices and thus the sweep volume was significantly increased (e.g., 0.35 PV vs. 0.06 PV at breakthrough).

In Paper VI, experiments were conducted to investigate the transport, placement, water-blocking ability, fluid diversion and sweep improvement, and matrix damage effect of microgels in reservoirs containing superpermeable channels. The impact of channel/matrix permeability contrast, the MSR in channels, and the MSR in matrices were studied. The favorable conditions of the tested microgels were identified.

(1) The microgel particles selectively penetrated and placed in the porous super-K channels. The pressure gradient during gel injection increased with the particle-to-pore matching size ratio. The pores in the channels were filled with the gel particles. The channel permeabilities were significantly reduced after microgel treatments. The channels were effectively blocked by the microgels.

(2) Delayed breakthrough of the gel particles was observed, which was partially resulted from the dehydration and retention of the gel particles in the channels, and the buildup of a filter cake at the inlet faces of the matrices.

(3) The sweep improvement after the gel treatment was evaluated by chemical tracer tests. The results clearly demonstrated delayed breakthrough, fluid diversion, and increased swept volume of the subsequent flooding fluids. In the experiments, the sweep improvement was in the range of 0.25-0.43 PV_t. A higher sweep improvement was achieved as the permeability contrast was higher (i.e., the reservoir was more heterogeneous).

(4) The effectiveness of the gel treatment is related to the quality of the gel placement in the channels. Better sweep improvement can be achieved when the gel particles have good injectivity and the gel particles can be placed at the in-depth sections of the channels. Insufficient placement of the gel materials can result in unsatisfactory sweep improvement.

(5) The damage of the gel materials to the matrices was evaluated by directly measuring matrix permeabilities after the gel treatment. A gel cake could be formed at the inlet faces of the matrices during treatment, but the cake could be removed with chemical breakers. The injectivity of the matrices was effectively recovered.

In Paper VII, experiments were carried out to test the effectiveness and applicable conditions of microgels in improving polymer flooding efficiency in heavy oil reservoirs containing superpermeable channels.

(1) Polymer flooding alone was insufficient to achieve a satisfactory oil recovery as the heterogeneity of the reservoir became more serious (e.g., permeability contrast $k_c/k_m > 50$). Additional conformance treatment efforts were required.

(2) The 260-μm microgel particles tested in this study were effective to attack the excessive water production problem and improve the oil recovery when the channel had a much higher permeability (>50 darcy). The gels were unlikely to be effective for channels below 30 darcy due to the penetration/transport difficulties.

(3) After the gels effectively penetrated and shut off the superpermeable channels, the subsequent flooding fluid was diverted to the reservoir matrices (i.e., the unswept oil zones) to displace the bypassed oil. The water cut was significantly reduced by as high as nearly 40 percentage units, and the sweep efficiency and overall oil recovery were improved.

(4) Overall, the results demonstrated the effectiveness of microgel particles in attacking the excessive water production issue caused by superpermeable channels under appropriate conditions. The essential principles to keep in mind when designing a gel treatment work include: 1) the microgels are effectively placed in the channels to prevent the flooding agent (water, polymer, etc.) from channeling vainly through such channels; 2) the microgels should not damage the matrices (or the low-permeability zones) where the majority of the remaining oil present; and 3) the subsequent flooding fluid can be diverted to the matrix to displace the bypassed remaining oil.

2.3. RECOMMENDATIONS

It would be beneficial to perform microscopic experiments using microfluidic models to investigate the enhanced oil recovery mechanisms of polymer flooding at low salinity conditions. The experiments are expected to demonstrate whether the low-salinity polymer can reduce the true residual oil saturation, and whether wettability alteration is an important mechanism responsible for the beneficial oil recovery improvement observed in coreflooding tests. Also, the experiments can demonstrate whether viscoelasticity of the polymer solutions can reduce the residual oil saturation under normal flow rate conditions.

In gel treatments, it is challenging to simultaneously achieve good injectivity, reliable water-blocking ability, and low matrix damage. Particular properties of the gels, such as the salinity-responsive behavior, can be further explored to help fulfill these requirements. In addition, it is encouraged to develop new gel products, such as softer but recrosslinkable gels. These gels are expected to possess the merits of good injectivity and easy placement. Meanwhile, a better water-blocking efficiency can be established compared with the gels with no recrosslinking ability.

The experimental MSRs to develop the diagrams of maximum propagation distance in Paper IV ranged from 0.67 to 1.77. The transport behaviors can be very different when the MSRs are much smaller (e.g., MSR<0.5). The critical pressure gradient may follow a substantially different trend compared with the situations in this study. It is meaningful to perform more experiments at lower MSRs.

The dehydration behavior of gels during propagation in channels or fractures is very important for gel placement. The channel model developed in this work can be improved to monitor the leak-off and dehydration during gel injection. Taps can be attached to the

matrices. Therefore, the water produced from the matrices can be obtained. The results are expected to be helpful in estimating the propagation distance when a given volume of gels is injected in scaleup applications. Scale-up numerical simulation studies are recommended to investigate the effect of different operational parameters on the microgel conformance treatment performance. In this way, guidelines can be worked out for field applications.

BIBLIOGRAPHY

Aldhaheri, M., Wei, M., Alhuraishawy, A. Bai, B. 2021. Field Performances, Effective Times, and Economic Assessments of Polymer Gel Treatments in Controlling Excessive Water Production from Mature Oil Fields. J. Energy Resour. Technol. 143 (8): 080804. https://doi.org/10.1115/1.4049019.

Aldhaheri, M., Wei, M., Zhang, N. Bai, B. 2020. Field Design Guidelines for Gel Strengths of Profile-Control Gel Treatments Based on Reservoir Type. J Pet Sci Eng 194 (November): 107482. https://doi.org/10.1016/j.petrol.2020.107482.

Alhuraishawy, A. K., Bai, B., Imqam, A., Wei, M. 2018. Experimental Study of Combining Low Salinity Water Flooding and Preformed Particle Gel to Enhance Oil Recovery for Fractured Carbonate Reservoirs. Fuel, 214: 342-350.

Attanasi, E.D. and Freeman, P.A., Evaluation of development options for Alaska North Slope viscous and heavy oil. Natural Resources Research, Vol. 24, No. 1, 2014.

Bai, B., Huang, F., Liu, Y., Seright, R. S., Wang, Y. 2008. Case Study on Preformed Particle Gel for In-depth Fluid Diversion. Paper presented at the SPE Symposium on Improved Oil Recovery, Tulsa, Oklahoma, USA. SPE-113997-MS. https://doi.org/10.2118/113997-MS.

Bai, B., Li, L., Liu, Y., Liu, H., Wang, Z., You, C. 2007a. Preformed Particle Gel for Conformance Control: Factors Affecting its Properties and Applications. SPE Res Eval & Eng. 10 (4): 415–421. SPE-89389-PA. http://dx.doi.org/10.2118/89389-PA.

Bai, B., Liu, Y., Coste, J. P. et al. 2007b. Preformed Particle Gel for Conformance Control: Transport Mechanism Through Porous Media. SPE Res Eval & Eng. 10 (2): 176–184. SPE-89468-PA. http://dx.doi.org/ 10.2118/89468-PA.

Bai, B., Wei, M., and Liu, Y. 2012. Injecting Large Volumes of Preformed Particle Gel for Water Conformance Control. Oil Gas Sci. Technol.–Rev. IFP Energies Nouvelles 67 (6): 941–952. https://doi.org/10.2516/ogst/2012058.

Bai, B., Wei, M., and Liu, Y. 2013. Field and Lab Experience with a Successful Preformed Particle Gel Conformance Control Technology. Paper presented at the SPE Production and Operations Symposium, Oklahoma City, Oklahoma, USA, 23–26 March. SPE-164511-MS. https://doi.org/10.2118/ 164511-MS.

Bai, B., Zhou, J., and Yin, M. 2015. A Comprehensive Review of Polyacrylamide Polymer Gels for Conformance Control. Pet. Explor. Dev. 42 (4): 525–532. https://doi.org/10.1016/S1876-3804(15)30045-8.

Chang, H., Zhang, Y., Dandekar, A., Ning, S., Barnes, J., Edwards, R., Schulpen, W., Cercone, D., Ciferno J. 2020. Experimental Investigation on Separation Behavior of Heavy-Oil Emulsion for Polymer Flooding on Alaska North Slope. SPE Prod & Oper 35 (3): 579–591. SPE-200369-PA. https://doi.org/10.2118/200369-PA.

Chavan M., Dandekar A., Patil S., Khataniar S. 2019. Low-salinity-based enhanced oil recovery literature review and associated screening criteria. Petrol Sci 16 (6): 1344–1360. https://doi.org/10.1007/s12182-019-0325-7.

Dandekar, A., Bai, B., Barnes, J., Cercone, D., Ciferno, J., Ning, S., Seright., R., Sheets, B., Wang, D., Zhang, Y. 2019. First Ever Polymer Flood Field Pilot–A Game Changer to Enhance the Recovery of Heavy Oils on Alaska's North Slope. Paper presented at the SPE Western Regional Meeting, San Jose, California, USA, 23–26 April. SPE-195257-MS. https:// doi.org/10.2118/195257-MS.

Dandekar, A., Bai, B., Barnes, J., Cercone, D., Ciferno, J., Edwards, R., Ning, S., Schulpen, W., Seright., R., Sheets, B., Wang, D., Zhang, Y. 2020. First Ever Polymer Flood Field Pilot to Enhance the Recovery of Heavy Oils on Alaska's North Slope– Pushing Ahead One Year Later. Paper presented at the SPE Western Regional Meeting, April 27-30, 2020, Bakersfield, California, USA. Note–postponed to virtual format in April 2021. SPE-200814-MS. https://doi.org/10.2118/200814-MS.

Dandekar, A., Bai, B., Barnes, J., Cercone, D., Ciferno, J., Edwards, R., Ning, S., Schulpen, W., Seright., R., Sheets, B., Wang, D., Zhang, Y. 2021. Heavy Oil Polymer EOR in the Challenging Alaskan Arctic–It Works! Paper prepared for presentation at the Unconventional Resources Technology Conference held in Houston, Texas, USA, 26-28 July 2021. URTeC-2021-5077. https://doi.org/10.15530/urtec-2021-5077.

Delamaide, E., Technologies, I. F. P., Alliance, E. O. R. 2018. A new Kind of EOR for Trinidad. Paper presented at the SPE Trinidad and Tobago Section Energy Resources Conference, 25–26 June, Port of Spain, Trinidad and Tobago. SPE-191205-MS. https://doi.org/10.2118/191205-MS.

Delamaide, E., Zaitoun, A., Renard, G., Tabary, R. 2014. Pelican Lake Field: First Successful Application of Polymer Flooding in a Heavy-Oil Reservoir. SPE Res Eval & Eng 17 (3): 340–354. https://doi.org/10.2118/165234-PA.

Dhaliwal, A., Zhang, Y., Dandekar, A., Ning, S., Barnes, J., Edwards, R., Schulpen, W., Cercone, D.P. Ciferno, J.P. 2021. Experimental Investigation of Polymer Induced Fouling of Heater Tubes in the First-Ever Polymer Flood Pilot on Alaska North Slope. SPE Prod & Oper 36 (1): 70–82. SPE-200463-PA. https://doi.org/10.2118/200463-PA.

Kang, W., Kang, X., Lashari, Z.A., Li, Z., Zhou, B., Yang, H., Sarsenbekuly, B. Aidarova, S. 2021. Progress of Polymer Gels for Conformance Control in Oilfield. Adv Colloid Interface Sci 289 (March): 102363.

Larkin, R. J. and Creel, P. G. 2008. Methodologies and Solutions to Remediate Inner-Well Communication Problems on the SACROC CO_2 EOR Project: A Case Study. Paper presented at the SPE Symposium on Improved Oil Recovery, Tulsa, Oklahoma, USA, 20–23 April. SPE-113305-MS. https://doi.org/10.2118/113305-MS.

Leng, J., Wei, M., and Bai, B. 2021. Review of Transport Mechanisms and Numerical Simulation Studies of Preformed Particle Gel for Conformance Control. J Pet Sci Eng, 109051. (In press; published online 6 June 2021) https://doi.org/10.1016/j.petrol.2021.109051.

Morrow, N. R. and Buckley, J. 2011. Improved Oil Recovery by Low-Salinity Waterflooding. J Petrol Techn, 63 (05): 106–112.

Ning, S., Barnes, J., Edwards, R., Dunford, K., Eastham, K., Dandekar, A., Zhang, Y., Cercone, D., Ciferno, J. 2019. First Ever Polymer Flood Field Pilot to Enhance the Recovery of Heavy Oils on Alaska's North Slope–Polymer Injection Performance. Paper presented at the SPE/AAPG/SEG Unconventional Resources Technology Conference, Denver, Colorado, USA, 22–24 July. URTEC-2019-643-MS. https://doi.org/10.15530/urtec-2019-643.

Ning S, Barnes J, Edwards R, Schulpen W, Dandekar A, Zhang Y, Cercone, D., Ciferno, J. 2020. First Ever Polymer Flood Field Pilot to Enhance the Recovery of Heavy Oils on Alaska North Slope–Producer Responses and Operational Lessons. Paper presented at the SPE Annual Technical Conference & Exhibition held in Denver, Colorado, USA, 5–7 October 2020 (postponed until 26–29 October 2020 and changed to a virtual event). SPE-201279-MS.

Paskvan, F., Turak, J., Jerauld, G., Gould, T., Skinner, R. and Garg, A. 2016. Alaskan viscous oil: EOR Opportunity, or Waterflood Sand Control First? Paper presented at the SPE Western Regional Meeting held in Anchorage, AK, USA, 23–26 May.

Peirce, J. W., Hutcherson, M. R., Jensen, M. D., Brice, B. W., Vasquez, J. E., Woods, A. 2014. An Overview of Conformance Control Efforts for the West Sak Field on the North Slope of Alaska. Paper presented at the SPE Improved Oil Recovery Symposium, Tulsa, Oklahoma, USA, 12–16 April. SPE-169073-MS. https://doi.org/ 10.2118/169073-MS.

Pu, J., Bai, B., Alhuraishawy, A., Schuman, T., Chen, Y., Sun, X. 2019. A Recrosslinkable Preformed Particle Gel for Conformance Control in Heterogeneous Reservoirs Containing Linear-Flow Features. SPE J. 24 (04): 1714–1725. SPE-191697-PA. https://doi.org/10.2118/191697-PA.

Pyziak, D. and Smith, D. 2007. Update on Anton Irish Conformance Effort. Paper presented at the 6th International Conference on Production Optimization-Reservoir Conformance-Profile Control-Water and Gas Shutoff, Houston, Texas, USA, 6–7 November.

Saboorian-Jooybari, H., Dejam, M., Chen, Z. 2016. Heavy Oil Polymer Flooding from Laboratory Core Floods to Pilot Tests and Field Applications: Half-century Studies. J Pet Sci Eng 142: 85–100.

Saleh, L. D., Wei, M., Zhang, Y., Bai, B. 2017. Data Analysis for Polymer Flooding That is Based on a Comprehensive Database. SPE Res Eval & Eng, 20 (4): 876–893. https://doi.org/10.2118/169093-PA.

Seright, R. S., Lane, R. H., and Sydansk, R. D. 2003. A Strategy for Attacking Excess Water Production. SPE Prod & Fac 18 (3): 158–169. SPE-84966-PA. https://doi.org/10.2118/84966-PA.

Seright, R. S, and Brattekas, B. 2021. Water Shutoff and Conformance Improvement: An Introduction. Pet. Sci. 18: 450–478. https://doi.org/10.1007/s12182-021-00546-1.

Sheng, J. J. 2014. Critical review of Low-Salinity Waterflooding. J Pet Sci Eng 120: 216–224.

Sun, X., Alhuraishawy, A. K., Bai, B., Wei, M. 2018. Combining Preformed Particle Gel and Low Salinity Waterflooding to Improve Conformance Control in Fractured Reservoirs. Fuel 221: 501-512.

Sun, X. and Bai, B. 2017. Comprehensive Review of Water Shutoff Methods for Horizontal Wells. Pet. Explor. Dev. 44 (6): 1022–1029. https://doi.org/10.1016/S1876-3804(17)30115-5.

Sun, X., Bai, B., Long, Y., Wang, Z. 2020. A Comprehensive Review of Hydrogel Performance under CO_2 Conditions for Conformance Control. J Pet Sci Eng 185: 106662.

Sydansk, R. D. and Romero-Zeron, L. 2011. Reservoir Conformance Improvement. Richardson, Texas, USA: Society of Petroleum Engineers.

Targac, G., Gallo, C., Smith, D., Huang, C. K., Autry, S., Peirce, J., Li, B. 2020. Case History of Conformance Solutions for West Sak Wormhole/Void Space Conduit with a New Reassembling Pre-Formed Particle Gel RPPG. Paper presented at the SPE Annual Technical Conference and Exhibition, Virtual, 26–29 October. SPE-201302-MS. https://doi.org/10.2118/201302-MS.

Vasquez, J. E., Dalrymple, E. D., Abbasy, I., Eoff L. S. 2008. Laboratory Evaluation of Water Swellable Materials for Fracture Shutoff. Paper presented at the SPE North Africa Technical Conference and Exhibition, Marrakech, Morocco, 12–14 March. SPE-111492-MS. https://doi.org/10.2118/111492-MS.

Wang, Z. and Bai, B. 2018. Preformed-Particle-Gel Placement and Plugging Performance in Fractures with Tips. SPE J. 23 (06): 2316–2326. SPE-193997-PA. https://doi.org/10.2118/193997-PA.

Wang, Z., Bai, B., Long, Y., Wang, L. 2019a. An Investigation of CO2-Responsive Preformed Particle Gel for Conformance Control of CO2 Flooding in Reservoirs with Fractures or Fracture-Like Channels. SPE J. 24 (05): 2398–2408. SPE-197046-PA. https://doi.org/10.2118/197046-PA.

Wang, Z., Bai, B., Sun, X., Wang, J. 2019b. Effect of Multiple Factors on Preformed Particle Gel Placement, Dehydration, and Plugging Performance in Partially Open Fractures. Fuel 251: 73-81.

Zhang, H. and Bai, B. 2011. Preformed-Particle-Gel Transport Through Open Fractures and Its Effect on Water Flow. SPE J. 16 (02): 388–400. SPE-129908-PA. https://doi.org/10.2118/129908-PA.

Zhang, Y., Wei, M., Bai, B., Yang, H., Kang, W. 2016. Survey and Data Analysis of the Pilot and Field Polymer Flooding Projects in China. SPE Improved Oil Recovery Conference, 11–13 April, Tulsa, Oklahoma, USA. SPE-179616-MS. https://doi.org/10.2118/179616-MS.

Zhu, D., Bai, B., and Hou, J. 2017. Polymer Gel Systems for Water Management in High-Temperature Petroleum Reservoirs: A Chemical Review. Energy Fuels 31 (12): 13063−13087.

VITA

Yang Zhao (赵阳) was born in Henan, China. He received his bachelor's degree in Petroleum Engineering in 2014 and Master of Science degree in Oil&Gas Well Engineering in 2017, both from China University of Petroleum (East China). His advisors were Prof. Zhiyuan Wang and Prof. Baojiang Sun. His research was focused on "Hydrate Blockage Formation and Development in Multiphase Flow in Deepwater Wellbore". He worked out models and procedures to predict and control hydrate blockage risk in deepwater wellbore and pipelines. Yang was accepted to Missouri University of Science and Technology as a Ph.D. student in August 2017 and joined Dr. Baojun Bai's research group. He received his Doctor of Philosophy in Petroleum Engineering from Missouri University of Science and Technology in July 2021. Based on the doctoral research, he was able to publish several papers.